Microcrystalline Silicon for High-Efficiency Thin-Film Photovoltaic Devices

THÈSE N^O 6288 (2014)

PAR

Simon HÄNNI

(EPFL)

ÉCOLE POLYTECHNIQUE
FÉDÉRALE DE LAUSANNE

Suisse
2014

Acknowledgements

Acknowledgements

Abstract

In this thesis, diverse aspects of hydrogenated microcrystalline silicon (μc-Si:H), when used as an absorber layer in thin-film silicon solar cells, are studied. Mainly single-junction μc-Si:H solar cells in the p–i–n configuration are investigated, but the presented concepts can be applied to a μc-Si:H solar cell bottom cell in multi-junction devices.

The microstructure of μc-Si:H is characterized by small crystalline grains, with a typical size on the order of ten to hundreds nanometers, usually clustered in columnar structures, and embedded in an amorphous matrix. Defective zones in μc-Si:H can hinder efficient collection of generated carriers. Hence, the best cell performance is usually achieved for solar cells containing an amorphous silicon matrix (typically between 30 and 50%), which is believed to passivate recombinative zones well. Due to the low absorption of μc-Si:H, the μc-Si:H absorber layer typically has to be made with a thickness of a few micrometers.

When μc-Si:H is used as an absorber layer in thin-film silicon solar cells, there is a trade-off between electrical and optical performance. High optical performance is achieved by thickening the absorber layer, or by using efficient light-trapping schemes. Light trapping is generally obtained via textured superstrates, here made of zinc oxide (ZnO). However, when growing μc-Si:H on sharp textures, porous zones can appear within the absorber layer, which are detrimental for the electrical properties of the solar cell, as well as for stability to ambient atmosphere exposure. Here, some concepts to overcome this trade-off are presented.

First, the development of stable high-efficiency solar cells is reported. It is shown that dense material is required, for both high and stable efficiency. This requirement can be achieved by adapting the morphology of the front texture, or by adapting the deposition process. Via advanced electron microscopy, it is demonstrated that porous zones, as induced by a textured superstrate, form an interconnected network of micropores that act as possible diffusion paths for moisture penetration. An independently verified record efficiency of 10.7% is reported for single-junction μc-Si:H solar cells, besting the previous world-record value by 0.6% absolute.

Then, the effect of post-deposition treatments on such solar cells is investigated. Starting with a post-deposition hydrogen plasma optimized for ZnO, effects induced by the hydrogen plasma or annealing are carefully decoupled in complete solar cells. A stable increase in electrical performance is demonstrated, due to curing of nanoporous zones. From Fourier-transform photocurrent spectroscopy (FTPS) analysis, it is proposed that defects in these porous zones do not consist of a pure bi-dimensional surface within the absorber layer, but have a probable spatial extension. These porous zones of defective material can be damaged by the deposition of a ZnO electrode, and restored by an adapted post-deposition process

Abstract

such as annealing in vacuum.

Next, a detailed study on the interplay between the quality of the μc-Si:H absorber layer and dedicated interfaces for the doped layers is presented. By using mixed-phase silicon oxide doped layers, improved resilience to rough surface morphology is demonstrated, especially on rough and textured superstrates, by mitigating their detrimental effect as shown by using a variable-illumination technique. The concept of passivated interfaces in μc-Si:H solar cells is then introduced, based on the use of amorphous silicon as the passivation layer on the μc-Si:H absorber layer surface. As a result, record open-circuit voltages (V_{oc}) are reached, with values of 0.608 V and 1.53 V in thin single-junction and tandem solar cells, respectively. Finally, a concept to probe the ultimate V_{oc} of thin μc-Si:H solar cells is presented.

In the last chapter, the development of highly crystallized absorber layers is reported, based on the use of silicon tetrafluoride (SiF_4) as a precursor, to obtain a high short-circuit current density (J_{sc}) without compromising material quality. Several growth regimes are investigated in terms of deposition rate (D_r) and Raman crystalline fraction (R_c). D_r values of up to 4 Å/s are demonstrated, combined with highly crystallized layers. These layers are compared to layers obtained with our standard deposition regime. Layers with both high and standard R_c are analyzed with secondary ion mass spectrometry (SIMS), Fourier transform infrared spectroscopy (FTIR), and X-ray diffraction (XRD). SIMS measurements show that the use of SiF_4 does not induce additional contamination in baseline processes. FTIR analysis of the hydride stretching modes reveals that similar hydrogen incorporation can be obtained in highly crystallized films deposited using SiF_4 or standard silane (SiH_4) precursors, whereas XRD analysis demonstrates that layers obtained with SiF_4 do not exhibit a (220) preferential orientation. This orientation, typically obtained with SiH_4-based chemistry is generally attributed to device-grade material. Such highly crystallized films are implemented as the absorber layer in single-junction solar cells, reaching V_{oc} values as high as 470 mV, and a conversion efficiency (η) of 8.3% (with $R_c > 80$%). Although superstrate roughness also limits cell efficiency, and especially fill factor, no porous zones, as can be observed by transmission electron microscopy for standard cells obtained with SiH_4-based chemistry, are detected. Structural defects are, however, found in large grains, and proposed as responsible for the low obtained V_{oc}. A record total J_{sc} value of 31.9 mA/cm^2 is demonstrated for a micromorph tandem cell with a total silicon thickness of 3.4 μm thanks to improved absorption in the near-infrared.

Key words: renewable energy, solar energy, photovoltaics, silicon, thin films, coatings, thin-film silicon solar cells, amorphous silicon, microcrystalline silicon, nanocrystalline silicon, stable efficiency, p–i–n, LPCVD, roughness, tandem solar cells, FTPS, FTIR, PECVD, micromorph, passivation, interfaces, electron microscopy, tomography, TEM, annealing, post-deposition treatment, hydrogen plasma, high efficiency, record, single-junction, multi-junction solar cells, simulation, PC1D, SiF_4, SiH_4, hydrogen, fully crystallized, defects, porous zones

Résumé

Divers aspects du silicium microcristallin hydrogéné (μc-Si:H) sont étudiés, lorsque celui-ci est utilisé comme couche absorbante de lumière dans des cellules solaires à couche mince de silicium, principalement dans des dispositifs à simple jonction, mais aussi dans des dispositifs à jonctions multiples, tels que des cellules solaires tandem de type "micromorphe".

La microstructure du matériau μc-Si:H est caractérisée par des grains cristallins, d'une taille charactéristique de l'ordre de dix à quelques centaines de nanomètres, généralement regroupées dans des structures colonnaires et entourés par une matrice de sillicium amorphe. La meilleure performance électrique est généralement obtenue pour des cellules solaires contenant une matrice de silicium amorphe (typiquement entre 30 et 50 %), considérée comme essentielle pour passiver les zones recombinatives présentes à l'intérieur du matériau. En raison de la faible absorption de la lumière par le μc-Si:H, une épaisseur de l'ordre de environ un à quelques micromètres est requise pour la couche absorbante.

Lorsque le μc-Si:H est utilisé comme couche absorbante de lumière en cellule solaire, il existe un compromis entre la performance électrique et optique. Une haute absorption de lumière est obtenue soit en épaississant la couche absorbante , ou alors en utilisant une technique efficace de piégeage de lumière dans la couche absorbante. Ce piégeage de lumière est généralement réalisé par l'intermédiaire de superstrats texturés, ici fabriqués en oxyde de zinc (ZnO). Cependant, lors de la croissance de μc-Si:H sur des textures rugueuses, des zones poreuses peuvent apparaître à l'intérieur de la couche absorbante. Ces zones poreuses sont préjudiciables à la fois pour les propriétés électriques de la cellule solaire, ainsi que pour sa stabilité à l'humidité ambiante.

Tout d'abord, le développement de cellules solaires à haute efficacité est rapporté . A cet effet, il est démontré qu'un matériau dense est nécessaire , tant pour obtenir une efficacité élevée que stable . Cette condition peut être réalisée par une morphologie adaptée de la texture avant, ou par un procédé de dépôt adapté . Via une reconstruction tridimensionelle de la couche absorbante par des images en coupe obtenues par microscopie électronique à balayage, il est démontré que les zones poreuses, induites par un superstrat texturé, forment un réseau interconnecté de micropores, agissant comme possible voie de diffusion par l'humidité. Grâce à un procdé de fabrication optimisé, une efficacité record de 10.7 % est montrée pour une cellule solaire μc-Si:H à simple jonction, certifiée par un institut de mesure indépendant, et constituant une amélioration de 0.6 % (absolu) par rapport au record du monde précédent.

Ensuite, à partir d'un traitement par plasma d'hydrogène développé pour améliorer les propriétés électriques du ZnO, les effets induits par un tel plasma et le recuit qui lui est

Résumé

associé sont étudiés et découplés dans des cellules solaires complètes. Par l'intermédiaire d'un recuit sous vide, une augmentation stable de la performance électrique est démontrée. Par analyse FTPS, il est proposé que les défauts dans ces zones poreuses ne constituent pas une surface bidimensionnelle, mais possèdent une extension spatiale. Ces zones poreuses du matériau μc-Si:H peuvent être rendues défectueuses par le dépôt d'une électrode en ZnO, et récupérées par un traitement thermique sous vide.

Une étude détaillée sur l'interaction entre la qualité de la couche absorbante et les couches dopées est egalement présentée . En utilisant des couches dopées faites d'oxyde de silicium, une meilleure résilience à une morphologie de superstrat rugueuse est mise en évidence. Le concept d'interfaces passivées est introduit, basé sur l'utilisation de silicium amorphe comme matériau passivant. En conséquence, des tensions en circuit ouvert (V_{oc}) élevées sont atteintes, avec des valeurs record de 0.608 V et 1.53 V pour des cellules solaires à simple jonction et en configuration tandem. Enfin, un concept pour évaluer le potentiel en V_{oc} pour une cellule solaire fine est présenté.

Dans le dernier chapitre, le développement de couches absorbantes hautement cristallisées est rapporté, basée sur l'utilisation du précurseur SiF$_4$. Plusieurs régimes de croissances sont examinés en termes de taux de dépôt (D_r) et de fraction cristalline (R_c), définie par spectromètrie Raman. Des taux de dépôts jusqu'à 4 Å/s sont obtenus, combinés avec des couches très cristallisées (R_c>80 %). Ces couches sont ensuite comparées à d'autres couches obtenues au moyen d'un régime de dépôt standard (SiH$_4$), au moyen d'analyses SIMS, FTIR et XRD. Les mesures SIMS montrent que l'utilisation de SiF$_4$ n'induit pas de contamination dans les procédés de référence, puis l'analyse FTIR montre qu'une incorporation d'hydrogène similaire aux couches obtenues par le precurseur standard (SiH$_4$) peut être obtenue dans des films hautement cristallisés, alors que l'analyse XRD révèle que si une orientation préferentielle de type (220) (en géneral requise pour de hautes efficacités) est présente pour les couches standard, celles obtenues par SiF$_4$ ne présentent pas ou peu d'orientation préférentielle. Toutefois, lorsqu'incorporés en cellule solaire, les films hautement cristallisés obtenus avec le précurseur SiF$_4$ permettent d'atteindre des V_{oc} de l'ordre de 470 mV et un rendement de 8.3 % (avec R_c>80 %) en cellule simple-junction. Bien que la rugosité du superstrat limite l'efficacité des cellules, des zones poreuses attendues sur des superstrats très texturés ne sont pas détectées. Toutefois, d'autres défauts structurels sont mis en évidence par microscopie électronique en transmission et cause de basses performances électriques. Ces couches absorbent néanmoins très efficacement l'infrarouge, conduisant à une densité de courant de court-circuit record de 31.9 mA/cm^2 en cellule micromoprhe, pour une épaisseur totale de silicium de 3.4 µm seulement.

Mots clefs : énergies renouvelables, solaire, photovoltaïque, silicium, couches minces de silicium, silicium amorphe, silicium microcristallin, efficacité stable, p–i–n, LPCVD, rugosité, tandem, PECVD, micromorphe, passivation, interfaces, microscopie électronique, tomographie, recuit, traitement, plasma d'hydrogène, haute efficacité, record, simple jonction, cellules solaires à multi-jonctions, simulation, FTPS, FTIR, PC1D, SiF$_4$, SiH$_4$, hydrogène, défauts, zones poreuses

Contents

Contents

List of Figures

List of Tables

List of Abbreviations and Symbols

$\alpha_{0.8}$	absorption coefficient at 0.8 eV, as evaluated by FTPS
η	conversion efficiency
μc-Si:H/nc-Si:H	hydrogenated microcrystalline/nanocrystalline silicon
μc-Si:F:H	μc-Si:H alloy deposited with a fluorinated precursor
σ_{RMS}	root mean square roughness
a-Si:H	hydrogenated amorphous silicon
CMM	current-matching machine
DD	dark degradation
DEZ	diethylzinc, a metalorganic precursor used for LPCVD-ZnO
D_r	deposition rate
EQE	external quantum efficiency
FCA	free-carrier absorption
FF	fill factor
FTIR	Fourier transform infrared spectroscopy
FTPS	Fourier transform photocurrent spectroscopy
In_2O_3:H	hydrogenated indium oxide, also referred to as IOH
IR	infrared
J_{sc}	short-circuit current density
LBIC	light-beam induced current
LPCVD	low-pressure chemical vapor deposition
LPCVD-ZnO	zinc oxide deposited by LPCVD
MFC	mass flow controller
nid	non-intentionally doped
NIR	near-infrared range of the light (∼750–1200 nm)
PECVD	plasma-enhanced chemical vapor deposition
P_{mpp} (V_{mpp},J_{mpp})	maximum power point (voltage,current density at P_{mpp})
R_c	Raman crystallinity factor
R_{oc}	open-circuit resistance
R_{sc}	short-circuit resistance

List of Tables

1 Introduction

1.1 Solar energy

1.1.1 General context

Mankind is facing one of its greatest challenges for the coming century. Indeed, our current energy supply is widely ensured by non-renewable and polluting resources such as oil, gas, and coal, which account for more than 80% of the world's production [IEA 13b]. These resources are restricted to defined areas and are therefore not equally shared between the world's population. Furthermore, the inherent risks of nuclear energy, as illustrated by the recent events in Fukushima in March, 2011, and the problem of nuclear waste disposal make nuclear power a potentially risky solution for the long term.

Renewable energies such as solar energy, hydropower, wind energy, and biomass offer solutions based on unlimited amounts of freely available energy. Among these technologies, photovoltaics (PV)—the direct conversion of light into electricity—is a proven solution to create renewable electricity [Jacobson 09]. Thanks to the continuous energy current from the sun that radiates towards the earth (1.5×10^{18} kWh/year) [Würfel 09], PV can be implemented virtually everywhere, in the form of localized, grid-connected installations generating hundreds of W up to large plants such as the Solar Star Projects under construction in California, United States, with a projected cumulative power of 579 MW.[1]

According to reports from the International Energy Agency [IEA 13a, IEA 13c], approximately 100 GW of PV capacity were installed worldwide by the end of 2012, with a record annual PV production of about 38 GW [Jäger-Waldau 13] in 2012 alone. In Switzerland, around 226 MW of grid-connected PV capacity were installed, which is more than all the PV capacity that was connected to the grid there during the whole period of 1987–2011 [Hüsser 13, Kaufmann 13]. As a comparison, these 226 MW represent about 20% of the nominal power of the Leibstadt nuclear power plant, which is the biggest in Switzerland. This rapid increase in PV installation is largely due to a continuous reduction of production and installation prices of PV modules,

---

[1]http://us.sunpower.com/solar-star/ accessed May, 2014

and to favorable government policies towards renewable energies.

Fig. 1.1 shows the difference between the levelized cost of electricity—which is the price at which electricity must be generated from a specific source to break even over the lifetime of the project—and the household retail price for PV in Europe.
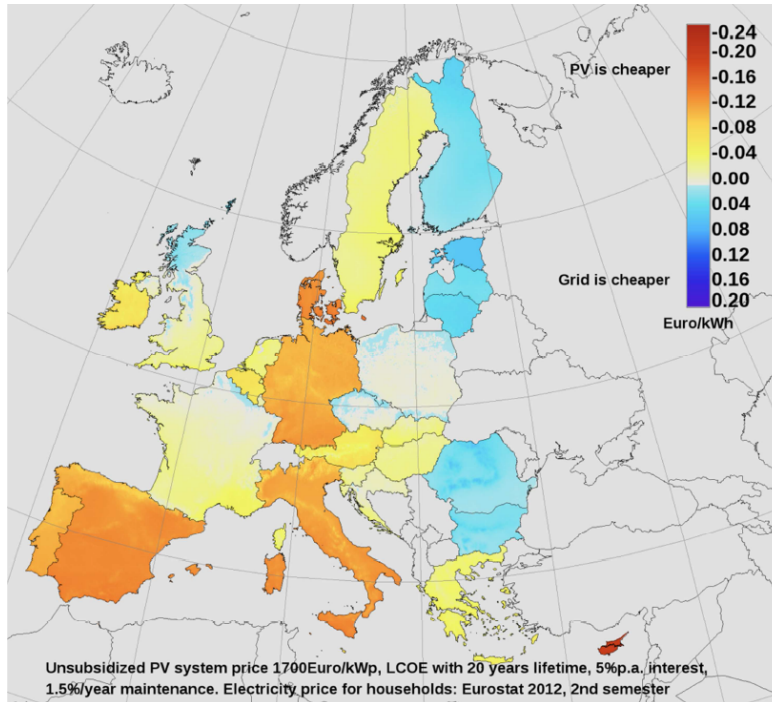
Figure 1.1: *Price difference between PV levelized electricity cost and household retail prices (reproduced from [Ossenbrink 13]).*

Even in the less sunny northern countries, PV can now be cheaper than other conventional sources (due to higher household retail prices), whereas in sunny southern countries, grid parity—*i.e.* PV generates electricity at a levelized cost that is less than or equal to the price of purchasing power from the grid—has already been reached. However, for a successful generalized implementation of PV, two issues will need to be solved. First, this low price has a meaning only if electricity can be sold, *e.g.* to an electricity supplier. Second, and maybe the most crucial step, grid management will have to be re-optimized. Indeed, a shift from the usual centralized production (the case in many western countries) towards localized production must be accompanied by efficient storage solutions, allowing for cloudy days and for the shaving of production peaks.

1.1.2 Some historical milestones

The photovoltaic principle was discovered by E. Becquerel in 1839. H.R. Hertz then established the photovoltaic effect, as it is known nowadays, but this effect was only fully explained by A.

Einstein in 1905 [Einstein 05], with the introduction of light as a finite number of fixed energy quanta, which led to the Nobel prize in Physics in 1923. C. Fritts is credited with fabricating the first working solar cell in 1883, which used the newly dicovered photoconductivity of selenium, and reached a conversion of about 1% by coating selenium with a very thin layer of gold [Fritts 83].

The first modern silicon solar cell, with a conversion efficiency of about 6%, was invented at Bell Labs by D. M. Chapin, C. S. Fuller and G. L. Pearson in 1954 [Chapin 54] and was obtained in the context of the emerging space applications. Indeed, on March 17, 1958, Vanguard I, the first solar-powered satellite was launched, equipped with silicon-based solar cell clusters from Hoffman Electronics, with a conversion efficiency of about 9%. Since these early years, the efficiency of silicon-based solar cells has continuously risen, up to a record value of 25.6% for a full-wafer back-contacted silicon heterojunction solar cell, as recently announced by Panasonic.

This rise in efficiency was accompanied by a strong reduction in fabrication costs. As a consequence of the wide use of crystalline silicon (c-Si) in the semiconductor industry, its production price has lowered drastically, going from prices as high as 1000 \$/W to lower than 0.5 \$/W, and dominating the PV market with about 85% of the market share.

1.1.3 Thin-film technologies

As just discussed, the PV market is dominated by the mature c-Si technology. However, to achieve more cost-effective production and higher throughput, a second generation of solar cells has been emerging. The most representative of them are technologies based on cadmium telluride (CdTe), on copper diselenide materials (CIGS), and on thin-film silicon.

Thin-film technologies offer the advantage of very low material costs, can be used on many kinds of substrates such as polyimide foils [Chirilă 13] and have a lower energy payback time and CO_2-eq/kWh as compared to c-Si technologies [de Wild-Scholten 13].

Other thin-film technologies are dye-sensitized solar cells (DSC), organic solar cells and perovskite-based solar cells [Burschka 13], which have emerged extremely fast with efficiencies of up to 17.9%. These technologies have the highest cost-reduction potential, but at the moment, the encapsulation requirements for these less stable cells with respect to ambient air exposition hinder their deployment for large-scale electricity production.

In Fig. 1.2, the most recent lab-scale record efficiencies for all PV technologies are shown, as reported and updated on a regular basis by the National Renewable Energy Laboratory (NREL).
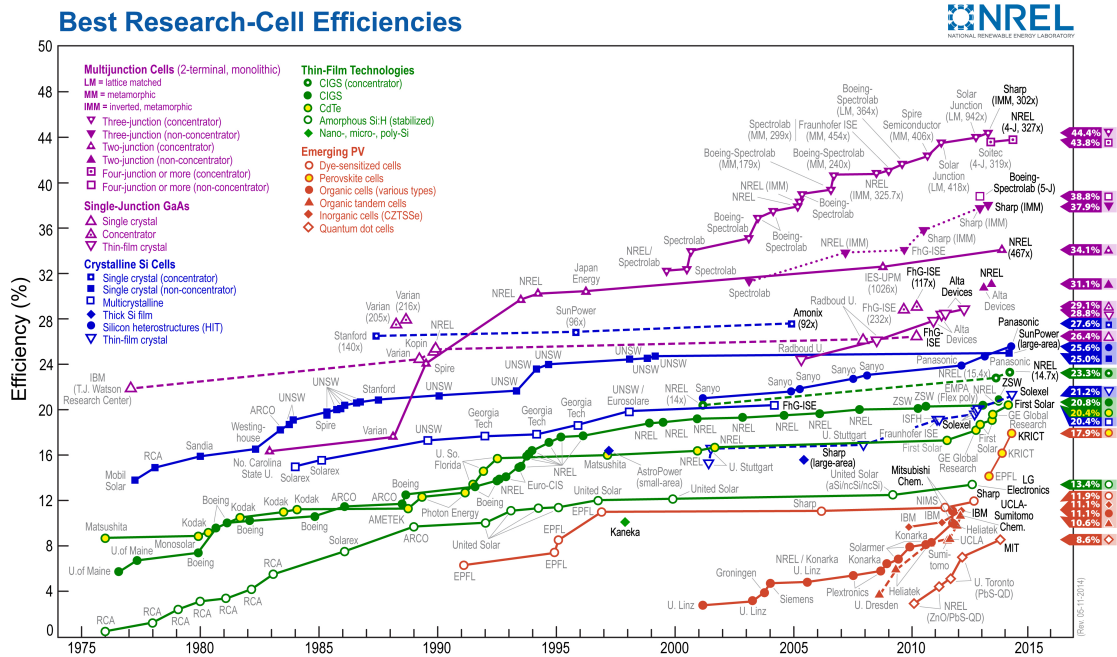
Figure 1.2: *Record efficiencies for the different photovoltaic technologies. Source: K. Emery et al., NREL 05/14 (http://www.nrel.gov/ncpv/), reproduced with authorization.*

1.2 Thin-film silicon photovoltaics

Since the manufacture of the first hydrogenated amorphous silicon (*a*-Si:H) layers [Sterling 65, Chittick 69] and the demonstration of their possible doping [Spear 75, Spear 76] leading to a first working device [Carlson 76], thin-film silicon has gained a tremendous interest for PV applications.

Nowadays these layers are generally deposited on coated glass, by plasma-enhanced chemical vapor deposition (PECVD), benefiting from the large experience of the flat-panel industry, and from the possibility to directly incorporate hydrogen in the layers, necessary for device-grade material.

Among the thin-film technologies, thin-film silicon has shown advantages from many points of view [Vallat-Sauvain 06b, Shah 10]:

- The materials are abundant and non-toxic, which is not the case for CIGS (limited indium resources and toxicity of cadmium) or CdTe (limited availability of tellurium and toxicity of cadmium).

- The energy payback time of thin-film silicon solar cells is lower than that of the present *c*-Si technology: less than a year for *a*-Si:H compared to 1.5 to 2 years for *c*-Si in southern Europe [Alsema 98, Fthenakis 11, de Wild-Scholten 13].

- Low-temperature processes can be employed, allowing for a large choice of substrates, including glass and plastic foils.

- Upscaling to larger areas has already been demonstrated, with a monolithically integrated series connection of cells to form modules with an area of up to $5.7\,m^2$.

- Low temperature coefficients have been reported [Meier 98], favorable for implementation in hot regions of the globe.

Thin-film silicon meets prerequisites to reduce the price per watt-peak (W_p), and, indeed, production prices as low as $0.5€/W_p$ have already been reported, for a production capacity of $120\,MW_p$/year [Kratzla 10, Meier 12]. It has a unique potential for large-scale deployment of renewable electricity production [Feltrin 08]. However, an efficiency increase will be required to stay competitive in the market and to alleviate the impact of the balance-of-system costs [Shah 13].

The technology is based on the use of two main building blocks as the absorber material, namely hydrogenated amorphous silicon (*a*-Si:H) and hydrogenated microcrystalline silicon (*μc*-Si:H). As these materials have bandgaps of ~1.75 eV (*a*-Si:H) and ~1.1 eV (*μc*-Si:H), they can be efficiently used in tandem configuration, where two cells are monolithically stacked and therefore connected in series. This "micromorph" concept—using an optimal bandgap combination for tandem cells [Meillaud 06b, Shah 10]—was pioneered in Neuchâtel [Meier 96]. In a micromorph solar cell, photons with wavelengths from ~350 to 1100 nm can be absorbed, as illustrated in Fig. 1.3.
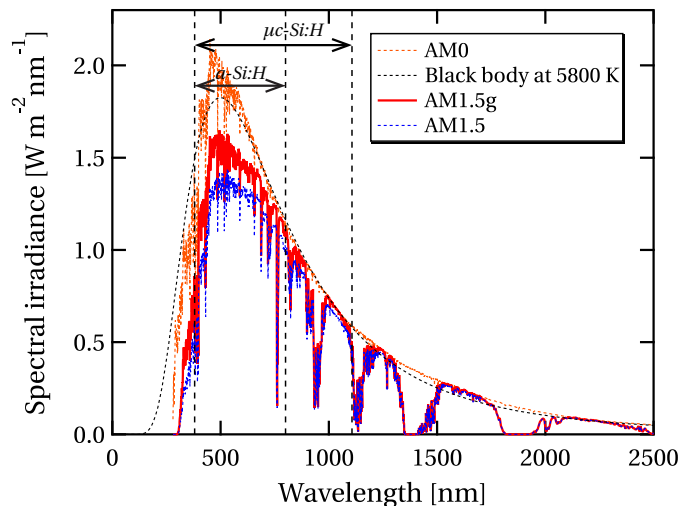
Figure 1.3: *Standard solar spectra, and absorption range of a-Si:H and μc-Si:H in a micromorph tandem cell. AM0 is the solar spectrum in space, AM1.5 is the solar spectrum for an incident angle of 48° (equivalent to an optical path length of 1.5 times the terrestrial atmosphere thickness) and AM1.5g is the AM1.5 spectrum with the additional diffuse component of the terrestrial atmosphere. For comparison, the spectrum of a black body at 5800 K is shown.*

Due to the high defect density in their layers, thin-film silicon solar cells are usually used in a configuration where an intrinsic absorber layer is sandwiched between a p-doped and an n-doped layer. Charge-carrier transport is assisted by the electric field created within the intrinsic layer (drift device), in opposition to a pure diffusion device. The doped layers are highly defective and charge carriers generated in them do not contribute to current. Hence, they have to be made thin to limit parasitic absorption.

The highest efficiency of 11.6% (after light-soaking) for a large-area micromorph module has very recently been reported by the Trübbach team of TEL Solar [Green 14b], with the lowest production costs of 0.35 €/W, corresponding to only 35 €/m². This type of module hence offers the lowest cost per m² and can benefit from additional advantages such as aesthetics. Such a module can be harmoniously implemented in beautiful architectural designs, such as the one presented in Fig. 1.4.

Figure 1.4: *Example of a photovoltaic wall, by the German company MASDAR PV.*

A scanning electron microscopy (SEM) cross section of a typical micromorph research cell, such as made in our laboratory, is presented in Fig. 1.5.

The cell in Fig. 1.5 is thicker than industrial solar cells, where the deposition rate and thickness of the bottom cell can be a limiting factor for high throughput and low production costs. In such a configuration, the current reported stable and certified record efficiency is 12.3%, obtained by Kaneka Corporation [Green 13b].

To further increase the conversion efficiency, triple-junction solar cells are used, reaching a reported initial efficiency of 16.3% [Yan 11] and a certified stable conversion efficiency of 13.4% [Kim 13]. Certified conversion efficiencies for single-junction a-Si:H and μc-Si:H solar cells are 10.1% (stable) and 10.8%,[2] respectively [Green 13b]. By using a quadruple-junction device and realistic assumptions for the contribution of each sub-cell, a simulated initial efficiency of 19.8% has recently been proposed [Isabella 14].

---

[2]improved to 11.0% by H. Sai *et al.*, 40th IEEE Photovoltaic Specialists Conference, Denver, Colorado, United States, June 8–13, 2014 (see also [Green 14b])
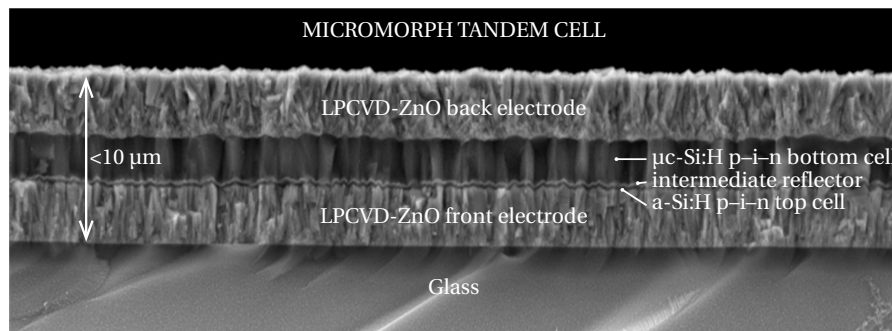
Figure 1.5: *Cross-sectional SEM image of a typical research micromorph tandem cell. It consists of two solar cells made of two different materials (a-Si:H and μc-Si:H) for efficient spectral utilization. Illumination is performed through the glass substrate. The front and back electrodes are made of a transparent conductive oxide, here zinc oxide. To optimize current repartition between the sub-cells, a intermediate reflector, generally made with a material with a lower refractive index than silicon, is inserted between the a-Si:H top cell and the μc-Si:H bottom cell. The total thickness is less than 10 μm.*

1.2.1 Amorphous silicon

a-Si:H is a disordered material, with some short-range order, but without translational symmetry. It is characterized by a bandgap of around 1.75 eV. Strictly speaking, this bandgap is not a well-defined bandgap such as in crystalline semiconductors (*i.e.* with no electronic states in the bandgap), but is defined as a "mobility gap," which is a range of energies in which there are electronic states that are localized and have zero mobility associated with them. These states are usually differentiated between "deep states" at around midgap, attributed to defects (dangling bonds), and "tail states," associated with strained bonds [Shah 10].

Soon after the demonstration of the first solar cell, D. L. Staebler and C. R. Wronski discovered the reversible light-induced degradation of photoconductivity in *a*-Si:H layers [Staebler 77]. This effect is still a limiting factor for further increasing the efficiency of thin-film silicon solar cells, as it has a direct impact on the stability of devices under light exposure. *a*-Si:H is sometimes divided into subcategories such as polymorphous silicon (dense *a*-Si:H containing very small crystallites [Hamers 00, Fontcuberta i Morral 01, Cabarrocas 02, Fontcuberta i Morral 04]) and protocrystalline silicon (*a*-Si:H grown close to the transition to μc-Si:H, which evolves into μc-Si:H if grown above a certain thickness [Collins 03, Yan 03, Stuckelberger 13]).

1.2.2 Microcrystalline silicon

μc-Si:H, often referred to as microcrystalline or nanocrystalline silicon, was discovered by S. Vepřek and V. Maraček in 1968 [Vepřek 68], by etching a piece of silicon with a hydrogen plasma and redepositing a layer on a substrate via a chemical transport technique at a process temperature of 600 °C. Doping of μc-Si:H layers was reported by S. Usui and M. Kikuchi in

1979 [Usui 79] and such layers were later implemented in solar cells [Uchida 82]. In 1992, a solar cell with a μc-Si:O:H absorber layer was reported [Faraji 92].

The first fully μc-Si:H working device was obtained by J. Meier *et al.* in 1994 at IMT Neuchâtel, with a conversion efficiency of 4.6%. They also showed that efficient absorber layers could be made by reducing impurities via the use of gas purifiers during deposition to reduce oxygen contamination [Torres 96].

Growth of microcrystalline silicon

μc-Si:H, as fabricated by PECVD, is generally grown in a transition regime and the deposition parameters can be used to control the crystalline fraction of the absorber layer. Microcrystalline growth is essentially determined by the species present in the plasma, and more specifically by the ratio of atomic hydrogen to radical flux towards the growing surface. This ratio was related to plasma properties by B. Strahm *et al.*, and a simple, but elegant, model was proposed, linking the transition to the concentration of silane in the plamsa c_p, and showing that μc-Si:H can be produced for any value of c_p, provided the silane depletion is high enough [Strahm 07].

In a review paper [Matsuda 99], the possible roles of hydrogen in the growth of μc-Si:H were summarized in three growth models, reproduced in Fig. 1.6:

(a) (b) (c)
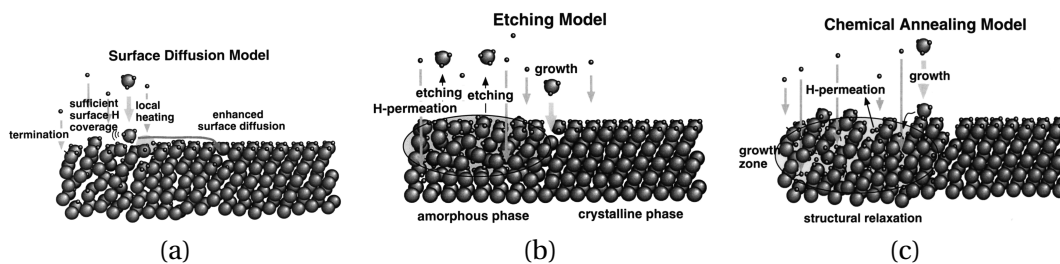
Figure 1.6: *(a) Surface diffusion, (b) etching and (c) chemical annealing models for the growth of μc-Si:H, reproduced with authorization from [Matsuda 99].*

- **The surface diffusion model** was originally proposed to explain a substrate temperature dependence for the crystalline volume fraction at a fixed silane-to-hydrogen ratio. Sufficient hydrogen flux density ensures full passivation of the surface and also produces local heating through hydrogen recombination on the growth surface of the film. This leads to an enhancement of the precursor diffusion length which can then find an energetically favorable site, favoring crystalline growth.

- **The etching model** was proposed to explain a growth rate decrease and an increase of the crystalline volume fraction when increasing the hydrogen dilution in the plasma. In this case, atomic hydrogen coming onto the surface breaks a (weak) Si—Si bond

(involved in the amorphous structure). This free place can then be replaced by a new precursor which would form a rigid crystalline structure.

- **The chemical annealing model** consists of a permeation of hydrogen in the sub-surface region leading to the crystallization of the amorphous network without removal of the Si atom (in opposition to the etching model).

Although the exact roles of atomic hydrogen in μc-Si:H growth are still debated, its importance is generally accepted [Fontcuberta i Morral 00, Sriraman 02, Kondo 03].

Microstructure of microcrystalline silicon absorber layers

The quality of μc-Si:H, as deposited by PECVD for photovoltaic applications, is directly linked to both intrinsic and extrinsic properties. Intrinsic properties are governed mainly by the deposition conditions—given by the reactor design (type, geometry)— such as deposition pressure, excitation frequency, inter-electrode gap, injected power, temperature of the substrate, deposition rate, gas type and flux, which determine the opto-electronic properties of the grown layer. Indeed, an extremely broad set of parameters can lead to any deposition from device-grade material to porous and useless material and from layers with many degrees of crystallinity to completely amorphous films.

Material with the highest quality is generally grown in the transition regime at a low deposition rate, below 1 nm/s, although lot of research effort is aimed at obtaining a higher deposition rate with maintained material quality. The aim here is to reduce the impact of ion bombardment on the growing film at high power. The use of very high frequencies [Curtins 87b, Curtins 87a, Kroll 97] or the high-pressure/high-depletion (HPD) regime [Guo 98, Kondo 00, Roschek 02, Rech 03], together with innovative reactor designs such as deposition with a multihole cathode [Niikura 04, Smets 06, Smets 08b], are proven solutions to obtain higher material quality at higher deposition rates. To completely remove ion bombardment, alternative non-plasma techniques, such as hot-wire chemical vapor deposition, can also be employed [Klein 01, Schropp 01, Klein 02].

Extrinsic properties, defined here as material properties that arise from external parameters, do not depend directly on the plasma conditions. For example, porous zones can be induced by the substrate and lead to post-deposition oxidation. As another example, the substrate's chemical nature can also impact the growth of μc-Si:H [Vallat-Sauvain 05]. However, as we will see throughout this thesis, these intrinsic and extrinsic properties can be strongly interlinked.

An important parameter to define device-grade material is the Raman crystallinity factor (R_c), which quantifies the crystalline fraction of μc-Si:H, as determined by Raman spectroscopy [Droz 04]. Device-grade material usually has R_c values around 60% [Vetterl 00, Mai 05]. It is generally assumed that an amorphous phase is required to passivate grain boundaries and to prevent their post-deposition oxidation [Bronneberg 11].

The microstructure of device-grade μc-Si:H is rather complex, as it is made of small crystalline grains embedded in an amorphous matrix [Vallat-Sauvain 00], in a columnar structure [Luysberg 97, Houben 98]. As an illustration, the structure of a typical p–i–n μc-Si:H cell, grown on textured zinc oxide (ZnO) is sketched in Fig. 1.7.
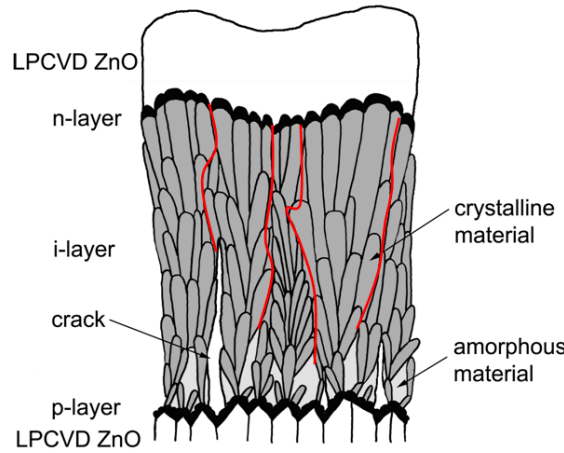
Figure 1.7: *Sketch of a typical p–i–n single-junction µc-Si:H solar cell, grown on textured ZnO, showing the microstructure of the µc-Si:H absorber layer, with clustered nanograins (red) embedded in an amorphous matrix. Reproduced with modification from [Bailat 03].*

Depending on the deposition conditions, the crystallinity generally evolves as a function of thickness. A large amorphous incubation layer at the p–i interface is not wanted, as it can hinder the collection of holes and thereby reduce the cell efficiency. "Cracks" will be discussed in Sec. 1.2.3, as they are the subject of many investigations presented in this thesis.

This figure also points out the importance of grain boundaries passivation, cluster boundaries passivation, and control of the interfaces, as generated charge carriers have to be extracted and collected at each side of the device. For the (lateral) transport of charge carriers in μc-Si:H layers, percolation via the crystalline parts is generally assumed, provided a minimum amount of crystalline fraction (about 20%, the percolation threshold) [Scher 70, Kirkpatrick 73, Tsu 82, Schellenberg 88, Hapke 93, Carius 97, Overhof 98, Shimakawa 00, Kočka 03, Azulay 05]. In solar cells, the relevant conductivity is, however, the perpendicular conductivity (along the growth direction) [Stiebig 00, Matsui 02a].

One of the main limiting factors in single-junction μc-Si:H solar cells is the V_{oc} decrease when increasing the crystalline volume fraction [Yamamoto 00, Droz 04, Nath 08, Johnson 08] and absorber layer thickness [Vetterl 01]. The thickness dependence is mainly attributed to bulk recombination [Yamamoto 00], as the material quality is still low compared to c-Si (a bulk lifetime on the order of 100 ns has been reported [Brammer 03]). The highest V_{oc} obtained so far is 603 mV [van den Donker 07], reached by using a buffer layer deposited by hot-wire CVD at the p–i interface, and attributed to the absence of ion bombardment at this interface. However, the low R_c of that cell implies that the high V_{oc} value was obtained by a

usual trade-off between high current (by enhanced absorption in the near-infrared for high R_c) and V_{oc}. This result also suggests that interface engineering is of crucial importance for high-efficiency μc-Si:H solar cells, as also discussed in [Mai 05, Mai 06, Söderström 08, Yue 08, Agbo 10, Despeisse 10, Bugnon 14].

1.2.3 Porous zones in microcrystalline silicon

As indicated previously, parameters not directly linked to the growth can modify the properties of a high-quality μc-Si:H layer. In thin-film silicon solar cells in general, a-Si:H layers have to be thin to reduce light-induced degradation, and due to the indirect nature of the μc-Si:H bandgap—associated with low optical absorption—and to ensure maximum current, the light path within the absorber layer has to be artificially elongated.

This is usually achieved by using efficient light in-coupling and trapping in the solar cells via randomly textured surfaces [Wenas 91, Faÿ 06, Berginski 07, Dominé 10, Rockstuhl 10], periodical grating to scatter light at well-defined angles [Soderstrom 10, Battaglia 12, Sai 13], modulated textures [Isabella 10], plasmonics [Atwater 10, Eminian 11, Paetzold 11, Tan 12], nano-structures with high aspect ratio [Kayes 05, Colombo 09, Vanecek 11, Krogstrup 13] and improved back reflectors [Sai 10, Sai 12, Söderström 12]. These light-scattering textures are of high theoretical and practical interest [Yablonovitch 82, Deckman 83b, Deckman 83a, Bittkau 08, Boccard 12e, Naqavi 13].

Methods using textured surfaces can lead to modified material quality in the a-Si:H and μc-Si:H absorber layers. For μc-Si:H, this often translates into the creation of porous zones within the absorber layer, especially when sharp textures are used as the substrate. Throughout this thesis, textured electrodes made of ZnO deposited by low-pressure chemical vapor deposition (LPCVD-ZnO) are employed. Their surface is characterized by pyramidal surface features, which can induce porous zones in the subsequently deposited μc-Si:H layer. These zones are often called "cracks" or "stripes" in the literature [Sakai 90, Bailat 02, Python 08, Python 09a, Li 09a, Li 09b, Python 10], as they usually appear as bright lines in micrographs, as obtained by transmission electron microscopy. Throughout this thesis, we will use the terms "porous zones"' or "zones of porous material," which reflect the physical nature of these defective areas. These zones were linked to the electrical properties of solar cells and to a two-diode model for solar cells [Merten 98], by acting as a second bad diode in parallel, with high dark saturation current.

These zones are generally attributed to strong "V-shaped" surface features, but it has recently been demonstrated that for a given substrate morphology, the creation of these porous zones is also influenced by the deposition process. Hence, a new model has been established, with two material phases, called "bulk" and "nanoporous zones," each phase being impacted differently by the deposition conditions and by post-deposition oxidation [Bugnon 12, Bugnon 13]. The porous zones still consist of μc-Si:H, but are highly defective.

1.3 Objectives of this thesis

The goals of this thesis are to

1. Identify fundamental limitations of single-junction μc-Si:H devices and find ways to surmount those limitations.

2. Separate contributions of the bulk μc-Si:H phase and of the p–i and i–n interfaces.

3. Identify the best μc-Si:H material and implement it in record devices.

4. Assess layers with high crystallinity for improved absorption in the near-infrared.

5. Identify how the growth of such material needs to be controlled and identify the impact of rough substrates on such devices.

A global objective is the identification of the limitations of single-junction μc-Si:H solar cells, without constraints on deposition rate, and to implement the processes required to reach this limit.

1.3.1 Structure of this thesis

This thesis is organized as follows.

Chap. 2 describes the structures of solar cells used in this thesis. The fabrication process of each layer is detailed and the general properties of standard ZnO layers, used as front and back electrodes, are given. Then, the main characterization tools used throughout this thesis are summarized. Nevertheless, this thesis has been written so that each chapter can be read separately, by repeating some experimental parts in each chapter, and by giving detailed information on processes which are used only in one chapter in that chapter.

Chap. 3 is first dedicated to the optimization of high-efficiency single-junction μc-Si:H solar cells in a small-area research system. Then, the impact of substrate roughness is analyzed, together with various combinations of doped layers and crystalline fraction of the μc-Si:H absorber layer. To evaluate the impact of surface features of increasing size, a novel front electrode is presented, based on the use of highly transparent hydrogenated indium oxide, allowing us to fabricate electrodes with similar sheet resistance, but varied surface feature sizes. The resilience of such high-efficiency devices to degradation in ambient atmosphere is evaluated. To further investigate the microstructure of μc-Si:H solar cells, a novel imaging technique is presented, based on 3-D tomographic reconstruction of the absorber layer.

In Chap. 4 the effect of post-deposition treatments, based on treatments developed for ZnO electrodes, on μc-Si:H solar cells is investigated. Careful evaluation of the effect of the treatments on the bulk material, the porous zones and the electrodes is performed. Special attention is given to further identify key properties of porous zones in the absorber layer.

These post-deposition treatments are then evaluated in the tandem configuration in terms of stability.

In Chap. 5, we investigate the effect of dedicated interfaces in p–i–n single-junction solar cells. We first investigate the role of the p–i interface and show that solar cells can be improved by using a SiO_x p-doped layer. Higher performance under lower illumination is demonstrated, linked to improved diode properties and improved shunt-quenching properties. Then, we introduce passivated interfaces for thin μc-Si:H solar cells, and demonstrate that an interface (here i–n) can be a limiting factor provided the bulk quality is high, which we confirm by a simple simulation model.

Finally, in Chap. 6, we detail a process based on the use of silicon tetrafluoride (SiF_4) as a precursor, for growing highly crystalline material to improve absorption in the infrared. We present a detailed comparison of the obtained absorber layers with our state-of-the-art layers, such as those presented in Chap. 3 and discuss the material requirements for obtaining high-efficiency devices. By implementing these layers in micromorph tandem cells, we obtain a record summed short-circuit current density of 31.9 mA/cm^2, with a total silicon thickness of only 3.4 μm.

1.3.2 Contribution of this thesis to the research field

In this thesis, several important findings for the field of thin-film silicon photovoltaics were obtained:

1. Thanks to advanced electron microscopy, it was demonstrated that porous zones form an interconnected network of micropores that can act as diffusion path for impurities. Degradation of solar cell performance under ambient atmosphere was successfully linked to the presence of porous zones in the absorber layer.

2. Thanks to careful investigation of post-deposition processes, it was demonstrated that these porous zones are also extremely sensitive to the deposition conditions of the back electrode, and that they can be cured by simple annealing in vacuum.

3. It was demonstrated that μc-Si:H solar cells are inherently limited by dead doped layers. By applying a passivating concept, a record V_{oc} of 0.608 V and 1.53 V was reached for thin single-junction μc-Si:H and micromorph tandem solar cells, respectively.

4. Using SiF_4, record infrared absorption was demonstrated in tandem solar cells, thanks to the use of highly crystallized layers. Although this result requires optimization, it paves the way to high-efficiency multi-junction solar cells.

Finally, this work led to two peer-reviewed publications [Hänni 13a, Hänni 13b], one conference proceeding [Hänni 11] as first author and various contributions as co-author

(list available at the end of this thesis). Two publications are to be submitted [Hänni 14a, Hänni 14b] and two patents are currently being filled.

Based of the developed processes, a new certified world-record conversion efficiency was obtained for single-junction μc-Si:H solar cells on an area >1 cm^2, with a value of 10.7%, as compared to the previous value of 10.1%. This value has now just been overtaken by AIST, Japan, with a certified value of 10.8%.[3] The topics presented in this thesis were also implemented in important results in the p–i–n configuration obtained by other members of the team, such as a certified world-record micromorph solar cell [Boccard 14] (12.6% stable) and an internal record for triple-junction solar cells [Schüttauf 14] (12.8% stable).

---

[3]improved to 11.0% by H. Sai *et al.*, 40th IEEE Photovoltaic Specialists Conference, Denver, Colorado, United States, June 8–13, 2014 (see also [Green 14b])

2 Preparation and characterization techniques

This chapter focuses on the standard experimental tools used in this thesis for the fabrication and characterization of microcrystalline Si (μc-Si:H) layers and solar cells. Most of them have already been described elsewhere [Python 09b, Cuony 11, Boccard 12c, Söderström 13, Biron 13b, Ding 13a, Bugnon 13] and will therefore only be summarized here. Details about special or more advanced techniques are given in the corresponding chapters.

2.1 Process flow for solar cell fabrication

The solar cells used in this thesis are deposited on glass using the p–i–n configuration. p–i–n and n–i–p refer to the sequence of deposition of the various doped (p, n) and intrinsic (i) silicon layers. Due to the lower mobility of holes as compared to that of electrons in amorphous silicon (a-Si:H), a thin-film Si solar cell is preferentially illuminated through the p-doped side. The p–i–n configuration hence needs a transparent superstrate, which is usually glass. Conversely, the n–i–p configuration allows for more freedom in the choice of the substrate,
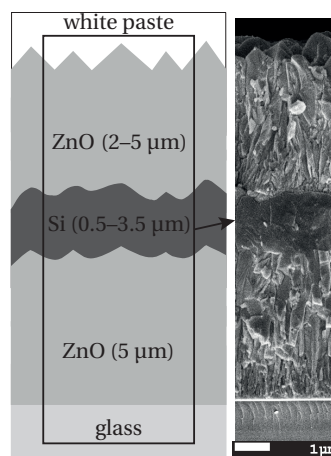
Figure 2.1: *Sketch and scanning electron microscopy (SEM) image of a typical μc-Si:H solar cell (no white paste on the SEM image).*

and opaque or flexible substrates such as plastic or metallic foils can be used. The standard glass used in this thesis is AF32 and AF45 glass from Schott, with a thickness of 0.5 mm and an area of 41x82 mm, usually cut into two pieces of 41x41 mm. After cleaning with soap and in acidic and alkaline ultrasonic baths, it serves as substrate for the deposition of all subsequent layers, and is the first window where the light enters the solar cell. Fig. 2.1 shows the standard structure of a solar cell in the $p–i–n$ configuration used in this thesis, with transparent zinc oxide (ZnO) front and back electrodes.

2.1.1 Zinc oxide deposited by low-pressure chemical vapor deposition

A typical superstrate for $p–i–n$ thin-film Si solar cells is glass coated with ZnO deposited by low-pressure chemical vapor deposition (LPCVD-ZnO). Diethylzinc (DEZ), which is a metalorganic compound ($Zn(C_2H_5)_2$), and water vapor are used as precursors. Doping is achieved by adding a small amount of diborane (B_2H_6) to the gas mixture. By choosing appropriate deposition conditions, a textured surface can be obtained, which is of high interest for better light trapping within the solar cell [Wenas 91, Faÿ 03, Faÿ 06, Faÿ 07, Steinhauser 07, Faÿ 10]. Indeed, when the growth temperature of LPCVD-ZnO is increased from 110 to 220 °C, the preferred orientation evolves from c-axis to a-axis, and then returns to c-axis at 380 °C. This transition is accompanied by a change in the surface morphology when the film thickness is increased: small rounded grains evolve to large V-shaped grains at a growth temperature of 150 °C [Nicolay 09], leading to a textured surface with random pyramids. The size of the surface pyramids is dependent on the film thickness, the doping and also the precursor flow ratio [Nicolay 12, Fanni 14], whereas the electrical properties of LPCVD-ZnO can also be adapted *e.g.* by tuning the doping level, by a multilayer approach or by post-deposition treatments [Ding 12b, Ding 12a, Ding 13b, Ding 13a].

In this thesis, the standard LPCVD-ZnO front and back electrodes are referred to as "Zx", where "x" stands for the nominal thickness of the ZnO film, in µm. The electrical properties of standard ZnO used as front and back electrodes are summarized in Tab. 2.1. 2-µm-thick Z2 is not an optimal electrode for μc-Si:H solar cells because of its higher doping and hence too high free-carrier absorbtion (FCA) in the near-infrared range of the solar spectrum. It is however used for amorphous silicon solar cells, which do not absorb light with wavelengths impacted by FCA. For a-Si:H/μc-Si:H micromorph tandem solar cells, electrodes with a maximal sheet resistance (R_{sq}) of up to 30 $\Omega/_{sq}$ can be used, as a consequence of the lower current of two solar cells connected in series, allowing for highly transparent front electrodes and still acceptable resistive losses [Boccard 12b]. For single-junction μc-Si:H solar cells, 10 $\Omega/_{sq}$ is a commonly accepted value for the R_{sq} of the front electrode in order to avoid too much resistive losses in the electrodes. Our standard superstrate for μc-Si:H solar cells is hence glass coated with a lightly doped 5-µm-thick Z5, which provides very efficient light trapping in the near infrared. This research superstrate is however not suited for industrialization, due to its large thickness.

Other common materials chosen for transparent conductive oxides (TCOs) in thin-film Si

Table 2.1: *Electrical and morphological properties of standard LPCVD-ZnO (taken and adapted from [Bugnon 13, Ding 13a]). Z2 and Z2.3 are usually used as superstrates for a-Si:H solar cells. Furthermore, Z2.3 is the standard superstrate for micromorph tandem solar cells. Z5 is used in this thesis as the standard superstrate for single-junction μc-Si:H solar cells, with an optimum treatment time of 45′. ZSE is employed in all types of thin-film Si solar cell, from single- to multi-junction devices. It provides a smooth surface morphology, favorable to the growth of high-quality μc-Si:H.*

Abbreviation	Z2	Z2.3	Z5	Z5 20'	Z5 45'	ZSE
Thickness [μm]	2.0	2.3–2.4	4.6–5.0	<5.0	<5.0	~0.6
(B_2H_6/DEZ)	(0.65)	(0.12)	(0.12)	(0.12)	(0.12)	–
σ_{RMS} [nm]	79	100	184	168	106	~130
Pyramid size [nm]	250	270	600	<600	<600	–
Average facet inclination [°]	40	-	45	-	18	–
Ironed surface factor [-]	1.55	1.38	1.67	1.37	1.15	–
Haze at 600 nm [%]	37	55	96	87	68	–
Sheet resistance [$\Omega/_{sq}$]	9	25	9	9	9	5–8
Mobility [cm^2/V s]	37	41	48	-	-	~40
Electron density [10^{19} cm^{-3}]	9.2	3.5	3.5	-	-	~37

solar cells in the *p–i–n* configuration include sputtered-etched ZnO (ZSE) and tin dioxide (SnO_2) such as *e.g.* TCOs from the Asahi Glass Company. ZSE is usually made by sputtering from an aluminium-doped ZnO target at a temperature usually between 200 and 400 °C. Its surface texture is usually achieved by etching with an acidic solution, typically by dipping in hydrochloric acid diluted in water at low concentrations (around 0.5%) for 30–40″. ZSE has a low R_{sq} (typically 5–8 $\Omega/_{sq}$) and provides a very smooth morphology with large craters more favorable to the growth of high-quality *μc*-Si:H [Rech 99, Agashe 03, Kluth 03, Müller 04, Hüpkes 06, Berginski 07, Beyer 07, Ruske 10, Hüpkes 12]. A few commercially available SnO_2-based TCOs are widely used, such as Asahi U (used for *a*-Si:H solar cells), Asahi VU and Asahi HU, which is multi-textured[1].

Multi-textured TCOs are employed as effective front electrodes in multi-junction devices, as they allow for optimized light in-coupling and light trapping in each sub-cell [Boccard 12a, Boccard 12d, Tan 13], similar to lacquer-based replicated textures coated with a sputtered conductive material [Battaglia 11c, Söderström 13, Paetzold 13]. Furthermore, in this thesis, a less common TCO that consists of high-mobility hydrogenated indium oxide (In_2O_3:H, or IOH) is also used. It was developed by C. Battaglia and L. Erni [Battaglia 11a], based on recent work done by Koida *et al.* at AIST [Koida 07, Koida 08, Koida 09, Koida 10b, Koida 10a]. Advantages of IOH include an unusually high carrier mobility above 100 cm^2/Vs, together with a relatively low carrier density, leading to very low FCA. The IOH TCO is obtained by sputtering an amorphous indium oxide film from a pure In_2O_3 target at room temperature, with argon (Ar) and a little water vapor for doping with hydrogen. Crystallization of the film is achieved

---

[1]http://www.agc.com/english/csr/env/products/3.html accessed April, 2014

by annealing, leading to a strong mobility increase together with a reduction by half of the carrier density. In our case, this annealing is obtained when depositing subsequent layers of the solar cell at higher temperatures. Details of the process can be found in [Boccard 12c].

Surface treatment of the front electrode

As previously mentioned, while the as-grown surface texture of LPCVD-ZnO is excellent for efficient light trapping, it is extremely challenging for the growth of high-quality μc-Si:H, resulting in decreased solar cell electrical performance [Python 08, Python 09a, Li 09b, Python 10] and long-term stability issues when porous zones are present within the bulk material [Matsui 06, Bronneberg 11, Cuony 11, Bugnon 12]. This interplay between superstrate morphology and μc-Si:H quality will be discussed in Chap. 3. In order to overcome these detrimental effects of a superstrate that is too rough, an Ar-plasma surface treatment can be used to improve the open-circuit voltage and the fill factor of the solar cell by smoothening the front electrode morphology, however at the cost of a reduced short-circuit current density [Bailat 06, Cuony 11, Boccard 12b]. The optimum treatment time on Z5 for a single-junction μc-Si:H solar cell was determined to be about 45 minutes. A transfer of these surface treatments of LPCVD-ZnO from one system to another occurred during this thesis. The treatment time was slightly shortened during the transfer for the same optical and electrical properties. Thus, a Z5 60' is the (old) equivalent of the Z5 45' if not specified otherwise.

2.1.2 Deposition of the silicon layers

Plasma-enhanced chemical vapor deposition (PECVD) was used throughout this thesis work to deposit the Si layers. PECVD takes place in a vacuum chamber where a substrate is heated at typical temperatures around $200\,^{\circ}$C between two electrodes. Silane (SiH$_4$) and hydrogen (H$_2$) are injected into the chamber. These gases would normally not decompose at such low temperatures, but by applying a radio-frequency (RF) signal (usually at a frequency of 13.56 MHz and multiples thereof) on one of the electrodes, a plasma is created between the electrodes, decomposing the gas precursors into radicals which can be used for layer growth. The multiple phenomena and reactions taking place in the plasma are rather complex and subject to an impressive number of publications and textbooks [Amanatides 01, Amanatides 02, Amanatides 05, Sansonnens 06, Strahm 07, Howling 07, Bartlome 09]. Reactions depend on the deposition conditions such as pressure, temperature, excitation frequency and power, gas mixture and fluxes, as well as on the reactor geometry.

In the following, the PECVD systems used during this thesis are briefly described, and are summarized in Tab. 2.2. Most of the work was performed in a small-area dual-chamber research system (SysB), in which each chamber contains an open parallel-plate reactor. For deposition of the absorber layers, a dedicated chamber was used, with a gas purifier for SiH$_4$ and H$_2$. All layers were deposited at $200\,^{\circ}$C, unless stated otherwise. The pressure and power

could in practice not be used as tunable process parameters, as acceptable homogeneity and reproducibility could be achieved only in a narrow range. On the other hand, dilution modification had a clear impact as a low-flow mass flow controller (MFC) was used for SiH_4, allowing good control of small fluxes and their grading. Ar was used in both chambers for pre-conditioning of the reactor after manual cleaning. Doping was performed with trimethylborane ($B(CH_3)_3$ or TMB) diluted in hydrogen (2% or 500 pppm) for p-type doping, whereas n-type doping was achieved by phosphine (PH_3) diluted in hydrogen (0.1%). In the chamber dedicated to doped layers, other gases such as carbon dioxide (CO_2), methane (CH_4), trimethylgallium (TMGA) were used as well. A detailed description of SysB is available in [Cuony 11].

Table 2.2: *Main parameters of the PECVD tools used during this thesis.*

System	Gap [mm]	Area of deposition [cm^2]	Pressure [mbar]	Frequency (p/i/n) [MHz]
SysB	15	10x10	0.2–0.7	110/70/110
OCTOPUS I	15	15x16	0.2–12	40/(13 & 81)/40
KAI-M	12	49x60	1–15	40/13/40

μc-Si:H was also routinely deposited in a dual-chamber R&D KAI-M system, described in detail in [Bugnon 13]. The baseline deposition for single-junction μc-Si:H and multi-junction solar cells was preferentially performed in this system, due to the large size available ($49 \times 60 \, cm^2$) and the reasonable deposition rate (3 Å/s). The same source gases as in SysB were used, except for the highly diluted TMB. Less diluted PH_3 (at 2%) was also available. Cleaning was performed after each deposition with a nitrogen trifluoride (NF_3) and Ar plasma followed by a H_2 plasma.

Details about the deposition and optimization of fluorinated microcrystalline silicon layers and cells, in KAI-M, with an alternative gas mixture consisting of silicon tetrafluoride (SiF_4), H_2 and Ar are described separately in Chap. 6.

2.1.3 Back contact and patterning

While plasma-treated Z5 is the standard superstrate for single-junction μc-Si:H solar cells, a lightly doped 2.3-μm-thick LPCVD-ZnO (Z2.3) is generally used as the back electrode. On each sample, 16 cells with an area of 0.25 cm^2 are typically patterned by lift-off of the back electrode between the cells. Access to the front electrode is ensured via dry-etching of the Si between the cells with a combined sulfur hexafluoride (SF_6)/oxygen (O_2) plasma. Larger cells can be obtained through a different patterning scheme, with six cells with a nominal area of 1 or 1.2 cm^2 each. In that case, however, Z2.3 is too resistive and a thicker Z5 must be used to avoid significant losses in the back electrode [Hanak 79]. The multi-junction solar cells presented in this thesis have an area larger or equal to 1 cm^2 and Z2.3 is used as the back electrode, unless specified differently.

2.1.4 Back reflectors

In combination with the LPCVD-ZnO back electrode, a white dielectric back reflector is typically applied to the back of the solar cells to reflect the transmitted light back into the cell and increase the short-circuit current density and the generation of charge carriers. The standard back reflector in our laboratory consists of a GORE[TM] layer (available with a thickness of 0.5 or 3 mm). The dielectric is applied directly onto the back of the solar cell, without gluing. If solar cells are encapsulated, white paint is applied onto the back electrode, after soldering of wires (two per contact). The soldered surface must be made as small as possible due to the poor reflectivity of soldered parts. To dry the two types of white paints provided by the manufacturer ("white opaque" and "white"), an annealing at 90 °C is performed in nitrogen atmosphere for about five hours. A fourth option is Tipp-Ex, a commercially available eraser[2] that can be easily applied.

Fig. 2.2 shows the total reflectance and transmittance (measured with a Perkin Elmer lambda 900 UV-vis-NIR spectrophotometer) of four possible white back reflectors.
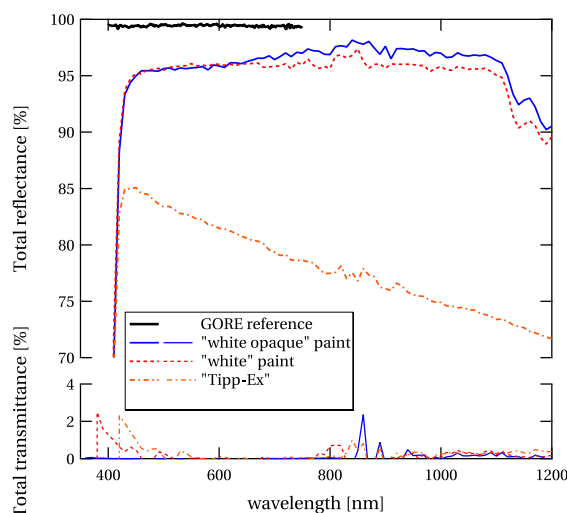
Figure 2.2: *Total reflectance and transmittance of four possible white back reflectors. "white opaque" and "white" paint are two types of white paint provided by the manufacturer, and "Tipp-Ex" is a commercially available ink eraser. The best reflection is obtained with the 3-mm-thick GORE[TM] reflector.*

The measurement of the 3-mm-thick GORE reflector is the one provided by the manufacturer. Internal measurement confirms that it has the best reflectance of all four white back reflectors, but it is not shown here due to artifacts in the measurement. Tipp-Ex has a poor reflectance compared to the white paint, but is easily applied and does not need an additional annealing such as is needed for drying the white paint.

Alternative possibilities exist for the back contact/reflector design, such as a metallic reflector

---

[2]http://www.bicworld.com/en/products/categories/13/correction accessed April, 2014

applied directly on the Si [Widenborg 07, Kunz 08] or on a thin TCO layer [Morris 90, Müller 04, Moulin 12, Khazaka 14].

2.1.5 Light soaking and dark degradation

Since the discovery of light-induced degradation in a-Si:H films (Stabler-Wronski effect) [Staebler 77], solar cells made of a-Si:H degrade when exposed to sun light. This degradation is linked to an increase of defect density within the absorber layer and is reversible by annealing. Thus, when illuminating the cells, an equilibrium between defect creation and recovery is established after a certain amount of time, depending on the illumination spectrum and intensity, the electrical-bias condition and the temperature. Although the degradation mechanisms are not fully understood, degradation can be lowered in a-Si:H solar cells by making them thin. With absorber layers with a thickness of typically 100 to 300 nm, the cell efficiency stabilizes after relative degradation of approximately 10 up to 30%.

Conversely, μc-Si:H is rather stable with respect to light-induced degradation [Meier 94, Yamamoto 99b] and is generally not light soaked when employed as an absorber layer in single-junction solar cells. This improved stability is largely utilized in multi-junction devices, as when μc-Si:H is used as a middle or bottom cell, its amorphous phase is not directly exposed to the high-energy photons, which are filtered by the top cell. In these configurations, μc-Si:H does not degrade, though in single junctions, some degradation (usually no more than 10%) can be observed if the Raman crystallinity factor (R_c) is low [Klein 03, Yan 04a, Yue 05a, Yue 05b, Yue 06, Meillaud 08]. To obtained stabilized values, solar cells containing at least one a-Si:H layer are therefore maintained under an illumination of one sun at a temperature of 50 °C, usually for 1000 h.

While light exposure is not a major concern for μc-Si:H, even in single junctions, dark degradation (DD) is critical. This phenomenon can take place when a cell is stored in ambient conditions and depends on the superstrate roughness or the PECVD, and is attributed to moisture ingression which leads to degradation of the solar cell efficiency.

Although there is no well-defined procedure for the evaluation of DD, which can also involve the degradation of LPCVD-ZnO, damp-heat tests [Bugnon 13] have been proposed as a method to accelerate DD for rapid assessment of the resilience of a solar cell to moisture exposure. In this thesis, DD is evaluated by leaving the cells in a dark drawer under ambient conditions for a certain number of days, without any control of the atmosphere.

2.2 Characterization

2.2.1 I-V measurements

Once the solar cells are complete, they must be characterized electrically in order to assess their conversion efficiency (η), also referred to simply as efficiency. This is defined as the ratio

of the electrical power output to the incident light power input under standard conditions (AM1.5g, $1000\,\text{W/m}^2$, $25\,°\text{C}$) and defined as:

$$\eta = \frac{P_{mpp}}{P_{ill}}\bigg|_{(\text{AM1.5g},\,1000\,\text{W/m}^2,\,25°\,\text{C})}$$

where P_{mpp} is the power density at the maximum power operational point of the solar cell, and P_{ill} the power density of the incident light. The efficiency can be derived from a current (density)–voltage ($I(J)$–V) curve under illumination, as presented in Fig. 2.3 in which relevant points are indicated on the curve.
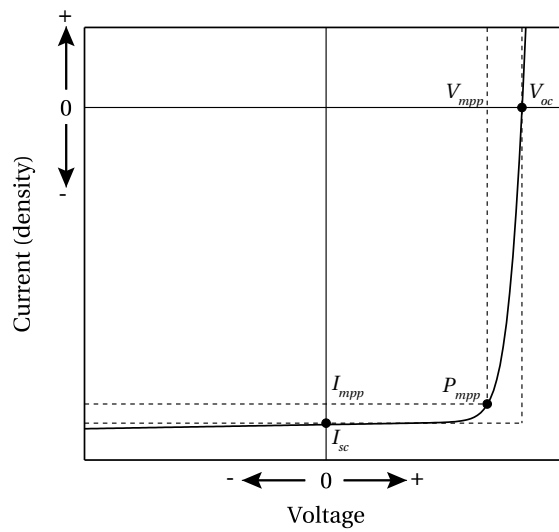
Figure 2.3: *Example of I(J)-V curve, with relevant points on the curve.*

The open-circuit voltage (V_{oc}) is the voltage of the device under illumination when no current is flowing. In thin-film Si solar cells, it is determined mainly by the doped layers (both materials and thicknesses), by the quality of the bulk material (which has an influence on the bulk recombination), by band offsets at the doped layer interfaces, and by the contact with the electrodes. It is also extremely sensitive to shunts, usually induced by pinholes directly contacting both sides of the cell, or bad-diode areas of the solar cells. These latter are linked to the presence of a nanoporous phase in the absorber layer, such as the one induced by rough superstrates [Python 08, Li 09b, Python 10, Cuony 11]. The short-circuit current density (J_{sc}) is the current density flowing through the device at zero voltage condition. Finally, the fill factor (*FF*) is the ratio of the $V_{mpp}I_{mpp}$-product over the $V_{oc}I_{sc}$-product. *FF* is sensitive to recombination (linked to the material quality), to shunts, and to the presence of electric-potential barriers in the solar cell which hinder the collection of the charge carriers. *FF* is also directly impacted by the many resistive losses which can occur in the solar cell.

Assuming an illumination of $1000\,\text{W/m}^2$ (standard test conditions), the conversion efficiency

is then simply given by

$$\eta\,[\%] = \frac{V_{oc}\,[\text{V}] \cdot I_{sc}\,[\text{mA}] \cdot FF\,[\%]}{A[\text{cm}^2] \cdot 100},$$

where *A* is the area of the solar cell.

The *J-V* curve is recorded experimentally using a four-terminal current-voltage measurement with a dual-lamp sun simulator from Wacom (WXS-220S-L2 AM1.5g) operating under standard test conditions. Apart from V_{oc} and *FF*, other parameters that are usually recorded are the open-circuit resistance R_{oc} (slope of the *J-V* curve at V_{oc}) and the short-circuit resistance R_{sc} (slope of the *I(J)-V* curve at J_{sc}). To achieve high efficiency, minimum R_{oc} and maximum R_{sc} values are necessary. J_{sc} can in principle be extracted from *J–V* curves as well. However, due to our cell design, a correct determination of J_{sc} requires special care. Indeed, lateral collection effects and trapping of light in the glass can typically impact the measurements. For this reason, J_{sc} of cells with an area larger than or equal to $1\,\text{cm}^2$ are measured with a dark mask (this defines a designated-area measurement, see Appendix A), while for smaller cells, J_{sc} is deduced from external quantum efficiency measurement as explained in the next section.

J-V curves can also be recorded at various degrees of illumination intensity with a variable illumination measurement (VIM) technique [Merten 98, Meillaud 06a]. Such measurements are performed by putting grey metallic filters between the sample and the light source to reduce the intensity of the incoming light. The technique can be used to determine the collection voltage of *p–i–n* devices [Meillaud 06c]. The VIM technique is here mainly used to assess V_{oc} losses as a function of illumination intensity, which is an important parameter when μc-Si:H is used in multi-junction devices.

2.2.2 External quantum efficiency

External quantum efficiency (EQE) is a unitless value giving the probability of collecting one electron-hole pair created by one incident photon of wavelength λ. It is evaluated by illuminating the cell in short-circuit condition with monochromatic light and measuring and comparing the resulting photocurrent with a photodetector reference of known EQE. As the generated photocurrent is low (the probe beam issued from a xenon lamp has a size of about 1x2 mm, smaller than the cell), lock-in amplification is used to improve the measurement. White light bias is used to approach real operation conditions. Negative-bias voltage measurement (usually at $-1\,\text{V}$), enhancing the internal electrical field, is routinely performed to evaluate the collection of photo-generated carriers in the solar cell.

In short-circuit condition, EQE is used to calculate J_{sc} by integrating the amount of photons from the AM1.5g spectrum[3] that contribute to photocurrent over the useful wavelength range (here from 370 to 1100 nm).

---

[3]http://rredc.nrel.gov/solar/spectra/am1.5/ accessed April, 2014

2.2.3 Raman spectroscopy

Raman spectroscopy is a widely used characterization setup for the evaluation of the crystalline volume in μc-Si:H, pioneered by Iqbal *et al.* in the early 80s [Iqbal 80, Iqbal 82]. A quantification of the crystallinity was introduced shortly afterwards by Tsu *et al.* [Tsu 82], based on the ratio of integrated parts of the spectrum originating from crystalline and amorphous parts. The crystalline volume fraction ρ is thus usually expressed as

$$\rho = \frac{I_c}{I_c + yI_a},$$

where I_c and I_a denote the integrated scattered intensity of the crystalline and amorphous phase, respectively and $y := \frac{\Sigma_c}{\Sigma_a}$ is the ratio of the corresponding integrated backscattering cross section (over the measured frequency range) [Bustarret 88]. A large set of values for y can be found in the literature [Brodsky 77, Bustarret 88, Vallat-Sauvain 06a]. We thus follow the approach proposed by Droz *et al.* [Droz 03, Droz 04] and arbitrarily set $y = 1$. The resulting Raman crystallinity factor R_c is then

$$R_c = \frac{I_{520} + I_{510}}{I_{520} + I_{510} + I_{480}},$$

where I_x is the integrated area of a Gaussian fit centered at x and the sum $I_{520} + I_{510} + I_{480}$ is the total integrated intensity.

R_c is not equal to the true crystalline volume fraction and should be considered as a lower bound for ρ [Houben 98]. In this thesis, the terms "Raman crystalline fraction", "Raman crystalline factor", and "Crystallinity" are always referring to R_c as defined above. The best devices are typically obtained near the transition regime, usually for R_c values ranging from 50 to 70% [Vetterl 00, Matsui 02b, Klein 02, Roschek 02, Mai 05].

In our laboratory, those measurements are performed with a Renishaw System 2000 Raman spectrometer, using a back-scattering geometry and green light excitation from the 514.5 nm emission line of an Ar ion laser, leading to a characteristic collection depth of approximately 150 nm in μc-Si:H. The measurements are usually performed on complete solar cells, both at the n-side through the back electrode or directly through the n-doped layer (on a small spot next to the cell which was protected during the patterning step) and through the glass for measurements at the p-side.

2.2.4 Fourier-transform photocurrent spectroscopy

The sub-gap absorption coefficient at 0.8 eV ($\alpha_{0.8}$) which is linked to defects in the bulk phase of the μc-Si:H material was evaluated by Fourier-transform photocurrent spectroscopy (FTPS). This method was originally developed by Vanecek *et al.* [Vanecek 02]. A Fourier-transform infrared spectrometer (Nicolet 8700 from Thermo Scientific) was used as a modulated infrared source and complete μc-Si:H solar cells as photodetectors. As the technique is very sensitive to

both roughness and doping of the superstrate [Python 09b], solar cells with similar absorber-layer thicknesses and R_c, as well as with similar front and back electrodes, were used in each study. The FTPS technique being a relative measurement, the curves were scaled at 1.35 eV with the known value of the absorption coefficient of crystalline silicon. $\alpha_{0.8}$ was taken as a figure of merit for material quality assignment, as it scales with the defect density in the absorber layer. A more detailed description of FTPS can be found in [Bailat 04].

2.2.5 Transmission electron microscopy

Direct evidence of the microstructure of μc-Si:H can be derived from transmission electron microscopy (TEM) images of cross sections of μc-Si:H layers and solar cells. The first TEM experiments on μc-Si:H were performed in the early 90s, when the first evidence of columnar growth parallel to the growth direction for undoped, phosphorus–doped and slightly boron–doped layers was shown [Chen 92, Kaneko 93]. Saha *et al.* studied the effects of the deposition parameters on grain size [Saha 93]. Two publications [Luysberg 97, Houben 98] from the Jülich group showed a detailed structural analysis of μc-Si:H samples by TEM. In [Luysberg 97], columnar growth was confirmed and dependence on growth parameters like pressure and excitation frequency was shown. The role of porous zones was extensively investigated with TEM, and was later linked to solar cell performance [Sakai 90, Bailat 03, Python 08, Duchamp 11, Naruse 12, Duchamp 13].

TEM images presented in this thesis, as well as sample preparation, were taken by the author, if not stated otherwise. For sample preparation, a wedge-polishing method by tripod, followed by smooth milling with Ar ions, was used [Benedict 91, Bailat 04, Python 09b]. The images were recorded with a Philips CM-200 microscope at CSEM SA, Neuchâtel, Switzerland.

3 High-efficiency microcrystalline silicon thin-film solar cells

In this chapter, we first summarize the development and optimization of high-efficiency microcrystalline silicon (μc-Si:H) solar cells (Sec. 3.1). In Sec. 3.2, we then show how the bulk properties of μc-Si:H, as well as the cell design impacts the performance of single-junction μc-Si:H solar cells. In particular, we show that a dense material, without porous zones is required to obtain both highly efficient and stable solar cells. The impact of increasing superstrate roughness is investigated in Sec. 3.3, by using an innovative superstrate based on the use of stacked transparent conductive oxide layers. It is showed that the resilience to sharp surface textures is highly dependent on the used deposition process of the absorber layer.

A combination of scanning electron microscopy (SEM) and tomography is presented in Sec. 3.4 to visualize the 3-D interconnected network of porous and defective zones which can appear when μc-Si:H is grown on highly textured superstrates. We finally present a record device in Sec. 3.5, with an independently confirmed conversion efficiency of 10.7%. Parts of these results are published in [Hänni 11, Hänni 13a, Hänni 13b].

3.1 Optimization of solar cells in a small-area PECVD reactor

Single-junction solar cells were deposited and optimized by the author in a small-area research reactor (SysB, see Chap. 2) by PECVD at a superstrate temperature of 200 °C. For the intrinsic layers, the excitation frequency was set at 70 MHz and a pressure of 0.7 mbar was chosen. To ensure a good homogeneity and given the reactor design of SysB, the pressure could not be increased above this value. Thus, promising deposition regimes such as a high-pressure/high-depletion regime [Guo 98, Kondo 00] were not accessible (see also Chap. 1). To evaluate the deposition rate and transition zone for the Raman crystallinity factor (R_c) of the intrinsic absorber layer, the silane (SiH_4) dilution in hydrogen (H_2), as well as the (low) input power, were varied. We investigated dilutions, defined here as the flux ratio of SiH_4 to H_2 ($[SiH_4]/[H_2]$), ranging from 3 to 6%, and power densities ranging from 0.02 to 0.06 W/cm^2. The obtained deposition rate was on the order of 1.4 to 1.8 Å/s, as assessed from thickness measurements of complete devices with doped layers of known
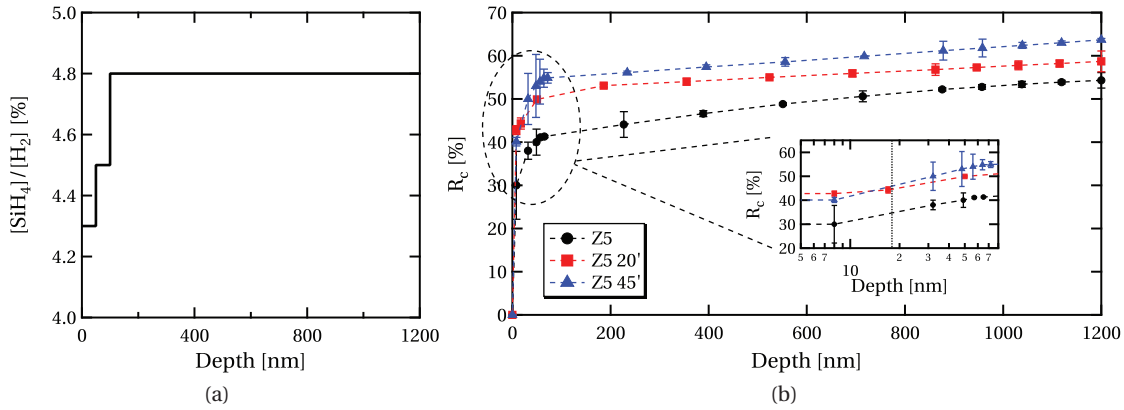
Figure 3.1: *Typical dilution (a) and R_c (b) profiles used in the optimized process. The R_c profiles were measured by Dr. Do Yun Kim from TU Delft [Kim 14], and the data are used here with his kind authorization. The p–i interface is shown in the magnified inset.*

thicknesses. A grading of [SiH$_4$] was employed at the p–i interface during the first 50 to 100 nm, without a plasma break, to ensure an early microcrystalline growth on the p-doped layer [Stiebig 00, Bailat 03, Vetterl 03, Yan 04b, van den Donker 05, Gordijn 05, Smets 08a].

With such optimized SiH$_4$ grading at the beginning of the growth, an optimum R_c was achieved both at the p–i interface (R_c~50–60%) and within the absorber layer (R_c~55–60%). Typical dilution and R_c profiles as a function of layer thickness are presented in Fig. 3.1. Note that R_c optimization was performed mainly for smooth superstrates, such as a 5-µm-thick zinc oxide layer deposited on glass by low-pressure chemical vapor deposition (LPCVD-ZnO) and treated for 45' with an argon plasma (Z5 45') (see Chap. 2). Slightly lower R_c values were measured on the untreated rough Z5 superstrate. We attribute this discrepancy to an overall thinner and hence less crystalline p-layer (which also acts as nucleation layer for the intrinsic layer), as Z5 has a higher ironed surface than Z5 45' or Z5 20' due to its bigger pyramidal surface features (see Tab. 2.1). The doped layers were deposited at an excitation frequency of 110 MHz with carbon dioxide (CO$_2$) in the gas mixture, based on the work of Cuony *et al.* [Cuony 10] and as described in the following section.

3.1.1 Silicon oxide doped layers

Silicon sub-oxide layers containing a microcrystalline phase (SiO$_x$) were introduced for doped layers by Sichanugrist *et al.* for thin-film silicon solar cells [Sichanugrist 93, Sichanugrist 94]. Intrinsic or doped SiO$_x$ is a multiphase material, whose properties can be tuned by adapted PECVD process [Cuony 12], allowing a wide range of crystalline fraction, refraction index and bandgap, making it a versatile layer to be used in efficient thin-film silicon solar cells [Lambertz 13]. SiO$_x$ can hence be used as an intermediate reflector in tandem solar cells [Buehlmann 07, Lambertz 11], benefiting from a low refraction-index and low lateral conductivity which prevents the interconnection of shunt paths, thanks to its multiphase

nature. This multiphase nature, composed of microcrystalline filaments embedded in an amorphous SiO_x matrix, is key to obtaining efficient shunt-quenching layers, thanks to anisotropic lateral and transverse conductivity [Despeisse 10, Cuony 11, Despeisse 11, Cuony 12]. SiO_x can also be efficiently implemented as a p-doped layer in $n–i–p$ amorphous silicon (a-Si:H) solar cells to enhance their open-circuit voltage (V_{oc}), due to the reduction of recombination at the $i–p$ interface as a consequence of the conduction band offset in this region [Biron 11, Biron 12]. In $p–i–n$ solar cells, an increased EQE can be obtained in the blue part of the spectrum, and a higher resilience to rougher superstrate morphologies has been demonstrated, when SiO_x layers are implemented as p-doped and n-doped layers [Veneri 10, Cuony 10].

Fig. 3.2 shows a bright-field transmission electron microscopy (TEM) cross-sectional picture of the $p–i$ interface of a single-junction μc-Si:H solar cell, such as obtained with the optimization step previously described. Although the R_c of such optimized p-doped SiO_x is relatively low (~30%), a good nucleation of the intrinsic μc-Si:H absorber layer can be obtained, leading to a thin incubation layer, as indicated by the white circle in Fig. 3.2, in good agreement with previous studies [Bailat 04].
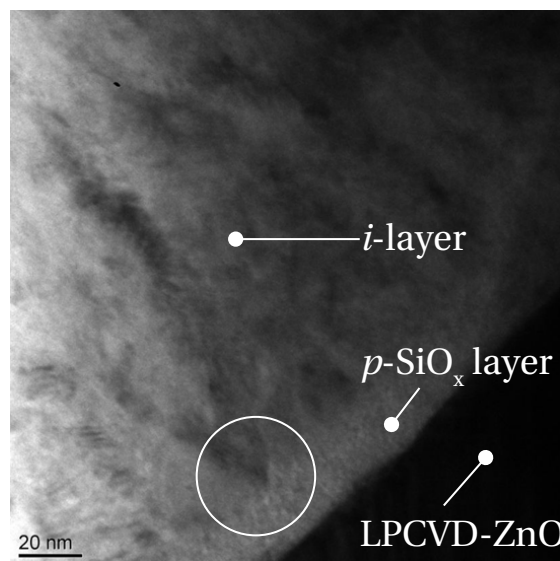
Figure 3.2: *Bright-field TEM picture of the nucleation phase of the intrinsic layer on a p-doped SiO_x layer.*

3.2 Effects of crystalline volume fraction and doped-layers design

After the first optimization step described in Sec. 3.1, single-junction μc-Si:H solar cells with R_c~50% (referred to as standard) as well as cells with higher R_c~65–70% were deposited on LPCVD-ZnO superstrates with varying roughness (Z5, Z5 20' and Z5 60', the latter being the smoothest surface), at a temperature of 180 °C. The thickness of the intrinsic

absorber layer was $1.8 \pm 0.1\,\mu m$, with two different designs for the doped layers: either p-μc-Si:H/i-μc-Si:H/n-μc-Si:H (μc-Si design), or p-SiO$_x$/i-μc-Si:H/n-SiO$_x$/n-μc-Si:H (SiO$_x$ design). The cells were annealed for 1.5 h at 180 °C in nitrogen atmosphere before degradation and were then stored in dark, ambient atmosphere after characterization. A sketch of the configurations can be found in Fig. 3.3.
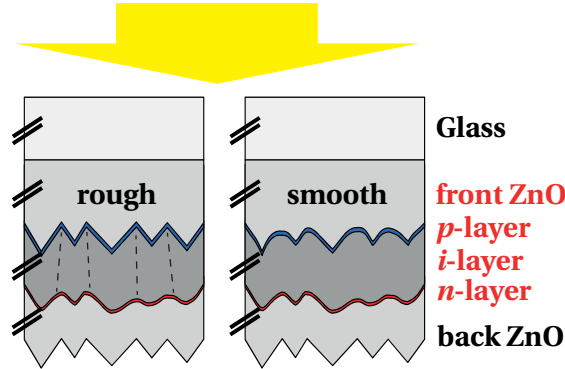
Figure 3.3: *Sketch of the configurations used to evaluate the impact of the doped layers and absorber-layer R_c upon ambient storage. The varied parameters are labeled in red. Devices deposited on rough (Z5) and smooth superstrates (Z5 60') are depicted. From [Hänni 11].*

Fig. 3.4 (a) shows the influence of long ambient storage (4m = 4 months), in the dark, on the V_{oc} of non-encapsulated cells.
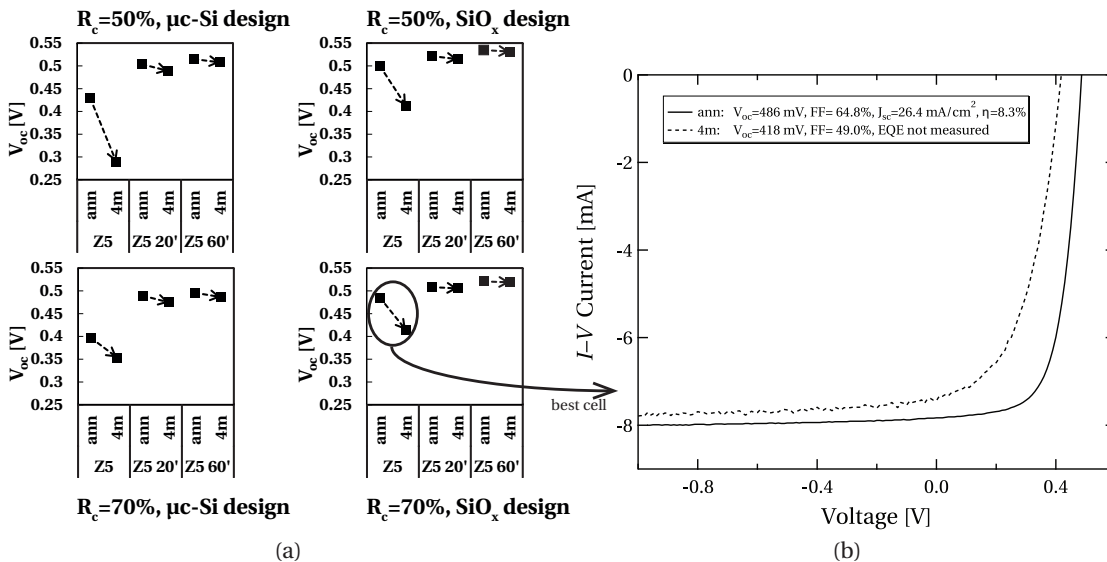
Figure 3.4: *V_{oc} losses between the annealed state (ann) and four months' ambient storage in the dark (4m) for different surface treatments of the front ZnO, two doped-layers designs and for high and low R_c (average values of the eight best cells) (a) and example of an I–V curve (not normalized with EQE J_{sc}) of a cell after dark degradation (best cell of degradation series marked by the arrow) (b). From [Hänni 11].*

The Ar plasma treatment of the superstrates improves V_{oc} in all configurations, linked to a reduction of porous zones, which are detrimental for cell performance [Python 08]. For both standard and high R_c, the use of SiO_x doped layers drastically improves the V_{oc}, particularly on the rougher superstrates, as previously demonstrated in [Cuony 10]. A similar trend can be observed for *FF* (not shown) and similar high efficiencies up to 9.4% (standard R_c) and 9.5% (high R_c) are obtained for both R_c values on Z5 60' with the SiO_x design.

Very stable V_{oc} values are achieved for solar cells deposited on Z5 60', and only limited degradation is observed for solar cells deposited on Z5 20'. However, for cells deposited on a superstrate with no surface treatment (Z5), a strong decrease in V_{oc} is observed in all cases after four months' storage. As an example, an *I–V* curve of the best cell with the high R_c and SiO_x doped-layers design is shown in Fig. 3.4 (b). For that cell, EQE after four months' storage was not measured, and the curves are thus shown as raw data, without normalization with J_{sc} calculated with the EQE.

We attribute this overall performance decrease—which we call dark degradation (DD)—to post-deposition oxidation of the porous zones present in solar cells grown on Z5. The decrease in V_{oc} is most clearly seen in the worst case, corresponding here to the standard R_c and μc-Si:H doped-layers design, where the V_{oc} decreases from an average value of 429 mV to only 290 mV after four months of DD. The smallest decrease is observed in the case of the high R_c and μc-Si:H doped-layers design, but the average V_{oc} value after four months of DD is very low (354 mV) as well. With the SiO_x design, the average V_{oc} value after four months of DD is higher (around 410 mV for both R_c values).

In [Bugnon 13], it is shown that SiO_x doped layers can improve the resilience of μc-Si:H solar cells to DD, attributed to a possible role of being a barrier to moisture [Taira 03] and to quenching the negative effects of such porous zones, due to higher lateral resistivity [Despeisse 10]. In our case, we see that DD is indeed slightly mitigated on Z5 20' and Z5 60'. Conversely, on Z5, DD seems to be independent of the doped-layers design, as the lowest DD is observed for cells with the μc-Si:H doped-layers design and high R_c. Importantly, the values after four months' DD presented here should not be considered as stabilized. Indeed, as shown in [Bronneberg 11], post-deposition oxidation of μc-Si:H layers is two-fold, with different kinetics, as assessed by Fourier-transform infrared spectroscopy (FTIR): one part consists of the oxidation of the crystalline grain boundaries' surface [Smets 08a] over a relatively brief timescale (< 60 days), and the other part concerns the amorphous material, especially when material with a high density of nanovoids is used, on a longer timescale (>100 days).

We believe however that the detrimental effects of DD on solar cells can be mitigated by SiO_x doped layers, following the quenching hypothesis of Despeisse *et al.* [Despeisse 10, Despeisse 11]. We also believe that the density of porous zones is not affect by the R_c values in our case, as shown by Python [Python 09b] for R_c values up to 70%. As our high R_c corresponds here to a value of 70%, we think that there is still enough *a*-Si:H for the passivation of the

crystalline grain boundaries (validated by V_{oc} values above 500 mV and the absence of narrow high stretching modes in the FTIR spectra of our absorber layers), and that this a-Si:H does not degrade on the short timeframe of four months presented here (validated by the stability of the solar cells on a smooth superstrate). This is not necessary true anymore for higher R_c above 80%, even for our best μc-Si:H layers, as we will show in Chap. 6.

The kinetics of the degradation of porous zones also needs further investigation. The damp-heat test (exposure of the solar cells to heat and high humidity [Cuony 11]) is a fast method to obtain information on the stability of solar cells, but is too harsh to provide insights into the kinetics of the degradation of such porous zones. Water vapor in-diffusion in porous zones induced by the texture is here proposed as the cause of post-deposition oxidation in our μc-Si:H solar cells, in accordance with several other studies [Sendova-Vassileva 05, Sendova-Vassileva 06, Boccard 11, Cuony 11]. This effect was also observed by Bugnon *et al.* [Bugnon 13] via damp-heat tests, where the porous zones induced by superstrate roughness or the PECVD process played a crucial role in the DD of μc-Si:H solar cells.

3.3 Effect of increased superstrate roughness

As shown in the previous section, the superstrate roughness can induce negative effects on solar cell efficiency during storage. To identify the effect of increasing pyramid size on this performance deterioration, more particularly the degradation kinetics during the first days of degradation, an innovative set of superstrates was studied. It was composed of non-intentionally-doped LPCVD-ZnO (Znid) of various thicknesses, on top of high-mobility sputtered indium oxide [Koida 07, Koida 10b] (In_2O_3:H, referred to as IOH) layers on glass.

3.3.1 Preparation of an innovative superstrate to study the effect of increasing superstrate roughness

The R_{sq} of LPCVD-ZnO has a strong dependence on its thickness [Faÿ 07]. Hence, to analyze the influence of variable pyramid sizes (including very small pyramids), the front electrode has to be adapted to have sufficiently low R_{sq}. A possibility to reduce R_{sq} while keeping high transparency is a multilayer approach [Ding 12b, Ding 12c]. We used an approach consisting of stacked layers with different R_{sq} to obtain total R_{sq} values around $10\,\Omega/_{sq}$. This method is justified by a very simple approximation of an in-plane resistive network put in parallel, in which high resistance of one plane can be canceled out by the lower resistance of another plane. This combination allows for the realization of front electrodes with various surface features sizes but of almost identical sheet resistance. Based on the work of Battaglia *et al.* [Battaglia 11a, Battaglia 11c], a flat highly transparent IOH film was deposited as a first layer with a thickness of 210 nm leading to a R_{sq} value of $15\,\Omega/_{sq}$. Znid—to keep the transparency high—with varying thickness was then deposited on top of the IOH layer. When using these bilayers as the superstrate for μc-Si:H solar cells, peeling of the solar cells was observed during

the lift-off of the back electrode. Furthermore, for the lowest Znid thicknesses, R_{sq} was still slightly too high.

Before the deposition of the Znid films with varying thickness and surface pyramid sizes, a 500-nm-thick doped LPCVD-ZnO layer (with $(B_2H_6/DEZ)=0.65$, Z2 recipe) was deposited on top of the IOH layer and subsequently treated for 20' with an Ar plasma treatment for flattening, reducing its thickness to about 300 nm. A SEM picture of this very smooth IOH/ZnO combination, as well as of the complete device structure, can be seen in Fig. 3.5.
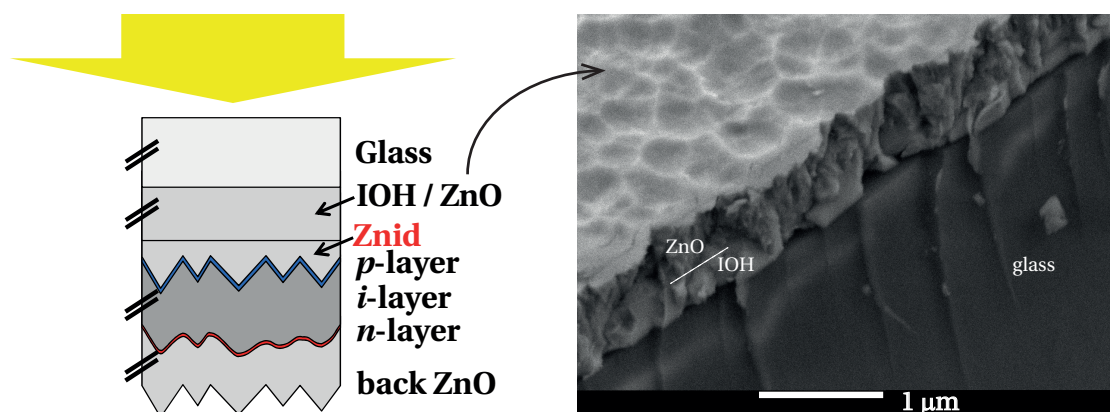
Figure 3.5: *Sketch of a cell using a IOH/ZnO/Znid stack as the front electrode and a SEM picture of the building block of this stack (IOH/ZnO). Znid of increasing thickness (and thus with associated increasing pyramid size) is then deposited on top of this IOH/ZnO combination. From [Hänni 11].*

Fig. 3.6 shows the sheet resistance of Znid deposited with increasing thickness (and hence surface pyramid sizes) on glass and on the IOH/ZnO bilayer. The thickness of the Znid refers to the thickness measurement on glass.

Whereas Znid on glass is too resistive for μc-Si:H solar cells, especially for low thicknesses, R_{sq} of the stacked layers becomes remarkably low (about 10–13 $\Omega/_{sq}$ before cell deposition, comparable to that of the Z5 60' (8 $\Omega/_{sq}$), and corresponding to typical initial open-circuit resistance (R_{oc}) in the cell of 2–2.8 Ω cm^2).

3.3.2 Effect of increasing superstrate roughness on μc-Si:H solar cells

Single-junction μc-Si:H solar cells were then deposited on these stacks, shown in SEM images in Fig. 3.7, with variable pyramid sizes going from almost flat for the lowest thickness to very rough for the Znid with a thickness of 2220 nm.

The deposition conditions were similar to those of the cells shown in Sec. 3.2, except the absorber layer thickness was decreased to 1.6 µm and the deposition temperature was increased to 200 °C. The SiO$_x$ doped-layers design was used. Due to space limitations in the
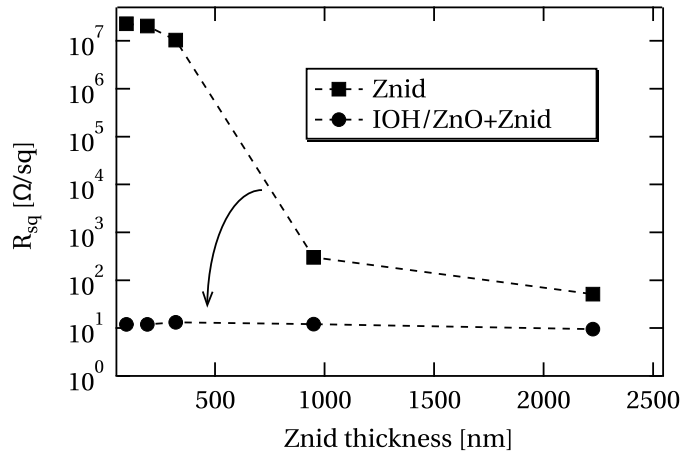
Figure 3.6: *R_{sq} as a function of the Znid thickness, in the case of Znid only (squares) and (IOH/ZnO)+Znid stack (circles). This figure demonstrates the reduction of R_{sq} with the stack versus the Znid layer only, particularly for low thicknesses. From [Hänni 11].*
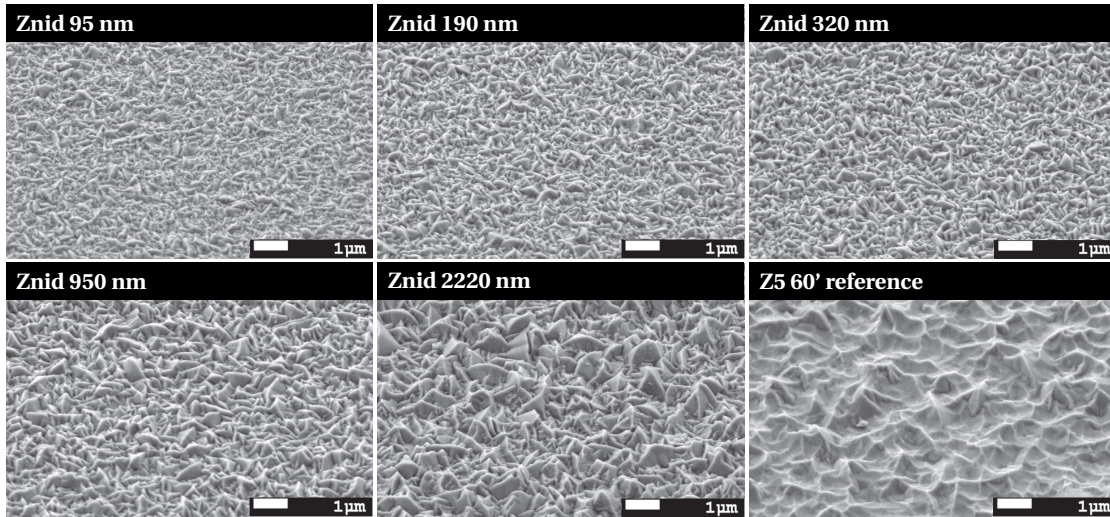
Figure 3.7: *SEM pictures of Znid layers of varying thickness deposited on very smooth IOH/ZnO. The indicated thickness refers to the measurement of the Znid thickness deposited directly on glass. From [Hänni 11].*

sample holder, the depostions were performed in two runs and each run contained a Z5 60' reference. The overall R_c yielded $55 \pm 7\%$ for all cells (n-side) and $40 \pm 2\%$ (p-side), except for the reference cells on Z5 60', which were slightly more crystalline (55% on both sides).

Single-junction μc-Si:H solar cells were also deposited on the same series of superstrates in the KAI-M system, using a regime developed by G. Bugnon *et al.*, at an excitation frequency of 13 MHz, a pressure of 9 mbar, and a deposition rate of 3 Å/s for the absorber layer [Bugnon 13]. Even though these cells were slightly thinner ($1.45\pm0.05\,\mu$m), we assume that the comparison with the 1.6-µm-thick solar cells deposited in SysB is still fair. Finally, a 5-µm-thick back

electrode (Z5) was used for all cells. After characterization in the initial as-deposited state, the cells were annealed at 180 °C in an inert atmosphere, and stored in dark ambient atmosphere for several days, without encapsulation, to study their DD.

Fig. 3.8 presents the electrical-performance evolution upon ambient storage time, based on the average of the eight best cells of each substrate at each stage (ini=as deposited, ann= annealed, n days=after n days' storage in dark ambient conditions).
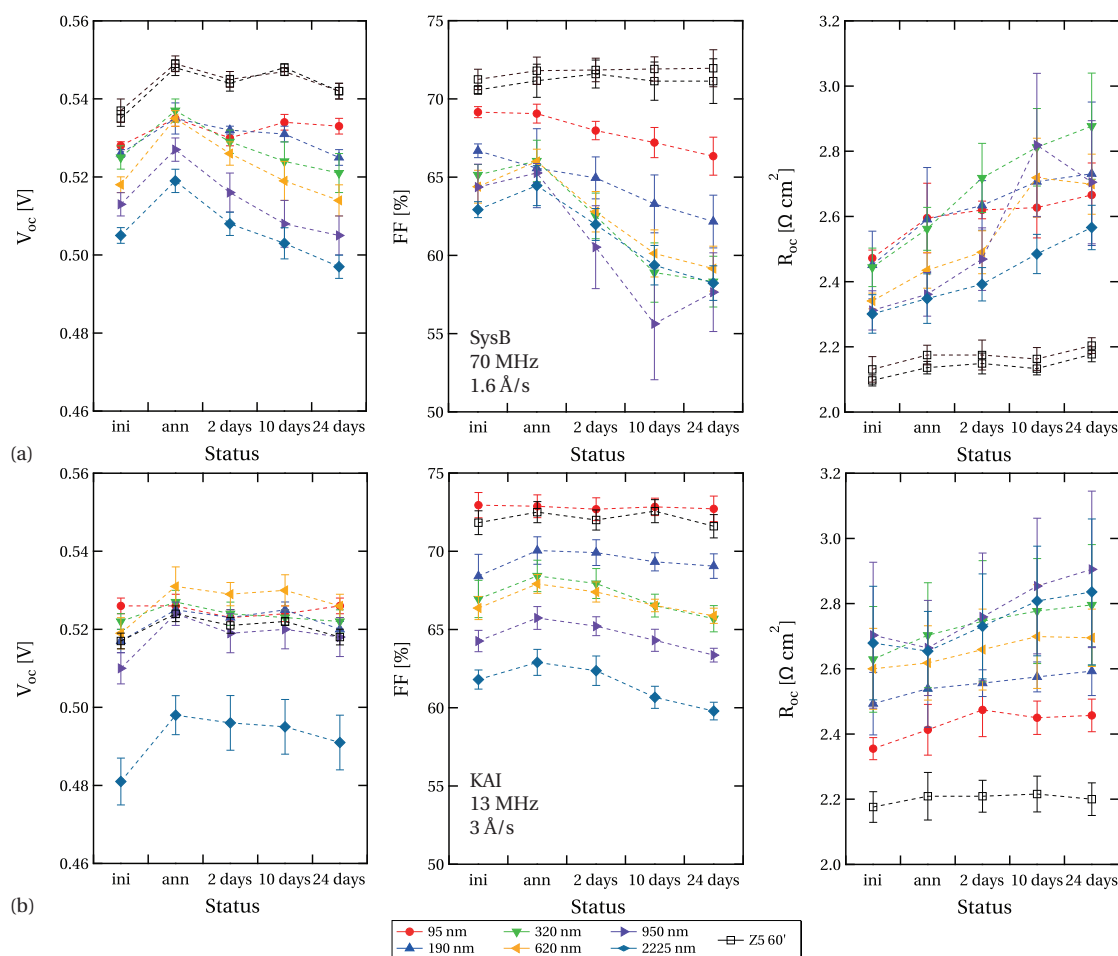
Figure 3.8: *Evolution of electrical parameters during DD for single-junction μc-Si:H solar cells with front electrodes composed of various thicknesses of Znid on top of an IOH/ZnO stack. The upper graphs (a) are for the cells deposited in SysB at low pressure and high frequency and the lower graphs (b) show the results for the high-pressure/high-depletion regime of KAI-M. From [Hänni 11].*

First, for the cells deposited in SysB at 70 MHz (part (a)), we observe decreasing as-deposited values (ini) of V_{oc}, *FF* and R_{oc} when going from very small to large pyramids, related to the presence of an increased density of porous zones on the V-shaped pyramids, as also discussed in the previous section. Note that for the SysB cells two reference cells deposited on Z5 60'

are shown, corresponding to the two PECVD deposition runs of silicon layers. We observe that small surface features as achieved for Znid thicknesses up to 320 nm lead to V_{oc} values only slightly below the Z5 60' reference values. *FF* drops very rapidly with increasing pyramid size and begins to decrease for the smallest Znid thickness, with an average value of 69.2%, as compared to the average value of 70.9% for cells deposited on the Z5 60' references. This *FF* drop is well correlated with an increase of R_{oc}. After annealing (ann), an increase in V_{oc} and *FF* is observed for all cells, which is the subject of Chap. 4.

When no Ar surface treatment is applied (which is the case for all cells except the reference), a general decrease in V_{oc} and *FF* is observed upon ambient storage, attributed to DD, which increases with Znid thickness (i.e. pyramid size). Even the smallest Znid thickness, leading to small but sharp surface features, is enough to allow this V_{oc} and *FF* loss to take place, attributed to the creation of porous zones. The results of Fig. 3.8 (a) demonstrate that stable cells can be obtained with a smooth superstrate, indicating that an appropriate superstrate with low associated crack density enhances the stability of our μc-Si:H solar cells upon non-encapsulated storage. It must also be noted that the process was optimized for smooth superstrates, especially the thickness of the p-doped layer, which was reduced as much as possible to reduce parasitic absorption.

The second series, deposited on the same superstrates but under a high-pressure/high-depletion regime (13 MHz, 9 mbar, 3 Å/s) and illustrated in Fig. 3.8 (b), shows a different behavior. Although the initial V_{oc} values are slightly lower than the 70-MHz series, the impact of increasing superstrate roughness is much smaller. Up to a Znid thickness of 950 nm, the initial values for V_{oc} remain very close to one another, at around 520 mV in the initial state and at around 530 mV after annealing. Moreover, these cells show a much higher stability to DD on all superstrates. The *FF* drop with increased roughness takes place at higher thickness of Znid (*i.e.* roughness), here up to 190 nm.

These results corroborate the model presented by G. Bugnon [Bugnon 13] in which denser material can be obtained on highly textured superstrates with the high-pressure/high-depletion regime at 13.56 MHz for low deposition rates such as the one used throughout this thesis. The higher resilience to superstrate roughness is therefore also linked to the deposition regime, which to some extent hinders the creation of porous defective zones at low deposition rates on textured superstrates. We will show in the following section that these porous zones form an interconnected network, acting as probable diffusion paths for impurity ingression.

3.4   3-D reconstruction of the microstructure of μc-Si:H solar cells

A solar cell was deposited on an as-grown rough superstrate (Z5) and was investigated with focused ion beam (FIB) "slice and view" tomography [Cantoni 10] in order to further investigate the μc-Si:H microstructure on such a challenging superstrate and more particularly the creation of porous zones. By first milling to obtain a smooth cross section of the sample

with a FIB column, then imaging the milled face with a SEM column, and after successively FIB milling in steps of some nm followed each time by SEM imaging, a 3-D data set of stacked SEM pictures was created. A voxel size (*i.e.* 3-D pixel size) of $7 \times 7 \times 7$ nm was used, recording the SEM images using an in-lens backscattered electron detector that gives mass contrast for the different layers (voids as dark regions), and grain contrast in the ZnO, as seen in Fig. 3.9. The same procedure was applied to a cell deposited on a smooth Z5 45' front electrode as a reference for dense μc-Si:H. Note that both solar cells, with 1.2-µm-thick absorber layers, were co-deposited using the optimized recipe of SysB, with SiO$_x$ p-doped layers. When considering
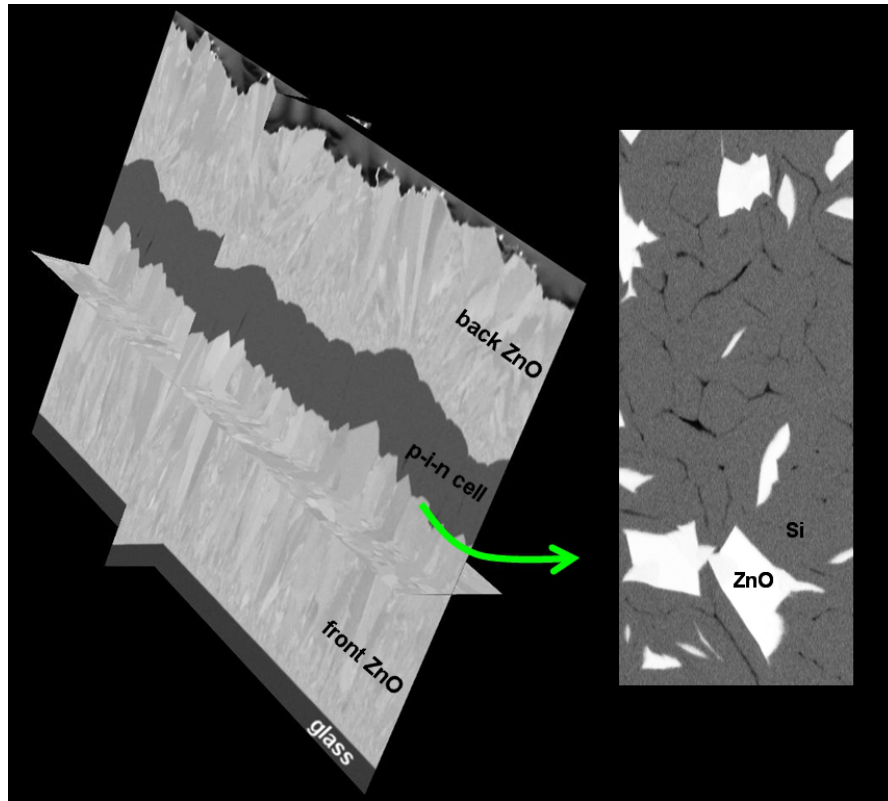
Figure 3.9: *FIB tomography of a μc-Si:H solar cell. A top view of the growth front in the reconstructed image at the ZnO–Si interface (planar cut at the level of the arrow, along the growth direction) reveals the 2-D porous network (black) in dense silicon (grey). The white areas are the top of the front ZnO pyramids. From [Hänni 13a].*

a planar cut in the 3-D data set at the Z5–Si interface (arrow in Fig. 3.9), perpendicular to the i-layer growth direction, the 2-D network formed by the porous material can be directly seen. Porous material develops in the bottom of the valleys and appears as dark zones within the silicon absorber layer.

Pseudo-color tomograms in Fig. 3.10 reveal the microstructure of cells co-deposited on the rough superstrate (Z5) and on smooth Z5 45' (current optimum superstrate). As expected from the standard 1-D image, a continuous network of porous zones is formed (bright orange) following the bottom of the valleys formed by the sharp ZnO pyramids. On Z5, this network is

present throughout the absorber layer, whereas on Z5 45' the porous zones are much smaller and do not form a continuous network, but are rather limited to a few zones of the upper part of the absorber layer.
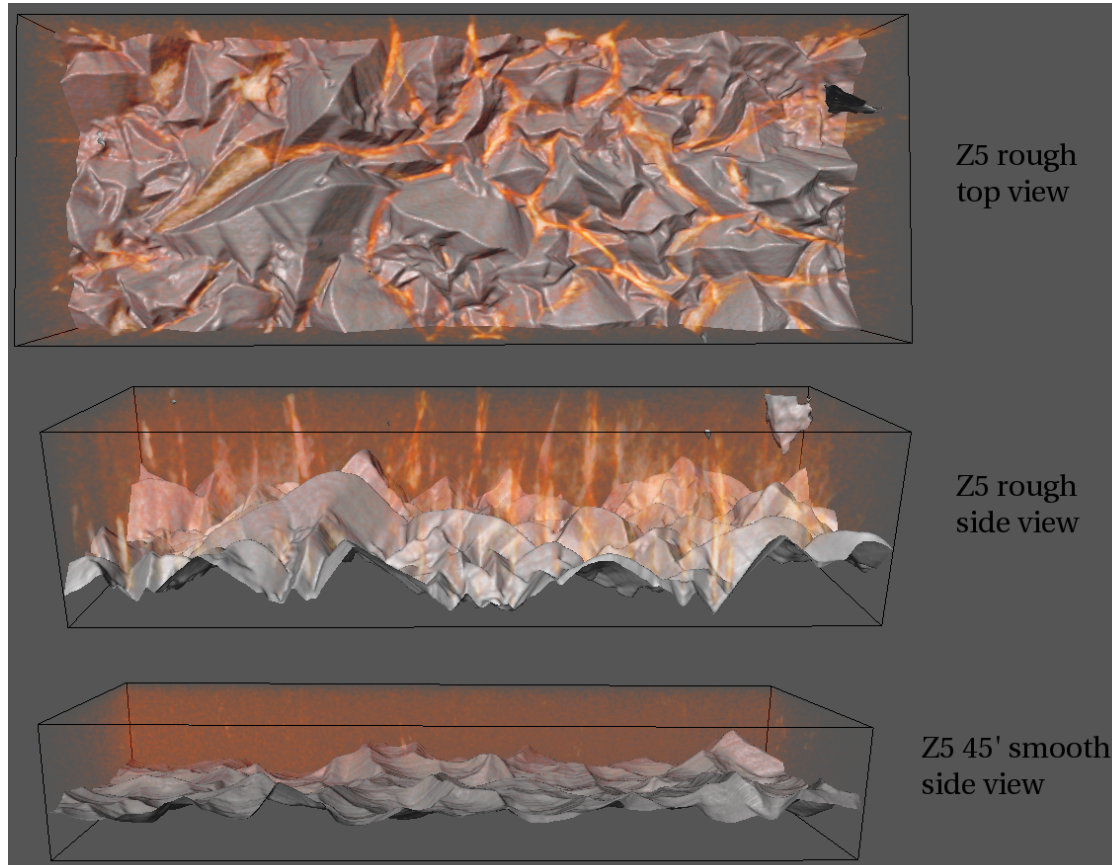
Figure 3.10: *Pseudo-color tomograms of the reconstructed network of porous zones (bright orange) in cells deposited on rough (Z5) and smooth (Z5 45') superstrates. From [Hänni 13a].*

Tomography thus provides additional insights into details of the μc-Si:H microstructure, and more particularly validates that when porous zones are present in solar cells deposited on rough LPCVD-ZnO, they form a continuous interconnected network. A high resilience to challenging superstrate morphologies is of paramount importance when developing multi-junction devices, as additional phenomena such as pinching (the creation of an increased surface sharpness by the top cell grown by PECVD) can significantly change the properties of the μc-Si:H bottom cell [Cuony 10]. In that view, 3-D tomography reveals the location of potential pinching points related to the growth of thin-film silicon (see Fig. 3.11). Indeed, these pinching points induced by the PECVD process are a limiting factor for multi-junction devices using μc-Si:H bottom (or middle) cells and methods such as valley-filling [Boccard 13] are a possible solution to reduce their impact on cell performance.

Tomographic reconstruction of complete solar cells thus opens new perspectives for detailed
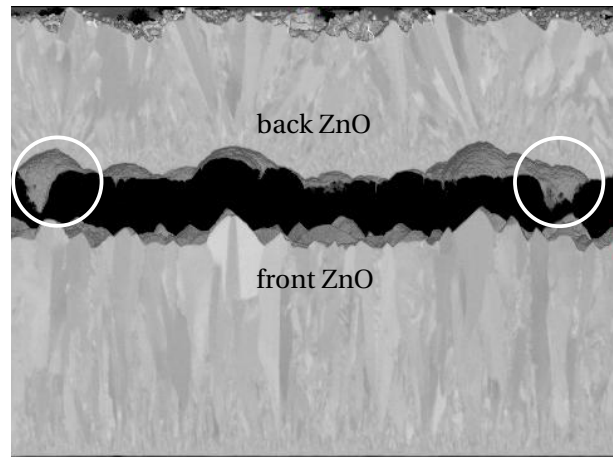
Figure 3.11: *Tomographic 3-D reconstruction of a single-junction μc-Si solar cell deposited on a rough Z5 superstrate, where the silicon layer was filtered out. The potential pinching points (in case an additional cell would be grown on top of the silicon layers, such as in the triple-cell configuration) can be seen in the white circles, here filled with the ZnO back electrode. From [Hänni 13a].*

analysis of the effect of superstrate features on the growth of μc-Si:H, even if it is too time intensive for routine diagnostics or high sample throughput analysis for materials development. This 3-D reconstruction could also be used as input data for 3-D growth models for thin-film solar cells. Nowadays, such growth models normally use data from atomic force microscopy pictures as growth template for solar cells to determine the morphological evolution and the conformality of the growth [Jovanov 13a, Jovanov 13b, Sever 13]. Our 3-D reconstruction offers the advantage to simultaneously provide information (in the same device) on the superstrate texture, its impact on the microstructure of the solar cell and the conformality of the PECVD growth.

3.5 World-record device

Tab. 3.1 presents a summary of the best electrical performances obtained so far for cells combining our current optimal superstrate texture (Z5 45'), the use of SiO_x doped layers and an adapted i-layer process to guarantee an optimal trade-off between optical and electrical performance. Through this careful optimization of the i-layer and of the cell design, state-of-the-art cells with efficiencies above 10% have routinely been obtained in several PECVD systems, both in small-area research systems (this thesis) and in large-area R&D KAI-M systems [Bugnon 13] at various excitation frequencies.

Fig. 3.12 shows a series of μc-Si:H cells, with various i-layer thicknesses, on Z5 45', using the optimized recipe of Sec. 3.1. The absorber-layer thickness was varied between 1 μm and 3.3 μm (typical range of bottom-cell thicknesses used in tandem solar cells), while the other layers were kept constant. $R_c = 57 \pm 5\%$ for all cells. Remarkable conversion efficiencies between 9.5%

Table 3.1: *Best results obtained for 2-µm-thick µc-Si:H solar cells deposited at PV-Lab. All cells have $R_c \geq 55\%$. A conversion efficiency of 10.9% was obtained in two different deposition systems.*

Area $[\text{cm}^2]$	V_{oc} [mV]	J_{sc} $[\text{mA/cm}^2]$	FF [%]	η [%]	Thickness [µm]	Front	Back	Ref.
0.25	535	27.5	74.2	10.9	2.0	Z5 45'	Z2.3	[Bugnon 12]
0.25	545	26.6	74.9	10.9	2.0	Z5 45'	Z5	[Hänni 13a]
1	541	27.0	71.3	10.4	2.0	Z5 45'	Z5	[Hänni 13a]

and 10.5% are obtained, with however no clear performance gain with cell thickness. Indeed, the loss of V_{oc} and FF observed for increased thickness is compensated by higher J_{sc} values. Improved V_{oc} and FF are obtained with a specific post-deposition treatement (hydrogen plasma), indicated by the "pH2"-values in Fig. 3.12 . The effect of this post-deposition treatment is detailed in Chap. 4.
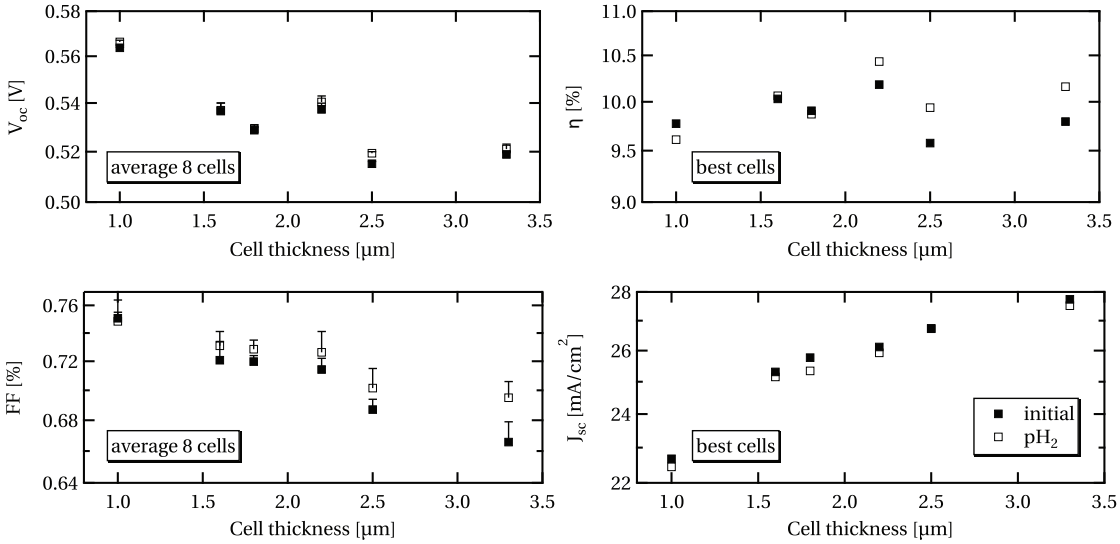
Figure 3.12: *Properties of solar cells deposited on smooth Z5 45' in the initial state (solid squares) and after hydrogen plasma post-deposition treatment (empty squares), as a function of the cell thickness. For V_{oc} and FF, the values of the eight best cells on each superstrate are given (ranked by $V_{oc} \times FF$). For J_{sc} and η, only the best cells are shown. From [Hänni 13a].*

Following further dedicated design and layer optimization, a world-record conversion efficiency was achieved for single-junction μc-Si:H solar cells, with a value of 10.69%, independently confirmed at ISE CalLab PV Cells, and reported in [Green 13b]. These record cells are 1.8-µm-thick, with R_c=57 ± 5%, and were co-deposited in the small-area SysB. They also contain a 1.4-nm-thick (evaluated with the deposition rate from a 100-nm-thick layer) intrinsic SiO_x buffer layer between the p-doped SiO_x layer and the intrinsic μc-Si:H absorber layer. Such buffer layer promotes the nucleation of μc-Si:H layers, and probably limits boron

cross contamination from the *p*-doped layer into the absorber layer [Bugnon 14].

Performance of this cell, as measured at PV-lab and ISE CalLab PV Cells, together with the measurements performed at ISE on two other cells, is reported in Tab. 3.2. The excellent

Table 3.2: *Electrical parameters of record cells, independently confirmed by ISE CalLab PV Cells. (da) means designated area. From [Hänni 13b].*

Sample	Area (da) $\left[\text{cm}^2\right]$	V_{oc} [mV]	J_{sc} $[\text{mA/cm}^2]$	*FF* [%]	η [%]
D2	1.0437 ± 0.0032	549.0 ± 2.7	26.55 ± 0.67	73.31 ± 0.73	10.69 ± 0.32
D5	1.0419 ± 0.0065	546.1 ± 2.7	26.61 ± 0.69	73.49 ± 0.73	10.68 ± 0.33
D5 (IMT meas)	1.043	551	26.1	73.8	10.61
C2	1.0437 ± 0.0032	548.8 ± 2.7	26.40 ± 0.67	73.24 ± 0.73	10.61 ± 0.32

agreement obtained for sample D5 between the certified and in-house values validates our measurement procedure. Details about the internal measurement of these cells are given in Appendix A.

The certified *I–V* and EQE curves of cell *D*2 are presented in Fig. 3.13 and 3.14. The latter is normalized to the measured current density. Note that an anti-reflective texture was applied on the glass side [Escarré 12b], boosting the current density to a high value of 26.55 mA/cm^2.
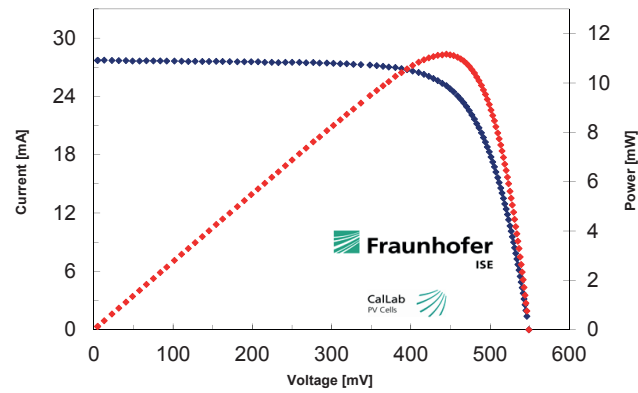
Figure 3.13: *Certified I–V curve of cell D2. From [Hänni 13b].*
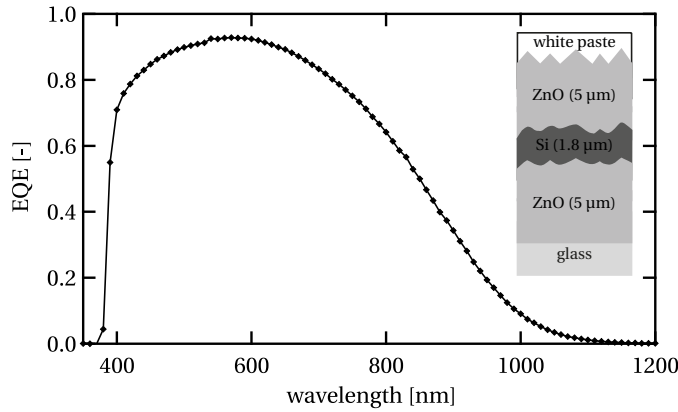
Figure 3.14: *Certified EQE of cell D2, normalized to a measured J_{sc} of 26.55 mA/cm^2, together with a sketch of the cell structure. The anti-reflection texture is not drawn. From [Hänni 13b].*

As compared to the previous record of Kaneka [Yamamoto 99b, Green 13a], these cells have a significantly lower *FF* (between 73.3 and 73.5% in our case, as compared to the previous value of 76.6%). This difference might partially be explained by the absence of metallic front or back electrodes (or grids), leading to higher resistive losses. Indeed, we obtained *FF* values around 75% (for same cell thickness) for smaller cells (0.25 cm^2) with a similar manufacturing process, due to lowered impact of R_{sq} with reduced cell surface. Higher efficiencies can thus still be expected if a clever metallization is introduced in the electrodes, with an optimal trade-off between shadowing and resistive losses in the electrodes. Note that if our result remains the best efficiency in *p–i–n* configuration, a higher efficiency value has recently been reported by Sai *et al.* in *n–i–p* configuration, on honeycomb textures, with a certified conversion efficiency of 10.8% [Green 14a].

The stability of these record cells under light soaking has not been investigated. We however light-soaked a non-encapsulated cell with similar performance, as reported in Tab. 3.3.

Table 3.3: *Performance of a 1.8-µm-thick single-junction µc-Si:H solar cell, in the initial state and after 1050 h of light soaking under standard conditions (50°C, 1-sun illumination, for more than 1000 h). The cell is not encapsulated and has a laser-scribed area of 0.996 cm^2.*

State	V_{oc} [mV]	J_{sc}(IV) [mA/cm^2]	*FF* [%]	η [%]
ini	539	25.0	70.0	9.4
light soaked for 1050 h	531	24.6	70.8	9.2
relative change [%]	-1.5	-1.7	+1.1	-2.1

A low degradation of 2% is observed, indicating a very stable µc-Si:H material. The highest degradation occurs in J_{sc}, and at least part of it is attributed to an increased free-carrier absorption of the front electrode, due to exposure to ultraviolet light during light-soaking [Ding 13a]. As reported by Yan *et al.* [Yan 04a], light-induced degradation in µc-Si:H solar cells

occurs in the amorphous matrix of the absorber layer. Hence, when used in a multi-junction device, no light-induced degradation is expected in the μc-Si:H bottom cell, as the light that would contribute to generation in the amorphous phase is mostly absorbed by the a-Si:H top cell.

3.6 Conclusion

We have demonstrated the importance of both the cell design and the absorber layer quality and microstructure to reach high-efficiency μc-Si:H solar cells. The role of porous zones which can appear for cells deposited on rough superstrates, in the dark degradation of μc-Si:H solar cells was discussed.

Although being inappropriate for routine diagnostics, 3-D tomography appears as an innovative and valuable technique to further probe details of the microstructure of μc-Si:H, directly revealing the interconnected network of the porous zones within the absorber layer. We showed that even minimal superstrate roughness, below that commonly used in light-trapping structures, as induced by thin LPCVD-ZnO layers, can cause a V_{oc} drop in single-junction μc-Si:H solar cells within a few days in ambient conditions. However, by selecting:

- appropriate superstrate, with smooth morphology allowing for the growth of high-quality μc-Si:H,

- appropriate cell design, with *e.g.* SiO$_x$ doped layers, and

- appropriate deposition conditions, such as a high-pressure/high-depletion regime,

a very high stability in ambient storage can be achieved even without encapsulation.

All these developments permitted us to reach a certified world-record efficiency for single-junction μc-Si:H solar cells with a conversion efficiency of 10.69%, independently confirmed at ISE CalLab PV Cells. Recently, this record value was overcome by a 10.8% efficiency, as achieved in the n–i–p configuration [Green 13b].[1] Still, we are confident that efficiencies above 11% for single-junction μc-Si:H solar cells can be expected in the very near future. Since smooth front electrodes are usually required to avoid the formation of porous zones within the silicon absorber layer, structures with (i) tunable aspect-ratios [Sai 12], (ii) replication or nanomoulding of dedicated morphologies [Battaglia 11b] or (iii) smoother as-grown ZnO layers [Nicolay 12] should enable higher electrical performances. These recent single-junction μc-Si:H record efficiencies, together with record tandem [Boccard 12d] and triple-junction solar cells [Kim 13] clearly support the potential of thin-film silicon multi-junction devices in reaching conversion efficiencies above 15%, with a minimal usage of abundant and non-toxic raw materials at low costs.

---

[1] improved to 11.0% by H. Sai *et al.*, 40th IEEE Photovoltaic Specialists Conference, Denver, Colorado, United States, June 8–13, 2014 (see also [Green 14b])

4 Post-deposition treatments of solar cells

In this chapter, we show how the performance of state-of-the-art thin-film microcrystalline-silicon (μc-Si:H) solar cells in the p–i–n configuration can be improved by a simple post-deposition treatment, especially when the cells are deposited on a rough zinc oxide (ZnO) superstrate. In particular, we investigate the effect of applying a hydrogen plasma treatment on finished non-encapsulated cells and decouple it from the annealing taking place simultaneously.

It is shown that although exposure of complete cells to a hydrogen plasma lowers the sheet resistance (R_{sq}) of the ZnO back electrode, annealing in vacuum is sufficient to induce large improvement in cell performance, with gain in open-circuit voltage (V_{oc}) and fill factor (*FF*) up to 30 mV and 4% (absolute), respectively.

We demonstrate that these gains are linked to the curing of intrinsic defects in the silicon absorber layer, which may appear during the deposition of the ZnO back electrode, as well as to an improvement in the conductivity of the ZnO back electrode, occurring during such a treatment. When the treatment is applied to tandem cells, the observed gains remain stable upon light soaking.

This curing of the porous zones is related to a reduction of the absorption coefficient at 0.8 eV, as observed by Fourier-transform photocurrent spectroscopy (FTPS), implying that defects in the porous zones are not limited to pure 2-D surfaces in the absorber layer, but can be considered as having a spatial extension in the absorber layer.

Except for the introductory part which is partly published in [Hänni 13a], the results presented in this chapter are not published. The second part is currently under a patent application and should be published later.

4.1 Introduction and motivation

μc-Si:H is usually considered as rather stable with respect to light-induced degradation as compared to amorphous silicon (a-Si:H), especially when used as bottom cell in a multi-junction device [Meier 94, Yamamoto 99b, Yan 04a, Meillaud 08, Guha 13]. On the other hand, it is known to be sensitive to contamination by impurities and moisture-related post-deposition oxidation [Finger 05, Matsui 06, Smets 08a, Kilper 09, Frammelsberger 10, Bronneberg 11, Boccard 11, Merdzhanova 12, Yue 12]. Indeed, even short times of storage in ambient atmosphere may induce losses in electrical performance. Nevertheless, these losses can often be minimized with an adequate deposition process for the absorber layer and recovered (at least partially) when the cells are annealed or properly encapsulated. The nanoporous phase induced by the superstrate roughness or the plasma-enhanced chemical vapor deposition (PECVD) process is a potential diffusion path for impurities [Python 10, Cuony 11]. There are very few methods available to directly probe the nature of this nanoporous phase. Advanced scanning electron microscopy, such as presented in Chap. 3, reveals the 2-D interconnected network of such defective material. The presence of porous zones has a direct impact on solar cell degradation linked to moisture ingression [Hänni 11, Bugnon 12]. Nano secondary ion mass spectrometry (Nano-SIMS) measurements show that oxygen is preferentially found in these zones, even in device-grade material [Python 10]. Advanced transmission electron microscopy demonstrates that oxygen can accumulate in such zones and is strongly correlated to the presence of ZnO, which can creep into a defective region during deposition of a ZnO electrode deposited by low-pressure chemical vapor deposition (LPCVD-ZnO) onto μc-Si:H [Duchamp 13]. This chapter demonstrates that an efficient, but indirect, way to probe the impact of these defective zones is to make full devices and submit them to various post-deposition treatments.

We first introduce a post-deposition treatment using a hydrogen plasma, which improves the electrical performance of μc-Si:H solar cells deposited on rough superstrates [Hänni 13a]. This post-deposition treatment was originally developed for LPCVD-ZnO layers deposited on glass [Ding 13b, Ding 13a]. Post-deposition treatment of ZnO, by *e.g.* ion implantation or simple annealing, is a widely investigated field as it typically leads to improved properties of ZnO [Major 84, Major 86, Minami 89, Kohiki 94, Baik 97, Lee 01, Theys 02, Ruske 10, Wimmer 12, Charpentier 13].

4.1.1 Effect of post-deposition treatments on LPCVD-ZnO

Fig. 4.1 shows the effect on R_{sq}, mobility (μ) and carrier density (N) of post-deposition treatments such as exposure to a hydrogen plasma at $200\,°C$ and annealing in vacuum at $230\,°C$ applied to our standard LPCVD-ZnO films. Before the treatment, the samples were preheated in vacuum for 20'. The number in parentheses is the ratio of the dopant gas diborane (B_2H_6) to the diethylzinc (DEZ) precursor during the deposition of LPCVD-ZnO. Z5 is a lightly doped 5-μm-thick LPVCD-ZnO typically used as the front electrode in our single-junction

μc-Si:H solar cells, Z2.3 is our standard 2.3-µm-thick front electrode for multi-junction solar cells (with the same doping as Z5) [Boccard 12b, Schüttauf 14], and Z2 is a highly doped 2-µm-thick LPCVD-ZnO which is typically used in our a-Si:H solar cells. Znid is a non-intentionally doped LPCVD-ZnO, with a thickness of 2 µm, which is usually used as a reference for LPCVD-ZnO development.
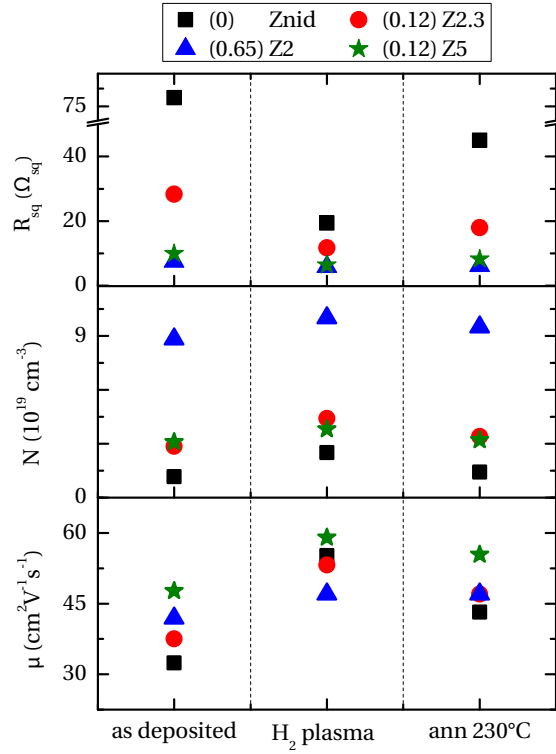
Figure 4.1: *Electrical properties of LPCVD-ZnO as deposited, after exposure to a hydrogen plasma, and after annealing in vacuum. The number in parentheses is the (B_2H_6/DEZ) ratio during deposition (courtesy of L. Ding).*

A strong increase in charge-carrier mobility and a moderate increase in carrier density are observed when applying a hydrogen plasma or annealing in vacuum, leading to a significant decrease in R_{sq}. The effect is more pronounced for Znid and lightly doped ZnO (Z5, Z2.3) and is attributed to modification in the charged trap density at the grain boundaries [Ding 13b]. A minimal treatment time of 20' is required to reach a plateau in the improved values. Although understanding of the effect of such treatments on LPCVD-ZnO is not the subject of this thesis, it will be useful to observe a few points for the following parts of the chapter: (i) Post-deposition hydrogen plasma treatment and annealing in vacuum improve the electrical properties of LPCVD-ZnO, (ii) hydrogen plasma treatment has a larger impact than annealing, and (iii) the effect of post-deposition treatments on the electrical properties of LPCVD-ZnO diminishes with increasing doping.

4.1.2 Typical effect of post-deposition treatments on *µc*-Si:H single-junction solar cells

When applying a hydrogen plasma to complete solar cells, we generally observe a reproducible improvement of up to 10 mV in V_{oc} and 1 to 2% (absolute) in *FF* for cells deposited on smooth superstrates, and up to 30 mV in V_{oc} and 4% (absolute) in *FF* for cells deposited on rough superstrates. The effect on short-circuit current density (J_{sc}) is usually small (± 0.2 mA/cm^2).

Tab. 4.1 demonstrates the typical effect on V_{oc}, the voltage at maximum-power point (V_{mpp}), *FF*, J_{sc}, the current density at maximum-power point (J_{mpp}), and the conversion efficiency (η) of a hydrogen plasma applied to complete 1.1-µm-thick *µc*-Si:H solar cells deposited on smooth (Z5 45') and rough (Z5 20') LPCVD-ZnO front electrodes.

Table 4.1: *Solar cell performance before and after a post-deposition hydrogen plasma treatment (best cell). From [Hänni 13a].*

Front	Treatment	V_{oc} [mV]	V_{mpp} [mV]	*FF* [%]	J_{sc} [mA/cm^2]	J_{mpp} [mA/cm^2]	η [%]
Z5 45'	-	552	446	73.6	23.5	21.4	9.5
	hydrogen plasma	561	459	75.4	23.7	21.8	10.0
Z5 20'	-	536	429	71.7	24.1	21.8	9.3
	hydrogen plasma	554	454	75.3	24.3	22.2	10.1

We observe a gain of 9 mV in V_{oc} and 1.8% (absolute) in *FF* for cells deposited on smooth Z5 45'. A similar trend is observed for the rougher front electrode, however with more pronounced gains of 18 mV in V_{oc} and 3.6% absolute in *FF*, as also shown in *J–V* curves in Fig. 4.2.
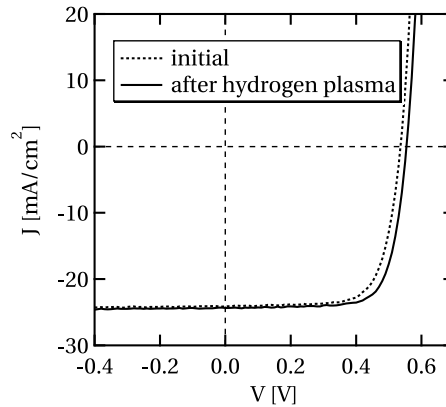
Figure 4.2: *Effect of post-deposition hydrogen plasma treatment on the J–V curve of a 1.1-µm-thick µc-Si:H solar cell (deposited on Z5 20'). From [Hänni 13a].*

Using following formula for the relative resistive losses in the back electrode for the output power (P) of a solar module at maximum-power point [Hanak 79, Battaglia 11c], where w is

the collection width of the module,

$$\frac{\Delta P}{P} = \frac{w^2 R_{sq} J_{mpp}}{3 V_{mpp}},$$

we can approximate the power losses before and after hydrogen plasma treatment for the solar cell deposited on Z5 20'. As one contact point is in the middle of the back contact, and the other one on the side of our cell (0.5 × 0.5 cm), our cell geometry corresponds approximately to a segment width of w=0.3 cm in a module configuration.

Based on the modification of Z2.3 (our standard back electrode) after hydrogen plasma treatment in Fig. 4.1, and more precisely a reduction of its R_{sq} from 28 to 12 $\Omega/_{sq}$, the resistive power loss due to the back electrode can be approximated to 4.3% (initial) and 1.8% (after hydrogen plasma treatment) respectively, so there is an absolute gain of 2.5% in relative power losses after hydrogen plasma treatment. Assuming that gain is the only source of the *FF* gain, an improvement in *FF* of 1.8% absolute is expected based on the calculation, below the true gain of 3.6% shown in Tab. 4.1. This calculation indicates that the observed increase in *FF* is related not only to a reduced R_{sq} of the back electrode, but also to an improvement in the μc-Si:H absorber layer. The same calculation can be made for the cell deposited on Z5 45', and the outcome is an expected gain in *FF* of 1.7% absolute, based on the reduced R_{sq} of the back electrode, in very good agreement with the observed gain of 1.8% absolute. Although the effect of reduced R_{sq} of the back electrode on *FF* is rather small with our cell geometry, and almost within the experimental error for the determination of *FF*, this gain has been observed consistently in many samples.

Finally, it is unlikely that the high V_{oc} gain observed with high reproducibility on rough superstrates is linked to a sole change of the electrical properties of the back electrode. Hence, the dependence on superstrate roughness suggests that post-deposition processes directly impact the μc-Si:H absorber layer.

In the following sections, we will present a detailed study of the effect of hydrogen plasma treatment versus annealing in vacuum on finished, non-encapsulated cells deposited on rough and smooth superstrates. The aim here is to discriminate between (i) the contribution of the temperature from the contribution of the hydrogen plasma and (ii) the contribution of the back electrode from the contribution of the μc-Si:H absorber layer. We will demonstrate that both the μc-Si:H absorber layer and the ZnO back electrode are affected by post-deposition treatments, and that annealing has a preponderant role on the improved performance of the solar cells. Our observations suggest that gains in performance would result from the curing of defects, as induced by the deposition of the LPCVD-ZnO back electrode on the absorber layer.

4.2   Experimental details

4.2.1   Solar cell preparation and characterization

Glass (0.5-mm-thick) coated with highly doped 2-µm-thick LPCVD-ZnO (Z2) was used as our textured superstrate. Z2 was chosen to minimize the change in its electrical properties induced by the post-deposition treatments (hydrogen plasma/annealing), as this change is highly dependent on doping. It must be noted that these highly doped electrodes are not optimal for high-efficiency μc-Si:H cells, as they are characterized by high free-carrier absorption in the near-infrared. They also provide limited light trapping in the 800–1100 nm wavelength range due to their smaller surface feature size. They do, however, provide a similar R_{sq} of about 9 $\Omega/_{sq}$ with respect to standard Z5 front electrodes, allowing a direct comparison with standard cells for the resistive losses in the front electrode.

When μc-Si:H solar cells are deposited on as-grown rough Z2 superstrates, porous defective zones (commonly referred to as "cracks") may appear in the μc-Si:H film, which can lead to local post-deposition oxidation and poorer cell performance [Sakai 90, Nasuno 01, Matsui 02c, Python 08, Kilper 09, Li 09b, Bugnon 12]. Prior to μc-Si:H deposition, an argon plasma was applied to the front electrode for 4 or 20' to obtain a rough (Z2 4') and a smooth (Z2 20') ZnO surface, more favorable to the growth of high-quality μc-Si:H material.

Single-junction solar cells in the p–i–n configuration were then deposited by PECVD at a superstrate temperature of 200 °C, using the process given in Chap. 3. The i-layer was deposited with an excitation frequency of 70 MHz, a pressure of 0.7 mbar and a deposition rate of 1.6 Å/s. An i-layer thickness of 1.1±0.1 µm was chosen for all experiments, unless stated otherwise. For the back electrode, LPCVD-ZnO with thicknesses of 2–2.3 µm and various doping was used, depending on the experiment. The cell area was defined to 0.25 cm^2, unless stated otherwise. The sub-gap absorption coefficient at 0.8 eV ($\alpha_{0.8}$) linked to defects in the bulk phase of the μc-Si:H material was evaluated by FTPS [Vanecek 02, Bugnon 12]. Dark degradation was evaluated by storing the samples in the dark and in ambient conditions, without specific control of the temperature or atmosphere. Dark degradation can indeed be expected on rough superstrates via moisture in-diffusion through the 2-D network of interconnected porous areas present within the μc-Si:H when deposited on rough superstrates, coming from the edges of the cell that are directly exposed to the atmosphere with our cell design (see Chap. 3). Post-deposition oxidation of this defective material can be related to an increase of dark saturation current through it [Boccard 11], which can happen in a very short timeframe as well as on a longer timescale for the post-deposition oxidation of the amorphous material surrounding the crystalline grains [Bronneberg 11].

4.2.2   Post-deposition treatments of complete solar cells

Post-deposition treatment with a hydrogen plasma was performed both in a medium-size PECVD KAI reactor and in a small-size R&D reactor from Indeotec (OCTOPUS I). The hydrogen

plasma treatment consisted first of 20' of preheating and outgassing at 200 °C under vacuum at a pressure of 2×10^{-6} mbar, directly followed by a hydrogen plasma, which was performed at a pressure of 0.5 mbar, a power density of 0.15 W/cm^2 and a temperature of 200 °C for 20 min. Annealing under vacuum was also performed in a small-area PECVD system, at temperatures between 200 °C and 245 °C for 20', with preheating conditions similar to those of the hydrogen plasma. For comparison with the hydrogen plasma treatment at 200 °C, an annealing temperature of 230 °C was chosen to approximate the additional temperature increase induced by the hydrogen plasma. The effect of varying the annealing temperature is analyzed in Sec. 4.3.3 to discriminate between effects from temperature plus hydrogen plasma and from temperature only.

Fig. 4.3 presents a sketch of the solar cells used for this experiment to decouple the impact of annealing in vacuum from hydrogen plasma treatment. In the first experiment, Z2 was chosen to minimize the effects on the doping level of back electrode. Two superstrate roughnesses were used to evaluate the role of cracks when applying post-deposition treatments. In the second experiment, solar cells were grown on a smooth highly doped superstrate (Z2 20') and the influence of the doping level of the ZnO back electrode (which is the part of the cell directly exposed to the hydrogen plasma) was characterized. Two different back electrodes were tested, with the same thickness (2 μm): a highly doped Z2 and a non-intentionally doped 2-μm-thick Znid.

Figure 4.3: *Schematic view of p–i–n μc-Si:H solar cells used to demonstrate the impact of superstrate roughness (a) and back electrode doping level (b) upon post-deposition treatment (hydrogen plasma or annealing in vacuum). Porous zones, typically appearing when μc-Si:H material is grown on a rough superstrate, are represented as dashed lines in the μc-Si:H material.*

4.3 Results and discussion

4.3.1 Effect of cell morphology

Fig. 4.4 presents the changes in V_{oc} and FF when applying different post-deposition treatments on complete μc-Si:H solar cells deposited on rough and smooth superstrates (see Fig. 4.3 (a)).

Figure 4.4: *Effect of a hydrogen plasma treatment and vacuum annealing (ann) on the V_{oc} (a) and FF (b) of μc-Si:H solar cells deposited on rough and smooth superstrates (averaged over eight 0.25-cm^2-cells), and their evolution after 40 days ambient storage in the dark (DD 40d).*

In all cases, an improvement in V_{oc} and FF is observed after the post-deposition treatment, with a strong dependence on the superstrate roughness. In the case of the rough superstrate, the electrical gains are much more pronounced, with absolute gains in V_{oc} and FF of up to 25–30 mV and 3–4%, respectively. Very high V_{oc} values above 540 mV are obtained on the rough superstrate after treatment. For the smooth superstrate, the absolute gain is lower

(10–15 mV in V_{oc} and 1–2% in *FF*). We suggest that this massive increase observed on the rough superstrate is related to a curing of the porous, defective, zones that appear in the silicon when grown on rougher superstrates. Note that both annealing and hydrogen plasma treatment lead to comparable results in terms of V_{oc} and *FF* improvements. It has also been checked (not shown here) that the gains observed upon post-deposition treatment are not linked to ultraviolet illumination of the plasma or the presence of hydrogen. This was tested by covering the cells with a piece of glass during the plasma treatment. We also observe that, while solar cells deposited on the rough superstrate suffer from dark degradation after storage in the dark under ambient atmosphere for 40 days, those deposited on smooth superstrates remain stable, also after treatment.

To further understand the origin of the observed electrical gains, and to see whether they are linked to curing of the μc-Si:H absorber layer, additional experiments were carried out. An additional annealing at 230 °C for 40' was performed on the solar cells just after the μc-Si:H deposition, according to the procedure describer hereafter. All these treatments took place before deposition of the back-electrode:

- **ref**: no annealing directly after the μc-Si:H PECVD (reference),

- **air break+ann**: the samples were cooled to room temperature after the μc-Si:H PECVD, and annealed after a short air break,

- **direct ann**: the samples were annealed directly after the μc-Si:H PECVD, without an air break,

- **double ann**: the samples were annealed directly after the μc-Si:H PECVD, and annealed again after a short air break.

Tab 4.2 shows the changes in V_{oc} and *FF* for 1-μm-thick μc-Si:H solar cells with different treatments performed before deposition of the back electrode (leading to the results labelled "ini"). The results of an annealing subsequent to the deposition of the back electrode (leading to the results labelled "ann") are also presented.

While V_{oc} and *FF* gains, similar to those reported before, are observed for annealing after the deposition of the back electrode, no improvement is observed for the various treatments performed before the deposition of the back electrode ("ini" values). This suggests either that the deposition of the back electrode might cancel a possible gain obtained when annealing the cell before the deposition, or that the gain is achieved only when the back electrode is present (improvement of the μc-Si:H–LPCVD ZnO interface). Further investigations should be performed to clarify this point, *e.g.* by using an alternative back electrode. However, the strong superstrate dependence tends to indicate that interface effects can be excluded, as well as improved doped layers upon annealing such as demonstrated in [Kondo 03], where it is suggested that p-doped layers can be improved by thermal annealing (removal of H from the B–H complex).

Table 4.2: *Effect of various treatments performed before the deposition of the LPCVD-ZnO back electrode on the electrical properties (best cell) of 1-µm-thick µc-Si:H solar cells (ini), and after annealing subsequent to deposition of the back electrode (ann).*

Superstrate	Treatment before LPCVD-ZnO	$V_{oc,ini}$ [mV]	$V_{oc,ann}$ [mV]	FF_{ini} [%]	FF_{ann} [%]
smooth Z2 20'	**ref**	544	552	74.1	75.7
	air break+ann	544	553	73.6	75.1
	direct ann	548	553	74.5	75.7
	double ann	544	552	73.6	75.4
rough Z2 4'	**ref**	527	548	69.0	72.7
	air break+ann	523	545	69.3	73.0
	direct ann	523	543	69.2	72.7
	double ann	517	537	69.0	72.2

Indeed, an improvement similar to the one shown in Fig. 4.4 is again observed when the solar cells are annealed after the deposition of the LPCVD-ZnO back electrode. An increase of 20–22 mV in V_{oc} and up to 3.7% in *FF* for the rough Z2 4' front electrode is achieved, while the gain remains moderate on the smooth Z2 20' (+5–9 mV in V_{oc} and +1.2–1.8% in *FF*), regardless of the treatment performed before the deposition of the LPCVD-ZnO back electrode.

The gains observed only when the annealing is performed after back electrode deposition further support our assumption that they are, at least partly, linked to the curing of defects induced by the LPCVD-ZnO in porous zones of the μc-Si:H absorber layer. Furthermore, the LPCVD method for ZnO film preparation can result in the introduction of foreign elements in those porous zones [Duchamp 13]. Indeed, exposure to water vapor during the deposition of LPCVD-ZnO at temperatures above 150 °C may lead to oxidation of those zones, which would be cured during annealing after the deposition of the back electrode.

4.3.2   Effect of post-deposition annealing analyzed by FTPS

To investigate our hypothesis of μc-Si:H absorber layer improvement by curing, we performed FTPS on these same μc-Si:H solar cells of Tab. 4.2. This technique allows us to assess the defect density in the absorber layer. Fig. 4.5 shows the sub-gap absorption at around 0.8 eV (linked to defects in the bulk) as evaluated by FTPS for solar cells deposited on rough and smooth superstrates. The curves were normalized with the absorption coefficient of crystalline silicon at 1.35 eV.

Results on rough superstrates demonstrate that a strong reduction in $\alpha_{0.8}$ is achieved only if annealing is performed after the deposition of the LPCVD-ZnO back electrode, while no significant difference is observed when the cells are annealed before the deposition of the back electrode. A similar behavior, although much less pronounced, is observed on the smooth superstrate (the solid curves are always below the corresponding dashed curves at 0.8 eV). This
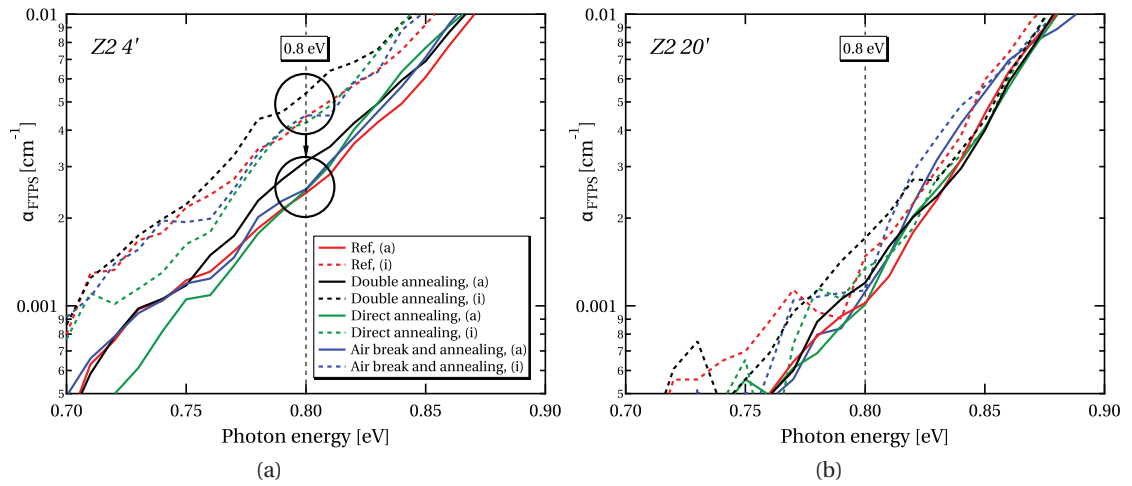
Figure 4.5: *FTPS measurement of the sub-gap absorption of solar cells deposited on rough Z2 4' (a) and smooth Z2 20' (b) LPCVD-ZnO, for various types of annealing before the deposition of the back electrode (dashed curves) and annealing after the deposition of the back electrode (solid curves).*

reduction in $\alpha_{0.8}$ is usually associated with a reduction of defects in the bulk μc-Si:H absorber layer. It is generally believed that this method is sensitive only to the bulk μc-Si:H absorber layer and not to 2-D surfaces such as porous zones present in the absorber layer [Python 09b]. However, by looking at the strong reduction of $\alpha_{0.8}$ in the case of the rough superstrate, we cannot exclude the possibility that part of this reduction in $\alpha_{0.8}$ may be related to a reduction of defects within the 2-D network of porous and defective material in the μc-Si:H absorber layer.

Thus, defects in these porous zones can not be considered as located on pure 2-D surfaces only, but also have a 3-D extension, allowing a detection of their curing by FTPS.

Note that the absolute value of $\alpha_{0.8}$ must be taken with caution as it can depend on the free-carrier density of the front and back electrodes and on their morphology [Python 09b]. In our case, such dependence is small as the texture is kept constant for each case (rough and smooth), and the highly doped front and back electrodes provide limited sensitivity to post-deposition treatments.

4.3.3 Effect of annealing temperature

Tab. 4.3 summarizes the performance of 1.35-µm-thick μc-Si:H solar cells deposited on a rough Z2 4' superstrate, characterized prior to and after annealing in vacuum at different temperatures. At an annealing temperature of 230 °C, a maximal enhancement in $V_{oc} \times FF$ is observed without collection losses in J_{sc} as could arise from potential boron diffusion from the p-doped layer into the absorber layer. According to Tab. 4.3, V_{oc} and FF gradually increase with increasing temperatures but tend to saturate at around 230 °C. At 245 °C, V_{oc} and FF

Table 4.3: *Evolution of the electrical parameters of solar cells (best cell, with area of 0.25 cm^2) exposed to different temperatures of annealing. The cells were deposited on rough Z2 4' and the i-layer had a thickness of 1.35±0.1 μm. "Ref" stands for the parameter measured for the same cell before annealing. *This cell was unfortunately irreversibly damaged after the FTPS measurement. Hence its EQE and J$_{sc}$ after annealing are not available.*

T [°C]	V_{oc} [mV] ref/ann	*FF* [%] ref/ann	J_{sc} [mA/cm^2] ref/ann	$\alpha_{0.8}$ [10^{-3} cm^{-1}] ref/ann
200	515/525	67.9/69.3	23.1/23.1	4.8/3.9
215	513/527	68.3/70.8	23.1/-*	4.3/3.0
230	514/531	68.9/71.5	22.9/22.9	4.2/2.7
245	510/531	69.4/71.5	22.9/22.7	4.2/2.2

remain similar but the blue response in the external quantum efficiency (EQE) (not shown) of the cell starts to be lower, due to possible boron diffusion from the *p*-doped layer into the absorber layer or a reduced transparency of the *p*-doped layer [Stuckelberger 14a]. An increased reduction of the absorption coefficient at 0.8 eV as measured by FTPS can be seen for increasing temperatures of annealing (see also Sec. 4.3.1). This study therefore validates our choice for the annealing temperature and supports our conclusion that the high electrical gains on rough superstrates are linked to thermally activated curing.

4.3.4 Effect of doping of the back electrode

As discussed in Sec. 4.1, while annealing in vacuum of LPCVD-ZnO films already results in a decrease in their R_{sq}, this decrease can be further lowered with a hydrogen plasma treatment, even drastically for Znid, due to modification in the charged trap density at the grain boundaries. Furthermore, according to [Ding 13a], the improved electrical properties of the ZnO films remain stable upon exposure to ambient atmosphere, except for Znid for which an increase of its R_{sq} can be observed when stored in dark ambient atmosphere. In the following experiment, we investigate the impact on cell performance of post-deposition annealing and hydrogen plasma treatment for μc-Si:H solar cells with a back electrode of two different doping levels (Z2, Znid). 1.1-μm-thick μc-Si:H solar cells were deposited on a smooth Z2 20' superstrate (the same as used in Sec. 4.3.1) to minimize the effect of porous zones in the μc-Si:H absorber layer on the cell performance and to highlight the effect of varying the doping level of the ZnO back electrode (see Fig. 4.3 (b)). The results are summarized in Tab. 4.4. Larger cells (1.2 cm^2) were chosen to enhance the impact of the R_{sq} of the back electrode on the *FF* due to resistive losses.

A similar increase in V_{oc} as presented in Sec. 4.3.1 after annealing and hydrogen plasma treatment is achieved. A very high increase in *FF* is observed for the cells with the Znid back electrode, but the low *FF* values before treatment should be considered with caution due to potential measurement artifacts. Nevertheless, this result corroborates the larger gains expected for the solar cells with Znid back electrodes. With the highly doped Z2 back electrode,

Table 4.4: *Electrical properties of p–i–n µc-Si:H solar cells (best cells, designated aperture area of 1.05 cm²) with non-intentionally doped (Znid) and highly doped (Z2) back electrodes in initial state and after treatment.*

Back electrode	Treatment	V_{oc} [mV]	*FF* [%]	$R_{sq,back}$ [Ω/□]
Znid	ref/H$_2$ plasma	526/530	(48.0)/70.9	85/24-33
	ref/ann	530/534	(52.2)/69.1	85/40-50
Z2	ref/H$_2$ plasma	542/549	71.0/72.1	10/8
	ref/ann	545/551	72.0/72.6	10/8

a much smaller enhancement is observed.

Depending on the cell geometry and more specifically the collection width of the solar cell (usually defined via laser scribing for monolithically series-interconnected cells in modules), a hydrogen plasma treatment can be worthwhile compared to annealing in vacuum. For large modules, a detailed analysis will be required to evaluate the need for a hydrogen plasma treatment, depending on the used laser scribe patterning and the R_{sq} of the back electrode.

4.3.5 Application to tandem cells

This section presents the application of post-deposition treatments described in the previous sections to solar cells in the micromorph (*a*-Si:H/μc-Si:H tandem) configuration. When a micromorph cell is deposited on a rough superstrate, the change of morphology induced by the *a*-Si:H top cell, or by an intermediate reflector, can negatively influence the growth template of the bottom cell, with so-called "pinching points" that can induce cracks in the μc-Si:H bottom cell [Cuony 10, Cuony 11, Boccard 12c, Biron 13a, Biron 13c]. As we suggested that improvements in single-junction μc-Si:H solar cells are linked to curing of porous zones in the absorber layer, improvement of the bottom cell can similarly be expected when the post-deposition treatments are applied to tandem solar cells deposited on a rough superstrate.

An *a*-Si:H top cell with a thickness of 250 nm was deposited on a Z2.3 4' superstrate and the baseline process from KAI-M was used to deposit a 1.2-µm-thick bottom cell at 3 Å/s [Bugnon 13]. A 40-nm-thick silicon oxide intermediate reflector (SOIR) was inserted between the top and the bottom cell. Details about the optimization of this tandem configuration can be found in [Despeisse 11]. Nine samples were co-deposited and compared, with three sets of back electrodes. The cells were patterned into an area of 1 cm². In addition to the Z2 and Znid tested in the previous section, Z2.3, which is lightly doped, was also used as a standard back electrode for the tandem cells. For each set of back electrodes, one sample was kept as a reference without any post-deposition treatment (referred to as (r)), one sample was annealed post-deposition (a), and one sample was given a post-deposition hydrogen plasma treatment (p). Light soaking was performed on each sample and the *J–V* characteristics were recorded just after the post-deposition treatment, after around 50 h of light soaking, and after around

200 h of light soaking.

Fig. 4.6 presents the V_{oc} and the *FF* of the best cells of the nine combinations of back electrodes and post-deposition treatments.
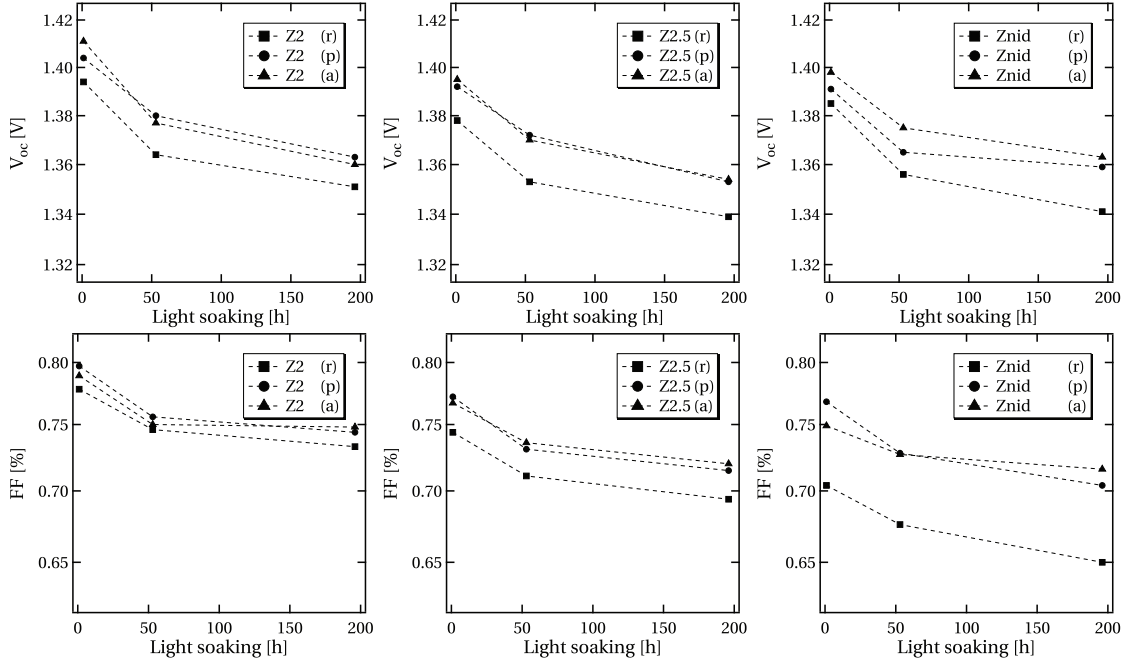
Figure 4.6: *Evolution of the V_{oc} and FF of micromorph tandem solar cells (a-Si:H (250 nm)/SOIR (40 nm) /μc-Si:H (1.2 μm)) upon light soaking for three back electrodes. (r)-cells are reference solar cells without any post-deposition treatment, (p)-cells are solar cells with a post-deposition hydrogen plasma treatment and (a)-cells are solar cells after a post-deposition annealing in vacuum. The FF values are not corrected with CMM (see text).*

An improvement of 10–20 mV in V_{oc} is observed for the (a) and (p) samples for all three back electrodes and the improvement is stable upon light soaking. The *FF* is also improved with the post-deposition treatments, but there is a clear dependence on the back electrode as expected from the doping and hence R_{sq} variations. The initial *FF* values also depend on the back electrodes since (i) the R_{sq} of the back electrode impacts *FF* [Boccard 12b] and (ii) different current repartition occurs in the top and bottom cell (mismatch) due to the doping level of the back electrode [Ulbrich 11, Bonnet-Eymard 13, Ulbrich 13].

Indeed, parasitic absorption by free carriers (FCA) in the back electrode changes the amount of light that is reflected back into the cell by the white back reflector, leading to different matching conditions and *FF*. We should mention that the *FF* curves in Fig. 4.6 were not corrected with a current-matching machine (CMM) [Bonnet-Eymard 13] for the different matching conditions to obtain a proper assessment of the stability of the gain obtained from the post-deposition treatments. CMM was originally developed to accelerate the development of high-efficiency micromorph solar cells, where the choice of superstrate is critical to optimize the current-

density in each subcell. CMM enables us to modify the AM1.5g spectrum by adding red or blue light in the spectrum while keeping the illumination intensity constant, and therefore allows us to evaluate the *FF* and the efficiency of micromorph solar cells for different superstrates or matching conditions without needing to adapt the layer thicknesses for each superstrate separately [Boccard 12c, Bonnet-Eymard 13].

In our case, the matching conditions should artificially be made identical in all cells together with a measurement of the R_{sq} of the back electrode to correctly evaluate the change in *FF* during light soaking due to (i) the change in R_{sq} especially for the untreated Znid which is directly exposed to air and is prone to degradation by moisture and (ii) the mismatch evolution due to the degradation of the top-cell EQE and the optical properties of the front and back electrodes [Ding 14].

However, this experiment demonstrates that the more resistive the back electrode, the higher the initial gain, as was observed in single-junction μc-Si:H solar cells. This gain is then stable upon light soaking, but from the experiment, it cannot be deduced unambiguously that the stability of the observed gain for the *FF* in micromorph tandems is provided solely by the post-deposition treatment.

Fig. 4.7 shows the EQE of all nine samples before light soaking. The corresponding J_{sc} of the top and bottom cells can be found in the legend.
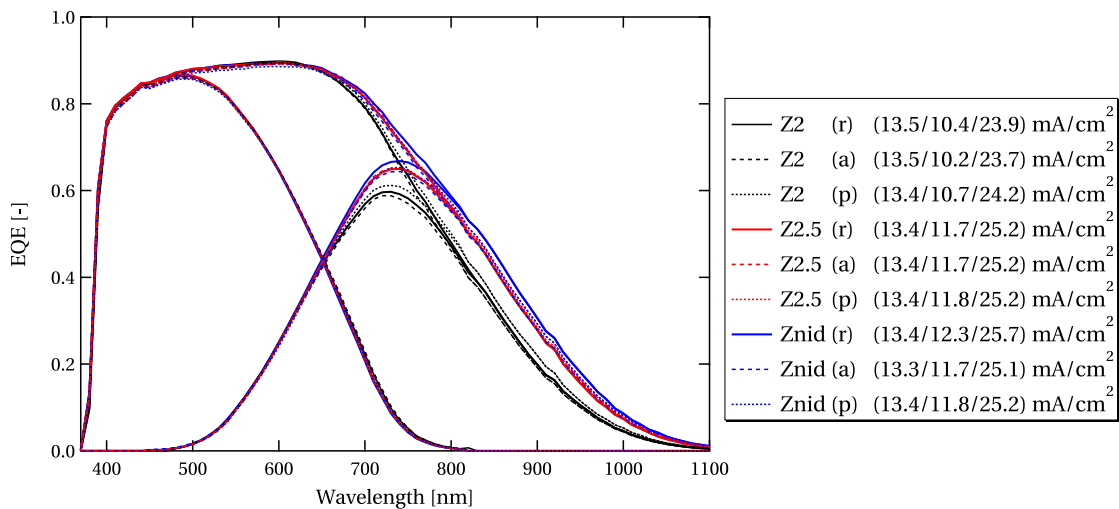
Figure 4.7: *EQE of tandem solar cells as a function of the doping of the back electrode. Solid curves are reference cells without any post-deposition treatment (r), dashed curves are cells with a post-deposition annealing treatment (a) and dotted curves are cells with a post-deposition hydrogen plasma treatment (p). The legend indicates the corresponding J_{sc} for the (top cell/ bottom cell/ total) EQE.*

The remarkable absence of change in the EQE of the top cell for the nine combinations demonstrates that the doping of the back-contact has little to no impact on the top-cell EQE

(for this tandem configuration). It also supports the conclusion that most of the improvement after post-deposition treatment happens in the μc-Si:H bottom cell, even though, as for single-junction μc-Si:H solar cells, the post-deposition treatments have only a small impact on the bottom-cell EQE. Note however that in the Znid case (which is also the most sensitive to post-deposition treatment), a slight reduction in the bottom cell EQE is observed. This small change in EQE is attributed to the increased free-carrier density and associated FCA induced by post-deposition treatments [Ding 13a].

4.4 Conclusion

In this chapter, we demonstrated the beneficial effect of two different post-deposition treatments (hydrogen plasma treatment and annealing in vacuum) on complete, non-encapsulated solar cells. Furthermore, effects arising from temperature or hydrogen plasma were decoupled. More particularly, it was shown that annealing the cells under vacuum is sufficient as compared to hydrogen-plasma exposure, with two main conclusions:

- A curing of the porous phase in the μc-Si:H absorber layer was obtained by annealing, as was especially observed on rough superstrates. An improvement of the porous zones in μc-Si:H was detected by FTPS measurements, implying that defects in these porous zones are not located on pure 2-D surfaces, but have a spatial extension. The deposition of LPCVD-ZnO induced additional defects in porous zones of the absorber layer, which were cured by annealing. This effect should thus be absent or very limited for sputtered back electrodes.

- A decreased R_{sq} of the LPCVD-ZnO was obtained with annealing, without requiring an exposure to a hydrogen plasma. This exposure to a hydrogen plasma is hence not needed to improve the cell performance, provided that LPCVD-ZnO electrodes with low enough R_{sq} are used.

Even though the post-deposition treatments can be beneficial, smooth front electrodes and a robust PECVD process are nevertheless required to avoid the formation of porous zones within the μc-Si:H absorber layer and ensure good stability upon ambient storage.

The post-deposition treatments are likely too time consuming for direct industrial application, especially the hydrogen plasma treatment which needs a dedicated PECVD chamber, thus giving it a non-negligible impact on the takt time and making it less cost-effective. However, a simple annealing in vacuum is probably more compatible with an industrial process, as it could in principle be performed in a simple heated vacuum chamber. A post-deposition annealing could offer *e.g.* the possibility to use larger stripes for laser scribing or less doped ZnO back electrodes for equivalent resistive losses in modules.

Finally, such an annealing was implemented in the record cell of Chap. 3, with a conversion efficiency of 10.7%, independently confirmed at ISE CalLab PV Cells [Hänni 13b], as well as

in our new world-record 12.6%-efficient tandem solar cell (after 1000 h of light soaking) [Boccard 14], independently confirmed at Newport Technology & Applications Center's Photovoltaic (TAC-PV Lab) and in our internal-record 12.8%-efficient triple-junction cell in the p–i–n configuration (after 1000 h of light soaking) [Schüttauf 14], all on an area larger than or equal to $1\,cm^2$.

5 Interface effects on solar cell performance

In this chapter, we show how dedicated interface engineering can improve the performance of microcrystalline silicon (μc-Si:H) solar cells. We first analyze the shunt-quenching effect of silicon oxide (SiO$_x$) p-doped layers with variable illumination measurements (VIM). It is demonstrated that such SiO$_x$ p-doped layers can very efficiently limit open-circuit voltage (V_{oc}) losses at lower illumination levels, also on rough superstrates, and improve the diode ideality factor of single-junction μc-Si:H solar cells deposited on rough superstrates.

Then, we introduce passivating hetero-interfaces in single-junction μc-Si:H solar cells and investigate the effect of different i–n layer stacks in thin (<1 μm) μc-Si:H devices, sensitive to recombination both at the interfaces and in the bulk material. By applying intrinsic amorphous silicon passivating layers at the μc-Si:H i–n interface, we show a device with a V_{oc} of 608 mV, reaching a value close to those of standard multicrystalline silicon solar cells, for a standard Raman crystalline fraction (R_c) of the i-layer (∼55%). This V_{oc} value is, to our knowledge, the highest reported value for a state-of-the-art μc-Si:H device made solely by plasma-enhanced chemical vapor deposition (PECVD).

By using this novel passivating interface, we thus demonstrate a state-of-the-art conversion efficiency of 9.5% for a solar cell with an absorber layer as thin as 650 nm. We also apply passivating interfaces in micromorph tandem solar cells and reach a record V_{oc} of 1.53 V by depositing such a thin μc-Si:H solar cell on an amorphous silicon (a-Si:H) solar cell with a wide-bandgap absorber layer.

By increasing the thickness of the absorber layer, the bulk quality of our μc-Si:H material is found to be a limiting factor for the cell efficiency, thereby canceling the beneficial effects from improved interfaces. This is also illustrated by simulation.

Finally, we introduce a concept to probe the ultimate V_{oc} limit of μc-Si:H solar cells.

Part of the results presented in this chapter are published in [Hänni 13a], and some are currently under a patenting process and should be submitted for publication later.

5.1 Contribution of SiO$_x$ *p*-doped layers

As discussed in Chap. 3, silicon suboxide (SiO$_x$) doped layers have been proposed as excellent candidates to mitigate the effect of localized porous and defective zones within the absorber layer (commonly called cracks), induced by inadequate surface morphology of the superstrate or the PECVD process [Sichanugrist 94, Cuony 10, Veneri 10, Despeisse 11, Cuony 12, Bugnon 12, Lambertz 13, Kim 13]. Here, we further investigate the quenching of these defective areas when adequate *p–i* interfaces are used, by studying the role of SiO$_x$ versus *μc*-Si:H *p*-doped layers by means of the VIM technique [Merten 98, Meillaud 06a]. The VIM technique consists of the measurement of *J–V* curves at various illumination levels, by using intensity filters (see also Chap. 2). For this analysis, 1.6-μm-thick solar cells with *μc*-Si:H or SiO$_x$ *p*-doped layers were deposited on superstrates made of LPCVD-ZnO of decreasing roughness, from very rough Z5 5' to smooth Z5 45', which is currently our optimum superstrate for high-efficiency single-junction *μc*-Si:H solar cells (see Chap. 2 and 3). *μc*-Si:H *n*-doped layers were used in all cases.

Tab. 5.1 shows a comparison of the short-circuit current density (J_{sc}), fill factor (*FF*), V_{oc}, conversion efficiency (η) and diode ideality factor (*n*) for these cells.

Table 5.1: *Performance of solar cells (best cells) as a function of the superstrate surface treatment time and the used p-doped layer. From [Hänni 13a].*

p	Superstrate	J_{sc} [mA/cm^2]	*FF* [%]	V_{oc} [mV]	η [%]	*n* [-]
	Z5 5'	23.9	67.2	493	7.9	1.8
μc-Si:H	Z5 20'	23.8	71.8	518	8.9	1.2
	Z5 45'	23.1	74.4	529	9.1	1.1
	Z5 5'	25.5	69.0	512	9.0	1.4
SiO$_x$	Z5 20'	25.3	72.7	528	9.7	1.2
	Z5 45'	24.6	74.5	543	10.0	1.1

Using SiO$_x$ *p*-doped layers, a J_{sc} gain of 1.5 mA/cm^2 is achieved on all superstrates, together with increased V_{oc} and *FF*. More remarkably, on the roughest superstrate (Z5 5'), absolute gains of 19 mV and 1.8% are obtained for V_{oc} and *FF*, respectively. On the smooth Z5 45' superstrate, an absolute gain in V_{oc} is maintained (14 mV), but that in *FF* is much lower (0.1%). These results are consistent with previous observations by Cuony *et al.* [Cuony 10], where improved V_{oc} and *FF* values, observed with SiO$_x$ *p*-doped layers in *μc*-Si:H cells, are ascribed to quenching of undesired current drains in porous zones, whereas the J_{sc} gain is related to increased external quantum efficiency (EQE) in the short wavelength range. The latter is due both to a reduction of parasitic absorption, and to a reduction of reflection at the ZnO–Si interface thanks to the low refraction index of the SiO$_x$ layer.

5.1.1 SiO$_x$ versus μc-Si:H p-doped layers studied with the VIM technique

Fig. 5.1 shows V_{oc} values as a function of the illumination level for the solar cells reported in Tab. 5.1. For very low illumination, the curve is dominated mainly by the shunt resistance. By fitting the linear part (in a semi-logarithmic plot) of such curves to a one-diode model, the value of the diode ideality factor (n) can be obtained [Merten 98], also reported in Tab. 5.1.
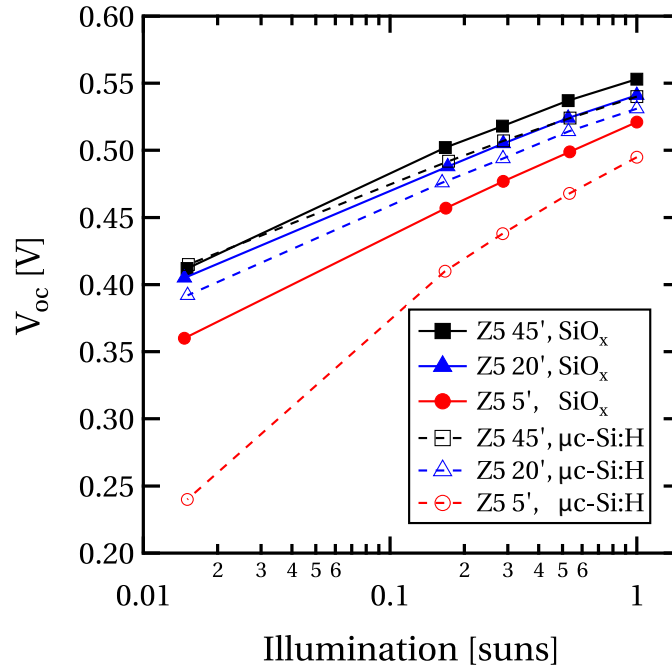
Figure 5.1: *V_{oc} values as a function of illumination level for 1.6-µm-thick single-junction μc-Si:H solar cells, with SiO$_x$ and μc-Si:H p-doped layers. The SiO$_x$ p-doped layer mitigates the detrimental effect arising from porous zones. Similar behavior was observed for FF (not shown here). From [Hänni 13a].*

In Fig. 5.1, the V_{oc} gain reported in Tab. 5.1 is visible at 1 sun illumination value. For the Z5 45' and Z5 20' superstrates, the V_{oc} reduction with lowered illumination level is independent of the p-doped layer, as also expressed in similar n values of 1.1 and 1.2, respectively.

For the rougher superstrate (Z5 5'), a higher V_{oc} value is maintained with the SiO$_x$ p-doped layer, as compared to the μc-Si:H p-doped layer, when reducing the illumination level, and correlated to a reduction of n from 1.8 to 1.4. At low illumination conditions, the benefit of the SiO$_x$ design is consistent with the conclusions of [Despeisse 10, Despeisse 11], where quenching of local current drains was proposed as an explanation for the improved performance on rough superstrates.

VIM on our samples thus further corroborates previous statements that a suitable choice of p–i interface has an impact on cell performance and that the detrimental effects of porous zones can successfully be mitigated. The higher maintained V_{oc} attributable to the SiO$_x$ p-

doped layers is important for multi-junction devices with high V_{oc}, as a μc-Si:H cell used as the middle or bottom cell typically receives only half or less of the illumination intensity.

5.2 Passivating interfaces for high open-circuit voltage

5.2.1 Introduction

State-of-the-art μc-Si:H solar cells deposited by PECVD [Meier 94] generally exhibit V_{oc} values in the 500–560 mV range. These values are far below the theoretical upper limit of above 800 mV that can be expected from the μc-Si:H bandgap (1.1 eV) [Tiedje 84, Meillaud 06b]. To improve V_{oc}, attention has lately been focused on developing both high-quality μc-Si:H material and a suitable cell design [Yamamoto 01, Roschek 04, Matsui 06, Smets 08a, Shah 13, Guha 13, Hänni 13a, Sai 13, Tan 13].

One way to increase the V_{oc} of μc-Si:H solar cells is to increase the amorphous fraction of the absorber layer (*e.g.* by modifying the deposition conditions), but the subsequent gain is generally accompanied by a loss in *FF* due to less efficient carrier collection and increased light-induced degradation [Flückiger 93, Droz 04, Yan 04a, Söderström 08, Johnson 08]. Recently, however, promising results have been obtained with alternative precursors and deposition conditions, yielding high V_{oc} values even with a large crystalline fraction in the absorber layer [Zhang 08, Dornstetter 13]. V_{oc} is sensitive to absorber layer material and quality, but also to interfaces. For example, the use of SiO_x not only for doped layers but also as a buffer layer at the p–i interface has recently been shown to boost the efficiency of thin-film silicon solar cells [Bugnon 14]. Furthermore, a high V_{oc} value of 603 mV was reported for a single-junction μc-Si:H solar cell that incorporated a buffer layer grown by hot-wire chemical vapor deposition at the p–i interface [van den Donker 07]. The absence of ion bombardment on the p–i interface was suggested as the cause of this high value [Mai 05, Mai 06, Finger 08].

5.2.2 Impact of passivated *i*–*n* interface on open-circuit voltage

Here, we investigate the interplay between the thickness of the μc-Si:H absorber layer and the thickness of an a-Si:H buffer layer applied at the μc-Si:H *i*–*n* interface [Yue 08, Hoetzel 11]. We use this buffer layer as a tool to probe the influence of interfaces and the bulk on the V_{oc} of very thin single-junction μc-Si:H solar cells, incorporating high-quality bulk material (Chap. 3) and an optimized SiO_x layer at the p–i interface [Bugnon 14]. The followed approach is similar to the amorphous/crystalline silicon heterojunction concept, where passivation of the crystalline surface drastically enhances V_{oc}, compared to traditional diffused-junction cells [De Wolf 12].

The R_c of the absorber layer was kept constant, above 50%, in all cases. For absorber layer thicknesses ranging from 0.4 to 2.5 μm, several designs for the *i*–*n* interfaces were compared.

Passivated design in thin μc-Si:H solar cells

First, two designs for the $i–n$ interface were compared, as sketched in Fig. 5.2, for solar cells with a 650-nm-thick absorber layer. One design utilizes a single SiO_x n-doped layer
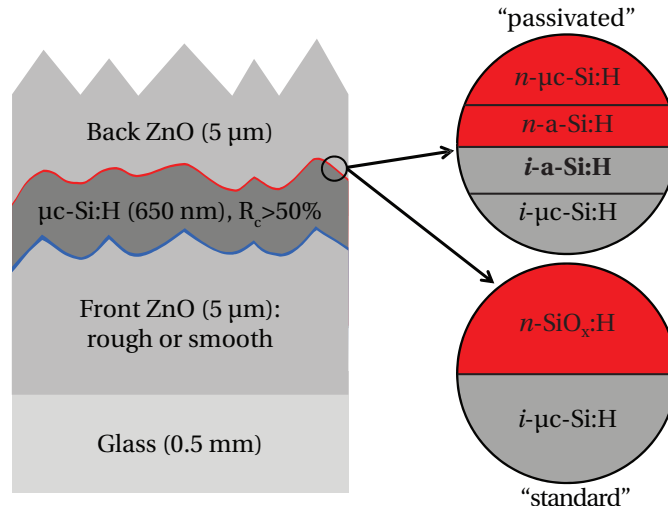
Figure 5.2: *Cross-sectional schematic of the device used to study the impact of specific $i–n$ interfaces on cell performance. Two front-electrode roughnesses and two cell designs with various $i–n$ interfaces are investigated: a standard SiO_x n-doped layer ("standard") and a design with a-Si:H layers ("passivated").*

("standard"); in the other a passivated interface was introduced, which consisted of a stack comprising a 20-nm-thick intrinsic a-Si:H buffer layer and an a-Si:H n-doped layer ("passivated"). In this latter design, a thin μc-Si:H n-doped layer was used to ensure good contact with the back electrode [Gerlach 13].[1]

Tab. 5.2 shows the performance of solar cells with a 650-nm-thick absorber layer for the two cell designs as a function of superstrate roughness. For such thin devices, the impact of the bulk defect density in the intrinsic absorber layer is reduced so that recombination at the interfaces plays a major role in V_{oc}.

We observe that state-of-the-art efficiencies are obtained on all superstrates with both standard and passivated designs. In both cases, V_{oc} and *FF* on very smooth (Z5 150') and smooth (Z5 45') superstrates are similar, indicating that the absorber layer contains almost no zones of porous and defective material. Still, although both cell designs yield similar efficiencies, a notably larger V_{oc} value is obtained for the passivated design. A V_{oc} gain of 26 mV with minor *FF* loss is reached on the smooth superstrates. However, on the rough superstrate, even though V_{oc} remains rather stable, *FF* is reduced compared to the standard design, due to less efficient

---

[1]We also investigated the configuration using an n-doped SiO_x layer instead of an n-doped μc-Si:H layer in the passivated design, but poor *FF* was obtained, probably due to the non-optimized n-a-Si:H/n-SiO_x interface. The proposed "passivated" design is a standard $i–n$ interface optimized for baseline a-Si:H cells. We therefore stuck to the comparison of our standard $i–n$ interface design for single-junction μc-Si:H solar cells (namely using SiO_x), and the novel passivated design.

Table 5.2: *Performance of thin p–i–n µc-Si:H solar cells with a 650-nm-thick absorber layer and two i–n-interface designs, as a function of argon plasma treatment of the front electrode (from very smooth for the Z5 150' to rough for the Z5 20').*

Design	Z5 treatment time	V_{oc} [mV]	*FF* [%]	J_{sc} [mA/cm^2]	η [%]	*n* [-]
	150' (very smooth)	589	78.0	16.3	7.5	1.1
"standard"	45' (smooth)	582	77.4	20.0	9.0	1.1
	20' (rough)	576	75.4	20.4	8.9	1.2
	150' (very smooth)	606	76.6	16.1	7.5	1.1
"passivated"	45' (smooth)	608	77.1	19.7	9.2	1.2
	20' (rough)	571	72.5	20.2	8.4	1.5

shunt quenching in the passivated design. This is demonstrated by using the VIM technique, as presented in Fig. 5.3.
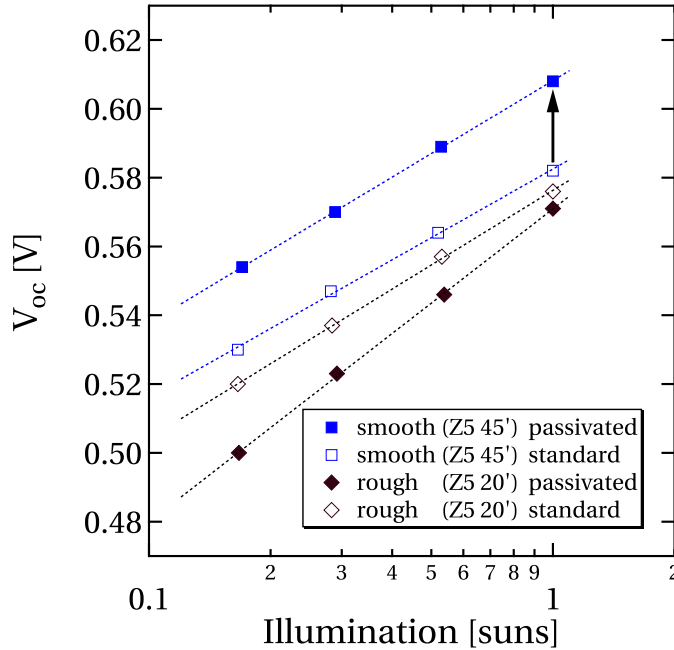
Figure 5.3: V_{oc} *values as a function of illumination level for single-junction µc-Si:H solar cells with a 650-nm-thick absorber layer, deposited on smooth and rough superstrates. The dotted lines represent fits with a one-diode model. The diode ideality factor was calculated from the slope of the fit.*

In this figure, the V_{oc} values of four of the cells in Tab. 5.2 are presented as a function of variable illumination level. Similarly as for the previous study, *n* can be extracted by fitting the V_{oc} vs. illumination data with a one-diode model [Merten 98]. Fig. 5.3 shows that for the smooth superstrate, the slope of V_{oc} as a function of illumination, and hence the diode ideality factor, is independent of the *i–n* interface design. On the contrary, for the rough superstrate,

shunt quenching is more efficient with the standard design (with a SiO_x n-doped layer), for a similar initial V_{oc}. This result shows that a high-quality absorber layer with no or few zones of defective and porous material is mandatory to obtain—and maintain at lower illumination—a gain with the passivated design. This is relevant for multi-junction solar cells in the p–i–n configuration, since in that case the μc-Si:H sub-cell is usually grown on a highly textured superstrate and it gets only half or less (for more than two junctions) of the illumination as compared to the single-junction configuration.

Fig. 5.4 shows the J–V and EQE curves of the best device of Tab. 5.2, obtained with the passivated design on Z5 45'. A V_{oc} value of 608 mV is reached, which yields a state-of-the-art efficiency of 9.2% (9.5% with an anti-reflective textured coating [Escarré 12b]) with an absorber layer thickness of only 650 nm.
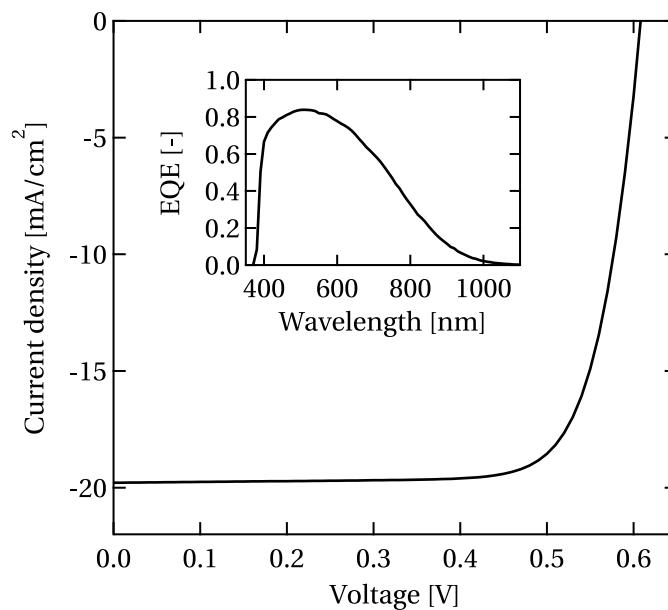
Figure 5.4: *J–V and EQE curves of the best cell reported in Tab. 5.2, yielding a V_{oc} value of 608 mV.*

Influence of absorber layer thickness in the passivated design

As previously mentioned, the second step of the study consists of evaluating the influence of the μc-Si:H absorber layer thickness in the passivated design. Although not shown here, an increase in V_{oc} is observed with increasing buffer layer thickness for all absorber layer thicknesses (from 0.4 to 2.5 μm). This increase in V_{oc} is accompanied by a reduction in *FF* if the buffer layer is too thick (*i.e.* >40 nm in our case) [Fujiwara 07, Holman 12].

Fig. 5.5 thus presents $V_{oc} \times FF$ as a function of the thickness of both the absorber layer and the intrinsic a-Si:H buffer layer. For these cells, a 2.5-μm-thick LPCVD-ZnO back electrode is used.
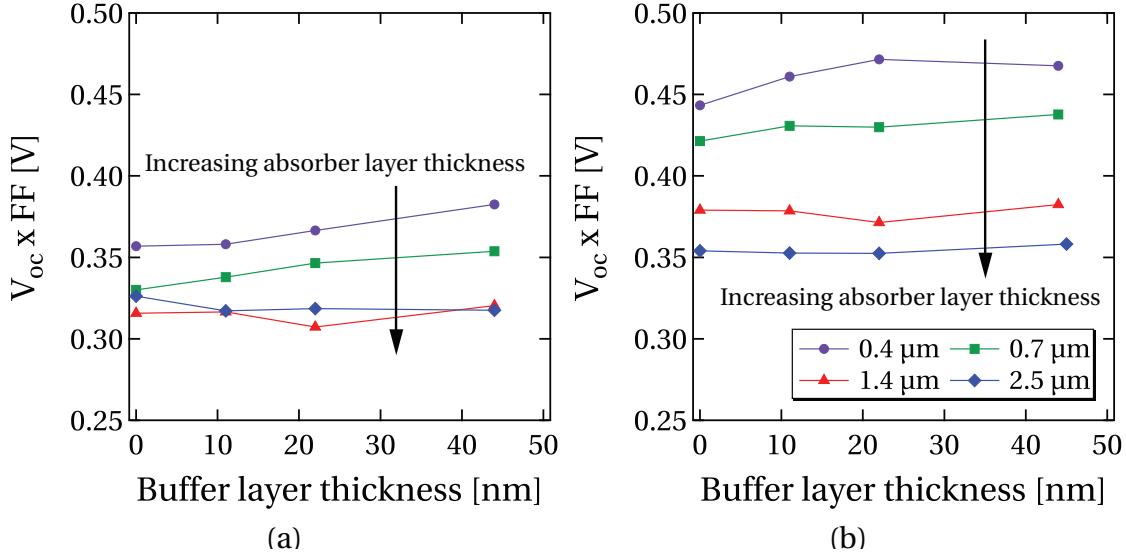
Figure 5.5: *Evolution of $V_{oc} \times FF$ on rough Z5 15' (a) and smooth Z5 45' (b) superstrates. For the cells without an a-Si:H buffer layer, the n-doped layer is unchanged (n-a-Si:H/n-μc-Si:H).*

For a very thin absorber layer, a large increase in $V_{oc} \times FF$ is observed on the smooth superstrate (Z5 45') as the buffer layer is thickened. Conversely, for thicker absorber layers or on rough superstrates such as a Z5 15' (slightly rougher than the Z5 20' of Tab. 5.2), only a slight gain is observed for increased buffer layer thickness, as the V_{oc} gain is canceled by a *FF* loss, linked to a too high defect density in the bulk, limiting the cell performance.

Limitations of *p–i–n μc*-Si:H devices by dead doped layers

Since very high V_{oc} values above 600 mV could be achieved experimentally for thin absorber layers, we wondered if the observed effects of the previous sections could be reproduced qualitatively, by simulating low-quality crystalline silicon, sandwiched between two "electronically dead" doped layers, and adding a passivation. Simulations were thus performed with the solar cell modeling program PC1D [Clugston 97, Yamamoto 03], assuming an absorber layer thickness of 500 nm.

We modeled a low-quality crystalline silicon layer with electron (μ_e) and hole (μ_h) mobility ($\mu_e = 10 \, cm^2/Vs$, $\mu_h = 1 \, cm^2/Vs$), sandwiched between two "electronically dead" doped layers with low bulk lifetimes (τ_{bulk}) and carrier mobilities (μ) ($\tau_{bulk,p} = \tau_{bulk,n} = 0.01 \, \mu s$, $\mu_e = 0.1 \, cm^2/Vs$, $\mu_h = 0.02 \, cm^2/Vs$). Furthermore, the bandgap of the *n*-doped layer was set at 1.75 eV, and the conduction-band offset at the heterojunction was set at 0.15 eV by using electron affinities of 4.05 eV for the crystalline layers and 3.9 eV for the *n*-doped layer [Matsuura 84]. The surface recombination velocity at the *p*-doped side was fixed at 10^4 cm/s.

Passivation at the *i–n* interface was subsequently introduced by varying the surface recombination velocity at this interface, for various τ_{bulk} of the absorber layer, linked to

the quality of the absorber layer. To assess what would happen for very high μc-Si:H bulk quality, the chosen parameters cover a wide range of surface recombination velocities, from that of a non-passivated silicon surface to that of a very well passivated surface [Yablonovitch 86], and τ_{bulk} values from below those reported for μc-Si:H (on the order of 100 ns [Brammer 03, Taretto 12]) up to those for low-quality crystalline silicon.

Simulation results are shown Fig. 5.6.
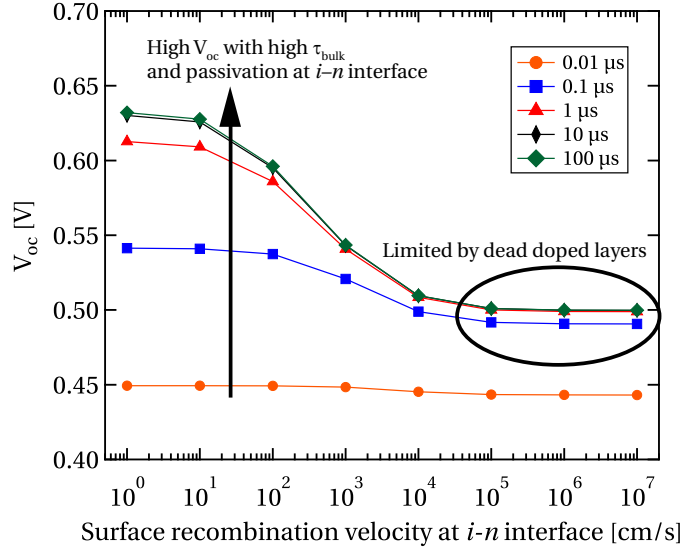
Figure 5.6: *PC1D simulation of a μc-Si:H solar cell with a 500-nm-thick absorber layer for different τ_{bulk} in the absorber layer and low-lifetime doped layers. Passivation at the i–n interface is simulated by reducing the surface recombination velocity at this interface.*

We observe that for poor passivation (high surface recombination velocities at the *i–n* interface) V_{oc} is not improved by reducing τ_{bulk}. For higher bulk quality (*i.e.* higher τ_{bulk}), passivation of the interface becomes increasingly relevant: the device is dominated by the interfaces and a gain in V_{oc} is observed in thin devices, as marked by an arrow in Fig. 5.3. Although further investigation of the exact passivation mechanism is required, the conduction-band offset is by nature not sufficient to fully passivate μc-Si:H. We believe that surface defect passivation must be present as well, in the same way that an amorphous phase is likely required to passivate grain- and column boundaries in the μc-Si:H bulk.

5.2.3   Implementation in thin tandem solar cells

Following the high performance achieved in the single-junction configuration, a solar cell with a 650-nm-thick absorber layer and 20-nm-thick buffer layer was implemented as the bottom cell in a micromorph tandem cell. Furthermore, to reach a global high V_{oc}, an *a*-Si:H top cell with a wide-bandgap absorber layer was used [Stuckelberger 14b]. Typical initial values of the top cell as a single junction (on a smooth superstrate) are 0.98–1 V for V_{oc}, 72% for *FF*

and 10–11 mA/cm^2 for J_{sc}. For the tandem cells, we used 2.3-μm-thick LPCVD-ZnO treated with an argon plasma for 7' (Z2.3 7') and 45' (Z2.3 45'). The second superstrate was chosen to provide a very smooth reference. For comparison, a sputtered-etched ZnO (ZSE) was also used, since it is known to provide a very favorable texture for the growth of high-quality silicon layers due to the large smooth craters on its surface (see Chap. 2). No optimization for the matching of the top- and bottom-cell current densities was performed and no intermediate reflector was used. For the back electrode, a lightly doped LPCVD-ZnO was chosen, with a reduced thickness of 1.5 μm, as compared to the standard 2.3 μm. The electrical performances are summarized in Tab. 5.3, and the *J–V* and EQE curves of these solar cells, as measured with a white dielectric back reflector, are shown in Fig. 5.7.

Table 5.3: *Performance (as-deposited) of thin micromorph tandem solar cells, implementing a wide-bandgap a-Si:H top cell and a high-V_{oc} μc-Si:H bottom cell. The designated area of the solar cells is 1 cm^2. The ZSE was kindly provided by Jürgen Hüpkes and Matthias Meier from Forschungszentrum Jülich in the frame of the FP7 project "Fast Track". The results are shown with their kind authorization.*

Superstrate	J_{sc} (EQE$_{top}$ / EQE$_{bottom}$) [mA/cm^2]	*FF* [%]	V_{oc} [V]	η (IV) [%]
Z2.3 45'	8.46 / 9.04	71.7	1.53	9.3
ZSE	9.29 / 8.89	78.7	1.49	9.9
Z2.3 7'	9.48 / 11.58	70.9	1.38	9.2
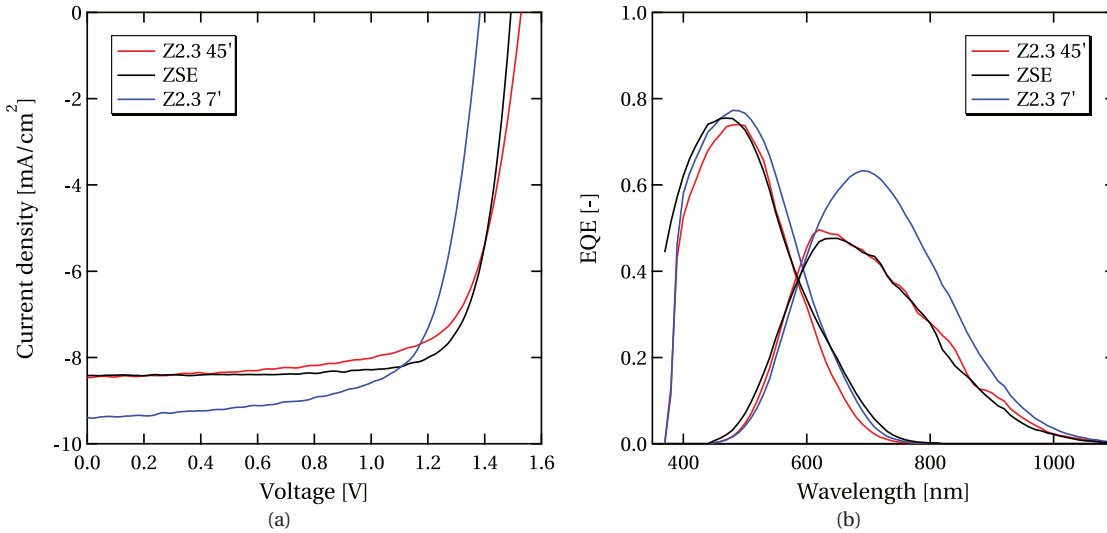
Figure 5.7: *J–V (a) and EQE (b) curves of thin micromorph tandem solar cells, implementing an a-Si:H top cell with wide bandgap and a high-V_{oc} μc-Si:H bottom cell.*

A record V_{oc} value of 1.53 V is obtained on the very smooth superstrate: In comparison, state-of-the-art V_{oc} values for micromorph tandem solar cells are in the range of 1.45 to 1.47 V, for bottom-cell thicknesses from 1.7 to 2.5 μm [Biron 13c, Tan 13, Feltrin 13].

A unexpected lower value of 1.49 V is obtained on the ZSE superstrate, which represents a drop of 40 mV that can not be fully attributed to the recombination junction between the top and bottom cells, or to reduced performance of the bottom cell. Indeed, a very high *FF* value above 78% is obtained for the bottom-limited tandem solar cell deposited on ZSE, indicating the high quality of the bottom cell. We thus attribute the drop in V_{oc} to the ZSE–p-doped layer interface in the a-Si:H top cell, which was not optimized for a ZSE superstrate, but for LPCVD-ZnO.

Except for the solar cell deposited on ZSE, the other two tandem cells are top limited, and present lower *FF* values of 71.7 and 70.9%. Furthermore, the tandem cell on Z2.3 7' has a much lower V_{oc} of 1.38 V, due to the inappropriate superstrate roughness. Note that in this case not only the bottom cell is affected by the lowered performance, but also the top cell with wide-bandgap absorber layer, which is very sensitive to superstrate roughness [Stuckelberger 13].

To clearly differentiate the losses of the top and bottom cells, further investigations must be performed, *e.g.* by means of a "current-matching machine" [Bonnet-Eymard 13], which permits one to properly evaluate the *FF* evolution as a function of the matching conditions.

The outstanding V_{oc} achieved for such thin micromorph solar cells are of significant importance for next-generation multi-junction devices, including triple- and quadruple-junction solar cells [Kim 13, Schüttauf 14, Isabella 14], but the deposition rate of both sub-cells is still too low. Still, this result paves the road towards single-junction μc-Si:H solar cells with efficiencies above 11% and multiple-junctions requiring the use of less silicon for similarly high efficiencies.

5.3 A fully passivated μc-Si:H device?

We have just shown that a very high V_{oc} can be reached with thin μc-Si:H devices, provided a high-quality bulk material is used. The remarkable V_{oc} of 608 mV which was obtained, together with a high *FF*, demonstrates the potential of μc-Si:H, when compared to the best values currently obtained with crystalline silicon on glass [Dore 14].

A natural extension of the concept used to further increase V_{oc} is to passivate the p–i interface as well. Indeed, assuming that the bulk material quality is optimum and the n-doped side is perfectly passivated, the p-doped side would then become the limiting interface of our device. However, using the same concept of an a-Si:H layer as a buffer layer in the p–i–n configuration implies growing a μc-Si:H absorber layer on top of an a-Si:H passivation layer, possibly hindering a good nucleation of μc-Si:H and leading to a too large (amorphous) incubation phase at the p–i interface. This limitation can be overcome by going to an n–i–p configuration [Yue 08], where a similar issue would then occur at the n-doped side. Another possibility would be to make a combination of both a-Si:H layers and seed layers for the μc-Si:H absorber layer using a very crystalline thin incubation layer on top of the a-Si:H layers. The control of this process would be difficult as this seed layer would be deposited

in a hydrogen-rich plasma, leading to potential etching of the layers below and to a not well-defined interface [Fontcuberta i Morral 00].

5.3.1 Method to reach the open-circuit voltage limit of μc-Si:H solar cells

A method to probe the ultimate V_{oc} for μc-Si:H solar cells is proposed as follows, drawn in Fig. 5.8.
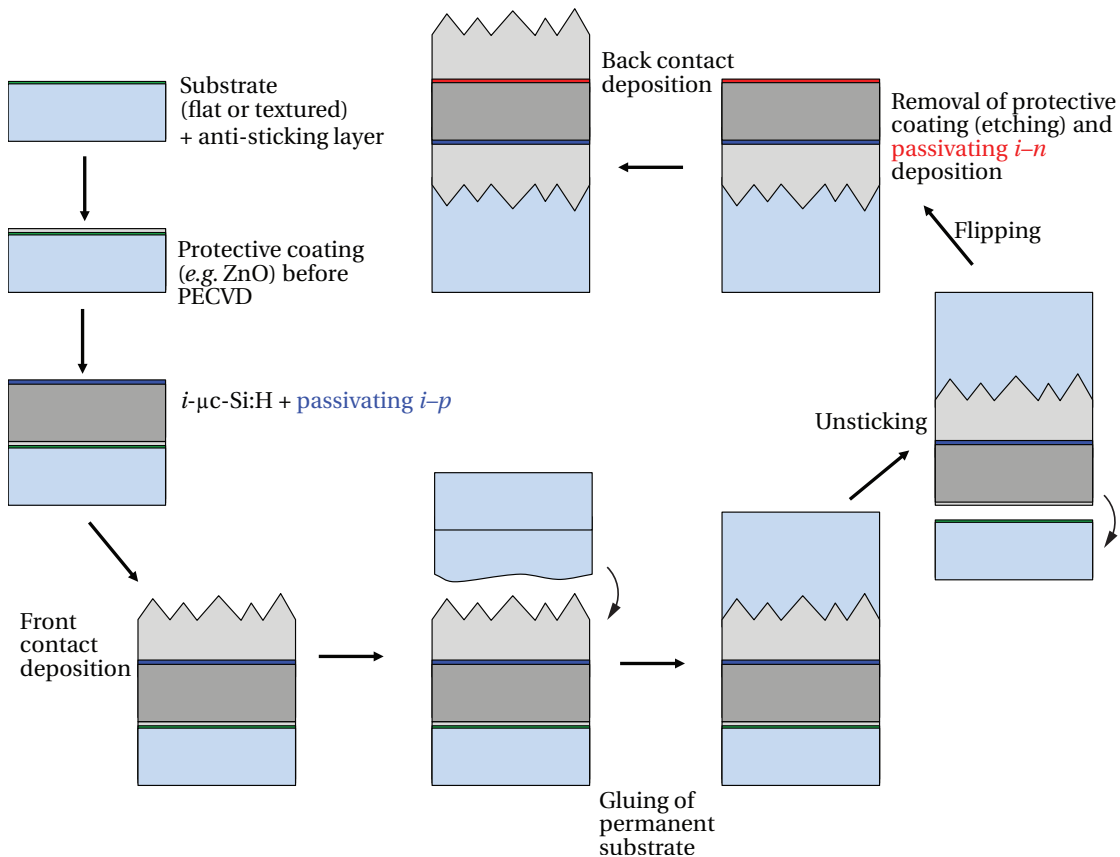
Figure 5.8: *Fabrication scheme of a fully passivated μc-Si:H device, involving a layer transfer technique.*

First, an anti-sticking layer is deposited on a temporary substrate. A protective layer (*e.g.* a thin ZnO layer) is then deposited on the anti-sticking layer to avoid a direct exposure to the plasma and remove any uncontrolled contamination. An absorber layer is then grown on top of the substrate, terminated by a passivated doped layer. After deposition of a front electrode, the layers are glued onto a permanent substrate and detached from the temporary substrate, thus flipping the layer sequence. The device is then finished by removing the protective coating (*e.g.* via chemical etching), by depositing the other passivated doped layer, and by depositing a back electrode.

This way, a high-quality μc-Si:H absorber layer can be deposited and both doped layers can be controlled independently. If present, an undesired incubation layer can be removed during the etching step. However, the process can be tedious and would need optimization of all steps. Moreover, the proposed design is optically not optimal, as a potentially highly reflective interface would be present (flat and non-scattering ZnO–Si interface). Such a process is however practicable: based on a nanomoulding process [Battaglia 11b], unsticking and flipping of a complete a-Si:H solar cell has already been demonstrated [Escarré 12a].

5.4 Conclusion

In Sec. 5.1, the shunt-quenching properties of SiO_x p-doped layers were compared to μc-Si:H p-doped layers. Such properties were evaluated by the VIM technique, and it was found that SiO_x p-doped layers can very efficiently limit V_{oc} losses at a lower illumination level.

In Sec. 5.2, we introduced passivating interfaces for single-junction μc-Si:H solar cells and implemented them at the μc-Si:H i–n interface of thin single-junction and tandem μc-Si:H solar cells, achieving record V_{oc} values of 0.608 V and 1.53 V, respectively. By increasing the thickness of the absorber layer, the bulk quality of our μc-Si:H material was found to be a limiting factor for the cell efficiency, thereby canceling any beneficial effects from improved interfaces, which was also illustrated by a simple simulation.

Finally, a concept to improve the V_{oc} values of single-junction μc-Si:H solar cells, based on passivation of both sides of a thin devices, was discussed in Sec. 5.3.

6 Highly crystalline absorber layers with fluorinated precursors

To obtain a high short-circuit current density (J_{sc}) without compromising on material quality, we investigate the potential of highly crystallized microcrystalline silicon (μc-Si:H) layers, as obtained by plasma-enhanced chemical vapor deposition (PECVD) with silicon tetrafluoride (SiF$_4$) as an additional precursor.

In Sec. 6.2, several growth regimes are investigated in terms of deposition rate (D_r) and Raman crystalline fraction (R_c). D_r values of up to 4 Å/s are demonstrated, combined with highly crystallized layers.

In Sec. 6.3, these layers are compared to layers obtained with standard deposition regimes, as described in Chap. 3. Layers with both high and standard R_c are analyzed with secondary ion mass spectrometry (SIMS), Fourier transform infrared spectroscopy (FTIR), and X-ray diffraction (XRD). First, SIMS measurements show that the use of SiF$_4$ does not induce additional contamination in baseline processes. FTIR analysis of the hydride stretching modes reveals that similar hydrogen incorporation can be obtained in highly crystallized films deposited using SiF$_4$ or silane (SiH$_4$) precursors, whereas XRD analysis demonstrates that layers obtained with SiF$_4$ do not exhibit a (220) preferential orientation. This orientation, typically obtained with SiH$_4$-based chemistry, is generally attributed to device-grade material.

In Sec. 6.4, we implement selected films as absorber layers in single-junction solar cells, reaching open-circuit voltages (V_{oc}) as high as 470 mV, and a conversion efficiency (η) of 8.3%, for highly crystalline solar cells (R_c>80%). Although superstrate roughness also limits cell efficiency, and especially fill factor (*FF*), no porous zones as can be observed by transmission electron microscopy (TEM) for standard cells obtained with SiH$_4$-based chemistry are observed. Structural defects are however found in large grains. A record total J_{sc} of 31.9 mA/cm^2 is demonstrated for a micromorph tandem cell, thanks to improved absorption in the near-infrared (NIR), for a total silicon thickness of 3.4 μm, which makes it the highest reported value for this configuration.

6.1 Historical development

Fluorinated precursors were first proposed as an alternative method for the fabrication of amorphous silicon (a-Si:H) in 1978, to reduce the instability problems associated with hydrogen in that material [Ovshinsky 78, Goodman 79, Madan 80]. Their use showed, among others, a potential for improved photo-conductivity, charge-carrier mobility and diffusion length, together with an increased light-soaking stability [Bruno 91, Kim 96, Cicala 98, Nishimoto 01, Zhang 04, Giangregorio 06, Bruno 09].

Fluorinated precursors were also used for the fabrication of intrinsic and doped fluorinated microcrystalline silicon (μc-Si:F:H) layers, at first obtained by chemical vapor deposition (microwave discharge system) at high temperatures above 250 °C [Hanna 86, Shibata 87a, Shibata 87b, Hanna 88, Hourd 91, Ishihara 93]. Several studies then showed that for such depositions, both crystallinity and crystallographic preferential orientation can be controlled by the precursor gas ratio [Tsu 80, Syed 97, Kamiya 99, Cicala 01, Kuo 03, Haddad-Adel 07].

The work reported here is based on the developments carried out at a lower temperature (~200 °C) by Ecole Polytechnique in Palaiseau (France). Kasouit *et al.* proposed to use small amounts of SiF$_4$ and hydrogen (H$_2$), highly diluted in argon (Ar), to grow fully crystallized layers for thin-film transistor applications [Kasouit 02, Vanderhaghen 02, Kasouit 03, Kasouit 04b]. It was suggested that crystals formed in the plasma contribute to the growth of μc-Si:F:H films, with no amorphous phase due to preferential etching of this phase by fluorine ions [Kasouit 04a]. It was also shown that for such highly crystallized layers, the use of SiF$_4$ led to films with improved electronic properties, thanks to the presence of larger grains, as compared to layers obtained with SiH$_4$ [Djeridane 07, Djeridane 08, Roca i Cabarrocas 08].

6.1.1 Use of fluorinated precursors in solar cells

Comprehensive studies on the effect of adding SiF$_4$ into radio frequency (RF) and very high frequency (VHF) plasmas for making a-Si:H, a-SiGe:H and μc-Si:H solar cells with improved material quality were conducted at Unisolar Ovonic and ECD. A small amount of SiF$_4$ did not show any observable effect on solar cell performance, and when the ratio of SiF$_4$ to SiH$_4$ was increased above a certain level, the material quality became poor.[1]

However, in a publication by Zhang *et al.* [Zhang 08], a solar cell with a V_{oc} of 523 mV and a conversion efficiency of 8.3% was demonstrated, together with a high R_c of 80%, using SiF$_4$ and H$_2$ diluted in Ar. This promising result suggested that a high defect density is not an intrinsic characteristic of highly crystallized material, even though in this particular case, the μc-Si:F:H absorber layer was additionally exposed to H$_2$ plasma to improve surface passivation of the crystalline grains.

In [Moreno 12], the influence of the grain size on the NIR absorption of such single-junction

---

[1]Dr. Baojie Yan (Unisolar Ovonic), private communication.

μc-Si:F:H solar cells was studied. In particular, it was shown that solar cells with absorber layers containing the largest grains presented the highest absorption in the NIR. It was also demonstrated that the ratio of SiF_4 to H_2 in the plasma was a key parameter to tune the fraction of large grains (as measured by spectroscopic ellipsometry) within the μc-Si:F:H layer. Even with increased NIR absorption, the highest J_{sc} reached only 20 mA/cm^2, which, combined with a V_{oc} of 480 mV and a *FF* of 60%, led to a relatively low conversion efficiency of 6%.

More promising results were achieved by Dornstetter *et al.* [Dornstetter 13, Dornstetter 14], demonstrating single-junction solar cells with a V_{oc} well above 500 mV leading to efficiencies above 9% for fully crystallized solar cells. The role of H_2 was particularly investigated and it was established that a certain amount of atomic hydrogen (H) was needed to evacuate fluorine atoms generated by the dissociation of SiF_4, in the form of HF molecules. Interestingly, the weak dependence of V_{oc} on absorber layer thickness (>500 mV for ~4 μm) indicated that high-quality material can be obtained with SiF_4, which was confirmed with measurements of low defect-induced sub-gap absorption.

Such highly crystallized layers with maintained electronic properties and increased absorption in the NIR are of high interest for use as an absorber layer in the bottom cell of multi-junction devices, as demonstrated in Sec. 6.4.5, with micromorph tandem cells matched at 15 mA/cm^2.

6.2 Deposition of fluorinated microcrystalline silicon layers

6.2.1 Description of experimental parameters

Throughout this work, the deposition of μc-Si:F:H layers and solar cells was performed in a large-area KAI-M^{TM} research system equipped with a closed plasma chamber [Bubenzer 90], with a fixed inter-electrode gap of 12 mm, an excitation frequency of 13 MHz and a typical base pressure of 2–3·10^{-7} mbar. The maximal allowed process temperature for long depositions (*i.e.* >1 h) was 230 °C. Following previous studies performed at Palaiseau [Djeridane 08], pressure and power series were performed at various dilutions "k:l:m" of the precursors, where k, l and m are integers denoting the flux setpoints, expressed in sccm, of SiF_4, H_2 and Ar respectively (*i.e.* [SiF_4], [H_2] and [Ar]), normalized by their greatest common divisor. Tab. 6.1 shows the current limitations of precursor fluxes due to the installed mass-flow controllers.

Table 6.1: *Limitations of the precursor fluxes by the mass-flow controllers.*

Gas	maximal flux [sccm]	minimal flux [sccm]
SiF_4	108	~2–5
H_2	3051	~80–90
Ar	2840	~60–80
SiH_4	181	~4–7

As previously mentioned, the [H$_2$]:[SiF$_4$] ratio was expected to be a key parameter determining both the microstructure and the electronic quality of the layers. Unfortunately, as high H$_2$ fluxes were daily used for baseline depositions of standard μc-Si:H deposition, the high-flux mass-flow controller in place was not very accurate nor reproducible at the minimum setpoint value, as needed for μc-Si:F:H. Moreover, for such low setpoint values, a significant discrepancy between the setpoint and the measured flux was observed (>10 sccm). Values below 1.5 for the [H$_2$]:[SiF$_4$] ratio were therefore not investigated. Furthermore, as the KAI-M was predominately operated for high-efficiency processes, the use of "extreme" or more "exotic" deposition regimes was prohibited and has been carefully avoided (such as *e.g.* leading to too high powder production).

Note that before each deposition, both the chamber and plate were coated with a thin intrinsic μc-Si:H layer. This layer, acting as a nucleation layer, was necessary to avoid peeling and obtain a successful μc-Si:F:H deposition (see details below). We used four substrates: two pieces of AF32 glass, a small piece of crystalline silicon (c-Si) wafer and AF32 glass coated with a 2-μm-thick zinc oxide layer deposited by low-pressure chemical vapor deposition (LPCVD-ZnO) and treated with an Ar plasma for 20' (Z2 20'). Standard cleaning with a nitrogen trifluoride (NF$_3$)/Ar-based plasma, followed by a H$_2$ plasma, was systematically performed after each layer deposition.

6.2.2 First depositions of fluorinated microcrystalline silicon layers at PV-lab

Fig. 6.1 shows the first depositions of μc-Si:F:H layers done at PV-lab on glass and ZnO.

(a)   (b)   (c)
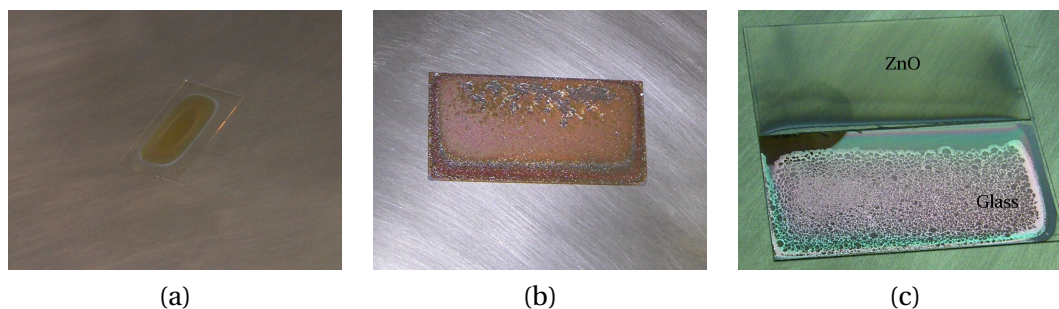
Figure 6.1: *(a) The first deposition of a μc-Si:F:H layer, which turned out to be etching and redeposition of the coating of the chamber. (b) Systematic peeling, which was observed when no pre-coating of the substrate or the chamber was used. This issue was solved by using a thin coating of the glass (p-doped μc-Si:H). (c) The first deposition on LPCVD-ZnO, which resulted in a strong reduction of the ZnO by the fluorinated plasma.*

In the first, unsuccessful, deposition trial of μc-Si:F:H, the μc-Si:H coating of the reactor and the plate was etched and redeposited on the substrates, while no μc-Si:F:H deposition occurred (see Fig. 6.1 (a)). No deposition was obtained with no pre-coating of the reactor, indicating that preconditioning of the reactor is crucial for μc-Si:F:H layer development. The

first successful deposition of a μc-Si:F:H layer directly on glass resulted in strong peeling of the layer (Fig. 6.1 (b)). In Fig. 6.1 (c), the experiment shown in Fig. 6.1 (b) was repeated with Z2 20' as additional substrate, resulting in a strong reduction of ZnO by the fluorinated plasma.

The strong chemical reaction observed between LPCVD-ZnO and the SiF$_4$ plasma can also be observed in Fig. 6.2, in which photographs of μc-Si:F:H solar cells before and after deposition are shown. In this case, the various superstrates were already covered with a p-doped silicon oxide (SiO$_x$) layer that, however, did not completely cover the superstrate, leaving an uncoated LPCVD-ZnO border of about 1 mm at the edges of the sample.

(a)   (b)
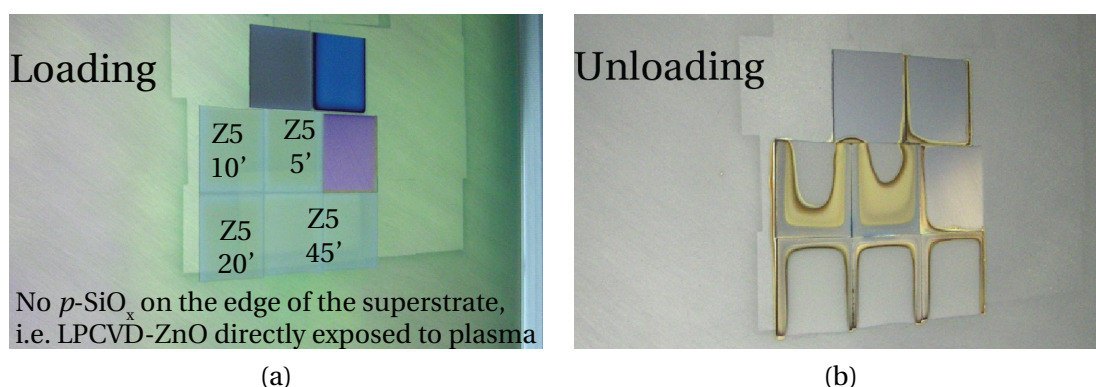
Figure 6.2: *Photographs of μc-Si:F:H solar cells before (a) and after (b) deposition, in which LPCVD-ZnO was directly exposed to a SiF$_4$-based plasma. A strong reaction occurred, extending to the other superstrates (a-Si:H top cells), while the plate was unaffected.*

Similarly as in the previous test with Z2 20', a strong reaction occurred between the SiF$_4$-plasma and LPCVD-ZnO, further extending to the whole superstrate, while deposition on the coated plate was unaffected. We established that solar cells deposited in such conditions were heavily p-type contaminated, following the doping of LPCVD-ZnO. Such experiments thus demonstrate that LPCVD-ZnO superstrates should completely be coated before μc-Si:F:H layer deposition.

Hence, to solve the issues of peeling on glass and the strong reaction of SiF$_4$ chemistry on LPCVD-ZnO, we always deposited a 20-nm-thick p-doped μc-Si:H layer on the substrates (in a dedicated, separate, deposition) in addition to the thin standard intrinsic μc-Si:H coating of the chamber walls and plate. Once optimum pre-conditoning conditions were established, we focused on assessing the useful deposition parameter space, concentrating on deposition rate and R_c.

6.2.3 Deposition rate as a function of deposition conditions

Fig. 6.3 (a) shows the evolution of the deposition rate of μc-Si:F:H layers deposited at 200 °C as a function of gas dilution and injected power, at an excitation frequency of 13 MHz and with [SiF$_4$]=78 sccm.
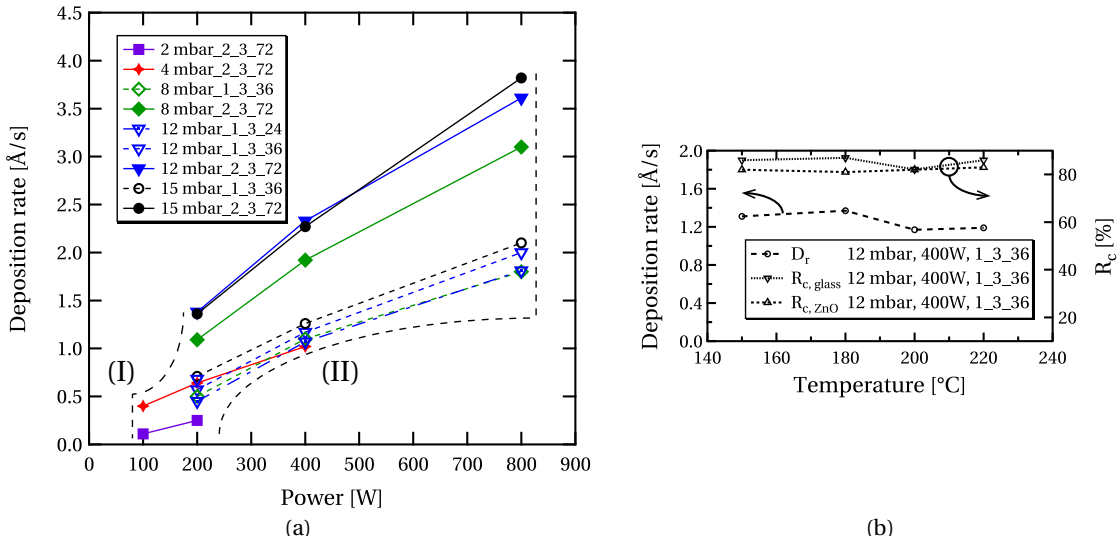
Figure 6.3: *Deposition rate as function of deposition conditions (a) and temperature (b) for several deposition regimes. Here, R_c is indicated as well, as measured both on glass and on a ZnO substrate (Z2 20').*

Based on the calculation of Strahm *et al.* [Strahm 07], assuming that all silicon atoms contribute to film growth and that μc-Si:F:H and μc-Si:H films have the same density, the maximal deposition rate ($D_{r,max}$) with [SiF$_4$]=78 sccm is

$$D_{r,max} = 0.0962 \frac{[SiF_4]}{A} \, [\text{Å/s}] = 12.2 \, \text{Å/s},$$

where A is the total surface of the plasma box. Note that no powder was observed on the plate after the deposition, for all data shown in Fig. 6.3. At low power values in zone (I) delimited by the dashed line, the plasmas were highly unstable: although ignition was feasible, the plasma was flashing and the process was highly irreproducible. Depositions performed in these conditions were thus excluded from the study. When the power was increased too much, zone (II) was reached, as delimited by the second dashed line, and sparks then appeared in the plasma. Depositions were thus not performed in this range either.

Between these two zones, the general trend observed is an increase of D_r with increased power and pressure. According to [Guo 98, Kondo 00, Roschek 02], for SiH$_4$-H$_2$ discharges, D_r is proportional to the generation rate of precursors ($\frac{dX}{dt}$), that is:

$$\frac{dX}{dt} = \sigma v_{th} [SiH_4] N_e,$$

where σ is the dissociation cross section of silane with electrons in the plasma having a higher energy than the dissociation energy threshold value, v_{th} is the thermal velocity of electrons, [SiH$_4$] is the density of SiH$_4$ molecules, and N_e is the density of energetic electrons responsible for the reaction. This equation implies that D_r is proportional to the SiH$_4$ partial pressure for

constant electron temperature [Guo 98, Rath 04].

A similar effect is probably observed here for the SiF_4 precursor, as we observe a systematic increase of D_r for increasing pressure (for the same dilution). Since we rejected "dusty" plasmas at high power, we did not explore regimes where D_r usually drops, either due to a reduction of the generation rate of precursors (due to the reduction of electron temperature at a higher pressure), or due to powder formation [Stuckelberger 13]. However, this drop in D_r was observed by Djeridane *et al.* [Djeridane 08] using similar SiF_4 chemistry for plasmas with powder.

When changing the $[SiF_4]{:}[H_2]{:}[Ar]$ dilution from 2:3:72 to 1:3:36 (*i.e.* doubling $[H_2]$), a strong reduction of D_r is observed for the used pressures, as can be observed in Fig. 6.3 by comparing the solid and empty symbols. Based on the recent growth model of Dornstetter *et al.* [Dornstetter 14], in which it is shown that a certain amount of H is needed in the plasma to evacuate fluorine ions in the form of HF molecules before obtaining film growth, we believe that adding more H can contribute to etching of the film [Tsai 89, Matsuda 99, Fontcuberta i Morral 02] and thus reduce D_r. Film growth is thus probably determined by the competitive effects of deposition of radicals and etching (by H and F), this latter effect being controlled by the amount of free H atoms in the plasma.

For a reduction of [Ar] by a factor of $\frac{2}{3}$ (changing the dilution from 1:3:36 to 1:3:24), no significant change in D_r is observed. Even though the exact role of Ar is yet still unclear, Djeridane *et al.* [Djeridane 08] suggested that a high dilution of Ar can enhance the dissociation of precursors and change the ratio of large to small grains while keeping R_c constant.

Using the deposition regimes shown in Fig. 6.3, deposition rates of up to 4 Å/s were obtained. We believe that higher D_r values should be possible by either further increasing the pressure—even though the maximum used pressure of 15 mbar is already quite high—, by further reducing $[H_2]$, by optimizing [Ar], by using higher excitation frequencies, or by narrowing the inter-electrode gap.

In a second step, the effect of the deposition temperature (T) was evaluated for a specific deposition regime (12 mbar, 400 W and dilution of 1:3:36). Fig. 6.3 (b) shows the evolution of D_r and R_c as a function of T. No significant dependence on T was observed for either D_r or R_c, confirming the results of Djeridane *et al.* [Djeridane 08] in the chosen narrow temperature range, which corresponds to the usual temperatures for solar cell fabrication.

6.2.4 Crystallinity as function of deposition conditions

Fig. 6.4 shows the measured R_c for the layers in Fig. 6.3, both on glass and on LPCVD-ZnO (Z2 20').

No significant difference is observed between glass and ZnO substrates for pressures above
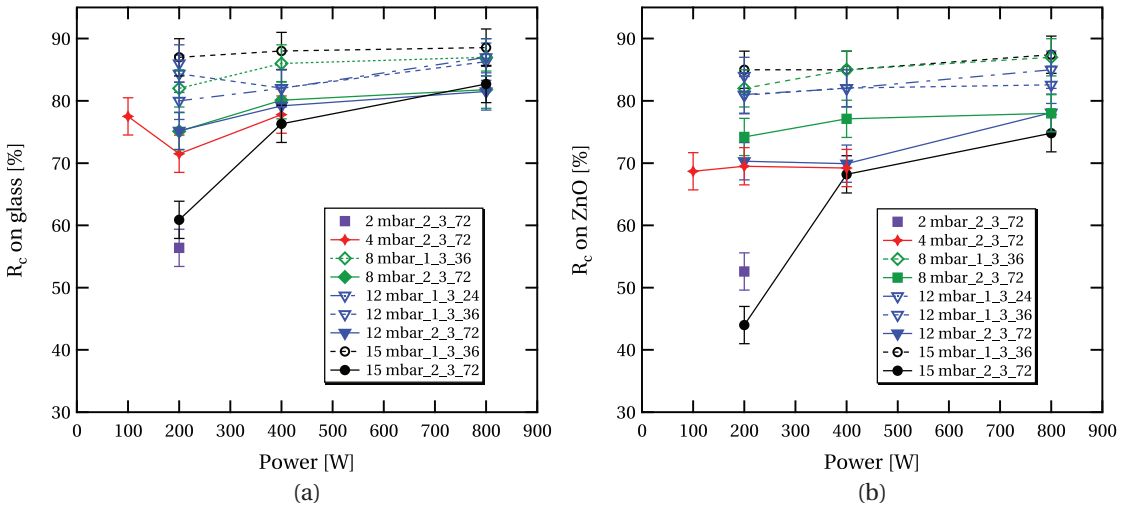
Figure 6.4: *Evolution of R_c as a function of pressure, precursor ratio and power, on glass (a) and on LPCVD-ZnO (Z2 20') (b).*

4 mbar. Note that the thicknesses of the films are not constant, ranging from 100 nm (for the points at the lowest possible power at pressures of 2 and 4 mbar) to 400 nm. However, since the obtained R_c values are very high (mostly between 75% and 85%), especially for layers with higher [H_2] and also for the thinnest films, we do not expect a large variation as could be induced by a thick a-Si:H incubation layer. Layers with R_c lower than about 75% are obtained only for the lowest possible power, below which the plasma is flashing and highly unstable. Note that the point at 2 mbar and 100 W from Fig. 6.3 is not evaluated here as its thickness is below the specified range.

When going to higher [H_2] (*i.e.* empty symbols), extremely high values of R_c are obtained (up to almost 90%), which, according to our fitting procedure [Droz 04], can be considered as fully crystallized. Indeed, for μc-Si:F:H layers, part of the left shoulder of Raman spectra, usually attributed to the amorphous phase of μc-Si:H, might be related to the crystalline part as well, with a peak linked to crystalline grain boundaries at around 500 cm^{-1} [Dornstetter 13], which was not implemented in our fitting procedure. This suggests that the R_c values we assessed are rather a lower bound for the "real" crystalline fraction. Our results hence suggest that the [H_2]:[SiF_4] ratio plays an important role in the growth and crystallization process in such plasma chemistry, as is also known for SiH_4-based discharges [Matsuda 99, Sriraman 02, Fujiwara 04], but as lower [H_2] was not investigated, further research is necessary. Our results suggest that lower [H_2] would lead to higher D_r and μc-Si:H with lower R_c. Thus, this research should include the study of the conjugate roles of gas dilutions (especially [Ar] and lower [H_2]), of other deposition parameters such as excitation frequency, inter-electrode gap, and temperature, and of the possibility of alloying or doping. Doping would be interesting, especially the development of p-doped μc-Si:F:H layers, as it is usually difficult to obtain such layers with high R_c [Jenq-Shiuh 92, Ghosh 92, Flückiger 94, Demichelis 94, Saleh 03, Cuony 10].

6.3   Comparison with standard microcrystalline silicon

We next investigated to what extent these highly crystalline layers are different from or similar to our usual μc-Si:H layers with standard and high R_c, and how they are compatible with our usual PECVD processes in terms of contamination of the reactor. SIMS analyses were therefore first performed on three layers, as discussed in the following.

6.3.1   Evaluation of impurities by SIMS analysis

Various layers were deposited on double-polished 250-μm-thick undoped c-Si wafers, coated with a fake p-μc-Si:H (using a recipe similar to the one for a standard p-doped layer, but without a dopant precursor) as the seed layer.

These layers correspond to (i) a reference high-quality 500-nm-thick μc-Si:H layer, deposited after the standard reactor cleaning and coating procedure and (ii) a layer stack made of μc-Si:F:H/p-doped SiO_x/SiO_x buffer/μc-Si:H.

Note that for the second layer stack, the sample was taken out of the reactor after the deposition of the μc-Si:F:H layer, and the standard reactor cleaning and coating procedure was performed before the deposition of the p-doped SiO_x layer, hence reproducing a subsequent deposition of a standard cell [Bugnon 14] on top of the μc-Si:F:H layer. The μc-Si:F:H layer was deposited at 12 mbar, a dilution of 1:3:36 and a power of 200 W (D_r=0.7 Å/s, R_c=85%). In this stack, both the μc-Si:F:H and μc-Si:H layers have the same thickness (340 nm). The SiO_x layers were deposited in a separate chamber and there was no vacuum break before the subsequent μc-Si:H layer deposition.

The measured elemental concentration profiles are shown in Appendix B. Concentrations of boron, zinc, phosphorus, carbon and nitrogen did not show any abnormal or unexpected results. The results of bulk concentrations as measured for O, F and H are summarized in Tab. 6.2.

Table 6.2: *Bulk O, F and H concentrations, as measured by SIMS, for several microcrystalline materials.*

Layer	O [cm^{-3}]	F [cm^{-3}]	H [cm^{-3}]
μc-Si:F:H	$(1.7 \pm 0.1) \cdot 10^{18}$	$(7.3 \pm 0.2) \cdot 10^{18}$	$(2.9 \pm 0.1) \cdot 10^{21}$
μc-Si:H reference	$(8.0 \pm 0.3) \cdot 10^{17}$	$(1.7 \pm 0.3) \cdot 10^{17}$	$(6.7 \pm 0.2) \cdot 10^{21}$
μc-Si:H after use of SiF_4	$(8.5 \pm 0.6) \cdot 10^{17}$	$(2.4 \pm 0.3) \cdot 10^{17}$	$(7.3 \pm 0.2) \cdot 10^{21}$

Using SiF_4-based plasma chemistry has no detrimental contamination effects in our reactor. Indeed, low O and F bulk concentrations are observed for both μc-Si:H reference layer and a μc-Si:H layer deposited after the use of SiF_4. The measured O concentrations, namely ~$8 \cdot 10^{17}$ cm^{-3}, are below a commonly admitted maximal accepted range of up to

~$1 \cdot 10^{19}$ cm^{-3} [Abramov 10, Shah 10]. The slight difference in F concentration ($1.7 \cdot 10^{17}$ cm^{-3} and $2.4 \cdot 10^{17}$ cm^{-3}) in both μc-Si:H layers is too low to have a significant effect on cell performance.

By comparing μc-Si:H and μc-Si:F:H layers together, it appears that a higher amount of F is incorporated in the μc-Si:F:H layer, with an average value of $7.3 \cdot 10^{18}$ cm^{-3} for μc-Si:F:H as compared to a value of around $2 \cdot 10^{17}$ cm^{-3} for standard μc-Si:H deposited without a fluorinated precursor.

For the μc-Si:F:H layer, the average O bulk concentration is slightly higher than for μc-Si:H layers ($1.7 \cdot 10^{18}$ cm^{-3} for the μc-Si:F:H layer and ~$8 \cdot 10^{17}$ cm^{-3} for standard μc-Si:H layers), but also below critical concentration.

However, a difference is observed for the H concentrations, with average values of $2.9 \cdot 10^{21}$ cm^{-3} for μc-Si:F:H and ~$7 \cdot 10^{21}$ cm^{-3} for standard μc-Si:H layers. The lower H concentration for the sample deposited with SiF$_4$ is linked to probable full crystallization of the layer and the low amount of a-Si:H tissue, as shown in the following section.

6.3.2 Structural evaluation by FTIR and Raman spectroscopy

To further investigate the differences between our best μc-Si:H layers and μc-Si:F:H layers, FTIR and Raman spectroscopy were performed. These Raman spectra were recorded for layers deposited on glass, with a Bruker Senterra spectrometer and an excitation wavelength of 532 nm [Choong 13].

FTIR spectra were recorded with a Nicolet 8700 spectrometer from Thermo Scientific. As with the SIMS analyses in Sec. 6.3.1, the layers were deposited on intrinsic c-Si wafers. For each sample, infrared transmittance (T) was evaluated by dividing the raw spectrum of the sample by the raw spectrum of the background (c-Si substrate). The spectrometer was constantly purged with nitrogen and a waiting time of 20' was used before each measurement. To minimize parasitic absorption of water and carbon dioxide due to the non-controlled atmosphere in the room, and artifacts from the infrared-source fluctuations, a new background was recorded and used for each sample. Absorbance (A) was calculated as $A = -\log_{10}(T)$, and normalized to unity at its maximum, then simply referred to as absorption. A linear baseline correction between 1800 and 2220 cm^{-1} was applied.

Tab. 6.3 shows the deposition conditions (plasma excitation frequency (v), pressure (p), power (P) and resulting D_r) for various μc-Si:H and μc-Si:F:H layers. R_c was calculated from the curves shown in Fig. 6.5. The thickness (t) of the layers was evaluated on glass with a profilometer. The "SiF" layers were deposited at 400 W, a dilution of 1:3:36, and T=200 °C, for three different pressures (8, 12 and 15 mbar).

A grading, *i.e.* a varying flux of the silicon precursor in the early stages of the growth, which is typically performed to achieve higher performance in the standard μc-Si:H solar cells

[Vetterl 03], was applied to the standard μc-Si:H layers here as well. All layers were grown on thin (<20 nm) μc-Si:H seed layers. Due to peeling, we were not able to get the same thickness for all layers, especially the ones deposited with SiF_4. Even though Smets *et al.* [Smets 08a] demonstrated that FTIR spectra of μc-Si:H layers can have a strong thickness dependence, highly correlated to an evolution of R_c as a function of thickness, we do not expect such variation here as deposition conditions of our standard layers (with lower R_c around 50–60%) ensure fast μc-Si:H nucleation and a minimal incubation layer (see Chap. 3). Moreover, the other layers have a high R_c(>75%), also the thinnest ones, suggesting a high-crystallinity growth from the start of the layer.

Table 6.3: *Selected intrinsic μc-Si:H and μc-Si:F:H layers investigated with FTIR, Raman spectroscopy and XRD. A grading, i.e. a varying flux of the silicon precursor in the early stages of the growth, is typically performed to achieve higher performance in the standard μc-Si:H solar cells.*

	SysB std	SysB high R_c	KAI std	KAI high R_c	SiF 8 mbar	SiF 12 mbar	SiF 15 mbar
ν [MHz]	70	70	13	13	13	13	13
p [mbar]	0.7	0.7	9	9	8	12	15
P [W]	3	3	350	500	400	400	400
D_r [Å/s]	1.1	1.0	2.8	2.2	1.1	1.2	1.3
R_c [%]	49	76	61	84	81	85	79
t [nm]	400	400	500	400	260	140	340
Grading?	[SiH$_4$]: 3 steps	no	[SiH$_4$]: 2 steps	no	no	no	no

Raman spectroscopy

As previously mentioned, these seven different layers were first evaluated by Raman spectroscopy. Fig. 6.5 shows the Raman shift spectra of the μc-Si:H and μc-Si:F:H layers presented in Tab. 6.3. For each layer, the corresponding calculated R_c is given [Droz 04].

For μc-Si:H layers, higher R_c values, on the order of 80%, were obtained by increasing the SiH$_4$ dilution in H$_2$ and increasing the power ("KAI high R_c" sample).

Interestingly, such high R_c values are obtained with SiF$_4$ chemistry for layers as thin as 140 nm, whereas larger thicknesses, as used in solar cells, lead to values well above 90%, which are not reachable with our standard μc-Si:H processes. We attribute this discrepancy to a different growth, with larger grains and increased nuclei density. This will be confirmed in this thesis by TEM images (see Sec. 6.4.3), but variations already appear here in the Raman spectra.

Indeed, we observe that for SiF$_4$-based layers, the main peak at 520 cm^{-1} is shifted towards higher wavenumbers, attributed in the case of standard μc-Si:H material to high compressive stress in the layers [Paillard 01, Vetushka 08]. Furthermore, the main peak of SiF$_4$-based material is not symmetrical around 520 cm^{-1}. In this material, such asymmetry has been attributed to the presence of column boundaries [Dornstetter 13]. When thicker such layers
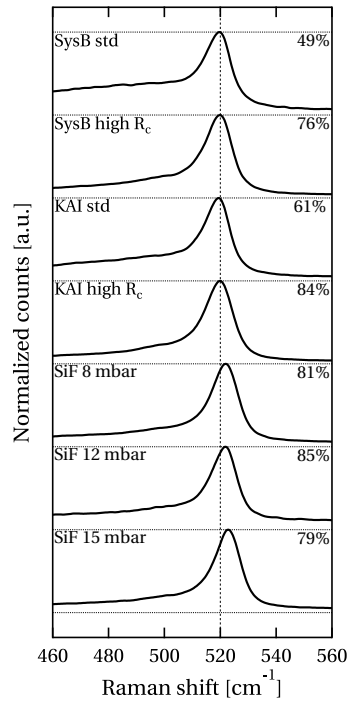
Figure 6.5: *Raman shift spectra of μc-Si:H layers with various R_c and μc-Si:F:H layers.*

were incorporated in solar cells (see Sec. 6.4), R_c values of up to 90–95% were measured, indicating probable complete crystallization with our fitting procedure.

As already mentioned, peeling issues were often encountered when depositing such μc-Si:F:H layers on glass, another indication that high compressive stress is present in these SiF_4-based layers.

Analysis of the hydride stretching mode with FTIR

For the analysis of the infrared (IR) spectra of Fig. 6.6, we use the nomenclature proposed by Smets *et al.* [Smets 03, Smets 08a, Smets 08b], briefly summarized hereafter. This model is based on the analysis of the hydride stretching modes (SM) present in the ~1800–2250 cm^{-1} wavenumber range in FTIR spectra of μc-Si:H layers, where these spectra are deconvoluted into a consistent set of 11 Gaussian curves, attributed to various hydrogen configurations and phases present in μc-Si:H, as summarized in Tab. 6.4.

When looking at the IR spectra of layers with average R_c, *e.g.* "SysB std" and "KAI std," we detect the presence of many features attributed to device-grade material. Indeed, we can recognize low SM (LSM), attributed to the amorphous part of the bulk, consistent with the measured R_c of 48 to 61%. Characteristic kinks of the extreme LSM (ELSM) can be observed at around 1900 cm^{-1}. High SM (HSM), attributed to both the amorphous tissue (2070–2100 cm^{-1}) and the microcrystalline phase (~2120 cm^{-1} and ~2150 cm^{-1}), are visible. It is important to
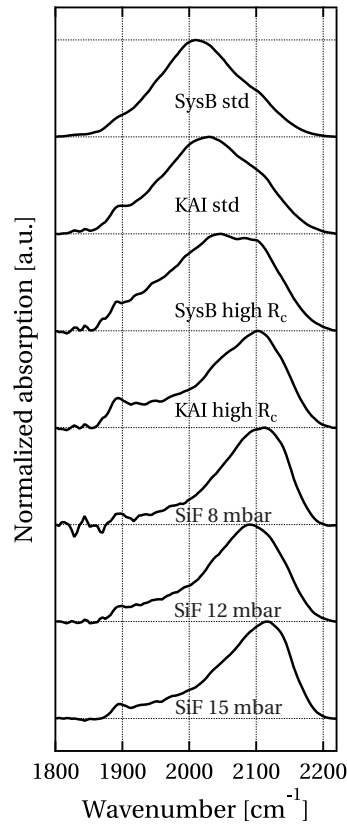
Figure 6.6: *FTIR spectra of the stretching modes of µc-Si:H and µc-Si:F:H (8, 12 and 15 mbar) layers.*

Table 6.4: *Hydride stretching modes in the infrared spectrum of a µc-Si:H layer and their attribution. Taken from [Smets 08a, Smets 08b, Bronneberg 11].*

Full name	Label	Position [cm^{-1}]	Attribution
low SM	LSM	1980–2010	amorphous tissue in bulk, SM in vacancies
medium SM	MSM	2030–2040	amorphous tissue in bulk, SM in vacancies
high SM	HSM	2070–2100	amorphous tissue in bulk, SM on nanovoid surfaces
		~2120	microcrystalline phase
		~2150	
narrow HSM NHSM		2083	mono-, di-, and trihydrides at crystalline grain boundaries
		2103	have large contribution in porous material, disappear when oxidized
		2137	absent in the best cells
extreme LSM ELSM		~1895	unique to µc-Si:H
		~1929	when going from a highly crystalline matrix to an amorphous matrix,
		~1950	they are maximum when NHSM are absent.

note that neither layer exhibits narrow HSM (NHSM), which can appear at 2083, 2103 and 2137 cm^{-1} and are related to crystalline grain boundaries not passivated with *a*-Si:H, and thus prone to post-deposition oxidation. This is confirmed by dark-degradation measurements

of solar cells containing these specific layers as absorber layers, and which show no effects related to post-deposition oxidation (see Chap. 3).

The "SysB high R_c" sample shows features similar to the "SysB std" sample. However, we observe that the LSM peaks (~1980 to 2010 cm^{-1}), attributed to the amorphous tissue, decrease with an increase in HSM (shift of the maximum peak to the right at around 2100 cm^{-1} [Kroll 96]).

For the remaining samples at very high R_c ("KAI high R_c" and "SiF"), different features are observed in the IR. These samples are characterized by a low amount of amorphous tissue, and exhibit rather similar spectra, with some differences in the HSM repartition. Although the "SiF 12 mbar" is the thinnest of all samples, it shows a spectrum similar to the thickest samples deposited with SiF$_4$, with a slight difference in the HSM balance, but with still quasi-absent LSM (*i.e.* at 1980 to 2010 cm^{-1}). This absence of LSM probably also accounts for the lower H content, as measured by SIMS in Sec. 6.3.1.

Conclusion

In conclusion, for these materials, it was shown with Raman and FTIR spectroscopy that:

- Highly crystallized samples can be obtained with SiF$_4$ at a range of deposition pressures.

- Compared to highly crystalline μc-Si:H layers deposited with SiH$_4$, high compressive stress is observed in μc-Si:F:H layers, based on the observation of a shift of the main peak towards higher wavenumbers in the Raman spectrum.

- The IR absorption spectra of hydride stretching modes of both SysB and KAI-M layers with standard R_c (*i.e.* 50–60%) exhibit device-grade material characteristics [Smets 08a].

- Layers with high R_c as obtained with SiF$_4$ exhibit IR spectra similar to standard μc-Si:H layers with very high R_c, although different device characteristics will be observed when these layers are used as absorber layers in solar cells (see Sec. 6.4.4).

6.3.3   Structural evaluation by X-ray diffraction

Device-grade μc-Si:H is generally reported to have (220) preferential orientation [Yamamoto 99a, Matsui 02b, Saito 11]. Due to this preferential orientation, many grain boundaries should be of the [220]–tilt type, and thus grow without broken bonds [Werner 01]. The consequences of this preferential orientation are however still under debate [Schicho 12]. Note that (220) preferential orientation seems not to be required for high-efficiency μc-Si:F:H solar cells [Dornstetter 13]. We thus carried out XRD measurements on the samples described in Tab. 6.3.

The samples were measured on a PANalytical X'Pert PRO MRD high-resolution diffractometer,

under 2θ (with a grazing incident angle of 1°) and $2\theta/\omega$ configurations in a range from 20 to 100° in 2θ axis (see Fig. 6.7 (a)).
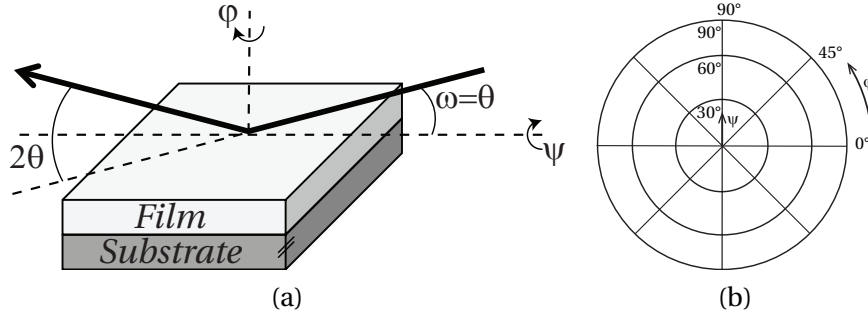
Figure 6.7: *Definition of angles for XRD measurements (a) and corresponding axes on pole figures (b).*

For the X-ray source, we used the $k_{\alpha,1}$ and $k_{\alpha,2}$ emission lines from a copper anode, at wavelengths of 1.5405980 and 1.5444260 Å, respectively, and with $k_{\alpha,2}/k_{\alpha,1} = 0.5$. According to Bragg's law, reflections occur only at specific angles θ between an incident X-ray beam and a sample, such as given by:

$$n\lambda = 2d\sin(\theta), \tag{6.1}$$

where d is the inter-planar distance, λ is the wavelength of the incident X-ray beam, and n is an integer determined by the order of a given reflection. This relationship describes the condition for constructive interference (and thus the appearance of a peak in the XRD pattern) from successive crystallographic planes given by their Miller indices (hkl).

Preferential orientation in μc-Si:H can in principle be deduced from deviations of peak intensity ratios, from the known values of a pure Si reference powder spectrum [Vallat-Sauvain 00]. To gain further information about the orientation distribution, we recorded pole figures. By tilting and rotating the sample (around ψ and ϕ), mounted onto a diffractometer, the intensity distribution of a (220) reflection over the orientation sphere—a pole figure—was recorded (see Fig. 6.7 (b)). Pole figures were analyzed and plotted with the MTEX MATLAB toolbox (version 3.5.0) [Bachmann 10]. For all pole figures, ψ values above around 60° should be discarded, as the incident beam is strongly defocused for such angles.

Fig. 6.8 shows the X-ray reflections of the samples of Tab. 6.3 using a $2\theta/\omega$ configuration, presented as raw data. The broad shoulder at low angles is caused by the amorphous glass substrate and is present for each sample.

Dashed lines correspond to the calculated position of reflections for planes in c-Si, using Eq. 6.1, together with the following relationship:

$$\frac{1}{d^2} = \frac{h^2 + k^2 + l^2}{a^2},$$
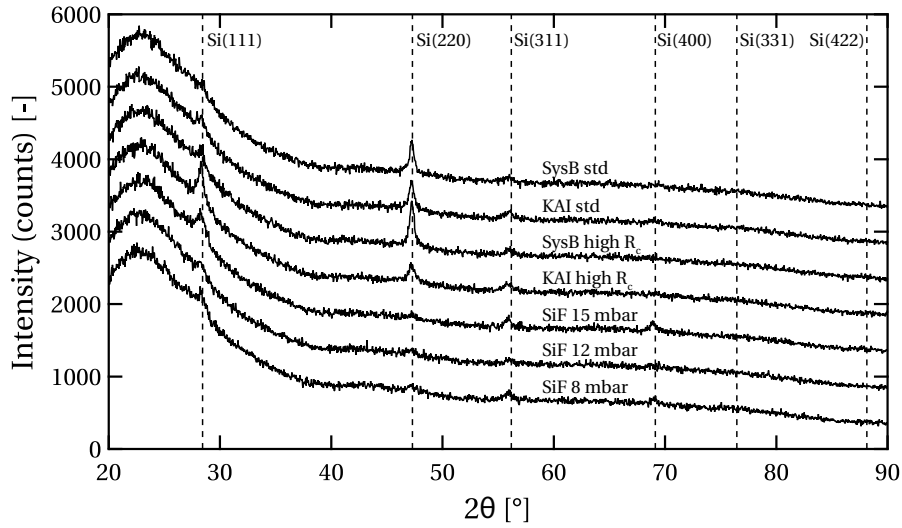
Figure 6.8: *$2\theta/\omega$ XRD pattern for the samples of Tab. 6.3. The broad shoulder at low 2θ angles is attributed to the glass substrate. The curves are shifted by 500 counts for better visualization.*

valid in cubic lattices, with a=5.4307 Å, the lattice parameter of c-Si.

Both "SysB" and "KAI" samples show peaks at d corresponding to the (111), (220), (311) and (400) planes. The "SiF" samples show peaks at d corresponding to the (111), (220), (311) and (400) planes, too. However, the peak intensity corresponding to the (220) orientation is much lower. For these samples, the overall signal-to-noise ratio is lower, due to the thinness of the films.

For the "SiF" samples, we therefore recorded XRD patterns at a low grazing incident angle of $1°$, *i.e.* a fixed ω, for a higher signal-to-noise ratio. The results are shown in Fig. 6.9, confirming the presence of peaks at d corresponding to the (111), (220), (311), (400), (311), and (422) planes, thus confirming the microcrystalline nature of μc-Si:F:H films.

From Fig. 6.8 we also estimated the mean size of the crystallites (τ) of the "SysB" and "KAI" samples from the (220) reflection, using the Scherrer equation:

$$\tau(2\theta) = \frac{K\lambda}{\beta\cos\theta}, \tag{6.2}$$

where K is the shape factor (set to 0.9, assuming spherical particles [Patterson 39, Langford 78]), and β is the broadening at half maximum intensity (FWHM) in rad. Results for mean crystallite sizes are summarized in Tab. 6.5. Due to the poor signal-to-noise ratio, mean crystallite sizes were not evaluated for the "SiF" samples. From the literature, larger grains would however be expected [Djeridane 07].

The absolute values for τ should be considered with extreme care, as they give only a lower bound for the crystallite sizes, assuming they are spherical, which is usually not the case. For similar crystallinity, the τ values can however be interpreted as trends: "SysB" layers have
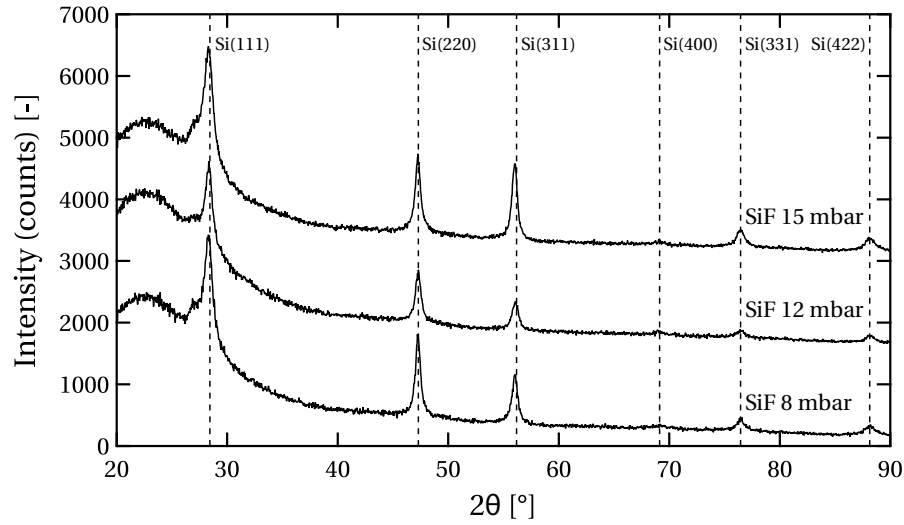
Figure 6.9: *2θ scan at a low grazing incident angle of 1° for the samples of Tab. 6.3 deposited with SiF_4. The curves are shifted by 1500 counts for better visualization.*

Table 6.5: *Mean size of the crystallites, as obtained with Eq. 6.2 for the (220) peak ($2\theta = 47.312°$). The resulting τ is a lower bound estimation, with about 5% uncertainty.*

Sample	FWHM [°]	τ [nm]
Reference	0.307	-
SysB std	0.471	53
KAI std	0.543	36
SysB high R_c	0.494	47
KAI high R_c	0.727	21

slightly larger crystallites than "KAI" layers, and in both cases increasing R_c by increased dilution leads to a reduction of the mean crystallite size. This can be attributed to the different deposition frequencies, as shown by Finger *et al.* [Finger 94], where selective etching of disordered material to create more space to develop crystalline grains was proposed when using higher frequencies, as is the case here for "SysB" layers.

To confirm the (220) preferential orientation of microcrystalline Si films, evaluation of pole figures on the (220) and (111) reflections was conducted. Fig. 6.10 shows the pole figures of the four samples deposited with SiH_4. For each sample, we measured pole figures at fixed $2\theta = 28.441°$, corresponding to the inter-planar distance of the {111} planes, and at fixed $2\theta = 47.3005°$, corresponding to the inter-planar distance of the {220} planes.

When looking at the "SysB std" sample, the pole density distribution for the (220) reflections is concentrated in the middle of the figure. The pole density distribution of the (111) reflections is concentrated in the region that matches the corresponding angle of the (220) with respect to the (111) plane ($\alpha_{(220),(111)} = 35.3°$). This implies that the (220) planes are mostly aligned approximately parallel to the substrate, or the [220] direction is aligned to the sample normal
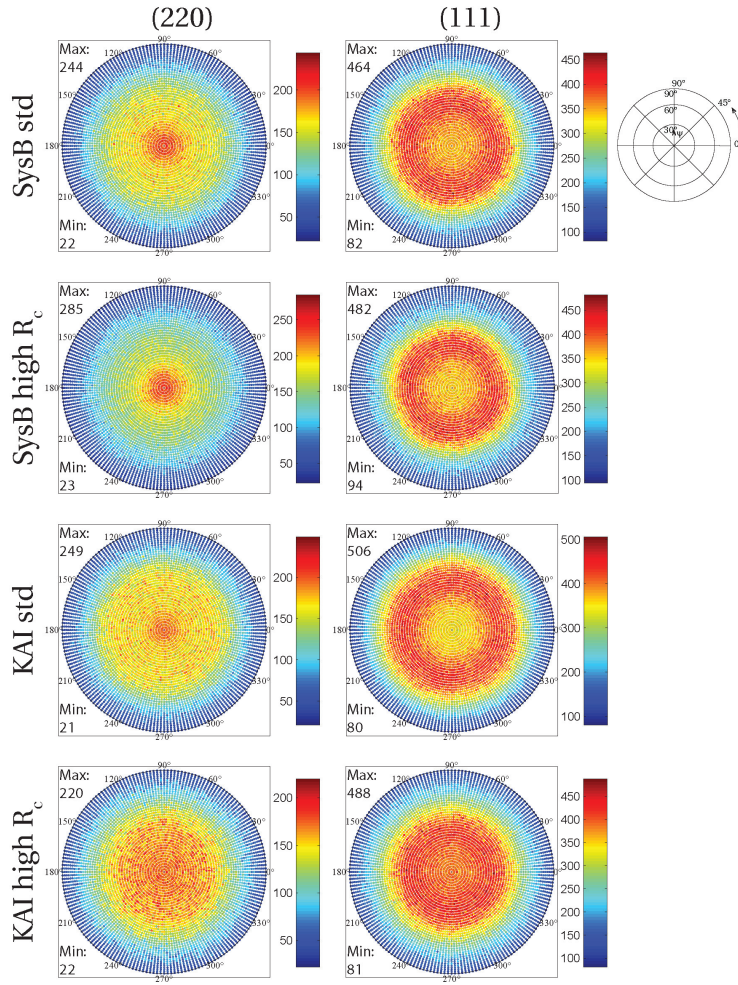
Figure 6.10: *Pole figures for layers deposited with SiH₄ at various pressures for the (220) and (111) orientations. The color scale represents counts at the detector.*

direction, also called the sample fiber direction. We hence deduce a weak but clearly recognizable (220) fiber texture. Similar observation can be made for the "SysB high R_c" sample, where the preferential orientation is even slightly more marked, as densification is observed for the peak in (220) and the ring becomes thinner. The "KAI std" sample also shows a (rather weak) (220) orientation, which diminishes when increasing the crystallinity [Meier 01], as observed for "KAI high R_c," where the preferential orientation almost completely vanishes.

Fig. 6.11 shows similar analysis for the "SiF" layers. No preferential orientation is observed for d corresponding to (220) or (111) planes. For the layer deposited at 15 mbar, we observe ring patterns, corresponding to the (400) preferential orientation, justified by the presence of the rings at angles corresponding to the calculated angles $\alpha_{(400),(111)} = 54.7°$ and $\alpha_{(400),(220)} = 45.0°$, and implying a (rather weak) (400) preferential orientation. This preferential orientation is absent in the "SiF" samples deposited at 12 and 8 mbar.
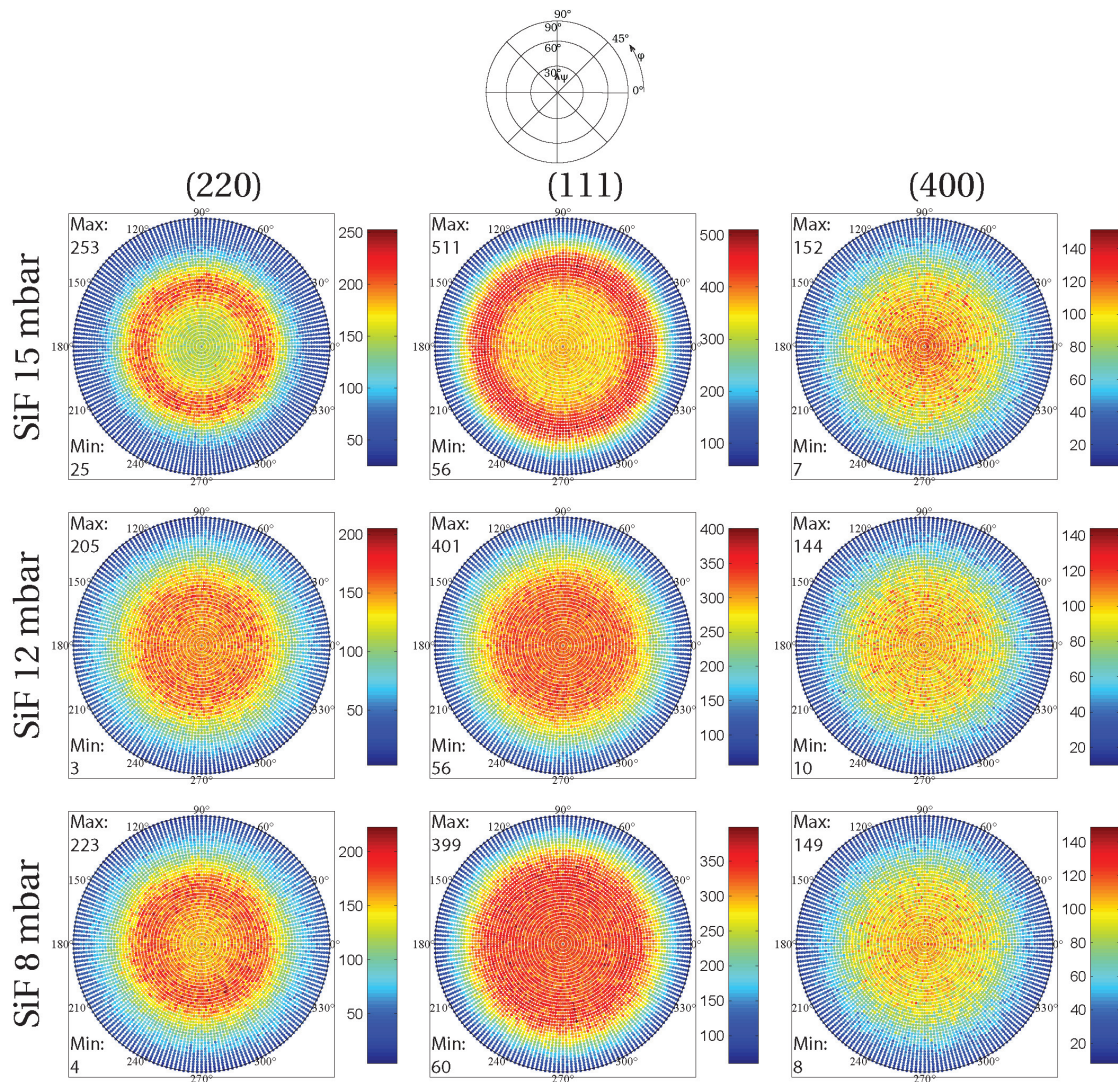
Figure 6.11: *Pole figures for layers deposited with SiF$_4$ at various pressures for the (220), (111) and (400) orientations. The color scale represents counts at the detector.*

Thus, our layers deposited with SiF$_4$ exhibit no—or very weak (400)—preferential orientation, though being highly crystalline, as suggested by Dornstetter *et al.* [Dornstetter 13].

6.3.4 Summary

The first part of this chapter was focussed on μc-Si:F:H layers and their characteristics. We presented a detailed structural analysis of selected μc-Si:F:H layers and compared them with standard μc-Si:H layers. In particular, it was shown that

- R_c values close to 90% can be achieved with SiF$_4$ at a deposition rate of up to 4 Å/s.

- At high pressure, the obtained layers are subject to compressive stress as indicated by Raman analysis.

- No NHSM are detected by FTIR in the hydride stretching modes and obtained μc-Si:H layers show similar infrared absorption spectra as standard layers with high R_c. However, as will be shown in Sec. 6.4, despite this similarity, high R_c μc-Si:H and μc-Si:F:H layers lead to different performance in devices, related to the higher R_c obtained with SiF$_4$, leading to higher infrared absorption in the device.

- A weak (400) preferential orientation can be present in μc-Si:F:H layers, whereas our standard μc-Si:H layers exhibit mostly (220) preferential orientation.

Note that the use of SiF$_4$ has no detrimental contamination effect on our reactor, as shown by SIMS analysis.

To further understand the growth mechanisms and the link between plasma conditions and microstructure, investigations of alternative deposition regimes for μc-Si:F:H with other dilutions, excitation frequencies and inter-electrode gaps could be very interesting.

In the following section, we will show the first results that were obtained when using μc-Si:F:H layers as the absorber layer in single-junction and tandem solar cells.

6.4 Solar cell results

6.4.1 Effect of adding a fluorinated precursor to standard chemistry

Before implementing the layers developed in Sec. 6.2 in solar cells, the effect on cell performance of adding a small amount of SiF$_4$ to the standard plasma chemistry of our high-efficiency μc-Si:H baseline process [Bugnon 13] was investigated. A small amount of SiF$_4$ (15% of the SiH$_4$ flux) was added to the plasma (SiH$_4$ highly diluted in H$_2$ at high pressure). To remove any effect that may arise from differences at the p–i interface, and also to keep the same nucleation of the absorber layer, SiF$_4$ was introduced, with no plasma break, only after the growth of 90 nm of the absorber layer.

Tab. 6.6 shows the electrical performance of solar cells deposited with this procedure on 5-μm-thick LPCVD-ZnO with increasing roughness (Z5 75', Z5 45', Z5 20' and Z5 5').

We observe that the electrical performance on Z5 45' is slightly lower than the standard baseline values for similar R_c and thickness. When using rougher superstrates, the overall efficiency decreases with the same trends as the baseline process (not shown here). This performance loss with roughness is attributed to the appearance of porous zones in the absorber layer, similarly as for standard SiH$_4$-based processes (see Chap. 3 and [Python 08, Cuony 11, Bugnon 12]). This experiment suggests that a simple, slight, addition of SiF$_4$ is not sufficient to modify the morphology of the material.

Table 6.6: *Electrical performance of a standard single-junction μc-Si:H solar cell (typical value from KAI-M baseline [Bugnon 13]) and single-junction solar cells deposited on superstrates of increasing roughness, with a small amount of SiF$_4$ (15% of the SiH$_4$ flux) added to the standard process. For these cells, V_{oc} and FF are presented based on the average of 12 cells on each superstrate, whereas J_{sc} and η are values given for the best cell only.*

Cell	Superstrate	V_{oc} [mV]	*FF* [%]	J_{sc} [mA/cm^2]	η [%]
standard [1.1 μm]	Z5 45'	540–550	74–75	23.6–24.3	9.5–10.0
standard + $\frac{[\mathrm{SiF_4}]}{[\mathrm{SiH_4}]} = 15\%$	Z5 75'	547 ± 2	74.9 ± 0.4	21.7	9.0
	Z5 45'	536 ± 2	72.5 ± 0.5	23.5	9.3
	Z5 20'	504 ± 2	71.0 ± 0.2	24.6	8.9
	Z5 5'	498 ± 4	69.5 ± 0.4	24.6	8.6

6.4.2 Solar cells with fluorinated absorber layers

We then implemented μc-Si:F:H films, developed in Sec. 6.2, as absorber layers in single-junction solar cells. If not stated otherwise, we used the SiO$_x$ doped layers and buffer layers from the baseline process [Bugnon 14], and varied only the deposition conditions of the absorber layer, at a fixed temperature of 200 °C. We did not use any precursor grading during the deposition of the absorber layer. For the superstrate, we again used 5-μm-thick LPCVD-ZnO of increasing roughness (Z5 45', Z5 20', Z5 10' and Z5 5'). For the back electrode, we used a lightly doped 2.3-μm-thick LPCVD-ZnO, and patterned 16 cells with an area of 0.25 cm^2. The presented results contain average values of at least six cells per sample for V_{oc} and *FF*. The values of J_{sc}, η and the sub-gap absorption coefficient at 0.8 eV ($\alpha_{0.8}$) as measured by Fourier-transform photocurrent spectroscopy (FTPS) [Vanecek 02] are given for the best cell only.

The solar cells presented in Fig. 6.12 have an absorber layer thickness of ~1.2 μm and R_c values ranging from 80 to 93%, as measured through the *n*-doped side of the solar cell. The absorber layer was deposited at low D_r, between 0.6 and 2.3 Å/s, at pressures ranging from 4 to 15 mbar and for two dilutions.

V_{oc} values around 450 mV and average *FF* values from 68 to 70% are obtained for samples deposited at high pressure, *i.e.* 8 mbar and above. For those cells, high J_{sc} are obtained, with values up to 25.8 mA/cm^2 for the solar cell deposited at 12 mbar, together with V_{oc} and *FF* values of 443 mV and 67.7%, respectively. This J_{sc} value is about 1.5 mA/cm^2 higher that our standard baseline cell for the same thickness, electrodes and doped layers. This enhanced J_{sc} is essentially attributed to higher absorption in the NIR due to the high R_c value of the μc-Si:F:H absorber layer, as it will be shown in Sec. 6.4.4. For the data presented in Fig. 6.12, the effect of hydrogen dilution is consistent with observations made with intrinsic layers, *i.e.*, a slightly higher R_c is reached. The best efficiency is achieved with a higher dilution thanks to a higher J_{sc}, for a constant V_{oc} and *FF*.

For the lower pressure (4 mbar), a strong degradation of all electrical parameters is observed.
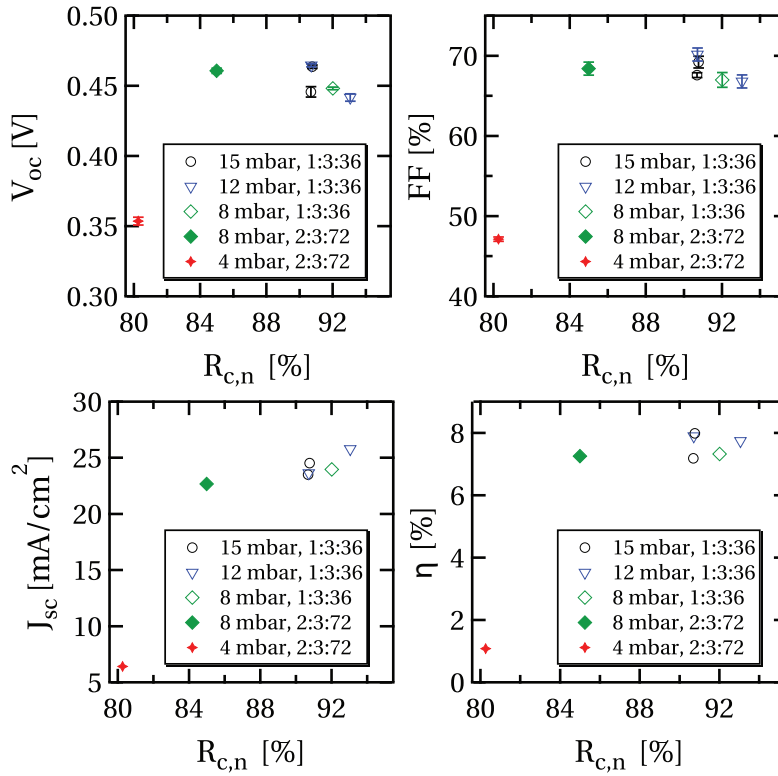
Figure 6.12: *Performance of single-junction µc-Si:F:H solar cells with a 1.2-µm-thick absorber layer with high R_c, deposited on Z5 45', as a function of the deposition conditions.*

Although only one sample is presented here, with V_{oc}=355 mV, FF=47.4% and J_{sc}=6.4 mA/cm^2, we observed reproducible lower performance for cells deposited at low pressure (in our case typically below 4 mbar) due to too high power. Cells with efficiencies above 7% could be obtained at pressures as low as to 4 mbar, but only with the lowest power and the low associated D_r of 0.4 Å/s, obtained for a slightly thinner cell deposited at 180 °C. We attribute the lower performance at low pressure and high power to bombardment by ions, arriving at the growing surface with high energy and generating defects in the absorber layer [Gordijn 06].

To get further insights into μc-Si:F:H material, we then studied defect-related absorption, $\alpha_{0.8}$, which is related to defect density in the bulk material. The obtained $\alpha_{0.8}$ values are plotted in Fig. 6.13 for the same solar cells.

From this figure, we observe an increase of $\alpha_{0.8}$ correlated with a higher defect density, when going to low pressure or higher power [Gordijn 06, Bugnon 13]. However, best obtained values are still 2–3 times higher than state-of-the art values. Even though both materials have similar bandgaps, the FTPS technique is not fully validated for μc-Si:F:H solar cells. Still, our layers are probably more defective than state-of-the-art μc-Si:H layers. Indeed, although a reasonable efficiency is obtained, V_{oc} is low.

We also measured the Urbach energy (slope of the absorption coefficient), which increased
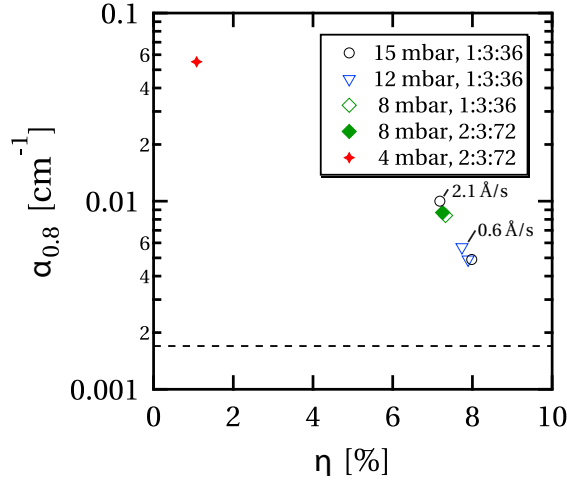
Figure 6.13: *Defect-related absorption as a function of conversion efficiency for μc-Si:F:H solar cells and for different deposition conditions. These cells have an absorber-layer thickness of 1.2 μm and were deposited on Z5 45'. The dashed line represents the best $\alpha_{0.8}$ value of a baseline μc-Si:H cell with same thickness and superstrate. Except for the two explicitly given values, the absorber layer was deposited at 1 Å/s. This figure suggests that μc-Si:F:H material is more defective than standard, high-quality μc-Si:H.*

from about 39 meV for cells deposited at 15 mbar to 54 meV for the cell deposited at 4 mbar and higher power, which is an indication of the presence of more strained bonds. We however observe that high-pressure regimes above 8 mbar are more favorable to the growth of high-quality μc-Si:F:H solar cells, similarly as for μc-Si:H obtained with SiH_4.

Best solar cells obtained with fluorinated precursors

Further tests were then performed by slightly adjusting the power to optimize the single-junction solar cell. Fig. 6.14 presents the *J-V* and EQE curves of our best cell with a 1.1-μm-thick absorber layer deposited at 1 Å/s, at a pressure of 12 mbar, a temperature of 200 °C, a dilution of 1:3:36 and on a Z5 20' superstrate. The measured R_c value is 90%. The other cells were co-deposited on superstrates of various roughnesses. Their electrical parameters are summarized in Tab. 6.7.

Table 6.7: *Electrical parameters of single-junction μc-Si:F:H solar cells, with an absorber layer thickness of 1.1 μm, as function of superstrate roughness. The best cell (area: 0.25 cm^2) is obtained on a Z5 20' superstrate, with a measured R_c value of 90%.*

Superstrate	V_{oc} [mV]	*FF* [%]	J_{sc} [mA/cm^2]	J_{-1V} [mA/cm^2]	η [%]
Z5 45'	467	71.6	23.6	23.7	7.9
Z5 20'	462	69.1	26.0	26.3	8.3
Z5 10'	467	59.9	25.7	25.9	7.2
Z5 5'	470	56.6	25.7	26.1	6.8
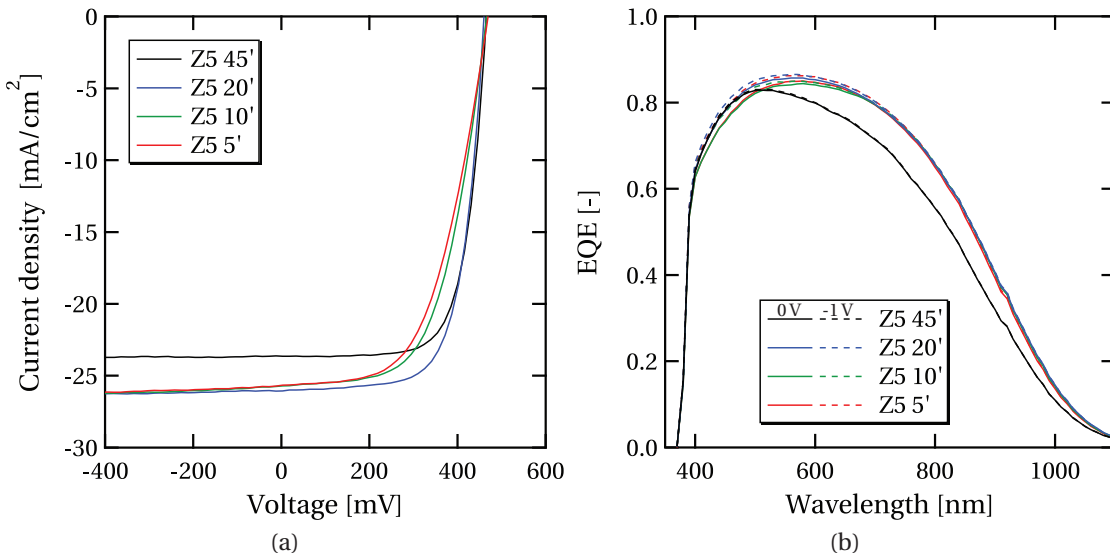
Figure 6.14: *J-V (left) and EQE (right) curves of single-junction μc-Si:F:H solar cells, with an absorber layer thickness of 1.1 μm, as a function of superstrate roughness. The best cell (area: 0.25 cm^2) is obtained on Z5 20' superstrate, with a measured R_c value of 90%. EQE are measured at 0 V and at reverse bias of -1 V. Note that for Z5 45', the curves are superimposed, indicating no collection problems on the smooth superstrate.*

According to Tab. 6.7 and Fig 6.14, V_{oc} values between 462 and 470 mV are achieved, with a highest η of 8.3%, which is close to the best reported value of 9.2% [Dornstetter 13, Dornstetter 14]. Interestingly, there is no V_{oc} dependence on superstrate roughness. This suggests that with such a low D_r, the superstrate roughness does not induce the creation of porous zones, as will indeed be shown in Sec. 6.4.3.

Furthermore, Tab. 6.7 and additional depositions suggest that in the case of μc-Si:F:H, the optimal superstrate is no longer the smooth Z5 45', but the rougher Z5 20'. This discrepancy is principally due to a large gain in J_{sc} in the NIR (+ 2.4 mA/cm^2 from Z5 45' to Z5 20') for similar V_{oc}. *FF* is slightly reduced because of collection losses, from 71.6 to 69.1% when going from Z5 45' to Z5 20', but there is a total positive gain.

Even though V_{oc} stays stable with respect to superstrate roughness, a drastic decrease in *FF* takes place with only 56% for the rough Z5 5' superstrate. This loss is mainly due to collection issues, as also seen in the low wavelengths of the EQE curves in Fig. 6.14 measured at 0 V and under reverse bias (-1 V).

Thick solar cells deposited with a fluorinated precursor

To evaluate the effect of the absorber layer thickness on solar cell performance, a solar cell with a 3.1-μm-thick absorber layer was deposited on Z5 20' with the same deposition process (*i.e.* pressure=12 mbar, dilution=1:3:36, D_r=1 Å/s). *J–V* and EQE curves (at reverse bias up to -4 V)

of this cell are shown in Fig. 6.15. V_{oc}, *FF* and J_{sc} values of 412 mV, 53.3% and 27.1 mA/cm^2, respectively, are reached. Bad collection is confirmed by EQE measurements at -4 V and the low *FF*, similarly as for the rough superstrate.
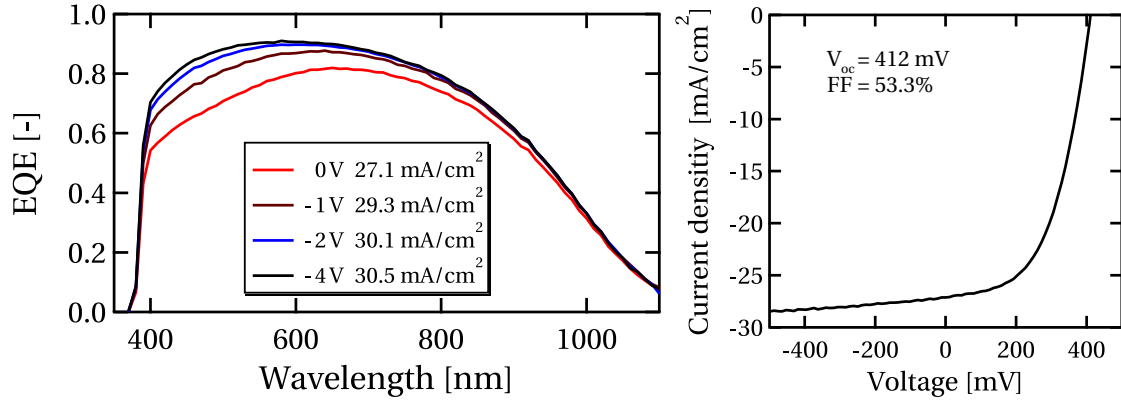
Figure 6.15: *EQE (left) and J–V curves of a solar cell with a 3.1-µm-thick µc-Si:F:H absorber layer, deposited on Z5 20'. EQE curves were measured under various electrical biases and corresponding calculated current densities are shown.*

The high EQE in the NIR is however extremely promising for multi-junction devices. To obtain more information on the quality of the μc-Si:F:H material and the possible causes for the low carrier collection, we carried out TEM analysis of a solar cell deposited on a rough superstrate, as discussed in the following section.

6.4.3   TEM imaging of a solar cell deposited on rough superstrate

To investigate the effect of superstrate roughness on material microstructure and defect formation, a TEM lamella was prepared by tripod polishing, followed by smooth Ar ion milling for a solar cell with a 1.1-µm-thick absorber layer, deposited at 15 mbar, with a dilution of 1:3:36, at D_r=1 Å/s, on a rough Z5 5' superstrate (V_{oc}=447 mV, *FF*=51.0%, J_{sc}=25.7 mA/cm^2). Such a sharp superstrate surface usually induces porous zones in the absorber layer of μc-Si:H solar cells. The electrical properties of a co-deposited cell (on Z5 45') are shown in Fig. 6.12.

A bright-field (BF) image of a cross section of this cell is shown in Fig. 6.16.

Zones I-III will be analyzed in detail in the following. Zone I potentially contains porous material (sharp V-shaped front LPCVD-ZnO), zone II is the location of the *i–n* interface and zone III is representative of the bulk material.

Fig. 6.16 shows the presence of columnar structures of highly crystallized μc-Si:F:H material, with large elongated grains of sizes up to ~ 100×800 nm. The columnar growth of single grains was also confirmed by dark field (DF) images (not shown here). This figure suggests that the grains are indeed larger than for standard μc-Si:H obtained from SiH$_4$, as expected from the literature [Houben 98, Bailat 03, Djeridane 08, Moreno 12].
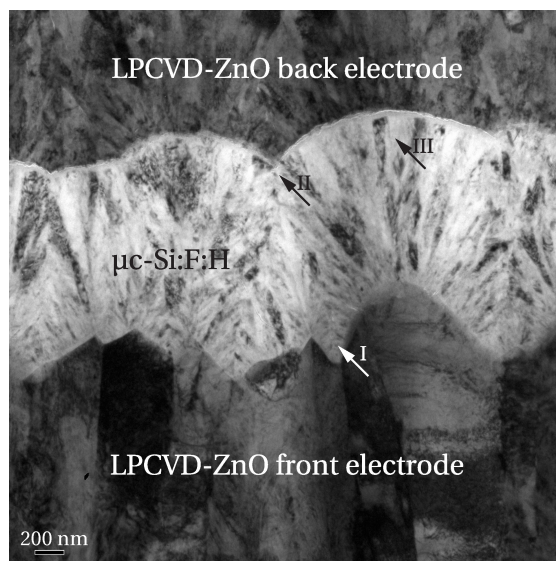
Figure 6.16: *BF TEM cross section of a solar cell deposited on rough ZnO (Z5 5'). The locations marked by arrows are analyzed in greater details in Fig. 6.17 to 6.19. Lamella preparation: M. Lebœuf, image: M. Dadras.*

Based on Fig. 6.16, another discrepancy between μc-Si:F:H and μc-Si:H is the absence of typical porous zones observed in μc-Si:H when solar cells are grown on such a rough superstrate. These defective zones usually appear as bright stripes going from the bottom of valleys of the V-shaped features—typically the front LPCVD-ZnO electrode—and throughout the absorber layer [Bailat 02, Python 08, Li 09b].

Fig. 6.17 shows a magnified micrograph of the Z5 5'/p-doped SiO_x/i-μc-Si:F:H interface corresponding to zone I in Fig. 6.16. Note that this figure is intentionally acquired slightly out-of-focus to gain information on porous defects.

The first observation which can be made is that no large amorphous incubation zone appears at the bottom of the μc-Si:F:H absorber layer, with crystalline growth starting directly on the 20-nm-thick p-doped SiO_x layer. On the other hand, nanoporous zones are clearly visible and are indicated by the arrows (a) and (b). Arrow (a) indicates nano-sized porous "filaments" that originate at the bottom of the V-shaped valleys, whereas arrow (b) shows these same filaments to be present on a locally flat area as well. We must mention that the filament-type defective zones observed here can be seen only in the out-of-focus mode, in opposition to larger porous zones, which can be more easily detected by TEM but also by scanning electron microscopy (SEM) images of polished cross sections [Python 09a]. Even though these porous zones are much smaller, they probably participate to the *FF* drop observed in Tab. 6.7 for a similar cell.

We then concentrate on zone II, a magnified view of the i–n interface in Fig. 6.18. Here, filaments are also observed, similar to the ones observed in Fig. 6.17. However, they are not necessary linked to V-shaped ZnO grains, but are found within the absorber layer, usually
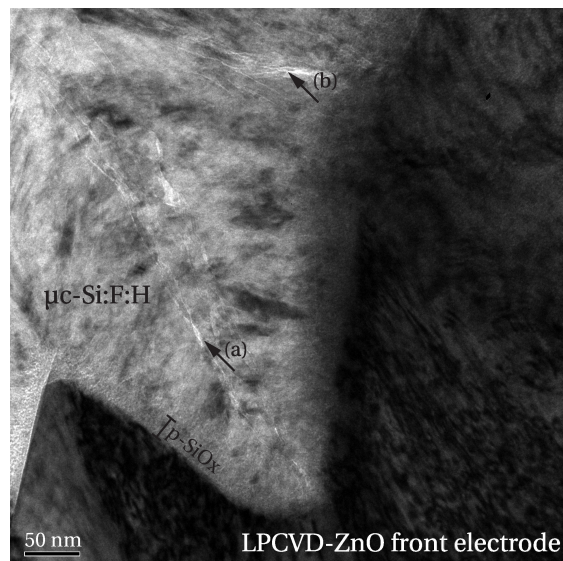
Figure 6.17: *BF TEM micrograph of the Z5 5'/p-doped SiO$_x$/i-µc-Si:F:H interface (zone I in Fig. 6.16). The two black arrows indicate defective nano-porous zones, originating from the bottom of V-shaped ZnO grains (a), as well as from a locally flat interface (b). Lamella preparation: M. Lebœuf, image: M. Dadras.*
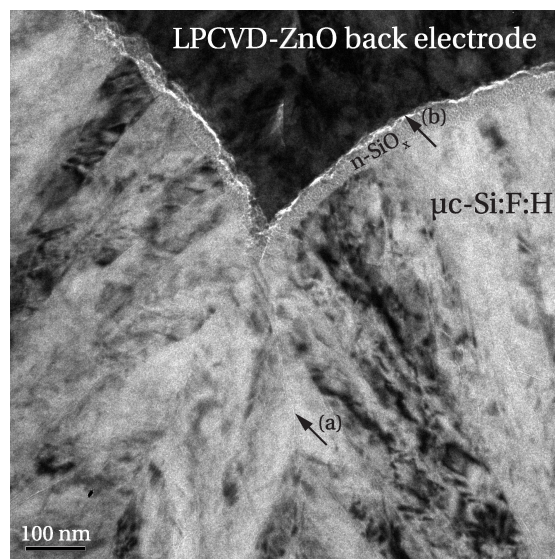
Figure 6.18: *BF TEM micrograph of the i–n interface (zone II in Fig. 6.16). In (a), a void crossing the cell is shown. In (b), a continuous porous zone between the n-doped SiO$_x$ layer and the LPCVD-ZnO back electrode can be seen, suggesting poor adhesion of the LPCVD-ZnO back electrode. Lamella preparation: M. Lebœuf, image: M. Dadras.*

where two columnar grains merge.

These filaments might be responsible for poor transport properties. However, they probably affect the electrical properties of solar cells differently than the usual porous zones which can

be observed with standard SiH_4-based plasma chemistry and also lead to a V_{oc} drop (and not only a *FF* drop as in our case) [Python 09b].

At the location pointed by the arrow (b), a continuous porous zone between the 30-nm-thick n-doped SiO_x layer and the LPCVD-ZnO back electrode is visible, indicating poor adhesion of the back electrode. This poor adhesion was observed when preparing the μc-Si:F:H solar cells, especially during the patterning steps, where delamination issues were often encountered. As a consequence, the n-doped layer should probably be optimized specifically for these μc-Si:F:H solar cells.

Fig. 6.19 shows the structure of large grains at higher magnification.
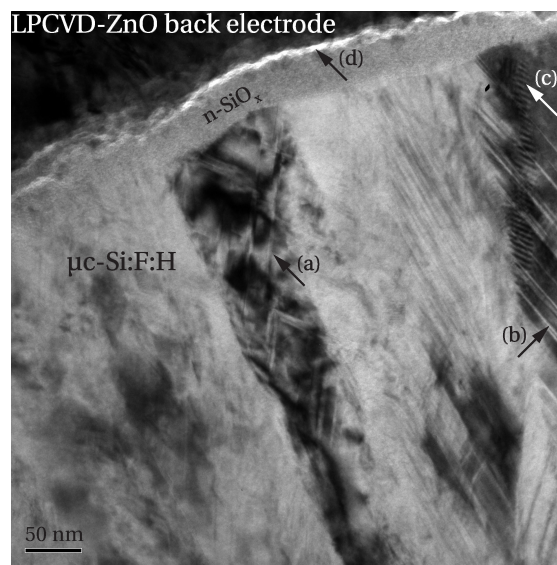
Figure 6.19: *BF TEM micrograph of large crystalline grains at the i–n interface (zone III in Fig. 6.16), at higher magnification. Structural defects are observed in (a) and (b). In (c), the overlapping of two grains creates a Moiré interference pattern. In (d), poor adhesion is observed between the n-doped layer and the LPCVD-ZnO back electrode. Lamella preparation: M. Lebœuf, image: M. Dadras.*

In locations marked by arrows (a) and (b), we detect parallel lines within the grains, which can be attributed to stacking faults within the grains, leading to nano-twins (not verified with a diffraction pattern) [Houben 03]. Thus, although we obtained decent V_{oc} values for such solar cells, the quality of the grains may be improved to further enhance the efficiency of such solar cells, especially to reach high V_{oc} above 500 mV at such high R_c. Arrow (c) points to dark and thick lines, which are Moiré interference fringes, coming from the spatial superposition of two grains. Finally, with arrow (d), we again observe poor adhesion of the LPCVD-ZnO back-electrode. This poor adhesion is however not the underlying reason for poor electrical performance on rough superstrate, as peeling of the LPCVD-back electrode was encountered mostly on smooth superstrates.

Summary of TEM observations

In summary, the TEM cross section made of a single-junction μc-Si:F:H solar cell deposited on a rough superstrate shows that

- Large columnar grains can be obtained with SiF_4-based plasma chemistry.

- Structural defects are present, appearing as nano-pores that can be observed at the column boundaries and to some extent, in the V-shaped valleys of the LPCVD-ZnO superstrate.

- Large grains, containing structural defects, are present. These defective grains are a probable cause of V_{oc} values below 500 mV.

- The adhesion between the n-doped layer and the LPCVD-ZnO back electrode is poor, also observed during preparation of the solar cells. This adhesion issue is however not the cause of poor performance observed on a rough superstrate.

These observations were made for a solar cell deposited at low D_r. It would be necessary to study a similar cell grown at higher D_r to assess whether SiF_4-based chemistry hinders the creation of porous zones, *e.g.* by selective etching induced by fluorine [Kasouit 02].

6.4.4 Comparison with standard solar cells with high cristallinity

In this section we compare the performance of our best μc-Si:F:H material with μc-Si:H obtained with standard SiH_4-based plasma, but with the highest feasible R_c.

In a single-junction μc-Si:H solar cell with a 2-µm-thick absorber layer, deposited at 2.2 Å/s on smooth Z5 45', with an R_c value of 80%, V_{oc}, *FF* and J_{sc} values of 397 mV, 62.2%, and 26.6 mA/cm^2, respectively, were reached. The obtained V_{oc} value is thus 22 mV below the value of a μc-Si:F:H cell (R_c=93%) of close thickness deposited with same doped layers on a similar superstrate, for which a V_{oc} value of 419 mV was measured. On the other hand, J_{sc} and *FF* values are quite similar, with 26.3 mA/cm^2 and 62.2%, respectively.

There is however a major difference in the EQE of such solar cells, as shown in Fig. 6.20.

It is clear from Fig. 6.20 that the μc-Si:F:H solar cell is subject to collection problems, already discussed previously for other μc-Si:F:H solar cells, as demonstrated by the difference in EQE at 0 V and -1 V bias and corresponding to a J_{sc} loss of 1.2 mA/cm^2.

Conversely, the SiH_4-based solar cell does not suffer from collection problems, but shows a lower EQE in the NIR, even for very high R_c. We could not compare cells of similar R_c as R_c> 80% could not be achieved. The absence of an amorphous phase is a characteristic of material obtained from SiF_4 [Dornstetter 13], associated to preferential etching by F ions [Kasouit 02].
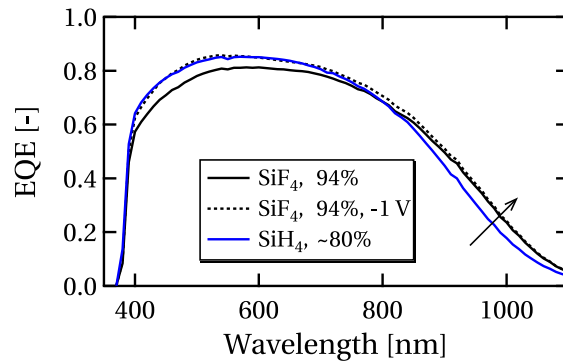
Figure 6.20: *EQE curves of solar cells with a ~ 2-μm-thick absorber layer at very high R_c, made with SiF₄- and SiH₄-based plasma chemistry. The cell deposited with SiF₄ shows clear collection issues, but a much higher response in the NIR.*

We hence believe that with further optimization of the process such as careful control of the hydrogen and fluorine in the plasma and control of ion bombardment, μc-Si:F:H solar cells have a significant potential as the absorber layer in multi-junction devices, thanks to very high absorption in the NIR. We thus believe that the fabrication of solar cells with similar absorption in the NIR, and with V_{oc} values above 500 mV, is feasible.

6.4.5   Application in micromorph tandem solar cells

The most promising material obtained so far in a single-junction solar cell (*i.e.* deposited with the same parameters as the best cell of Tab. 6.7) was then implemented in micromorph tandem cells, to evaluate the highest possible J_{sc} in a realistic device (*i.e.* with reasonable thickness, deposited on as-grown LPCVD-ZnO, and with standard doped layers and back electrode).

A 250-nm-thick *a*-Si:H top cell, optimized for higher current, was thus deposited on an as-grown lightly doped 2.3-μm-thick superstrate (Z2.3) [Boccard 12b]. This top cell was followed by a SiOₓ-based intermediate reflector (SOIR) [Buehlmann 07] with various thicknesses (0, 70, 90 and 120 nm) and a 3.1-μm-thick bottom cell deposited with SiF₄, at 12 mbar, with an absorber layer D_r of 1 Å/s. The EQE curves, as a function of SOIR thickness, are presented in Fig. 6.21.

Fig. 6.21 demonstrates that a very high total current density of 31.9 mA/cm² can be achieved on 1 cm² for the cell without a SOIR. Note that an anti-reflective foil is used on the glass side, leading to a total-current gain of ~1 mA/cm². For increasing SOIR thickness, we observe an expected increase in current density of the top cell, however with a reduced total current density. These losses are attributed to both increased reflectance of the cell, and increased parasitic absorption of the SOIR [Buehlmann 07]. We still obtain a solar cell matched above 15 mA/cm² for the 70-nm-thick SOIR. Compared to a similar tandem cell deposited with SiH₄ (70-nm-thick SOIR, similar thickness, high R_c), this represents an absolute gain in bottom-cell
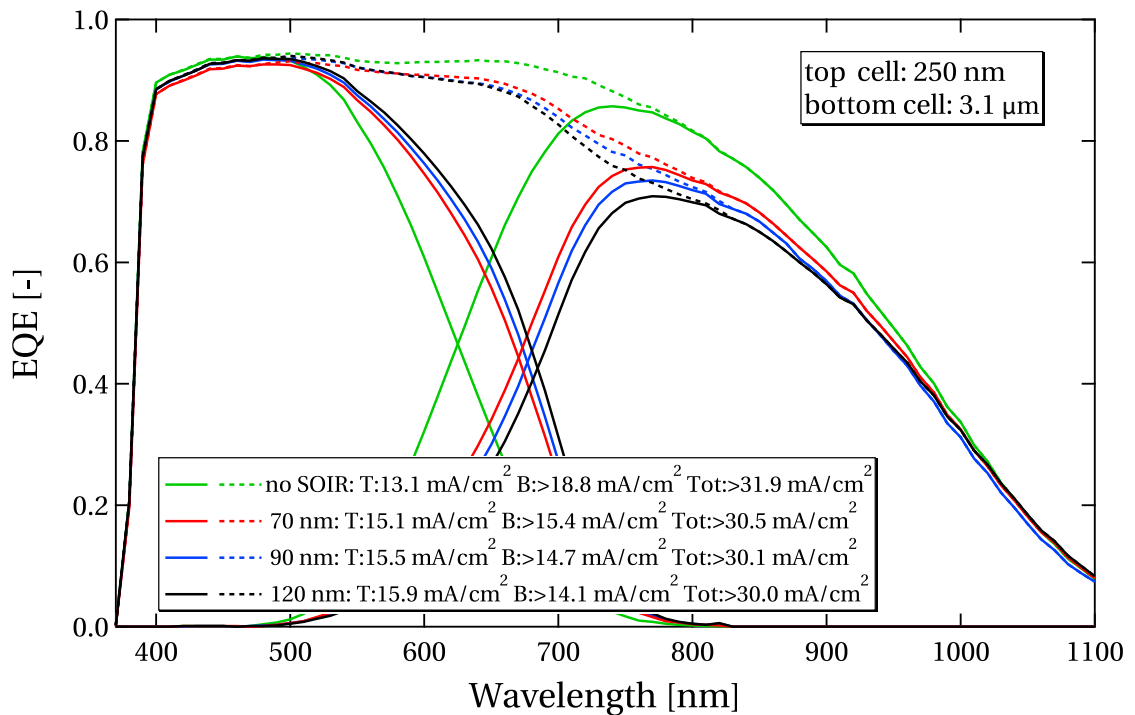
Figure 6.21: *EQE and corresponding top (T), bottom (B), and total (Tot) current densities of micromorph solar cells with a 250-nm-thick top cell and a 3.1-μm-thick highly crystallized bottom cell, as a function of the SOIR thickness. EQE were measured at 0 V bias with an anti-reflective foil applied on the glass.*

current density of 1.2 mA/cm^2, demonstrating the superior potential of absorption in the NIR for cells deposited from SiF$_4$.

The other electrical parameters of these cells (V_{oc}, *FF*) are low (~1 V and 63%) for the cell without a SOIR. For cells with a SOIR, S-shaped *J–V* curves were obtained, leading to a very low *FF* down to ~35% for the cell with the thickest SOIR (120 nm). We attribute this loss to a too high oxygen content in the SOIR, rendering it too resistive [Buehlmann 07]. The low V_{oc} can not be attributed to the bottom cell only, as the co-deposited reference bottom cell has a V_{oc} of 414 mV on Z5 20'. Hence, the effect of SiF$_4$-based plasma on the top cell during the growth of the bottom cell requires further investigation.

6.5   Conclusion and outlook

This chapter focused on microcrystalline silicon developments based on SiF$_4$. We first detailed the development of μc-Si:F:H layers and showed that a highly crystallized layer can be obtained. We then characterized selected layers by SIMS, Raman spectroscopy, FTIR and XRD. We also implemented μc-Si:F:H layers as absorber layers in single- and multi-junction solar cells. In particular, we showed that

- The use of SiF_4-based plasma chemistry is compatible with other standard PECVD processes and does not induce additional contamination.

- From a structural point of view, these layers exhibit similar properties to standard SiH_4-based layers with high R_c, but with no or limited preferential orientation.

- Large grains, of sizes up to ~ 100×800 nm, can be obtained, but containing stacking faults and nano-twins. At low D_r, porous zones, which are usually visible in standard SiH_4-based solar cells, are absent.

- In single-junction solar cells, V_{oc} values above 460 mV were obtained, together with very high R_c, and J_{sc} of 26 mA/cm^2, leading to an efficiency of 8.3% for 1.2-µm-thick solar cells, and showed the potential for J_{sc} values above 30 mA/cm^2 for thicker solar cells.

- The optimum superstrate roughness was shifted towards higher roughness, thanks to enhanced absorption in the NIR, with the consequence of a reduction in *FF*, but not in V_{oc}.

- μc-Si:F:H layers have the potential to reach record J_{sc} when used as the absorber layers in multi-junction devices, thanks to unequaled absorption in the NIR, as demonstrated here with micromorph tandem solar cells with total J_{sc} of 31.9 mA/cm^2 and micromorph tandem solar cells matched above 15 mA/cm^2.

Many points however still require further investigation: first, as observed, both the deposition rate and Raman crystallinity factor are sensitive to the ratio of SiF_4 and H_2 in the plasma, with the existence of a probable optimum specific to each D_r–R_c, which needs to be assessed. Second, since significant compressive stress was observed for layers on glass, it should be clarified whether this stress has an impact on solar cell performance and, if so, how it can be controlled. In [Bugnon 13], it was shown that, indeed, stress leads to worse solar cell performance in the case of standard μc-Si:H, strongly correlated to an increasing bulk defect density as measured from FTPS and increased ion bombardment energy. The role of precursor grading in μc-Si:F:H absorber layer growth, as well as the possibility to dope or alloy μc-Si:F:H, should be carefully studied as well.

Finally, to match industrial requirements, higher D_r are required. For that purpose, the use of very high frequencies—combined with an optimized inter-electrode gap—might be an attractive solution to reduce detrimental ion bombardment [Curtins 87b, Meier 04, Bugnon 13]. On the other hand, a low deposition rate might be advantageous for processes where nanometric precision is required, such as thin highly crystalline doped layers, or the fabrication of quantum dots.

7 Conclusion and Perspectives

This chapter summarizes the main findings and achievements of this thesis. At the end, some perspectives for the future of the technology are given.

7.1 Conclusion

7.1.1 Requirements for high-efficiency devices

In Chap. 3, the development of high-efficiency single-junction hydrogenated microcrystalline silicon (μc-Si:H) solar cells in a small-area research reactor was presented. It was shown that both an adequate cell design and high-quality μc-Si:H material are required for high-efficiency solar cells. Then, the impact of defective porous zones in the μc-Si:H absorber layer, which appear when a μc-Si:H layer is deposited on highly textured superstrates, was investigated. The relation between the presence of such porous zones and dark degradation of solar cells was confirmed. This dark degradation occurred when finished solar cells were stored in ambient conditions, and was attributed to moisture ingression through the porous zones in the absorber layer. It was also demonstrated that dark degradation can be limited with a smooth superstrate morphology or an adapted deposition process. To demonstrate the interconnection of this porous phase within the absorber layer, advanced scanning electron microscopy was employed for a tomographic 3-D reconstruction of the absorber layer, showing for the first time the interconnection of such defective zones within the absorber layer. Finally, we reported a certified record efficiency for single-junction μc-Si:H solar cells, with an efficiency of 10.7%, on an area >1 cm^2, as well as an efficiency of 10.9% on smaller area (0.25 cm^2).

7.1.2 Post-deposition processes

In Chap. 4, it was shown that the detrimental effect of porous zones in the absorber layer can partly be mitigated by dedicated post-deposition treatments. By using a post-deposition hydrogen plasma treatment that was first developed to improve the electrical properties of

zinc oxide deposited by low-pressure chemical vapor deposition (LPCVD-ZnO), it was shown that exposure to such a hydrogen plasma could be beneficial for solar cells that have very resistive LPCVD-ZnO electrodes. However, curing of porous zones was demonstrated by annealing in vacuum. This improvement of the porous zones in μc-Si:H was detected both in complete solar cells (leading to improvements in open-circuit voltage (V_{oc}) and fill factor (*FF*) of up to 30 mV and 4%, respectively), and by Fourier-transform photocurrent spectroscopy with lowered defect-related absorption. It was finally demonstrated that the deposition of LPCVD-ZnO could induce additional defects in these porous zones, and that annealing in vacuum can lead to the subsequent curing of these defects.

7.1.3 Towards fully passivated μc-Si:H

We then investigated the effect of dedicated interfaces on solar cell performance, also under lower illumination levels. It was demonstrated that silicon oxide SiO_x *p*-doped layers are extremely efficient as shunt-quenching layers. These SiO_x *p*-doped layers were moreover shown to be especially effective on rough superstrates. Passivated interfaces in μc-Si:H solar cells were then introduced, based on the addition of amorphous silicon layers, similar to a concept used in crystalline silicon heterojunction solar cells. A large increase in V_{oc} for thin μc-Si:H solar cells was demonstrated. This concept led to record values of 608 mV in a single-junction solar cell, and 1.53 V in a micromorph tandem cell. By investigating the interplay between passivation and cell thickness, we concluded that even though μc-Si:H absorber layers were of high quality, solar cells were mostly limited by the quality of the bulk material when made thicker. A simulation of a thin μc-Si:H device confirmed that an understanding of each interface is crucial in thin μc-Si:H solar cells, and that the passivation of electronically dead doped layers is essential to avoid an interface-limited device.

7.1.4 Potential of highly crystallized material

In the last chapter, the potential to obtain a high short-circuit current density (J_{sc}) without compromising on material quality was evaluated. In particular, highly crystalline absorber layers, made with the additional silicon tetrafluoride (SiF_4) precursor, were investigated. Highly crystalline layers were indeed obtained, with crystallinity values as defined by Raman spectroscopy (R_c) well above 80% and above the values that could be obtained with standard silane-based plasma chemistry. We compared these layers with highly crystalline layers obtained with our state-of-the art processes. It was concluded that although layers obtained with SiF_4 were similar in many points to highly crystalline layers obtained with silane, layers obtained with SiF_4 showed no or very little crystallographic preferential orientation in films, and contained a high compressive stress.

When such highly crystallized films were implemented as absorber layers in single-junction solar cells, V_{oc} values as high as 470 mV, and a conversion efficiency (η) of 8.3% were obtained in single-junction solar cells (with $R_c \sim 90\%$). Although it was found that superstrate roughness

was a limiting factor, no porous zones were detected in the absorber layer by transmission electron microscopy (TEM). TEM also revealed the presence of very large crystalline grains, but containing structural defects (nano-twins and porous filaments), likely responsible for the lower electrical performance when cells were made thicker. A record total J_{sc} of 31.9 mA/cm^2 was however demonstrated for a micromorph tandem cell, thanks to improved absorption in the near-infrared, for a total silicon thickness of 3.4 μm, which makes it the highest reported value for such a configuration. For this material obtained with SiF$_4$, many questions remain open, especially concerning the feasibility of producing high-quality material at a high deposition rate, which is a key requirement for implementation as the bottom cell in multi-junction devices.

7.2 Perspectives

Thin-film silicon technology has a unique potential for large-scale deployment of renewable electricity production. Apart from very high efficiency, it meets every requirement for a photovoltaic technology. First, it is based on the use of abundant and non-toxic materials. This criterion will be of high importance in a society where photovoltaics will reach terawatt levels of electricity production. Second, the low temperature coefficients and lowest production cost per square meter makes it one of the best candidates for large power plants in hot areas, but also for building integration due to its proven aesthetics potential. Then, thin-film silicon technology is one of the technologies with small gap between the lab-scale best values and the record module efficiency. Indeed, improvements, such as the one obtained in this thesis, can in principle be implemented in industrial production lines in a reasonable amount of time, as both research and industry are based on the same technological concepts.

However, due to the very low price of the well-established crystalline silicon technology and to become competitive in the current market, a significant leap in conversion efficiency will be required. The current state-of-the-art efficiency is a triple-junction solar cell with a stable efficiency of 13.4% [Kim 13] (V_{oc}= 1.96 V, J_{sc}= 9.5 mA/cm^2 and *FF*= 72%).

We believe that solar cells based on thin-film silicon have a stabilized efficiency potential of 15% without needing a major breakthrough. Indeed, by assuming a triple-junction solar cell matched at 10 mA/cm^2 with a stable *FF* of 73%, combining a top cell with a wide bandgap delivering 1 V, a high-V_{oc} middle cell delivering 560 mV, and an optimized bottom cell based on SiF$_4$ chemistry, such as the one presented in Chap. 6, delivering 490 mV, an efficiency above 15% is within reach. To go beyond this limit, major improvements will be required, such as both drastically minimizing light-induced degradation in amorphous silicon and optimizing the bandgap utilization of each subcell in the multi-junction configuration, as very recently demonstrated by simulation [Isabella 14]. According to this study, 19.8% is a realistic limit for quadruple-junction solar cells. However, mastering quadruple-junction cells will be a technical challenge. These cells would also have to be optimized for a given spectrum, as a slight spectrum mismatch can quickly lead to a decrease in efficiency.

A Measurements of cells on highly textured superstrates

In this appendix, we will present some considerations that should be taken into account when performing current-voltage (J–V) measurements of solar cells deposited on textured superstrates. It has been known for a long time that artifacts can be induced into efficiency measurements by scattering interfaces [Meier 94, Golay 00]. Indeed, if silicon is removed around the cells to access the front electrode, light hitting bare zinc oxide (ZnO) at the side of the cell can be trapped in the glass and scattered back into the neighbor cell, artificially increasing its short-circuit current density (J_{sc}) and thus its calculated conversion efficiency (η). This artifact can be eliminated by applying a mask the exact size of the cell, defining its area [Green 12]. However, in that case, light entering just at the edge of the mask is lost (being scattered out of the cell), which would not happen in standard laser-scribed modules with monolithic interconnection. To illustrate this effect, Fig. A.1 shows a light-beam-induced current (LBIC) measurement (developed in-house by Jonas Geissbühler) of a laser-scribed and non-shunted single-junction microcrystalline silicon (μc-Si:H) solar cell. The silicon and
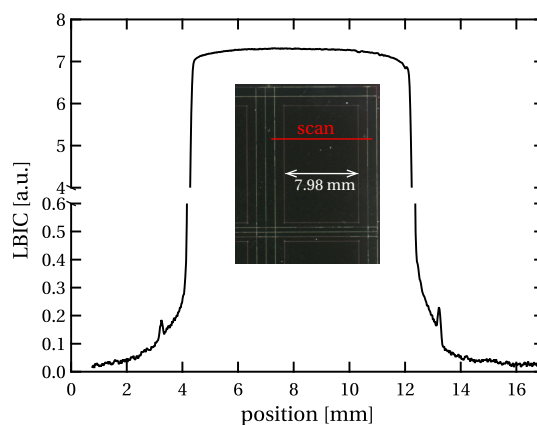
Figure A.1: *LBIC measurement performed by scanning across a laser-scribed cell with a 650-nm laser beam under short-circuit conditions. The scribing was developed and performed by Linus Löfgren and Moritz Schmidlin.*

Appendix A. Measurements of cells on highly textured superstrates

ZnO back electrode were removed around the cell with a laser-scribing process (P3) to isolate the cell and a second similar but slightly thicker scribing was performed approximately 1 mm away from the first scribe to access the front contact. On the LBIC signal, lateral collection from the edge of the cell can be seen. The two spikes on the sides of the cell are the parts of the thicker second scribe with more bare ZnO exposed to the laser beam, where even more light is injected into the cell.

To reproduce closely and fairly a true module measurement, the mask should therefore be just slightly bigger than the cell area, to compensate for the lost light (absent or limited to a very small dead area in a module) and the true area of the cell should be taken into account for efficiency computation (aperture area measurement). However, this is difficult to achieve with our cell design due to the anti-reflective texture applied to the glass, which makes the cell look "blurry" through the glass and hinders a precise determination of its area by an independent measurement.

The contact at the rear of the device is created by soldering two wires onto the back ZnO electrode, inducing a non-negligible J_{sc} loss, as the soldered part has very poor reflection compared to the white paint that covers the remaining part of the rear electrode.

By applying a mask smaller than the cell area, the (slightly) overestimated J_{sc} (some light enters the device and is scattered to the side) is in our opinion largely compensated for by the losses at the soldered part and the shading-induced open-circuit voltage (V_{oc}) loss (*e.g.* by a mask), analyzed with a simple one-diode model in the following.

With n the diode ideality factor, k_B the Boltzmann constant, T the temperature, q the electronic charge, J_0 the reverse saturation current, and J the current density (assumed proportional to the illumination), defining the shading factor κ as the ratio of the illuminated area of the solar cell over the total solar cell area, and starting from the one-diode equation for the V_{oc}:

$$V_{oc} = \frac{nk_B T}{q} \ln\left(\frac{J}{J_0} + 1\right),$$

one gets the following expression for the V_{oc} loss (ΔV_{oc}) due to shading:

$$\Delta V_{oc} = \frac{nk_B T}{q} \ln\left(\frac{1}{\kappa}\right) = 25.8 \, \text{mV} \cdot n \cdot \ln\left(\frac{1}{\kappa}\right) \tag{A.1}$$

at room temperature.

Fig A.2 shows the J–V measurement performed in-house with masks of different sizes of the record cell of Chap. 3 which has a nominal area of $1.20 \, \text{cm}^2$. This cell is patterned with the standard process (lift-off/dry-etching, without laser scribing). The masks were kindly prepared via laser-cutting by Jonas Geissbühler and their areas were precisely determined before being used in the computation of J_{sc} and η.
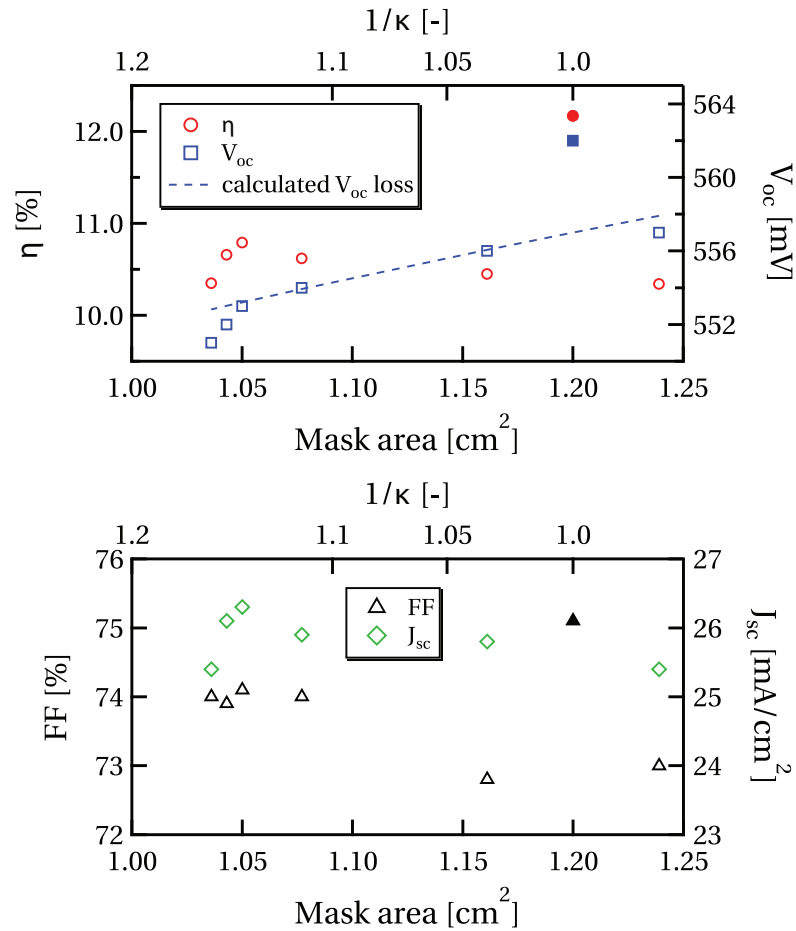
Figure A.2: *Electrical parameters of the record cell presented in this work, as function of the aperture size. The plain symbols are the values without a mask, where the cell nominal area (1.2 cm²) was taken for the efficiency measurement.*

Plain symbols show the measurement of this cell without a mask and the nominal area of the cell being taken into account for the calculation of the efficiency. The resulting efficiency is clearly overestimated due to effects explained in the beginning of this appendix. By applying masks of different sizes on the cell and using their areas to define the efficiency, an increasing J_{sc} is expected and seen for masks smaller than the cell, due to light being trapped under the mask and still contributing to the generation of charge carriers. The fill factor (*FF*) is slightly increased. The trend for *FF* is more complicated due to the many parameters which influence it (*e.g.* carrier collection, resistive losses, and the presence of localized microshunts and cracks). The V_{oc} losses are computed with Eq. A.1, assuming a nominal V_{oc} of 557 mV and $n = 1.1$, as found experimentally with the variable illumination measurements (VIM) technique in Chap. 5. A good agreement with the measured V_{oc} is observed. A slight discrepancy is observed for $\frac{1}{\kappa}$ values above 1.15, probably due to microshunts and microcracks within the absorber layer which are not taken into account with a one-diode model (especially the J_{02} contribution).

Appendix A. Measurements of cells on highly textured superstrates

For a designated area of 1.05 cm^2, a conversion efficiency of 10.8% is measured, in very good agreement with the certified value of 10.7%. For reasons mentioned above, we believe this measured efficiency is still a lower bound compared to what could be obtained in a scribed module.

B SIMS profiles for reference intrinsic microcrystalline silicon layers

This appendix presents concentrations of foreign atoms as a function of depth in reference intrinsic μc-Si:H layers, as obtained by secondary ion mass spectrometry (SIMS). Fig. B.1 shows comparisons of two samples, a single μc-Si:H layer and a layer stack (μc-Si:F:H+μc-Si:H). For details on the preparation of these samples and their purpose, the reader is referred to Sec.6.3, where bulk concentrations of oxygen, fluorine and hydrogen are evaluated, based on these measurements.
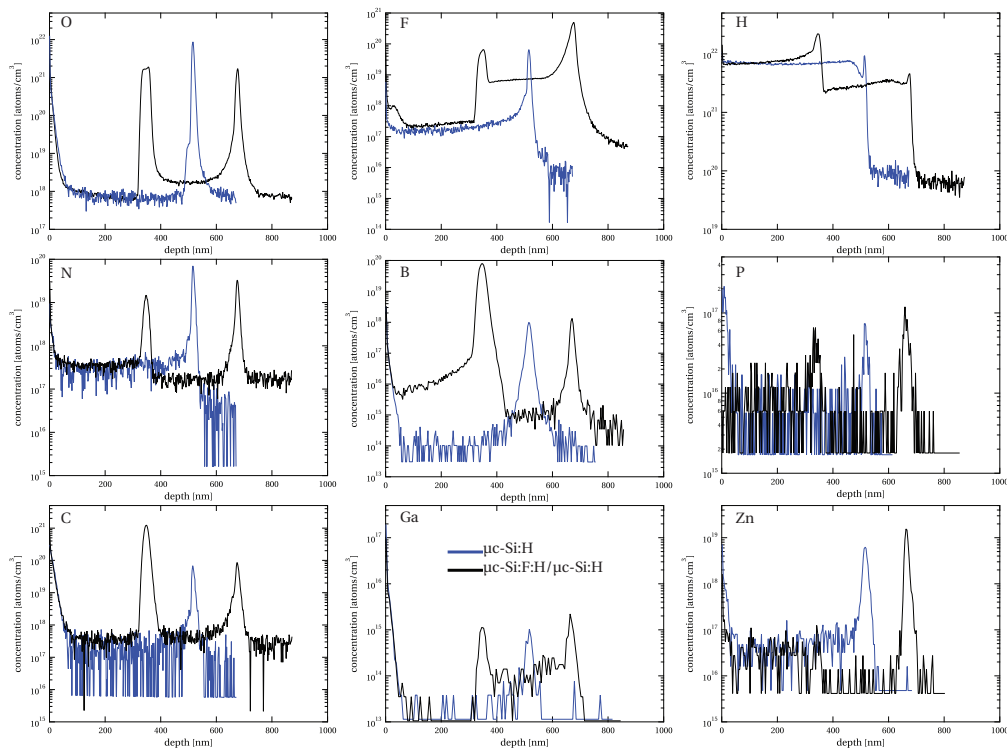
Figure B.1: *Concentrations of foreign atoms as a function of depth in reference intrinsic microcrystalline silicon layers, as measured by SIMS, for oxygen, fluorine, hydrogen, nitrogen, boron, phosphorus, carbon, gallium and zinc.*

Bibliography

[Abramov 10]   A. Abramov & P. Roca i Cabarrocas. *Addition of SiF$_4$ to standard SiF$_4$+H$_2$ plasma: an effective way to reduce oxygen contamination in μc-Si:H films.* physica status solidi (C), vol. 7, no. 3–4, pages 529–532, 2010.

[Agashe 03]   Chitra Agashe, Oliver Kluth, Gunnar Schöpe, Hilde Siekmann, Jürgen Hüpkes & Bernd Rech. *Optimization of the electrical properties of magnetron sputtered aluminum-doped zinc oxide films for opto-electronic applications.* Thin Solid Films, vol. 442, no. 1–2, pages 167–172, 2003. Selected papers from the 4th International Conference on Coatings on Glass.

[Agbo 10]   S. N. Agbo, J. Krč, R. A. C. M. M. van Swaaij & M. Zeman. *Optimization of the p-i interface properties in thin film microcrystalline silicon solar cells.* Solar Energy Materials & Solar Cells, vol. 94, pages 1864–1868, 2010.

[Alsema 98]   Erik Alsema. *Energy requirements of thin-film solar cell modules–a review.* Renewable and Sustainable Energy Reviews, vol. 2, no. 4, pages 387–415, 1998.

[Amanatides 01]   E. Amanatides, S. Stamou & D. Mataras. *Gas phase and surface kinetics in plasma enhanced chemical vapor deposition of microcrystalline silicon: The combined effect of rf power and hydrogen dilution.* Journal of Applied Physics, vol. 90, no. 11, pages 5786–5798, 2001.

[Amanatides 02]   E. Amanatides, D. Mataras & D. E. Rapakoulias. *Combined effect of electrode gap and radio frequency on power deposition and film growth kinetics in SiH4/H2 discharges.* Journal of Vacuum Science & Technology A: Vacuum, Surfaces, and Films, vol. 20, no. 1, pages 68–75, 2002.

Bibliography

[Amanatides 05]   E. Amanatides, A. Hammad, E. Katsia & D. Mataras. *High pressure regime of plasma enhanced deposition of microcrystalline silicon.* Journal of Applied Physics, vol. 97, no. 7, page 073303, 2005.

[Atwater 10]   Harry A. Atwater & Albert Polman. *Plasmonics for improved photovoltaic devices.* Nature Materials, vol. 9, pages 205–213, Sep 2010.

[Azulay 05]   D. Azulay, I. Balberg, V. Chu, J. P. Conde & O. Millo. *Current routes in hydrogenated microcrystalline silicon.* Physical Review B, vol. 71, no. 11, page 113304, Mar 2005.

[Bachmann 10]   F. Bachmann, R. Hielscher & H. Schaeben. *Texture Analysis with MTEX–Free and Open Source Software Toolbox.* Solid State Phenomena, vol. 160, pages 63–68, 2010.

[Baik 97]   Seung Jae Baik, Jae Hoon Jang, Chang Hyun Lee, Woo Yeong Cho & Koeng Su Lim. *Highly textured and conductive undoped ZnO film using hydrogen post-treatment.* Applied Physics Letters, vol. 70, no. 26, pages 3516–3518, 1997.

[Bailat 02]   J. Bailat, E. Vallat-Sauvain, L. Feitknecht, C. Droz & A. Shah. *Influence of substrate on the microstructure of microcrystalline silicon layers and cells.* Journal of Non-Crystalline Solids, vol. 299-302, Part 2, no. 0, pages 1219–1223, 2002. 19th International Conference on Amorphous and Microcrystalline Semiconductors.

[Bailat 03]   J. Bailat, E. Vallat-Sauvain, L. Feitknecht, C. Droz & A. Shah. *Microstructure and open-circuit voltage of n − i − p microcrystalline silicon solar cells.* Journal of Applied Physics, vol. 93, no. 9, pages 5727–5732, 2003.

[Bailat 04]   Julien Bailat. *Growth, microstructure and electrical properties of thin film microcrystalline silicon solar cells.* PhD thesis, Université de Neuchâtel, Institut de microtechnique, 2004.

[Bailat 06]   J. Bailat, Dominé D., R. Schlüchter, J. Steinhauser, S. Faÿ, F. Freitas, C. Bücher, L. Feitknecht, X. Niquille, R. Tscharner, A. Shah & C. Ballif. *High-efficiency p-i-n microcrystalline and micromorph thin film silicon solar cells deposited on LPCVD ZnO coated glass substrates.* In Conference Record of the 2006 IEEE 4th World Conference on Photovoltaic Energy Conversion, Hawaï, USA, volume 2, pages 1533–1536, 2006.

[Bartlome 09]   R. Bartlome, A. Feltrin & C. Ballif. *Infrared laser-based monitoring of the silane dissociation during deposition of silicon thin films.* Applied Physics Letters, vol. 94, no. 20, pages –, 2009.

[Battaglia 11a]   Corsin Battaglia, Lukas Erni, Mathieu Boccard, Loris Barraud, Jordi Escarré, Karin Söderström, Grégory Bugnon, Adrian Billet, Laura Ding, Matthieu Despeisse, Franz-Josef Haug, Stefaan De Wolf & Christophe Ballif. *Micromorph thin-film silicon solar cells with transparent high-mobility hydrogenated indium oxide front electrodes.* Journal of Applied Physics, vol. 109, no. 11, page 114501, 2011.

[Battaglia 11b]   Corsin Battaglia, Jordi Escarré, Karin Söderström Mathieu Charrière, Matthieu Despeisse, Franz-Josef Haug & Christophe Ballif. *Nanomoulding of transparent zinc oxide electrodes for efficient light trapping in solar cells.* Nature Photonics, vol. 5, no. 9, pages 535–538, 2011.

[Battaglia 11c]   Corsin Battaglia, Jordi Escarré, Karin Söderström, Lukas Erni, Laura Ding, Grégory Bugnon, Adrian Billet, Mathieu Boccard, Loris Barraud, Stefaan De Wolf, Franz-Josef Haug, Matthieu Despeisse & Christophe Ballif. *Nanoimprint Lithography for High-Efficiency Thin-Film Silicon Solar Cells.* Nano Letters, vol. 11, no. 2, pages 661–665, 2011.

[Battaglia 12]   Corsin Battaglia, Ching-Mei Hsu, Karin Söderström, Jordi Escarré, Franz-Josef Haug, Mathieu Charrière, Mathieu Boccard, Matthieu Despeisse, Duncan T. L. Alexander, Marco Cantoni, Yi Cui & Christophe Ballif. *Light Trapping in Solar Cells: Can Periodic Beat Random?* ACS Nano, vol. 6, no. 3, pages 2790–7, 2012.

[Benedict 91]   John Benedict, Ron Anderson & Stanley J. Klepeis. *Recent Developments in the use of the Tripod Polisher for TEM Specimen Preparation.* MRS Proceedings, vol. 254, 1 1991.

[Berginski 07]   Michael Berginski, Jürgen Hüpkes, Melanie Schulte, Gunnar Schöpe, Helmut Stiebig, Bernd Rech & Matthias Wuttig. *The effect of front ZnO:Al surface texture and optical transparency on efficient light trapping in silicon thin-film solar cells.* Journal of Applied Physics, vol. 101, no. 7, page 074903, 2007.

[Beyer 07]   W. Beyer, J. Hüpkes & H. Stiebig. *Transparent conducting oxide films for thin film silicon photovoltaics.* Thin Solid Films, vol. 516, no. 2–4, pages 147–154, 2007.

[Biron 11]   Rémi Biron, Celine Pahud, Franz-Josef Haug, Jordi Escarré, Karin Söderström & Christophe Ballif. *Window layer with p doped silicon oxide for high Voc thin-film silicon n-i-p solar cells.* Journal of Applied Physics, vol. 110, no. 12, page 124511, 2011.

Bibliography

[Biron 12]   Rémi Biron, Céline Pahud, Franz-Josef Haug & Christophe Ballif. *Origin of the Voc enhancement with a p-doped nc-SiOx:H window layer in n-i-p solar cells.* Journal of Non-Crystalline Solids, vol. 358, no. 17, pages 1958–1961, 2012. Proceedings of the 24th International Conference on Amorphous and Nanocrystalline Semiconductors (ICANS 24) Nara, Japan August 21-26, 2011.

[Biron 13a]   R. Biron, S. Hänni, M. Boccard, C. Pahud, G. Bugnon, L. Ding, S. Nicolay, G. Parascandolo, F. Meillaud, M. Despeisse, F.-J. Haug & C. Ballif. *Optimization of the Asymmetric Intermediate Reflector Morphology for High Stabilized Efficiency Thin n–i–p Micromorph Solar Cells.* IEEE Journal of Photovoltaics, vol. 3, no. 1, pages 41–45, Jan 2013.

[Biron 13b]   Rémi Biron. *Layers with advanced optoelectronic properties for high-efficiency micromorph solar cells on opaque substrates.* PhD thesis, EPFL, 2013.

[Biron 13c]   Rémi Biron, Simon Hänni, Mathieu Boccard, Céline Pahud, Karin Söderström, Martial Duchamp, Rafal Dunin-Borkowski, Grégory Bugnon, Laura Ding, Sylvain Nicolay, Gaetano Parascandolo, Fanny Meillaud, Matthieu Despeisse, Franz-Josef Haug & Christophe Ballif. *New progress in the fabrication of n–i–p micromorph solar cells for opaque substrates.* Solar Energy Materials & Solar Cells, vol. 114, no. 0, pages 147–155, 2013.

[Bittkau 08]   Karsten Bittkau, Thomas Beckers, Stephan Fahr, Carsten Rockstuhl, Falk Lederer & Reinhard Carius. *Nanoscale investigation of light-trapping in a-Si:H solar cell structures with randomly textured interfaces.* physica status solidi (A), vol. 205, no. 12, pages 2766–2776, 2008.

[Boccard 11]   M. Boccard, P. Cuony, M. Despeisse, D. Dominé, A. Feltrin, N. Wyrsch & C. Ballif. *Substrate dependent stability and interplay between optical and electrical properties in single junction solar cells.* Solar Energy Materials & Solar Cells, vol. 95, no. 1, pages 195–198, 2011. 19th International Photovoltaic Science and Engineering Conference and Exhibition (PVSEC-19) Jeju, Korea, 9-13 November 2009.

[Boccard 12a]   M. Boccard, P. Cuony, C. Battaglia, S. Hänni, S. Nicolay, L. Ding, M. Benkhaira, G. Bugnon, A. Billet, M. Charrière, K. Söderström, J. Escarré, F. Sculati-Meillaud, M. Despeisse & C. Ballif. *Nanometer- and Micrometer-Scale Texturing for High-Efficiency Micromorph*

122

Thin-Film Silicon Solar Cells. IEEE Journal of Photovoltaics, vol. 2, no. 2, pages 83–87, Apr 2012.

[Boccard 12b]   M. Boccard, T. Söderström, P. Cuony, C. Battaglia, S. Hänni, S. Nicolay, L. Ding, M. Benkhaira, G. Bugnon, A. Billet, M. Charrière, F. Meillaud, M. Despeisse & C. Ballif. *Optimization of ZnO Front Electrodes for High-Efficiency Micromorph Thin-Film Si Solar Cells.* IEEE Journal of Photovoltaics, vol. 2, no. 3, pages 229–235, Jul 2012.

[Boccard 12c]   Mathieu Boccard. *Novel Micromorph Solar Cell Structures for Efficient Light Trapping and High-Quality Absorber Layers.* PhD thesis, EPFL, 2012.

[Boccard 12d]   Mathieu Boccard, Corsin Battaglia, Simon Hänni, Karin Söderström, Jordi Escarré, Sylvain Nicolay, Fanny Meillaud, Matthieu Despeisse & Christophe Ballif. *Multiscale Transparent Electrode Architecture for Efficient Light Management and Carrier Collection in Solar Cells.* Nano Letters, vol. 12, no. 3, pages 1344–1348, 2012.

[Boccard 12e]   Mathieu Boccard, Corsin Battaglia, Franz-Josef Haug, Matthieu Despeisse & Christophe Ballif. *Light trapping in solar cells: Analytical modeling.* APL, vol. 101, no. 15, page 151105, 2012.

[Boccard 13]   M. Boccard, C. Battaglia, N. Blondiaux, R. Pugin, M. Despeisse & C. Ballif. *Smoothening intermediate reflecting layer for tandem thin-film silicon solar cells.* Solar Energy Materials & Solar Cells, vol. 119, no. 0, pages 12–17, 2013. Thin-film Photovoltaic Solar Cell.

[Boccard 14]   Mathieu Boccard, Matthieu Despeisse, Jordi Escarre, Xavier Niquille, Grégory Bugnon, Simon Hänni, Maximilien Bonnet-Eymard, Fanny Meillaud & Christophe Ballif. *High-stable-efficiency tandem thin-film silicon solar cell with low-refractive-index silicon-oxide interlayer.* submitted, 2014.

[Bonnet-Eymard 13]   M. Bonnet-Eymard, M. Boccard, G. Bugnon, F. Sculati-Meillaud, M. Despeisse & C. Ballif. *Optimized short-circuit current mismatch in multi-junction solar cells.* Solar Energy Materials & Solar Cells, vol. 117, no. 0, pages 120–125, 2013. Dye Sensitized Solar Cells, Organic, Hybrid Solar Cells and New Concepts Dye Sensitized Solar Cells, Organic, Hybrid Solar Cells and New Concepts.

[Brammer 03]   T. Brammer & H. Stiebig. *Defect density and recombination lifetime in microcrystalline silicon absorbers of highly efficient thin-film solar cells determined by numerical device simulations.* Journal of Applied Physics, vol. 94, no. 2, pages 1035–1042, 2003.

Bibliography

[Brodsky 77]   M. H. Brodsky, M. Cardona & J. J. Cuomo. *Infrared and Raman spectra of the silicon-hydrogen bonds in amorphous silicon prepared by glow discharge and sputtering.* Physical Review B, vol. 16, no. 8, pages 3556–3571, Oct 1977.

[Bronneberg 11]   A. C. Bronneberg, A. H. M. Smets, M. Creatore & M. C. M. van de Sanden. *On the oxidation mechanism of microcrystalline silicon thin films studied by Fourier transform infrared spectroscopy.* Journal of Non-Crystalline Solids, vol. 357, no. 3, pages 884–887, 2011.

[Bruno 91]   G. Bruno, P. Capezzuto & G. Cicala. *rf glow discharge of SiF4–H2 mixtures: Diagnostics and modeling of the a?Si plasma deposition process.* Journal of Applied Physics, vol. 69, no. 10, pages 7256–7266, 1991.

[Bruno 09]   Giovanni Bruno, Pio Capezzuto, Maria M. Giangregorio, Giuseppe V. Bianco & Maria Losurdo. *From amorphous to microcrystalline silicon: Moving from one to the other by halogenated silicon plasma chemistry.* Philosophical Magazine, vol. 89, no. 28–30, pages 2469–2489, 2009.

[Bubenzer 90]   A. Bubenzer & J.P.M. Schmitt. *Plasma processes under vacuum conditions.* Vacuum, vol. 41, no. 7–9, pages 1957–1961, 1990.

[Buehlmann 07]   P. Buehlmann, J. Bailat, D. Dominé, A. Billet, F. Meillaud, A. Feltrin & C. Ballif. *In situ silicon oxide based intermediate reflector for thin-film silicon micromorph solar cells.* Applied Physics Letters, vol. 91, no. 14, page 143505, 2007.

[Bugnon 12]   Grégory Bugnon, Gaetano Parascandolo, Thomas Söderström, Peter Cuony, Matthieu Despeisse, Simon Hänni, Jakub Holovský, Fanny Meillaud & Christophe Ballif. *A New View of Microcrystalline Silicon: The Role of Plasma Processing in Achieving a Dense and Stable Absorber Material for Photovoltaic Applications.* Advanced Functional Materials, vol. 22, no. 17, pages 3665–3671, 2012.

[Bugnon 13]   Grégory Bugnon. *High-Quality Microcrystalline Silicon for Efficient Thin-Film Solar Cells.* PhD thesis, EPFL, 2013.

[Bugnon 14]   Grégory Bugnon, Gaetano Parascandolo, Simon Hänni, Michael Stuckelberger, Mathieu Charrière, Matthieu Despeisse, Fanny Meillaud & Christophe Ballif. *Silicon oxide buffer layer at the p-i interface in amorphous and microcrystalline silicon solar cells.* Solar Energy Materials & Solar Cells, vol. 120, Part A, no. 0, pages 143–150, 2014.

[Burschka 13]   Julian Burschka, Norman Pellet, Soo-Jin Moon, Robin Humphry-Baker, Peng Gao, Mohammad K. Nazeeruddin & Michael Grätzel. *Sequential deposition as a route to high-performance perovskite-sensitized solar cells.* Nature, vol. 499, pages 316–320, Jul 2013.

[Bustarret 88]   E. Bustarret, M. A. Hachicha & M. Brunel. *Experimental determination of the nanocrystalline volume fraction in silicon thin films from Raman spectroscopy.* Applied Physics Letters, vol. 52, no. 20, pages 1675–1677, 1988.

[Cabarrocas 02]   P. Roca i Cabarrocas, A. Fontcuberta i Morral & Y. Poissant. *Growth and optoelectronic properties of polymorphous silicon thin films.* Thin Solid Films, vol. 403–404, no. 0, pages 39–46, 2002. Proceedings of Symposium P on Thin Film Materials for Photovoltaics.

[Cantoni 10]   Marco Cantoni, Christel Genoud, Cécile Hébert & Graham Knott. *Large Volume, Isotropic, 3D Imaging of Cell Structure on the Nanometer Scale.* Microscopy and Microanalysis, vol. 24, pages 13–16, May 2010.

[Carius 97]   R. Carius, F. Finger, U. Backhausen, M. Luysberg, P. Hapke, L. Houben, M. Otte & H. Overhof. *Electronic Properties of Microcrystalline Silicon.* MRS Proceedings, vol. 467, 1 1997.

[Carlson 76]   D. E. Carlson & C. R. Wronski. *Amorphous silicon solar cell.* Applied Physics Letters, vol. 28, no. 11, pages 671–673, 1976.

[Chapin 54]   D. M. Chapin, C. S. Fuller & G. L. Pearson. *A New Silicon p–n Junction Photocell for Converting Solar Radiation into Electrical Power.* Journal of Applied Physics, vol. 25, no. 5, pages 676–677, 1954.

[Charpentier 13]   C. Charpentier, P. Prod'homme & P. Roca i Cabarrocas. *Microstructural, optical and electrical properties of annealed ZnO:Al thin films.* Thin Solid Films, vol. 531, no. 0, pages 424–429, 2013.

[Chen 92]   Y. L. Chen, C. Wang, G. Lucovsky, D. M. Maher & R. J. Nemanich. *Transmission electron microscopy and vibrational spectroscopy studies of undoped and doped Si,H and Si,C:H films.* Journal of Vacuum Science & Technology A: Vacuum, Surfaces, and Films, vol. 10, no. 4, pages 874–880, Jul 1992.

[Chirilă 13]   Adrian Chirilă, Patrick Reinhard, Fabian Pianezzi, Patrick Bloesch, Carolin Fella, Lukas Kranz, Debora Keller, Christina Gretener, Harald Hagendorfer, Dominik Jaeger, Rolf Erni, Shiro Nishiwaki,

Bibliography

Stephan Buecheler & Ayodhya N. Tiwari. *Potassium-induced surface modification of Cu(In,Ga)Se$_2$ thin films for high-efficiency solar cells.* Nature Materials, vol. 12, pages 1107–1111, Dec 2013.

[Chittick 69]   R. C. Chittick, J. H. Alexander & H. F. Sterling. *The Preparation and Properties of Amorphous Silicon.* Journal of The Electrochemical Society, vol. 116, no. 1, pages 77–81, 1969.

[Choong 13]   G. Choong, E. Vallat Sauvain, X. Multone, L. Fesquet, U. Kroll & J. Meier. *Measurements of Raman crystallinity profiles in thin-film microcrystalline silicon solar cells.* The Journal of Physics D: Applied Physics, vol. 46, no. 23, page 235105, 2013.

[Cicala 98]   G. Cicala, G. Bruno & P. Capezzuto. *Plasma deposition chemistry of amorphous silicon–carbon alloys from fluorinated gas.* Journal of Vacuum Science & Technology A: Vacuum, Surfaces, and Films, vol. 16, no. 5, pages 2762–2767, 1998.

[Cicala 01]   G. Cicala, P. Capezzuto & G. Bruno. *From amorphous to microcrystalline silicon deposition in SiF$_4$–H$_2$–He plasmas: in situ control by optical emission spectroscopy.* Thin Solid Films, vol. 383, no. 1-2, pages 203–205, 2001. Proceedings of Symposium O on.

[Clugston 97]   Donald.A. Clugston & Paul.A. Basore. *PC1D version 5: 32-bit solar cell modeling on personal computers.* In Conference Record of the Twenty-Sixth IEEE Photovoltaic Specialists Conference, Anaheim, USA, pages 207–210, 1997.

[Collins 03]   R.W. Collins, A.S. Ferlauto, G.M. Ferreira, Chi Chen, Joohyun Koh, R.J. Koval, Yeeheng Lee, J.M. Pearce & C.R. Wronski. *Evolution of microstructure and phase in amorphous, protocrystalline, and microcrystalline silicon studied by real time spectroscopic ellipsometry.* Solar Energy Materials & Solar Cells, vol. 78, no. 1-4, pages 143–180, 2003.

[Colombo 09]   C. Colombo, M. Heiss, M. Grätzel & A. Fontcuberta i Morral. *Gallium arsenide p-i-n radial structures for photovoltaic applications.* Applied Physics Letters, vol. 94, no. 17, page 173108, 2009.

[Cuony 10]   P. Cuony, M. Marending, D. T. L. Alexander, M. Boccard, G. Bugnon, M. Despeisse & C. Ballif. *Mixed-phase p-type silicon oxide containing silicon nanocrystals and its role in thin-film silicon solar cells.* Applied Physics Letters, vol. 97, no. 21, page 213502, 2010.

[Cuony 11]   Peter Cuony. *Optical Layers for Thin-film Silicon Solar Cells.* PhD thesis, EPFL, 2011.

[Cuony 12]   Peter Cuony, Duncan T. L. Alexander, Ivan Perez-Wurfl, Matthieu Despeisse, Gregory Bugnon, Mathieu Boccard, Thomas Soderstrom, Aicha Hessler-Wyser, Cecile Hebert & Christophe Ballif. *Silicon filaments in silicon oxide for next-generation photovoltaics.* Advanced Materials, vol. 24, no. 9, pages 1182–1186, Mar 2012.

[Curtins 87a]   H. Curtins, N. Wyrsch, M. Favre & A.V. Shah. *Influence of plasma excitation frequency for a-Si:H thin film deposition.* Plasma Chemistry and Plasma Processing, vol. 7, no. 3, pages 267–273, 1987.

[Curtins 87b]   H. Curtins, N. Wyrsch & A. V. Shah. *High-rate deposition of amorphous hydrogenated silicon: effect of plasma excitation frequency.* Electronics Letters, vol. 23, pages 228–230, Feb 1987.

[de Wild-Scholten 13]   M.J. (Mariska) de Wild-Scholten. *Energy payback time and carbon footprint of commercial photovoltaic systems.* Solar Energy Materials & Solar Cells, vol. 119, no. 0, pages 296–305, 2013. Thin-film Photovoltaic Solar Cells.

[De Wolf 12]   Stefaan De Wolf, Antoine Descoeudres, Zachary C. Holman & Christophe Ballif. *High-efficiency Silicon Heterojunction Solar Cells: A Review.* Green, vol. 2, no. 1, pages 7–24, Mar 2012.

[Deckman 83a]   H. W. Deckman, C. B. Roxlo & E. Yablonovitch. *Maximum statistical increase of optical absorption in textured semiconductor films.* Optics Letters, vol. 8, no. 9, pages 491–493, Sep 1983.

[Deckman 83b]   H. W. Deckman, C. R. Wronski, H. Witzke & E. Yablonovitch. *Optically enhanced amorphous silicon solar cells.* Applied Physics Letters, vol. 42, no. 11, pages 968–970, 1983.

[Demichelis 94]   F. Demichelis, G. Crovini, C. F. Pirri, E. Tresso, M. Fanclulli, T. Piesarkiewicz & T. Stapinski. *Structural and optoelectronic properties of doped microcrystalline silicon carbide films.* Semiconductor Science and Technology, vol. 9, no. 8, pages 1543–1548, 1994.

[Despeisse 10]   M. Despeisse, G. Bugnon, A. Feltrin, M. Stuckelberger, P. Cuony, M. Meillaud, A. Billet & C. Ballif. *Resistive interlayer for improved performance of thin film silicon solar cells on highly textured substrate.* Applied Physics Letters, vol. 96, no. 7, page 073507, 2010.

Bibliography

[Despeisse 11]	Matthieu Despeisse, Corsin Battaglia, Mathieu Boccard, Gregory Bugnon, Mathieu Charrière, Peter Cuony, Simon Hänni, Linus Löfgren, Fanny Meillaud, Gaetano Parascandolo, Thomas Söderström & Christophe Ballif. *Optimization of thin film silicon solar cells on highly textured substrates.* physica status solidi (A), vol. 208, no. 8, pages 1863–1868, 2011.
[Ding 12a]	L. Ding, M. Benkhaira, S. Nicolay & C. Ballif. *Enhanced mobility of hydrogenated MO-LPCVD ZnO contacts for high performances thin film silicon solar cells.* MRS Proceedings, vol. 1426, pages 51–56, 2012.
[Ding 12b]	L. Ding, M. Boccard, G. Bugnon, M. Benkhaira, S. Nicolay, M. Despeisse, F. Meillaud & C. Ballif. *Highly transparent ZnO bilayers by LP-MOCVD as front electrodes for thin-film micromorph silicon solar cells.* Solar Energy Materials & Solar Cells, vol. 98, no. 0, pages 331–336, 2012.
[Ding 12c]	L. Ding, Mathieu Boccard, G. Bugnon, M. Benkhaira, M. Despeisse, F. Sculati-Meillaud, S. Nicolay, P.A. Losio, O. Kluth, P. Carroy, O. Caglar & C. Ballif. *New Generation Transparent LPCVD ZnO Electrodes for Enhanced Photocurrent in Micromorph Solar Cells and Modules.* IEEE Journal of Photovoltaics, vol. 2, no. 2, pages 88–93, Apr 2012.
[Ding 13a]	Laura Ding. *Low-Pressure Chemical Vapor Deposited Zinc Oxide Films: Toward Decoupled Opto-Electrical and Morphological Properties for More Efficient Electrodes.* PhD thesis, EPFL, 2013.
[Ding 13b]	Laura Ding, Sylvain Nicolay, Jérôme Steinhauser, Ulrich Kroll & Christophe Ballif. *Relaxing the Conductivity/Transparency Trade-Off in MOCVD ZnO Thin Films by Hydrogen Plasma.* Advanced Functional Materials, vol. 23, no. 41, pages 5177–5182, 2013.
[Ding 14]	Laura Ding, Michael Stuckelberger, Monica Morales Masis, Sylvain Nicolay & Christophe Ballif. *Stability of the opto-electrical properties of Zinc Oxide Electrodes in Thin-Film Silicon Solar Cells under Light Soaking.* in prep., 2014.
[Djeridane 07]	Y. Djeridane, A. Abramov & P. Roca i Cabarrocas. *Silane versus silicon tetrafluoride in the growth of microcrystalline silicon films by standard radio frequency glow discharge.* Thin Solid Films, vol. 515, no. 19, pages 7451–7454, 2007. Proceedings of Symposium I on Thin Films for Large Area Electronics EMRS 2007 Conference - EMRS 2006 - Symposium I.

128

[Djeridane 08]   Yassine Djeridane. *Synthèse de nanocristaux par plasma froid et leur rôle dans la croissance de couches minces de silicium microcristallin : Application aux transistors.* PhD thesis, Ecole Polytechnique, LPICM, 2008.

[Dominé 10]   Didier Dominé, Franz-Josef Haug, Corsin Battaglia & Christophe Ballif. *Modelling of light scattering from micro- and nanotextured surfaces.* Journal of Applied Physics, vol. 107, no. 044504, 2010.

[Dore 14]   J. Dore, D. Ong, S. Varlamov, R. Egan & M.A. Green. *Progress in Laser-Crystallized Thin-Film Polycrystalline Silicon Solar Cells: Intermediate Layers, Light Trapping, and Metallization.* IEEE Journal of Photovoltaics, vol. 4, no. 1, pages 33–39, Jan 2014.

[Dornstetter 13]   J.-C. Dornstetter, S. Kasouit & P. Roca i Cabarrocas. *Deposition of High-Efficiency Microcrystalline Silicon Solar Cells Using SiF$_4$ / H$_2$ / Ar Mixtures.* IEEE Journal of Photovoltaics, vol. 3, no. 1, pages 581–586, Jan 2013.

[Dornstetter 14]   Jean-Christophe Dornstetter, Junkang Wang, Bastien Bruneau, Erik V. Johnson & Pere Roca I Cabarrocas. *Material and Growth Mechanism Studies of Microcrystalline Silicon Deposited from SiF$_4$/H$_2$/Ar Gas Mixtures.* Canadian Journal of Physics, vol. 0, no. 0, pages 1–4, 2014.

[Droz 03]   Corinne Droz. *Thin Film Microcrystalline Silicon Layers and Solar Cells: Microstructure and Electrical Performances.* PhD thesis, Université de Neuchâtel, Institut de microtechnique, 2003.

[Droz 04]   C. Droz, E. Vallat-Sauvain, J. Bailat, L. Feitknecht, J. Meier & A. Shah. *Relationship between Raman crystallinity and open-circuit voltage in microcrystalline silicon solar cells.* Solar Energy Materials & Solar Cells, vol. 81, no. 1, pages 61–71, 2004.

[Duchamp 11]   M Duchamp, A Ramar, A Kovács, T Kasama, F.-J. Haug, S B Newcomb, C Ballif & R E Dunin-Borkowski. *Conventional and 360 degree electron tomography of a micro-crystalline silicon solar cell.* Journal of Physics: Conference Series, vol. 326, no. 1, page 012057, 2011.

[Duchamp 13]   M. Duchamp, M. Lachmann, C. B. Boothroyd, A. Kovács, F.-J. Haug, C. Ballif & R. E. Dunin-Borkowski. *Compositional study of defects in microcrystalline silicon solar cells using spectral decomposition in the scanning transmission electron microscope.* Applied Physics Letters, vol. 102, no. 13, page 133902, 2013.

Bibliography

[Einstein 05]   A. Einstein. *Über einen die Erzeugung und Verwandlung des Lichtes betreffenden heuristischen Gesichtspunkt.* Annalen der Physik, vol. 322, no. 6, pages 132–148, 1905.

[Eminian 11]   C. Eminian, F.-J. Haug, O. Cubero, X. Niquille & C. Ballif. *Photocurrent enhancement in thin film amorphous silicon solar cells with silver nanoparticles.* Progress in Photovoltaics: Research and Applications, vol. 19, no. 3, pages 260–265, 2011.

[Escarré 12a]   Jordi Escarré, Sylvain Nicolay, Corsin Battaglia, Matthieu Boccard, Laura Ding, Matthieu Despeisse, Franz-Josef Haug & Christophe Ballif. *Nanomoulded front ZnO contacts for thin film silicon solar cell applications.* In Proceedings of the 27th European Photovoltaic Solar Energy Conference and Exhibition, 2012, Frankfurt, Germany, pages 2632–2634, 2012.

[Escarré 12b]   Jordi Escarré, Karin Söderström, Matthieu Despeisse, Sylvain Nicolay, Corsin Battaglia, Grégory Bugnon, Laura Ding, Fanny Meillaud, Franz-Josef Haug & Christophe Ballif. *Geometric light trapping for high efficiency thin film silicon solar cells.* Solar Energy Materials & Solar Cells, vol. 98, no. 0, pages 185–190, 2012.

[Fanni 14]   L. Fanni, B. A. Aebersold, D.T.L. Alexander, L. Ding, M. Morales Masis, S. Nicolay & C. Ballif. *c-texture versus a-texture LP-MOCVD ZnO films: lower resistivity despite smaller grain size.* submitted, 2014.

[Faraji 92]   M. Faraji, Sunil Gokhale, S. M. Choudhari, M. G. Takwale & S. V. Ghaisas. *High mobility hydrogenated and oxygenated microcrystalline silicon as a photosensitive material in photovoltaic applications.* Applied Physics Letters, vol. 60, no. 26, pages 3289–3291, 1992.

[Faÿ 03]   Sylvie Faÿ. *L'oxyde de zinc par dépôt chimique en phase vapeur comme contact électrique transparent et diffuseur de lumière pour les cellules solaires.* PhD thesis, Université de Neuchâtel, Institut de microtechnique, 2003.

[Faÿ 06]   S. Faÿ, L. Feitknecht, R. Schlüchter, U. Kroll, E. Vallat-Sauvain & A. Shah. *Rough ZnO layers by LP-CVD process and their effect in improving performances of amorphous and microcrystalline silicon solar cells.* Solar Energy Materials & Solar Cells, vol. 90, no. 18-19, pages 2960–2967, Nov 2006.

[Faÿ 07]   Sylvie Faÿ, Jérôme Steinhauser, Nuno Oliveira, Evelyne Vallat-Sauvain & Christophe Ballif. *Opto-electronic properties of rough LP-*

CVD ZnO:B for use as TCO in thin-film silicon solar cells. Thin Solid Films, vol. 515, no. 24, pages 8558–8561, 2007. First International Symposium on Transparent Conducting Oxides.

[Faÿ 10]   Sylvie Faÿ, Jérôme Steinhauser, Sylvain Nicolay & Christophe Ballif. *Polycrystalline ZnO:B grown by {LPCVD} as {TCO} for thin film silicon solar cells.* Thin Solid Films, vol. 518, no. 11, pages 2961–2966, 2010. Transparent Oxides for Electronics and Optiocs (TOEO-6).

[Feltrin 08]   Andrea Feltrin & Alex Freundlich. *Material considerations for terawatt level deployment of photovoltaics.* Renewable Energy, vol. 33, no. 2, pages 180–185, 2008. E-MRS 2006 Symposium M: Materials, Devices and Prospects for Sustainable Energy, 2006 Spring Meeting of the European Materials Research Society.

[Feltrin 13]   Andrea Feltrin, Tomomi Meguro, Elisabeth Van Assche, Takashi Suezaki, Mitsuru Ichikawa, Takashi Kuchiyama, Daisuke Adachi, Osamu Inaki, Kunta Yoshikawa, Gensuke Koizumi, Hisashi Uzu, Hiroaki Ueda, Toshihiko Uto, Takahisa Fujimoto, Toru Irie, Hironori Hayakawa, Naoaki Nakanishi, Masashi Yoshimi & Kenji Yamamoto. *Advanced light trapping designs for high efficiency thin film silicon solar cells.* Solar Energy Materials & Solar Cells, vol. 119, no. 0, pages 219–227, 2013. Thin-film Photovoltaic Solar Cells.

[Finger 94]   F. Finger, P. Hapke, M. Luysberg, R. Carius, H. Wagner & M. Scheib. *Improvement of grain size and deposition rate of microcrystalline silicon by use of very high frequency glow discharge.* Applied Physics Letters, vol. 65, no. 20, pages 2588–2590, 1994.

[Finger 05]   F. Finger, R. Carius, T. Dylla, S. Klein, S. Okur & M. Günes. *Instability phenomena in microcrystalline silicon films.* Journal of Optoelectronics and Advanced Materials, vol. 7, no. 1, pages 83–90, 2005.

[Finger 08]   F. Finger, Y. Mai, S. Klein & R. Carius. *High efficiency microcrystalline silicon solar cells with Hot-Wire {CVD} buffer layer.* Thin Solid Films, vol. 516, no. 5, pages 728–732, 2008. Proceedings of the Fourth International Conference on Hot-Wire {CVD} Cat-CVD Process.

[Flückiger 93]   R. Flückiger, J. Meier, H. Keppner, M. Götz & A. Shah. *PREPARATION OF UNDOPED AND DOPED MICROCRYSTALLIINE SILICON (μc-Si:H) BY VHF-GD FOR P-I-N SOLAR CELLS.* In Proceedings of the 23rd IEEE PV Conference, Louisville, pages 839–844, 1993.

[Flückiger 94]   Roger Flückiger, J. Meier, A. Shah, A. Catana, M. Brunel, H. V. Nguyen, R. W. Collins & R. Carius. *Structural, Optical and Electrical*

Bibliography

Properties of μ c-Si:H Very Thin Films Deposited by the VHF-GD Technique. MRS Proceedings, vol. 336, 1 1994.

[Fontcuberta i Morral 00]   A. Fontcuberta i Morral, J. Bertomeu & P. Roca i Cabarrocas. *The role of hydrogen in the formation of microcrystalline silicon.* Materials Science and Engineering: B, vol. 69–70, no. 0, pages 559–563, 2000.

[Fontcuberta i Morral 01]   A. Fontcuberta i Morral & P. Roca i Cabarrocas. *Shedding light on the growth of amorphous, polymorphous, protocrystalline and microcrystalline silicon thin films.* Thin Solid Films, vol. 383, no. 1–2, pages 161–164, 2001. Proceedings of Symposium O on.

[Fontcuberta i Morral 02]   A. Fontcuberta i Morral & P. Roca i Cabarrocas. *Etching and hydrogen diffusion mechanisms during a hydrogen plasma treatment of silicon thin films.* Journal of Non-Crystalline Solids, vol. 299-302, Part 1, no. 0, pages 196–200, 2002. 19th International Conference on Amorphous and Microcrystalline Semiconductors.

[Fontcuberta i Morral 04]   A. Fontcuberta i Morral, P. Roca i Cabarrocas & C. Clerc. *Structure and hydrogen content of polymorphous silicon thin films studied by spectroscopic ellipsometry and nuclear measurements.* Physical Review B, vol. 69, no. 12, page 125307, Mar 2004.

[Frammelsberger 10]   W. Frammelsberger, P. Lechner, R. Lechner, W. Psyk, R. Geyer, S. Dandl, A. Haslauer & H. Maurus. *STATUS OF THE DEVELOPMENT OF MICROMORPH CELLS AND MODULES AT SCHOTT SOLAR THIN FILM GMBH.* In Proceedings of the 25th European Photovoltaic Solar Energy Conference and Exhibition / 5th World Conference on Photovoltaic Energy Conversion, 6-10 September 2010, Valencia, Spain, pages 2788–2792, 2010.

[Fritts 83]   C. E. Fritts. *On a new form of selenium cell, and some electrical discoveries made by its use.* American Journal of Science, vol. Series 3, Vol. 26, no. 156, pages 465–472, 1883.

[Fthenakis 11]   V.M. Fthenakis & H.C. Kim. *Photovoltaics: Life-cycle analyses.* Solar Energy, vol. 85, no. 8, pages 1609–1628, 2011. Progress in Solar Energy.

[Fujiwara 04]   Hiroyuki Fujiwara, Michio Kondo & Akihisa Matsuda. *Nucleation mechanism of microcrystalline silicon from the amorphous phase.* Journal of Non-Crystalline Solids, vol. 338–340, no. 0, pages 97–101, 2004. Proceedings of the 20th International Conference on Amorphous and Microcrystalline Semiconductors.

[Fujiwara 07]   Hiroyuki Fujiwara & Michio Kondo. *Effects of a-Si:H layer thicknesses on the performance of a-Si:H/c-Si heterojunction solar cells.* Journal of Applied Physics, vol. 101, no. 5, page 054516, 2007.

[Gerlach 13]   D. Gerlach, R. G. Wilks, D. Wippler, M. Wimmer, M. Lozac'h, R. Félix, A. Mück, M. Meier, S. Ueda, H. Yoshikawa, M. Gorgoi, K. Lips, B. Rech, M. Sumiya, J. Hüpkes, K. Kobayashi & M. Bär. *The silicon/zinc oxide interface in amorphous silicon-based thin-film solar cells: Understanding an empirically optimized contact.* Applied Physics Letters, vol. 103, no. 2, page 023903, 2013.

[Ghosh 92]   Sukriti Ghosh, Abhijit De, Swati Ray & A. K. Barua. *Role of hydrogen dilution and diborane doping on the growth mechanism of p?type microcrystalline silicon films prepared by photochemical vapor deposition.* Journal of Applied Physics, vol. 71, no. 10, pages 5205–5211, 1992.

[Giangregorio 06]   M.M. Giangregorio, M. Losurdo, A. Sacchetti, P. Capezzuto & G. Bruno. *Correlation between structure and optical properties of Si-based alloys deposited by {PECVD}.* Thin Solid Films, vol. 511-512, no. 0, pages 598–602, 2006. {EMSR} 2005 - Proceedings of Symposium F on Thin Film and Nanostructured Materials for Photovoltaics.

[Golay 00]   S. Golay, J. Meier, S. Dubail, U. Kroll & A. Shah. *Laser Scribing of p-i-n/p-i-n "Micromorph" (a-Si:H/μ c-Si:H) Tandem Cells.* In Proceedings of the 16th EU Photovoltaic Solar Energy Conference, pages 494–497, 2000.

[Goodman 79]   C. H. L. Goodman. *Improved amorphous semiconductors for solar cells.* Nature, vol. 279, page 349, May 1979.

[Gordijn 05]   Aad Gordijn. *Microcrystalline Silicon for Thin-Film Solar Cells.* PhD thesis, Universiteit Utrecht, 2005.

[Gordijn 06]   A. Gordijn, L. Hodakova, J.K. Rath & R.E.I. Schropp. *Influence on cell performance of bulk defect density in microcrystalline silicon grown by VHF PECVD.* Journal of Non-Crystalline Solids, vol. 352, no. 9–20, pages 1868–1871, 2006. Amorphous and Nanocrystalline Semiconductors - Science and Technology - Proceedings of the 21st International Conference on Amorphous and Nanocrystalline Semiconductors - Science and Technology - 21st International Conference on Amorphous and Nanocrystalline Semiconductors.

[Green 12]   Martin A. Green, Keith Emery, Yoshihiro Hishikawa, Wilhelm Warta & Ewan D. Dunlop. *Solar cell efficiency tables (version 39).* Progress

in Photovoltaics: Research and Applications, vol. 20, no. 1, pages 12–20, 2012.

[Green 13a]   Martin A. Green, Keith Emery, Yoshihiro Hishikawa, Wilhelm Warta & Ewan D. Dunlop. *Solar cell efficiency tables (version 41)*. Progress in Photovoltaics: Research and Applications, vol. 21, no. 1, pages 1–11, 2013.

[Green 13b]   Martin A. Green, Keith Emery, Yoshihiro Hishikawa, Wilhelm Warta & Ewan D. Dunlop. *Solar cell efficiency tables (version 42)*. Progress in Photovoltaics: Research and Applications, vol. 21, no. 5, pages 827–837, 2013.

[Green 14a]   Martin A. Green, Keith Emery, Yoshihiro Hishikawa, Wilhelm Warta & Ewan D. Dunlop. *Solar cell efficiency tables (version 43)*. Progress in Photovoltaics: Research and Applications, vol. 22, no. 1, pages 1–9, 2014.

[Green 14b]   Martin A. Green, Keith Emery, Yoshihiro Hishikawa, Wilhelm Warta & Ewan D. Dunlop. *Solar cell efficiency tables (version 44)*. Progress in Photovoltaics: Research and Applications, vol. 22, no. 7, pages 701–710, 2014.

[Guha 13]   Subhendu Guha, Jeffrey Yang & Baojie Yan. *High efficiency multi-junction thin film silicon cells incorporating nanocrystalline silicon*. Solar Energy Materials & Solar Cells, vol. 119, no. 0, pages 1–11, 2013. Thin-film Photovoltaic Solar Cells.

[Guo 98]   Lihui Guo, Michio Kondo, Makoto Fukawa, Kimihiko Saitoh & Akihisa Matsuda. *High Rate Deposition of Microcrystalline Silicon Using Conventional Plasma-Enhanced Chemical Vapor Deposition*. Japanese Journal of Applied Physics, vol. 37, no. 10A, page L1116, 1998.

[Haddad-Adel 07] A. Haddad-Adel, T. Inokuma, Y. Kurata & S. Hasegawa. *Roles of SiH4 and SiF4 in growth and structural changes of poly-Si films*. Surface Science, vol. 601, no. 5, pages 1429–1436, 2007.

[Hamers 00]   E. A. G. Hamers, A. Fontcuberta i Morral, C. Niikura, R. Brenot & P. Roca i Cabarrocas. *Contribution of ions to the growth of amorphous, polymorphous, and microcrystalline silicon thin films*. Journal of Applied Physics, vol. 88, no. 6, pages 3674–3688, 2000.

[Hanak 79]   J.J. Hanak. *Monolithic solar cell panel of amorphous silicon*. Solar Energy, vol. 23, no. 2, pages 145–147, 1979.

[Hanna 86]   J. Hanna, S. Oda, H. Shibata, H. Shirai, A. Miyauchi, A. Tanabe, K. Fukuda, T. Ohtoshi, O. Tokuhiro, H. Nguyen & I. Shimizu. *Reactive Deposition of a-Silicon and Si-Based Alloys.* MRS Proceedings, vol. 70, 1986.

[Hanna 88]   Jun-Ichi Hanna, Akira Kamo, Masanobu Azuma, Naoki Shibata, Hajime Shirai & Isamu Shimizu. *Propagation of Si-Network in Hr-Cvd and Spontaneous Chemical Deposition.* MRS Proceedings, vol. 118, 1988.

[Hänni 11]   S. Hänni, C. Battaglia, M. Boccard, G. Bugnon, P. Cuony, M. Despeisse, L. Ding, S. Nicolay, F. Meillaud & C. Ballif. *Towards Better Understanding of Long-Term Stability in Thin Film Microcrystalline Silicon Solar Cells.* In Proceedings of the 26th European Photovoltaic Solar Energy Conference and Exhibition, 2011, Hamburg, Germany, pages 2699–2703, 2011.

[Hänni 13a]   S. Hänni, D. T. L. Alexander, L. Ding, G. Bugnon, M. Boccard, C. Battaglia, P. Cuony, J. Escarré, G. Parascandolo, S. Nicolay, M. Cantoni, M. Despeisse, F. Meillaud & C. Ballif. *On the Interplay Between Microstructure and Interfaces in High-Efficiency Microcrystalline Silicon Solar Cells.* IEEE Journal of Photovoltaics, vol. 3, no. 1, pages 11–16, Jan 2013.

[Hänni 13b]   Simon Hänni, Grégory Bugnon, Gaetano Parascandolo, Mathieu Boccard, Jordi Escarré, Matthieu Despeisse, Fanny Meillaud & Christophe Ballif. *High-efficiency microcrystalline silicon single-junction solar cells.* Progress in Photovoltaics: Research and Applications, vol. 21, no. 5, pages 821–826, 2013.

[Hänni 14a]   Simon Hänni, Mathieu Boccard, Grégory Bugnon, Matthieu Despeisse, Jan-Willem Schüttauf, Franz-Josef Haug, Fanny Meillaud & Christophe Ballif. *Microcrystalline silicon solar cells with passivated interfaces for high open-circuit voltage.* to be subm., vol. –, no. –, pages –, 2014.

[Hänni 14b]   Simon Hänni, Laura Ding, Grégory Bugnon, Mathieu Boccard, Sylvain Nicolay, Fanny Meillaud & Christophe Ballif. *Post-Deposition Treatment of Microcrystalline Silicon Solar Cells For Improved Performance on Rough Superstrates.* to be subm., vol. –, no. –, pages –, 2014.

[Hapke 93]   P. Hapke, F. Finger, R. Carius, H. Wagner, K. Prasad & R. Flückiger. *Annealing Studies of the Microcrystalline Silicon System.* Journal of Non-Crystalline Solids, vol. 164–166, no. Part 2, pages 981–984,

1993. Proceedings of the Fifteenth International Conference on Amorphous Semiconductors-Science and Technology.

[Hoetzel 11]   Jochen Hoetzel, Evelyne Vallat-Sauvain, Stefano Benagli, Lucie Castens, Xavier Multone & Daniel Borrello. *THIN FILM SOLAR CELL WITH MICROCRYSTALLINE ABSORPBER LAYER AND PASSIVATION LAYER AND METHOD FOR MANUFACTURING SUCH A CELL.* Patent Application, Dec 2011. WO 2011/160246 A1.

[Holman 12]   Z.C. Holman, A. Descoeudres, L. Barraud, F.Z. Fernandez, J.P. Seif, S. De Wolf & C. Ballif. *Current Losses at the Front of Silicon Heterojunction Solar Cells.* IEEE Journal of Photovoltaics, vol. 2, no. 1, pages 7–15, Jan 2012.

[Houben 98]   L. Houben, M. Luysberg, P. Hapke, R. Carius, F. Finger & H. Wagner. *Structural properties of microcrystalline silicon in the transition from highly crystalline to amorphous growth.* Philosophical Magazine A, vol. 77, no. 6, pages 1447–1460, 1998.

[Houben 03]   L. Houben, M. Luysberg & R. Carius. *Microtwinning in microcrystalline silicon and its effect on grain-size measurements.* Physical Review B, vol. 67, page 045312, Jan 2003.

[Hourd 91]   A. C. Hourd, D. L. Melville & W. E. Spear. *Electronic properties of amorphous and microcrystalline silicon prepared in a microwave plasma from SiF4.* Philosophical Magazine B, vol. 64, no. 5, pages 533–550, 1991.

[Howling 07]   A. A. Howling, B. Strahm, P. Colsters, L. Sansonnens & Ch. Hollenstein. *Fast equilibration of silane/hydrogen plasmas in large area RF capacitive reactors monitored by optical emission spectroscopy.* Plasma Sources Science and Technology, vol. 16, no. 4, pages 679–696, 2007.

[Hüpkes 06]   J. Hüpkes, B. Rech, O. Kluth, T. Repmann, B. Zwaygardt, J. Müller, R. Drese & M. Wuttig. *Surface textured MF-sputtered ZnO films for microcrystalline silicon-based thin-film solar cells.* Solar Energy Materials & Solar Cells, vol. 90, no. 18–19, pages 3054–3060, 2006. 14th International Photovoltaic Science and Engineering Conference 14th International Photovoltaic Science and Engineering Conference.

[Hüpkes 12]   Jürgen Hüpkes, Jorj I. Owen, Sascha E. Pust & Eerke Bunte. *Chemical Etching of Zinc Oxide for Thin-Film Silicon Solar Cells.* ChemPhysChem, vol. 13, no. 1, pages 66–73, 2012.

[Hüsser 13]   Pius Hüsser. *National Survey Report of PV Power Applications in Switzerland 2012*. Rapport technique, International Energy Agency (IEA), Photovoltaic Power Systems Programme (PVPS), Sep 2013.

[IEA 13a]   IEA. *annual report 2012*. Rapport technique, International Energy Agency (IEA), Photovoltaic Power Systems Programme (PVPS), Apr 2013.

[IEA 13b]   IEA. *Key World Energy statistics 2013*. Rapport technique, International Energy Agency (IEA), 2013.

[IEA 13c]   IEA. *TRENDS 2013 IN PHOTOVOLTAIC APPLICATIONS – Survey Report of Selected IEA Countries between 1992 and 2012*. Rapport technique Report IEA-PVPS T1-23:2013, International Energy Agency (IEA), Photovoltaic Power Systems Programme (PVPS), Nov 2013.

[Iqbal 80]   Z. Iqbal, A. P. Webb & S. Veprek. *Polycrystalline silicon films deposited in a glow discharge at temperatures below* 250 °C. Applied Physics Letters, vol. 36, no. 2, pages 163–165, 1980.

[Iqbal 82]   Z. Iqbal & S. Veprek. *Raman scattering from hydrogenated microcrystalline and amorphous silicon*. The Journal of Physics C: Solid State Physics, vol. 15, no. 2, page 377, 1982.

[Isabella 10]   Olindo Isabella, Janez Krč & Miro Zeman. *Modulated surface textures for enhanced light trapping in thin-film silicon solar cells*. Applied Physics Letters, vol. 97, no. 10, page 101106, 2010.

[Isabella 14]   Olindo Isabella, Arno Hendrikus Marie Smets & Miro Zeman. *Thin-film silicon-based quadruple junction solar cells approaching 20% conversion efficiency*. Solar Energy Materials & Solar Cells, no. 0, pages –, 2014.

[Ishihara 93]   Shun-Ichi Ishihara, Deyan He, Masami Nakata & Isamu Shimizu. *Preparation of High-Quality Microcrystalline Silicon from Fluorinated Precursors by a Layer-by-Layer Technique*. Japanese Journal of Applied Physics, vol. 32, no. Part 1, No. 4, pages 1539–1545, 1993.

[Jacobson 09]   Mark Z. Jacobson. *Review of solutions to global warming, air pollution, and energy security*. Energy & Environmental Science, vol. 2, no. 2, pages 148–173, 2009.

[Jäger-Waldau 13]   Arnulf Jäger-Waldau. *PV Status Report 2013*. Rapport technique EUR 26118 EN, European Commission, DG Joint Research Centre,

Bibliography

Institute for Energy, Renewable Energy Unit, Via Enrico Fermi 2749; TP 450 I – 21027 Ispra (VA), Italia, Sep 2013.

[Jenq-Shiuh 92] Chou Jenq-Shiuh, Sah Wen-Jyh, Lee Si-Chen, Chang T'ien-Chih & Wang Jon-Ching. *Microcrystalline silicon deposited by glow discharge decomposition of heavily diluted silane.* Materials Chemistry and Physics, vol. 32, no. 3, pages 273–279, 1992.

[Johnson 08] E. V. Johnson, M. Nath, P. Roca i Cabarrocas, A. Abramov & P. Chatterjee. *Why does the open-circuit voltage in a micro-crystalline silicon PIN solar cell decrease when increasing the crystalline volume fraction?* Journal of Non-Crystalline Solids, vol. 354, pages 2455–2459, 2008.

[Jovanov 13a] V. Jovanov, X. Xu, S. Shrestha, M. Schulte, J. Hüpkes, M. Zeman & D. Knipp. *Influence of interface morphologies on amorphous silicon thin film solar cells prepared on randomly textured substrates.* Solar Energy Materials & Solar Cells, vol. 112, no. 0, pages 182–189, 2013.

[Jovanov 13b] Vladislav Jovanov, Xu Xu, Shailesh Shrestha, Melanie Schulte, Jürgen Hüpkes & Dietmar Knipp. *Predicting the Interface Morphologies of Silicon Films on Arbitrary Substrates: Application in Solar Cells.* ACS Applied Materials & Interfaces, vol. 5, no. 15, pages 7109–7116, 2013.

[Kamiya 99] T. Kamiya, K. Nakahata, A. Miida, C.M. Fortmann & I. Shimizu. *Control of orientation from random to (220) or (400) in polycrystalline silicon films.* Thin Solid Films, vol. 337, no. 1–2, pages 18–22, 1999.

[Kaneko 93] Toshiki Kaneko, Ken-ichi Onisawa, Masatoshi Wakagi, Yoshiaki Kita & Tetsuroh Minemura. *Crystalline Fraction of Microcrystalline Silicon Films Prepared by Plasma-Enhanced Chemical Vapor Deposition Using Pulsed Silane Flow.* Japanese Journal of Applied Physics, vol. 32, no. Part 1, No. 11A, pages 4907–4911, 1993.

[Kasouit 02] S. Kasouit, S. Kumar, R. Vanderhaghen, P. Roca i Cabarrocas & I. French. *Fluorine and hydrogen effects on the growth and transport properties of microcrystalline silicon from SiF4 precursor.* Journal of Non-Crystalline Solids, vol. 299–302, Part 1, no. 0, pages 113–117, 2002. 19th International Conference on Amorphous and Microcrystalline Semiconductors.

[Kasouit 03] S. Kasouit, P. Roca i Cabarrocas, R. Vanderhaghen, Y. Bonassieux, M. Elyaakoubi, I. French, J. Rocha & B. Vitoux. *Effect of deposition conditions and dielectric plasma treatments on the electrical*

properties of microcrystalline silicon {TFTs}. Thin Solid Films, vol. 427, no. 1–2, pages 67–70, 2003. Proceedings of Symposium K on Thin Film Materials for Large Area Electronics of the European Materials Research Society (E-MRS) 2002 Spring Conference.

[Kasouit 04a]   S. Kasouit, J. Damon-Lacoste, R. Vanderhaghen & P. Roca i Cabarrocas. *Contribution of plasma generated nanocrystals to the growth of microcrystalline silicon thin films.* Journal of Non-Crystalline Solids, vol. 338–340, no. 0, pages 86–90, 2004. Proceedings of the 20th International Conference on Amorphous and Microcrystalline Semiconductors.

[Kasouit 04b]   S. Kasouit, P. Roca i Cabarrocas, R. Vanderhaghen, Y. Bonnassieux, M. Elyaakoubi & I.D. French. *Effects of grain size and plasma-induced modification of the dielectric on the mobility and stability of bottom gate microcrystalline silicon {TFTs}.* Journal of Non-Crystalline Solids, vol. 338–340, no. 0, pages 369–373, 2004. Proceedings of the 20th International Conference on Amorphous and Microcrystalline Semiconductors.

[Kaufmann 13]   Urs Kaufmann. *Schweizerische Statistik der erneuerbaren Energien, Ausgabe 2012.* Rapport technique, Schweizerische Eidgenossenschaft, Bundesamt für Energie BFE, Sep 2013.

[Kayes 05]   Brendan M. Kayes, Harry A. Atwater & Nathan S. Lewis. *Comparison of the device physics principles of planar and radial p-n junction nanorod solar cells.* Journal of Applied Physics, vol. 97, no. 11, page 114302, 2005.

[Khazaka 14]   Rami Khazaka, Etienne Moulin, Mathieu Boccard, Loïc Garcia, Simon Hänni, Franz-Josef Haug, Fanny Meillaud & Christophe Ballif. *Silver versus white paste as a back reflector for microcrystalline silicon solar cells deposited on LPCVD-ZnO electrodes of various textures.* submitted to Progress in Photovotaics: Research and Applications, vol. –, no. –, pages –, 2014.

[Kilper 09]   T. Kilper, W. Beyer, G. Bräuer, T. Bronger, R. Carius, M. N. van den Donker, D. Hrunski, A. Lambertz, T. Merdzhanova, A. Mück, B. Rech, W. Reetz, R. Schmitz, U. Zastrow & A. Gordijn. *Oxygen and nitrogen impurities in microcrystalline silicon deposited under optimized conditions: Influence on material properties and solar cell performance.* Journal of Applied Physics, vol. 105, no. 7, page 074509, 2009.

[Kim 96]   Jung-Hyung Kim, Sang-Hun Seo, Seok-Min Yun, Hong-Young Chang, Kwang-Man Lee & Chi-Kyu Choi. *The deposition of SiOF*

film with low dielectric constant in a helicon plasma source. Applied Physics Letters, vol. 68, no. 11, pages 1507–1509, 1996.

[Kim 13]   Soohyun Kim, Jin-Won Chung, Hyun Lee, Jinhee Park, Younho Heo & Heon-Min Lee. *Remarkable progress in thin-film silicon solar cells using high-efficiency triple-junction technology.* Solar Energy Materials & Solar Cells, vol. 119, no. 0, pages 26–35, 2013. Thin-film Photovoltaic Solar Cells.

[Kim 14]   Do Yun Kim, R.A.C.M.M. van Swaaij & M. Zeman. *Optical and Electrical Simulation μc-Si:H Solar Cells: Effect of Substrate Morphology and Crystalline Fraction.* IEEE Journal of Photovoltaics, vol. 4, no. 1, pages 22–27, Jan 2014.

[Kirkpatrick 73]   Scott Kirkpatrick. *Percolation and Conduction.* Review of Modern Physics, vol. 45, no. 4, pages 574–588, Oct 1973.

[Klein 01]   Stefan Klein, Friedhelm Finger, Reinhard Carius, Heribert Wagner & Martin Stutzmann. *Intrinsic amorphous and microcrystalline silicon by hot-wire-deposition for thin film solar cell applications.* Thin Solid Films, vol. 395, no. 1–2, pages 305–309, 2001. Proceedings of the First International Conference on Cat-CVD (Hot-Wire CVD) Process.

[Klein 02]   Stefan Klein, Johannes Wolff, Friedhelm Finger, Reinhard Carius, Heribert Wagner & Martin Stutzmann. *Microcrystalline Silicon Prepared by Hot-Wire Chemical Vapour Deposition for Thin Film Solar Cell Applications.* Japanese Journal of Applied Physics, vol. 41, no. 1A, page L10, 2002.

[Klein 03]   Stefan Klein, Friedhelm Finger, Reinhard Carius, Thorsten Dylla, Bernd Rech, Michael Grimm, Lothar Houben & Martin Stutzmann. *Intrinsic microcrystalline silicon prepared by hot-wire chemical vapour deposition for thin film solar cells.* Thin Solid Films, vol. 430, no. 1-2, pages 202–207, 2003. Proceedings of the Second International Conference on Cat-CVD (Hot Wire CVD) Process.

[Kluth 03]   Oliver Kluth, Gunnar Schöpe, Jürgen Hüpkes, Chitra Agashe, Joachim Müller & Bernd Rech. *Modified Thornton model for magnetron sputtered zinc oxide: film structure and etching behaviour.* Thin Solid Films, vol. 442, no. 1–2, pages 80–85, 2003. Selected papers from the 4th International Conference on Coatings on Glass.

[Kohiki 94]   Shigemi Kohiki, Mikihiko Nishitani, Takahiro Wada & Takashi Hirao. *Enhanced conductivity of zinc oxide thin films by ion implantation*

of hydrogen atoms. Applied Physics Letters, vol. 64, no. 21, pages 2876–2878, 1994.

[Koida 07]   Takashi Koida, Hiroyuki Fujiwara & Michio Kondo. *Hydrogen-doped In$_2$O$_3$ as High-mobility Transparent Conductive Oxide.* Japanese Journal of Applied Physics, vol. 46, no. 28, pages L685–L687, 2007.

[Koida 08]   T. Koida, H. Fujiwara & M. Kondo. *Structural and electrical properties of hydrogen-doped films fabricated by solid-phase crystallization.* Journal of Non-Crystalline Solids, vol. 354, no. 19–25, pages 2805–2808, 2008. Proceedings of the 22nd International Conference on Amorphous and Nanocrystalline Semiconductors - Science and Technology.

[Koida 09]   T. Koida, H. Fujiwara & M. Kondo. *High-mobility hydrogen-doped transparent conductive oxide for a-Si:H/c-Si heterojunction solar cells.* Solar Energy Materials & Solar Cells, vol. 93, no. 6–7, pages 851–854, 2009. 17th International Photovoltaic Science and Engineering Conference.

[Koida 10a]   Takashi Koida, Michio Kondo, Koichi Tsutsumi, Akio Sakaguchi, Michio Suzuki & Hiroyuki Fujiwara. *Hydrogen-doped In$_2$O$_3$ transparent conducting oxide films prepared by solid-phase crystallization method.* Journal of Applied Physics, vol. 107, no. 3, page 033514, 2010.

[Koida 10b]   Takashi Koida, Hitoshi Sai & Michio Kondo. *Application of hydrogen-doped In2O3 transparent conductive oxide to thin-film microcrystalline Si solar cells.* Thin Solid Films, vol. 518, no. 11, pages 2930–2933, 2010. Transparent Oxides for Electronics and Optics (TOEO-6).

[Kondo 00]   Michio Kondo, Makoto Fukawa, Lihui Guo & Akihisa Matsuda. *High rate growth of microcrystalline silicon at low temperatures.* Journal of Non-Crystalline Solids, vol. 266–269, Part 1, no. 0, pages 84–89, 2000.

[Kondo 03]   Michio Kondo. *Microcrystalline materials and cells deposited by RF glow discharge.* Solar Energy Materials & Solar Cells, vol. 78, no. 1–4, pages 543–566, 2003. Critical review of amorphous and microcrystalline silicon materials and solar cells.

[Kočka 03]   J. Kočka, A. Fejfar, H. Stuchlíková, J. Stuchlík, P. Fojtík, T. Mates, B. Rezek, K. Luterová, V. Švrček & I. Pelant. *Basic features of transport in microcrystalline silicon.* Solar Energy Materials & Solar Cells,

vol. 78, no. 1-4, pages 493–512, 2003. Critical review of amorphous and microcrystalline silicon materials and solar cells.

[Kratzla 10]   T. Kratzla, A. Zindel & R. Benz. *Oerlikon Solar's Key Performance Drivers to Grid Parity*. In Proceedings of the 25th European Photovoltaic Solar Energy Conference and Exhibition / 5th World Conference on Photovoltaic Energy Conversion, 6-10 September 2010, Valencia, Spain, 2010.

[Krogstrup 13]   Peter Krogstrup, Henrik Ingerslev Jørgensen, Martin Heiss, Olivier Demichel, Jeppe V. Holm, Martin Aagesen, Jesper Nygard & Anna Fontcuberta i Morral. *Single-nanowire solar cells beyond the Shockley–Queisser limit*. Nature Photonics, vol. 7, pages 306–310, 2013.

[Kroll 96]   U. Kroll, J. Meier, A. Shah, S. Mikhailov & J. Weber. *Hydrogen in amorphous and microcrystalline silicon films prepared by hydrogen dilution*. Journal of Applied Physics, vol. 80, no. 9, pages 4971–4975, Nov 1996.

[Kroll 97]   U. Kroll, A. Shah, H. Keppner, J. Meier, P. Torres & D. Fischer. *Potential of VHF-plasmas for low-cost production of a-Si: H solar cells*. Solar Energy Materials & Solar Cells, vol. 48, no. 1–4, pages 343–350, 1997.

[Kunz 08]   O. Kunz, Z. Ouyang, J. Wong & A. G. Aberle. *Advances in Evaporated Solid-Phase-Crystallized Poly-Si Thin-Film Solar Cells on Glass (EVA),*. Advances in OptoElectronics, vol. 2008, no. 532351, pages 1–10, 2008.

[Kuo 03]   Ming-Tsun Kuo, Chorng-Jye Huang, Cheng-Ting Chen, Shin-Cheng Lin, Chien-Sheng Huang & Lee-Ching Kuo. *Crystallographic control of microcrystalline silicon films in a $SiF_4/SiH_4/H_2$ plasma by VHF-PECVD*. In Proceedings of 3rd World Conference on Photovoltaic Energy Conversion, volume 2, pages 1718–1721, May 2003.

[Lambertz 11]   A. Lambertz, T. Grundler & F. Finger. *Hydrogenated amorphous silicon oxide containing a microcrystalline silicon phase and usage as an intermediate reflector in thin-film silicon solar cells*. Journal of Applied Physics, vol. 10, no. 11, page 113109, 2011.

[Lambertz 13]   A. Lambertz, V. Smirnov, T. Merdzhanova, K. Ding, S. Haas, G. Jost, R.E.I. Schropp, F. Finger & U. Rau. *Microcrystalline silicon-oxygen alloys for application in silicon solar cells and modules*. Solar Energy Materials & Solar Cells, vol. 119, no. 0, pages 134–143, 2013. Thin-film Photovoltaic Solar Cells.

[Langford 78]   J. I. Langford & A. J. C. Wilson. *Scherrer after sixty years: A survey and some new results in the determination of crystallite size.* Journal of Applied Crystallography, vol. 11, no. 2, pages 102–113, Apr 1978.

[Lee 01]   Ji-Myon Lee, Kyoung-Kook Kim, Seong-Ju Park & Won-Kook Choi. *Low-resistance and nonalloyed ohmic contacts to plasma treated ZnO.* Applied Physics Letters, vol. 78, no. 24, pages 3842–3844, 2001.

[Li 09a]   Hongbo B. T. Li, Karine H. M. van der Werf, Jatin K. Rath & Ruud E. I. Schropp. *Hot wire CVD deposition of nanocrystalline silicon solar cells on rough substrates.* Thin Solid Films, vol. 517, pages 3476–3480, 2009.

[Li 09b]   Hongbo B.T. Li, Ronald H. Franken, Jatindra K. Rath & Ruud E.I. Schropp. *Structural defects caused by a rough substrate and their influence on the performance of hydrogenated nano-crystalline silicon n-i-p solar cells.* Solar Energy Materials & Solar Cells, vol. 93, no. 3, pages 338–349, 2009.

[Luysberg 97]   M. Luysberg, P. Hapke, R. Carius & F. Finger. *Structure and growth of hydrogenated microcrystalline silicon: Investigation by transmission electron microscopy and Raman spectroscopy of films grown at different plasma excitation frequencies.* Philosophical Magazine A, vol. 75, no. 1, pages 31–47, 1997.

[Madan 80]   A. Madan & S.R. Ovshinsky. *Properties of amorphous Si:F:H alloys.* Journal of Non-Crystalline Solids, vol. 35–36, Part 1, no. 0, pages 171–181, 1980.

[Mai 05]   Y. Mai, S. Klein, R. Carius, H. Stiebig, X. Geng & F. Finger. *Open circuit voltage improvement of high-deposition-rate microcrystalline silicon solar cells by hot wire interface layers.* Applied Physics Letters, vol. 87, no. 7, page 073503, 2005.

[Mai 06]   Y. Mai, S. Klein, R. Carius, H. Stiebig, L. Houben, X. Geng & F. Finger. *Improvement of open circuit voltage in microcrystalline silicon solar cells using hot wire buffer layers.* Journal of Non-Crystalline Solids, vol. 352, no. 9-20, pages 1859–1862, 2006. Amorphous and Nanocrystalline Semiconductors - Science and Technology - Proceedings of the 21st International Conference on Amorphous and Nanocrystalline Semiconductors - Science and Technology.

[Major 84]   S. Major, A. Banerjee & K.L. Chopra. *Annealing studies of undoped and indium-doped films of zinc oxide.* Thin Solid Films, vol. 122, no. 1, pages 31–43, 1984.

Bibliography

[Major 86]   S. Major, Satyendra Kumar, M. Bhatnagar & K. L. Chopra. *Effect of hydrogen plasma treatment on transparent conducting oxides.* Applied Physics Letters, vol. 49, no. 7, pages 394–396, 1986.

[Matsuda 99]   Akihisa Matsuda. *Growth mechanism of microcrystalline silicon obtained from reactive plasmas.* Thin Solid Films, vol. 337, no. 1–2, pages 1–6, 1999.

[Matsui 02a]   Takuya Matsui, Riza Muhida, Tomohiro Kawamura, Toshihiko Toyama, Hiroaki Okamoto, Tsutomu Yamazaki, Shinya Honda, Hideyuki Takakura & Yoshihiro Hamakawa. *Microstructural dependence of electron and hole transport in low-temperature-grown polycrystalline-silicon thin-film solar cells.* Applied Physics Letters, vol. 81, no. 25, pages 4751–4753, 2002.

[Matsui 02b]   Takuya Matsui, Masaharu Tsukiji, Hiroyuki Saika, Toshihiko Toyama & Hiroaki Okamoto. *Correlation between Microstructure and Photovoltaic Performance of Polycrystalline Silicon Thin Film Solar Cells.* Japanese Journal of Applied Physics, vol. 41, no. Part 1, No. 1, pages 20–27, 2002.

[Matsui 02c]   Takuya Matsui, Masaharu Tsukiji, Hiroyuki Saika, Toshihiko Toyama & Hiroaki Okamoto. *Influence of substrate texture on microstructure and photovoltaic performances of thin film polycrystalline silicon solar cells.* Journal of Non-Crystalline Solids, vol. 299–302, Part 2, no. 0, pages 1152–1156, 2002. 19th International Conference on Amorphous and Microcrystalline Semiconductors.

[Matsui 06]   Takuya Matsui, Akihisa Matsuda & Michio Kondo. *High-rate microcrystalline silicon deposition for p-i-n junction solar cells.* Solar Energy Materials & Solar Cells, vol. 90, no. 18-19, pages 3199–3204, 2006. 14th International Photovoltaic Science and Engineering Conference.

[Matsuura 84]   Hideharu Matsuura, Tetsuhiro Okuno, Hideyo Okushi & Kazunobu Tanaka. *Electrical properties of n?amorphous/p?crystalline silicon heterojunctions.* Journal of Applied Physics, vol. 55, no. 4, pages 1012–1019, 1984.

[Meier 94]   J. Meier, R. Flückiger, H. Keppner & A. Shah. *Complete microcrystalline p-i-n solar cell—Crystalline or amorphous cell behavior?* Applied Physics Letters, vol. 65, no. 7, pages 860–862, 1994.

[Meier 96]   J. Meier, P. Torres, R. Platz, S. Dubail, U. Kroll, J.A. Anna Selvan, N. Pellaton-Vaucher, C. Hof, D. Fischer, H. Keppner, A. Shah, K.-D.

144

Ufert, P. Giannoulès & J. Köhler. *On the Way towards High-Efficiency Thin Film Silicon Solar Cells by the "Micromorph" Concept.* In Proceedings of the Material Research Society Symposium, Spring meeting (San Francisco), 1996.

[Meier 98] J. Meier, H. Keppner, S. Dubail, Y. Ziegler, L. Feitknecht, P. Torres, C. Hof, U. Kroll, D. Fischer, J. Cuperus, J. A. Anna Selvan & A. Shah. *Microcrystalline and Micromorph Thin-Film Silicon Solar Cells.* In Proceedings of the 2nd World Conference on Photovoltaic Energy Conversion, vol. I, pages 375–380, 1998.

[Meier 01] J. Meier, E. Vallat-Sauvain, S. Dubail, U. Kroll, J. Dubail, S. Golay, L. Feitknecht, P. Torres, S. Fay, D. Fischer & A. Shah. *Microcrystalline/micromorph silicon thin-film solar cells prepared by VHF-GD technique.* Solar Energy Materials & Solar Cells, vol. 66, no. 1-4, pages 73–84, 2001.

[Meier 04] J. Meier, U. Kroll, E. Vallat-Sauvain, J. Spitznagel, U. Graf & A. Shah. *Amorphous solar cells, the micromorph concept and the role of VHF-GD deposition technique.* Solar Energy, vol. 77, no. 6, pages 983–993, 2004. Thin Film {PV}.

[Meier 12] J. Meier, U. Kroll, S. Benagli, L. Fesquet, J. Steinhauser, D. Borello, J.-B. Orhan, Y. Djeridane, E. Vallat-Sauvain, M. Fecioru-Morariu, B. Mereu, J. Kalas, J. Hoetzel, P. Losio, M. Kupich, O. Kluth, T. Eisenhammer, D. Weidman, S. Marjanovic & G. Kohnke. *From R& D to Mass Production of Micromorph Thin Film Silicon {PV}.* Energy Procedia, vol. 15, no. 0, pages 179–188, 2012. International Conference on Materials for Advanced Technologies 2011, Symposium O.

[Meillaud 06a] F. Meillaud, A. Shah, J. Bailat, E. Vallat Sauvain, T. Roschek, B. Rech, D. Dominé, T. Söderström, M. Python & C. Ballif. *Microcrystalline silicon solar cells: Theory and diagnostic tools.* In Proceedings of the 4th WCPEC Conference, Hawaii, USA, pages 1572–1575, 2006.

[Meillaud 06b] F. Meillaud, A. Shah, C. Droz, E. Vallat-Sauvain & C. Miazza. *Efficiency limits for single-junction and tandem solar cells.* Solar Energy Materials & Solar Cells, vol. 90, no. 18-19, pages 2952–2959, 2006. 14th International Photovoltaic Science and Engineering Conference.

[Meillaud 06c] Fanny Meillaud. *MICROCRYSTALLINE SILICON SOLAR CELLS: THEORY, DIAGNOSIS AND STABILITY.* PhD thesis, Université de Neuchâtel, Institut de microtechnique, 2006.

Bibliography

[Meillaud 08]   F. Meillaud, E. Vallat-Sauvain, Arvind Shah & C. Ballif. *Kinetics of creation and of thermal annealing of light-induced defects in microcrystalline silicon solar cells.* Journal of Applied Physics, vol. 103, no. 5, page 054504, 2008.

[Merdzhanova 12]   T. Merdzhanova, J. Woerdenweber, W. Beyer, T. Kilper, U. Zastrow, M. Meier, H. Stiebig & A. Gordijn. *Impurities in thin-film silicon: Influence on material properties and solar cell performance.* Journal of Non-Crystalline Solids, vol. 358, no. 17, pages 2171–2178, 2012. Proceedings of the 24th International Conference on Amorphous and Nanocrystalline Semiconductors (ICANS 24) Nara, Japan August 21-26, 2011.

[Merten 98]   J. Merten, J. M. Asensi, C. Voz, A.V. Shah, R. Platz & J. Andreu. *Improved equivalent circuit and analytical model for amorphous silicon solar cells and modules.* IEEE Transactions on Electron Devices, vol. 45, no. 2, pages 423–429, Feb 1998.

[Minami 89]   T. Minami, H. Sato, H. Nanto & S. Takata. *Heat treatment in hydrogen gas and plasma for transparent conducting oxide films such as ZnO, SnO$_2$ and indium tin oxide.* Thin Solid Films, vol. 176, no. 2, pages 277–282, 1989.

[Moreno 12]   M. Moreno, R. Boubekri & P. Roca i Cabarrocas. *Study of the effects of different fractions of large grains of μc-Si:H:F films on the infrared absorption on thin film solar cells.* Solar Energy Materials & Solar Cells, vol. 100, no. 0, pages 16–20, 2012. Photovoltaics, Solar Energy Materials, and Technologies: Cancun 2010.

[Morris 90]   J. Morris, R. R. Arya, J. G. O'Dowd & S. Wiedeman. *Absorption enhancement in hydrogenated amorphous silicon-based solar cells.* Journal of Applied Physics, vol. 67, no. 2, pages 1079–1087, 1990.

[Moulin 12]   E. Moulin, U.W. Paetzold, K. Bittkau, M. Ermes, L. Ding, L. Fanni, S. Nicolay, J. Kirchhoff, D. Weigand, A. Bauer, A. Lambertz, C. Ballif & R. Carius. *Thin-film silicon solar cells applying optically decoupled back reflectors.* Materials Science and Engineering: B, no. 0, pages –, 2012.

[Müller 04]   Joachim Müller, Bernd Rech, Jiri Springer & Milan Vanecek. *TCO and light trapping in silicon thin film solar cells.* Solar Energy, vol. 77, no. 6, pages 917–930, 2004.

[Naqavi 13]   Ali Naqavi, Franz-Josef Haug, Corsin Battaglia, Hans Peter Herzig & Christophe Ballif. *Light trapping in solar cells at the extreme*

146

coupling limit. Journal of the Optical Society of America B, vol. 30, no. 1, pages 13–20, Jan 2013.

[Naruse 12]   Y. Naruse, M. Matsumoto, T. Sekimoto, M. Hishida, Y. Aya, W. Shinohara, A. Fukushima, S. Yata, A. Terakawa, M. Iseki & M. Tanaka. *Identification of defective regions in thin-film Si solar cells for new-generation energy devices.* In Proceedings of the Photovoltaic Specialists Conference (PVSC), 2012 38th IEEE, pages 003118–003123, Jun 2012.

[Nasuno 01]   Yoshiyuki Nasuno, Michio Kondo & Akihisa Matsuda. *Effects of Substrate Surface Morphology on Microcrystalline Silicon Solar Cells.* Japanese Journal of Applied Physics, vol. 40, no. Part 2, No. 4A, pages L303–L305, 2001.

[Nath 08]   Madhumita Nath, P. Roca i Cabarrocas, E. V. Johnson, A. Abramov & P. Chatterjee. *The open-circuit voltage in microcrystalline silicon solar cells of different degrees of crystallinity.* Thin Solid Films, vol. 516, pages 6974–6978, 2008.

[Nicolay 09]   S. Nicolay, S. Faÿ & C. Ballif. *Growth Model of MOCVD Polycrystalline ZnO.* Crystal Growth & Design, vol. 9, no. 11, pages 4957–4962, 2009.

[Nicolay 12]   S. Nicolay, M. Benkhaira, L. Ding, J. Escarre, G. Bugnon, F. Meillaud & C. Ballif. *Control of CVD-deposited ZnO films properties through water/DEZ ratio: Decoupling of electrode morphology and electrical characteristics.* Solar Energy Materials & Solar Cells, vol. 105, no. 0, pages 46–52, 2012.

[Niikura 04]   Chisato Niikura, Michio Kondo & Akihisa Matsuda. *Preparation of microcrystalline silicon films at ultra high-rate of 10 nm/s using high-density plasma.* Journal of Non-Crystalline Solids, vol. 338–340, no. 0, pages 42–46, 2004. Proceedings of the 20th International Conference on Amorphous and Microcrystalline Semiconductors.

[Nishimoto 01]   Tomonori Nishimoto, Tomoko Takagi, Michio Kondo & Akihisa Matsuda. *Effect of halogen additives on the stability of a-Si:H films deposited at a high-growth rate.* Solar Energy Materials & Solar Cells, vol. 66, no. 1-4, pages 179–185, 2001. {PVSEC} 11 - Part {II}.

[Ossenbrink 13]   H. Ossenbrink, T. Huld, A. Jäger-Waldau & N. Taylor. *Photovoltaic Electricity Cost Maps.* Rapport technique JRC 83366, European Commission, DG Joint Research Centre, Institute for Energy and Transport, Renewable Energy Unit, Via Enrico Fermi 2749; TP 450 – 21027 Ispra (VA), Italia, Sep 2013.

Bibliography

[Overhof 98]   H. Overhof, M. Otte, M. Schmidtke, U. Backhausen & R. Carius. *The transport mechanism in micro-crystalline silicon.* Journal of Non-Crystalline Solids, vol. 227–230, no. Part 2, pages 992–995, 1998.

[Ovshinsky 78]   Stanford R. Ovshinsky & Arun Madan. *A new amorphous silicon-based alloy for electronic applications.* Nature, vol. 276, pages 482–484, Nov 1978.

[Paetzold 11]   U. W. Paetzold, E. Moulin, D. Michaelis, W. Böttler, C. Wächter, V. Hagemann, M. Meier, R. Carius & U. Rau. *Plasmonic reflection grating back contacts for microcrystalline silicon solar cells.* Applied Physics Letters, vol. 99, no. 18, page 181105, 2011.

[Paetzold 13]   Ulrich Wilhelm Paetzold, Wendi Zhang, Michael Prömpers, Joachim Kirchhoff, Tsvetelina Merdzhanova, Stephan Michard, Reinhard Carius, Aad Gordijn & Matthias Meier. *Thin-film silicon solar cell development on imprint-textured glass substrates.* Materials Science and Engineering: B, vol. 178, no. 9, pages 617–622, 2013. Advanced materials and characterization techniques for solar cells.

[Paillard 01]   V. Paillard, P. Puech, R. Sirvin, S. Hamma & P. Roca i Cabarrocas. *Measurement of the in-depth stress profile in hydrogenated microcrystalline silicon thin films using Raman spectrometry.* Journal of Applied Physics, vol. 90, no. 7, pages 3276–3279, 2001.

[Patterson 39]   A. L. Patterson. *The Scherrer Formula for X-Ray Particle Size Determination.* Physical Review, vol. 56, pages 978–982, Nov 1939.

[Python 08]   Martin Python, Evelyne Vallat-Sauvain, Julien Bailat, Didier Dominé, Luc Fesquet, Arvind Shah & Christophe Ballif. *Relation between substrate morphology and microcrystalline silicon solar cell performance.* Journal of Non-Crystalline Solids, vol. 354, no. 19-25, pages 2258–2262, 2008. Amorphous and Nanocrystalline Semiconductors, 22nd International Conference on Amorphous and Nanocrystalline Semiconductors – Science and Technology.

[Python 09a]   M. Python, O. Madani, D. Dominé, F. Meillaud, E. Vallat-Sauvain & C. Ballif. *Influence of the substrate geometrical parameters on microcrystalline silicon growth for thin-film solar cells.* Solar Energy Materials & Solar Cells, vol. 93, no. 10, pages 1714–1720, 2009.

[Python 09b]   Martin Python. *Microcrystalline Silicon Solar Cells: Growth and Defects.* PhD thesis, Université de Neuchâtel, Institut de microtechnique, 2009.

[Python 10]   M. Python, D. Dominé, T. Söderström, F. Meillaud & C. Ballif. *Microcrystalline silicon solar cells: effects of substrate temperature on cracks and their role in post-oxidation.* Progress in Photovoltaics: Research and Applications, vol. 18, no. 7, pages 491–499, Nov 2010.

[Rath 04]   J.K. Rath, R.H.J. Franken, A. Gordijn, R.E.I. Schropp & W.J. Goedheer. *Growth mechanism of microcrystalline silicon at high pressure conditions.* Journal of Non-Crystalline Solids, vol. 338–340, no. 0, pages 56–60, 2004. Proceedings of the 20th International Conference on Amorphous and Microcrystalline Semiconductors.

[Rech 99]   B. Rech & H. Wagner. *Potential of amorphous silicon for solar cells.* Applied Physics A: Materials Science & Processing, vol. 69, no. 2, pages 155–167, 1999.

[Rech 03]   B. Rech, T. Roschek, T. Repmann, J. Müller, R. Schmitz & W. Appenzeller. *Microcrystalline silicon for large area thin film solar cells.* Thin Solid Films, vol. 427, no. 1–2, pages 157–165, 2003. Proceedings of Symposium K on Thin Film Materials for Large Area Electronics of the European Materials Research Society (E-MRS) 2002 Spring Conference.

[Roca i Cabarrocas 08]   Pere Roca i Cabarrocas, Yassine Djeridane, V.D. Bui, Yvan Bonnassieux & Alexey Abramov. *Critical issues in plasma deposition of microcrystalline silicon for thin film transistors.* Solid State Electronics, vol. 52, no. 3, pages 422–426, 2008. Special Issue: Papers Selected from the 3rd International TFT Conference - ITC'07.

[Rockstuhl 10]   C. Rockstuhl, S. Fahr, K. Bittkau, T. Beckers, R. Carius, F.-J. Haug, T. Söderström, C.Ballif & F. Lederer. *Comparison and optimization of randomly textured surfaces in thin-film solar cells.* Optics Express, vol. 18, no. S3, pages A335–A341, Sep 2010.

[Roschek 02]   T. Roschek, T. Repmann, J. Müller, B. Rech & H. Wagner. *Comprehensive study of microcrystalline silicon solar cells deposited at high rate using 13.56 MHz plasma-enhanced chemical vapor deposition.* Journal of Vacuum Science & Technology A: Vacuum, Surfaces, and Films, vol. 20, no. 2, pages 492–498, 2002.

[Roschek 04]   Tobias Roschek, Bernd Rech, Joachim Müller, Ralf Schmitz & Heribert Wagner. *Influence of the total gas flow on the deposition of microcrystalline silicon solar cells.* Thin Solid Films, vol. 451–452, no. 0, pages 466–469, 2004. Proceedings of Symposium D on Thin Film and Nano-Structured Materials for Photovoltaics, of the E-MRS 2003 Spring Conference.

149

Bibliography

[Ruske 10]   F. Ruske, M. Roczen, K. Lee, M. Wimmer, S. Gall, J. Hüpkes, D. Hrunski & B. Rech. *Improved electrical transport in Al-doped zinc oxide by thermal treatment.* Journal of Applied Physics, vol. 107, no. 1, page 013708, 2010.

[Saha 93]   S. C. Saha, A. K. Barua & Swati Ray. *The role of hydrogen dilution and radio frequency power in the formation of microcrystallinity of n-type Si:H thin film.* Journal of Applied Physics, vol. 74, no. 9, pages 5561–5568, 1993.

[Sai 10]   Hitoshi Sai, Haijun Jia & Michio Kondo. *Impact of front and rear texture of thin-film microcrystalline silicon solar cells on their light trapping properties.* Journal of Applied Physics, vol. 108, no. 4, page 044505, 2010.

[Sai 12]   Hitoshi Sai, Kimihiko Saito & Michio Kondo. *Enhanced photocurrent and conversion efficiency in thin-film microcrystalline silicon solar cells using periodically textured back reflectors with hexagonal dimple arrays.* Applied Physics Letters, vol. 101, no. 17, page 173901, 2012.

[Sai 13]   Hitoshi Sai, Kimihiko Saito, Nana Hozuki & Michio Kondo. *Relationship between the cell thickness and the optimum period of textured back reflectors in thin-film microcrystalline silicon solar cells.* Applied Physics Letters, vol. 102, no. 5, page 053509, 2013.

[Saito 11]   Kimihiko Saito & Michio Kondo. *Control of preferential orientation of microcrystalline silicon and its impact on solar cell performance.* Progress in Photovoltaics: Research and Applications, vol. 19, no. 7, pages 858–864, 2011.

[Sakai 90]   Hiroshi Sakai, Takasi Yoshida, Toshio Hama & Yukimi Ichikawa. *Effects of Surface Morphology of Transparent Electrode on the Open-Circuit Voltage in a-Si:H Solar Cells.* Japanese Journal of Applied Physics, vol. 29, no. Part 1, No. 4, pages 630–635, 1990.

[Saleh 03]   R. Saleh & N.H. Nickel. *Raman spectroscopy of B-doped microcrystalline silicon films.* Thin Solid Films, vol. 427, no. 1–2, pages 266–269, 2003. Proceedings of Symposium K on Thin Film Materials for Large Area Electronics of the European Materials Research Society (E-MRS) 2002 Spring Conference.

[Sansonnens 06]   L. Sansonnens, A. A. Howling & Ch. Hollenstein. *Electromagnetic field nonuniformities in large area, high-frequency capacitive plasma reactors, including electrode asymmetry effects.* Plasma

150

Sources Science and Technology, vol. 15, no. 3, pages 302–313, 2006.

[Schellenberg 88]   J. J. Schellenberg & R. D. McLeod. *A percolation model for microcrystalline silicon films.* Solid State Communications, vol. 66, no. 2, pages 159 – 162, 1988.

[Scher 70]   Harvey Scher & Richard Zallen. *Critical Density in Percolation Processes.* The Journal of Chemical Physics, vol. 53, no. 9, pages 3759–3761, 1970.

[Schicho 12]   S. Schicho, F. Köhler, R. Carius & A. Gordijn. *The relationship of structural properties of microcrystalline silicon to solar cell performance.* Solar Energy Materials & Solar Cells, vol. 98, no. 0, pages 391–397, 2012.

[Schropp 01]   R.E.I Schropp. *Status of Cat-CVD (Hot-Wire CVD) research in Europe.* Thin Solid Films, vol. 395, no. 1–2, pages 17–24, 2001. Proceedings of the First International Conference on Cat-CVD (Hot-Wire CVD) Process.

[Schüttauf 14]   Jan-Willem Schüttauf, Grégory Bugnon, Michael Stuckelberger, Simon Hänni, Mathieu Boccard, Matthieu Despeisse, Franz-Josef Haug, Fanny Meillaud & Christophe Ballif. *Thin-Film Silicon Triple-Junction Solar Cells on Highly Transparent Front Electrodes With Stabilized Efficiencies up to 12.8%.* IEEE Journal of Photovoltaics, vol. 4, no. 3, pages 757–762, May 2014.

[Sendova-Vassileva 05]   M. Sendova-Vassileva, F. Finger, S. Klein & A. Lambertz. *Impact of instability in μc-Si:H i-layers on the performance of solar cells.* Journal of Optoelectronics and Advanced Materials, vol. 7, no. 1, pages 481–484, 2005.

[Sendova-Vassileva 06]   M. Sendova-Vassileva, S. Klein & F. Finger. *Instability phenomena in μc-Si:H solar cells prepared by hot-wire CVD.* Thin Solid Films, vol. 501, no. 1–2, pages 252–255, 2006. Proceedings of the Third International Conference on Hot-Wire {CVD} (Cat-CVD) Process.

[Sever 13]   Martin Sever, Benjamin Lipovšek, Janez Krč, Andrej Čampa, Guillermo Sánchez Plaza, Franz-Josef Haug, Martial Duchamp, Wim Soppe & Marko Topič. *Combined model of non-conformal layer growth for accurate optical simulation of thin-film silicon solar cells.* Solar Energy Materials & Solar Cells, vol. 119, no. 0, pages 59–66, 2013. hin-film Photovoltaic Solar Cells.

[Shah 10]   Arvind Shah. Thin-Film Silicon Solar Cells. EPFL Press, 2010.

[Shah 13]   Arvind Shah, Etienne Moulin & Christophe Ballif. *Technological status of plasma-deposited thin-film silicon photovoltaics.* Solar Energy Materials & Solar Cells, vol. 119, no. 0, pages 311–316, 2013. Thin-film Photovoltaic Solar Cells.

[Shibata 87a]   N. Shibata, K. Fukuda, H. Ohtoshi, J. Hanna, S. Oda & I. Shimizu. *Growth of Amorphous and Crystalline Silicon by HR-CVD (Hydrogen Radical Enhanced CVD).* MRS Proceedings, vol. 95, 1987.

[Shibata 87b]   Naoki Shibata, Kaichi Fukuda, Hirokazu Ohtoshi, Jun ichi Hanna, Shunri Oda & Isamu Shimizu. *Preparation of Polycrystalline Silicon by Hydrogen-Radical-Enhanced Chemical Vapor Deposition.* Japanese Journal of Applied Physics, vol. 26, no. Part 2, No. 1, pages L10–L13, 1987.

[Shimakawa 00]   K. Shimakawa. *Percolation-controlled electronic properties in microcrystalline silicon: effective medium approach.* Journal of Non-Crystalline Solids, vol. 266–269, no. Part 1, pages 223–226, 2000.

[Sichanugrist 93] P. Sichanugrist, T. Yoshida, Y. Ichikawa & H. Sakai. *Amorphous silicon oxide with microcrystalline Si phase.* Journal of Non-Crystalline Solids, vol. 164–166, Part 2, no. 0, pages 1081–1084, 1993.

[Sichanugrist 94] P. Sichanugrist, T. Sasaki, A. Asano, Y. Ichikawa & H. Sakai. *Amorphous silicon oxide and its application to metal/n-i-p/ITO type a-Si solar cells.* Solar Energy Materials & Solar Cells, vol. 34, no. 1–4, pages 415–422, 1994.

[Smets 03]   A. H. M. Smets, W. M. M. Kessels & M. C. M. van de Sanden. *Vacancies and voids in hydrogenated amorphous silicon.* Applied Physics Letters, vol. 82, no. 10, pages 1547–1549, 2003.

[Smets 06]   A. H. M. Smets, T. Matsui & M. Kondo. *Optimization of the High Rate Microcrystalline Silicon Deposition Conditions of the Multi-Hole-Cathode Very High Frequency SiH4/H2 Plasma.* In Conference Record of the 2006 IEEE 4th World Conference on Photovoltaic Energy Conversion, volume 2, pages 1592–1595, May 2006.

[Smets 08a]   A. H. M. Smets, T. Matsui & M. Kondo. *High-rate deposition of microcrystalline silicon p–i–n solar cells in the high pressure depletion regime.* Journal of Applied Physics, vol. 104, no. 3, page 034508, 2008.

[Smets 08b]   A. H. M. Smets, T. Matsui & M. Kondo. *Infrared analysis of the bulk silicon-hydrogen bonds as an optimization tool for high-rate deposition of microcrystalline silicon solar cells*. Applied Physics Letters, vol. 92, no. 3, page 033506, 2008.

[Söderström 08]   T. Söderström, F.-J. Haug, V. Terrazzoni-Daudrix, X. Niquille, M. Python & C. Ballif. *N/I buffer layer for substrate microcrystalline thin film silicon solar cell*. Journal of Applied Physics, vol. 104, no. 10, page 104505, Nov 2008.

[Soderstrom 10]   Karin Soderstrom, F. Haug, Jordi Escarre, Oscar Cubero & C. Ballif. *Photocurrent increase in n-i-p thin film silicon solar cells by guided mode excitation via grating coupler*. Applied Physics Letters, vol. 96, no. 21, pages 213508–213508, May 2010.

[Söderström 12]   Karin Söderström, Grégory Bugnon, Rémi Biron, Céline Pahud, Fanny Meillaud, Franz-Josef Haug & Christophe Ballif. *Thin-film silicon triple-junction solar cell with 12.5% stable efficiency on innovative flat light-scattering substrate*. Journal of Applied Physics, vol. 112, no. 11, page 114503, 2012.

[Söderström 13]   Karin Söderström. *Coupling light into thin silicon layers for high-efficiency solar cells*. PhD thesis, EPFL, 2013.

[Spear 75]   W.E. Spear & P.G. Le Comber. *Substitutional doping of amorphous silicon*. Solid State Communications, vol. 17, no. 9, pages 1193–1196, 1975.

[Spear 76]   W. E. Spear & P. G. Le Comber. *Electronic properties of substitutionally doped amorphous Si and Ge*. Philosophical Magazine, vol. 33, no. 6, pages 935–949, 1976.

[Sriraman 02]   Saravanapriyan Sriraman, Sumit Agarwal, Eray S. Aydil & Dimitrios Maroudas. *Mechanism of hydrogen-induced crystallization of amorphous silicon*. Nature, vol. 418, pages 62–65, 2002.

[Staebler 77]   D. L. Staebler & C. R. Wronski. *Reversible conductivity changes in discharge-produced amorphous Si*. Applied Physics Letters, vol. 31, no. 4, pages 292–294, 1977.

[Steinhauser 07]   J. Steinhauser, S. Faÿ, N. Oliveira, E. Vallat-Sauvain & C. Ballif. *Transition between grain boundary and intragrain scattering transport mechanisms in boron-doped zinc oxide thin films*. Applied Physics Letters, vol. 90, no. 14, page 142107, 2007.

Bibliography

[Sterling 65]   H.F. Sterling & R.C.G. Swann. *Chemical vapour deposition promoted by r.f. discharge.* Solid State Electronics, vol. 8, no. 8, pages 653–654, 1965.

[Stiebig 00]   H. Stiebig, T. Brammer, J. Zimmer, O. Vetterl & H. Wagner. *Investigation of the optoelectronic properties of μc-Si:H pin solar cells.* Journal of Non-Crystalline Solids, vol. 266–269, Part 2, no. 0, pages 1104–1108, 2000.

[Strahm 07]   B. Strahm, A. A. Howling, L. Sansonnens & Ch. Hollenstein. *Plasma silane concentration as a determining factor for the transition from amorphous to microcrystalline silicon in SiH$_4$/H$_2$ discharges.* Plasma Sources Science and Technology, vol. 16, no. 1, pages 80–89, 2007.

[Stuckelberger 13]   M. Stuckelberger, M. Despeisse, G. Bugnon, J.-W. Schüttauf, F.-J. Haug & C. Ballif. *Comparison of amorphous silicon absorber materials: Light-induced degradation and solar cell efficiency.* Journal of Applied Physics, vol. 114, no. 15, page 154509, 2013.

[Stuckelberger 14a]   Michael Stuckelberger. *Amorphous silicon: Impact of process conditions on material properties and solar cell efficiency.* PhD thesis, EPFL, 2014. in prep.

[Stuckelberger 14b]   Michael Stuckelberger, Adrian Billet, Yannick Riesen, Mathieu Boccard, Matthieu Despeisse, Jan-Willem Schüttauf, Franz-Josef Haug & Christophe Ballif. *Comparison of amorphous silicon absorber materials: kinetics of light-induced degradation.* submitted, 2014.

[Syed 97]   Moniruzzaman Syed, Takao Inokuma, Yoshihiro Kurata & Seiichi Hasegawa. *Effects of the Addition of SiF$_4$ to the SiH$_4$ Feed Gas for Depositing Polycrystalline Silicon Films at Low Temperature.* Japanese Journal of Applied Physics, vol. 36, no. Part 1, No. 11, pages 6625–6632, 1997.

[Taira 03]   S. Taira, M. Shima, K. Murata & M. Tanaka. *A ROLE OF A-SI:H BUFFER LAYER FOR CONTROLLING THE IMPURITY PROFILES NEAR P/I INTERFACE OF MICROCRYSTALLINE SILICON SOLAR CELL.* In Proceedings of 3rd World Conference on Photovoltaic Energy Conversion, 11–18 May 2003, Osaka, Japan, pages 1816–1819, May 2003.

[Tan 12]   Hairen Tan, Rudi Santbergen, Arno H. M. Smets & Miro Zeman. *Plasmonic Light Trapping in Thin-film Silicon Solar Cells with Improved Self-Assembled Silver Nanoparticles.* Nano Letters, vol. 12, no. 8, pages 4070–4076, 2012.

154

[Tan 13]   Hairen Tan, Efthymia Psomadaki, Olindo Isabella, Marinus Fischer, Pavel Babal, Ravi Vasudevan, Miro Zeman & Arno H. M. Smets. *Micro-textures for efficient light trapping and improved electrical performance in thin-film nanocrystalline silicon solar cells.* Applied Physics Letters, vol. 103, no. 17, 2013.

[Taretto 12]   Kurt Taretto. *New explicit current/voltage equation for p-i-n solar cells including interface potential drops and drift/diffusion transport.* Progress in Photovoltaics: Research and Applications, pages n/a–n/a, 2012.

[Theys 02]   Bertrand Theys, Vincent Sallet, François Jomard, Alain Lusson, Jean-François Rommeluère & Zéphyrin Teukam. *Effects of intentionally introduced hydrogen on the electrical properties of ZnO layers grown by metalorganic chemical vapor deposition.* Journal of Applied Physics, vol. 91, no. 6, pages 3922–3924, 2002.

[Tiedje 84]   T. Tiedje, E. Yablonovitch, G.D. Cody & B.G. Brooks. *Limiting efficiency of silicon solar cells.* IEEE Transactions on Electron Devices, vol. 31, no. 5, pages 711–716, May 1984.

[Torres 96]   P. Torres, J. Meier, R. Flückiger, U. Kroll, J. A. Anna Selvan, H. Keppner, A. Shah, S. D. Littelwood, I. E. Kelly & P. Giannoulès. *Device grade microcrystalline silicon owing to reduced oxygen contamination.* Applied Physics Letters, vol. 69, no. 10, pages 1373–1375, 1996.

[Tsai 89]   C.C. Tsai, G.B. Anderson, R. Thompson & B. Wacker. *Control of silicon network structure in plasma deposition.* Journal of Non-Crystalline Solids, vol. 114, Part 1, no. 0, pages 151–153, 1989. Proceedings of the Thirteenth International Conference on Amorphous and Liquid Semiconductors.

[Tsu 80]   R. Tsu, M. Izu, S.R. Ovshinsky & F.H. Pollak. *Electroreflectance and Raman scattering investigation of glow-discharge amorphous Si:F:H.* Solid State Communications, vol. 36, no. 9, pages 817–822, 1980.

[Tsu 82]   R. Tsu, J. Gonzalez-Hernandez, S. S. Chao, S. C. Lee & K. Tanaka. *Critical volume fraction of crystallinity for conductivity percolation in phosphorus-doped Si:F:H alloys.* Applied Physics Letters, vol. 40, no. 6, pages 534–535, 1982.

[Uchida 82]   Yoshiyuki Uchida, Takeshige Ichimura, Masakazu Ueno & Hiromu Haruki. *Microcrystalline Si: H Film and Its Application to Solar Cells.* Japanese Journal of Applied Physics, vol. 21, no. Part 2, No. 9, pages L586–L588, 1982.

Bibliography

[Ulbrich 11]	C. Ulbrich, C. Zahren, J. Noll, B. Blank, A. Gerber, A. Gordijn & U. Rau. *Power matching of tandem solar cells.* In Proceedings of the 26th European Photovoltaic Solar Energy Conference and Exhibition, 2011, Hamburg, Germany, pages 302–305, 2011.
[Ulbrich 13]	C. Ulbrich, C. Zahren, A. Gerber, B. Blank, T. Merdzhanova, A. Gordijn & U. Rau. *Matching of Silicon Thin-Film Tandem Solar Cells for Maximum Power Output.* International Journal of Photoenergy, vol. 2013, no. 314097, pages 1–7, 2013.
[Usui 79]	S. Usui & M. Kikuchi. *Properties of heavily doped GD—Si with low resistivity.* Journal of Non-Crystalline Solids, vol. 34, no. 1, pages 1–11, 1979.
[Vallat-Sauvain 00]	E. Vallat-Sauvain, U. Kroll, J. Meier, A. Shah & J. Pohl. *Evolution of the microstructure in microcrystalline silicon prepared by very high frequency glow-discharge using hydrogen dilution.* Journal of Applied Physics, vol. 87, no. 6, pages 3137–3142, 2000.
[Vallat-Sauvain 05]	E. Vallat-Sauvain, J. Bailat, J. Meier, X. Niquille, U. Kroll & A. Shah. *Influence of the substrate's surface morphology and chemical nature on the nucleation and growth of microcrystalline silicon.* Thin Solid Films, vol. 485, no. 1–2, pages 77–81, 2005.
[Vallat-Sauvain 06a]	E. Vallat-Sauvain, C. Droz, F. Meillaud, J. Bailat, A. Shah & C. Ballif. *Determination of Raman emission cross-section ratio in hydrogenated microcrystalline silicon.* Journal of Non-Crystalline Solids, vol. 352, no. 9–20, pages 1200–1203, 2006. Amorphous and Nanocrystalline Semiconductors – Science and Technology – Proceedings of the 21st International Conference on Amorphous and Nanocrystalline Semiconductors – Science and Technology.
[Vallat-Sauvain 06b]	Evelyne Vallat-Sauvain, Arvind Shah & Julien Bailat. Advances in Microcrystalline Silicon Solar Cell Technologies, pages 133–165. Wiley Series in Materials for Electronic & Optoelectronic Applications, 2006.
[van den Donker 05]	M. N. van den Donker, B. Rech, F. Finger, W. M. M. Kessels & M. C. M. van de Sanden. *Highly efficient microcrystalline silicon solar cells deposited from a pure SiH$_4$ flow.* Applied Physics Letters, vol. 87, no. 26, page 263503, 2005.
[van den Donker 07]	M. N. van den Donker, S. Klein, B. Rech, F. Finger, W. M. M. Kessels & M. C. M. van de Sanden. *Microcrystalline silicon solar cells with an open-circuit voltage above 600 mV.* Applied Physics Letters, vol. 90, no. 183504, 2007.

[Vanderhaghen 02]   R. Vanderhaghen, S. Kasouit, R. Brenot, V. Chu, J.P. Conde, F. Liu, A. de Martino & P. Roca i Cabarrocas. *Electronic transport in microcrystalline silicon controlled by trapping and intra-grain mobility.* Journal of Non-Crystalline Solids, vol. 299–302, Part 1, no. 0, pages 365–369, 2002. 19th International Conference on Amorphous and Microcrystalline Semiconductors.

[Vanecek 02]   M. Vanecek & A. Poruba. *Fourier-transform photocurrent spectroscopy of microcrystalline silicon for solar cells.* Applied Physics Letters, vol. 80, no. 5, pages 719–721, 2002.

[Vanecek 11]   Milan Vanecek, Oleg Babchenko, Adam Purkrt, Jakub Holovsky, Neda Neykova, Ales Poruba, Zdenek Remes, Johannes Meier & Ulrich Kroll. *Nanostructured three-dimensional thin film silicon solar cells with very high efficiency potential.* Applied Physics Letters, vol. 98, no. 16, page 163503, 2011.

[Veneri 10]   Paola Delli Veneri, Lucia V. Mercaldo & Iurie Usatii. *Silicon oxide based n-doped layer for improved performance of thin film silicon solar cells.* Applied Physics Letters, vol. 97, no. 2, page 023512, 2010.

[Vepřek 68]   S. Vepřek & V. Maraček. *The preparation of thin layers of Ge and Si by chemical hydrogen plasma transport.* Solid State Electronics, vol. 11, pages 683–684, 1968.

[Vetterl 00]   O. Vetterl, F. Finger, R. Carius, P. Hapke, L. Houben, O. Kluth, A. Lambertz, A. Mück, B. Rech & H. Wagner. *Intrinsic microcrystalline silicon: A new material for photovoltaics.* Solar Energy Materials & Solar Cells, vol. 62, no. 1-2, pages 97–108, 2000.

[Vetterl 01]   O. Vetterl, A. Lambertz, A. Dasgupta, F. Finger, B. Rech, O. Kluth & H. Wagner. *Thickness dependence of microcrystalline silicon solar cell properties.* Solar Energy Materials & Solar Cells, vol. 66, no. 1–4, pages 345–351, 2001.

[Vetterl 03]   O. Vetterl, M. Hülsbeck, J. Wolff, R. Carius & F. Finger. *Preparation of microcrystalline silicon seed-layers with defined structural properties.* Thin Solid Films, vol. 427, no. 1-2, pages 46–50, 2003. Proceedings of Symposium K on Thin Film Materials for Large Area Electronics of the European Materials Research Society (E-MRS) 2002 Spring Conference.

[Vetushka 08]   A. Vetushka, M. Ledinský, J. Stuchlík, T. Mates, A. Fejfar & J. Kočka. *Mapping of mechanical stress in silicon thin films on silicon cantilevers by Raman microspectroscopy.* Journal of Non-Crystalline Solids, vol. 354, no. 19–25, pages 2235–2237, 2008. Amorphous

and Nanocrystalline Semiconductors Proceedings of the 22nd International Conference on Amorphous and Nanocrystalline Semiconductors.

[Wenas 91]   Wilson W. Wenas, Akira Yamada, Makoto Konagai & Kiyoshi Takahashi. *Textured ZnO Thin Films for Solar Cells Grown by Metalorganic Chemical Vapor Deposition.* Japanese Journal of Applied Physics, vol. 30, no. Part 2, No. 3B, pages L441–L443, 1991.

[Werner 01]   J.H. Werner, R. Dassow, T.J. Rinke, J.R. Köhler & R.B. Bergmann. *From polycrystalline to single crystalline silicon on glass.* Thin Solid Films, vol. 383, no. 1–2, pages 95–100, 2001. Proceedings of Symposium O on.

[Widenborg 07]   Per I. Widenborg & Armin G. Aberle. *Polycrystalline Silicon Thin-Film Solar Cells on AIT-Textured Glass Superstrates.* Advances in OptoElectronics, vol. 2007, no. 24584, pages 1–7, 2007.

[Wimmer 12]   Mark Wimmer, Florian Ruske, Simone Scherf & Bernd Rech. *Improving the electrical and optical properties of DC-sputtered ZnO:Al by thermal post deposition treatments.* Thin Solid Films, vol. 520, no. 12, pages 4203–4207, 2012. 8th International Conference on Coatings on Glass and Plastics –ICCG8.

[Würfel 09]   Peter Würfel. Physics of solar cells: From basic principles to advanced concepts. Wiley-VCH Verlag GmbH, 2009.

[Yablonovitch 82] Eli Yablonovitch. *Statistical Ray Optics.* Journal of the Optical Society of America, vol. 72, no. 7, page 899, Jul 1982.

[Yablonovitch 86] E. Yablonovitch, D. L. Allara, C. C. Chang, T. Gmitter & T. B. Bright. *Unusually Low Surface-Recombination Velocity on Silicon and Germanium Surfaces.* Physical Review Letters, vol. 57, pages 249–252, Jul 1986.

[Yamamoto 99a]   K. Yamamoto. *Very thin film crystalline silicon solar cells on glass substrate fabricated at low temperature.* IEEE Transactions on Electron Devices, vol. 46, no. 10, pages 2041–2047, Oct 1999.

[Yamamoto 99b]   K. Yamamoto, M. Yoshimi, Y. Tawada, Y. Okamoto, A. Nakajima & S. Igari. *Thin-film poly-Si solar cells on glass substrate fabricated at low temperature.* Applied Physics A: Materials Science & Processing, vol. 69, pages 179–185, 1999.

[Yamamoto 00]   Kenji Yamamoto, Masashi Yoshimi, Yuko Tawada, Yoshifumi Okamoto & Akihiko Nakajima. *Thin film Si solar cell fabricated*

at low temperature. Journal of Non-Crystalline Solids, vol. 266-269, no. Part 2, pages 1082–1087, 2000.

[Yamamoto 01]   Kenji Yamamoto, Masashi Yoshimi, Yuko Tawada, Yoshifumi Okamoto & Akihiko Nakajima. *Cost effective and high-performance thin film Si solar cell towards the 21st century.* Solar Energy Materials & Solar Cells, vol. 66, no. 1-4, pages 117–125, 2001. PVSEC 11 - Part II.

[Yamamoto 03]   Kenji Yamamoto. *Thin-film crystalline silicon solar cells.* JSAP International, vol. 7, pages 12–19, 2003.

[Yan 03]   Baojie Yan, Jeffrey Yang & Subhendu Guha. *Effect of hydrogen dilution on the open-circuit voltage of hydrogenated amorphous silicon solar cells.* Applied Physics Letters, vol. 83, no. 4, pages 782–784, 2003.

[Yan 04a]   Baojie Yan, Guozhen Yue, Jessica M. Owens, Jeffrey Yang & Subhendu Guha. *Light-induced metastability in hydrogenated nanocrystalline silicon solar cells.* Applied Physics Letters, vol. 85, no. 11, pages 1925–1927, 2004.

[Yan 04b]   Baojie Yan, Guozhen Yue, Jeffrey Yang, Subhendu Guha, D. L. Williamson, Daxing Han & Chun-Sheng Jiang. *Hydrogen dilution profiling for hydrogenated microcrystalline silicon solar cells.* Applied Physics Letters, vol. 85, no. 11, pages 1955–1957, 2004.

[Yan 11]   Baojie Yan, Guozhen Yue, Laura Sivec, Jeffrey Yang, Subhendu Guha & Chun-Sheng Jiang. *Innovative dual function nc-SiO[sub x]:H layer leading to a > 16% efficient multi-junction thin-film silicon solar cell.* Applied Physics Letters, vol. 99, no. 11, page 113512, 2011.

[Yue 05a]   Guozhen Yue, Baojie Yan, Jeffrey Yang & Subhendu Guha. *Effect of electrical bias on metastability in hydrogenated nanocrystalline silicon solar cells.* Applied Physics Letters, vol. 86, no. 9, page 092103, 2005.

[Yue 05b]   Guozhen Yue, Baojie Yan, Jeffrey Yang & Subhendu Guha. *Enhancement of light-induced degradation under reverse bias in hydrogenated nanocrystalline silicon solar cells.* Journal of Applied Physics, vol. 98, no. 7, page 074902, 2005.

[Yue 06]   Guozhen Yue, Baojie Yan, Gautam Ganguly, Jeffrey Yang, Subhendu Guha & Charles W. Teplin. *Material structure and metastability of hydrogenated nanocrystalline silicon solar cells.* Applied Physics Letters, vol. 88, no. 26, page 263507, 2006.

Bibliography

[Yue 08]   Guozhen Yue, Baojie Yan, Charles Teplin, Jeffrey Yang & Subhendu Guha. *Optimization and characterization of i/p buffer layer in hydrogenated nanocrystalline silicon solar cells.* Journal of Non-Crystalline Solids, vol. 354, no. 19–25, pages 2440–2444, 2008. Amorphous and Nanocrystalline Semiconductors Proceedings of the 22nd International Conference on Amorphous and Nanocrystalline Semiconductors - Science and Technology.

[Yue 12]   Guozhen Yue, Baojie Yan, Laura Sivec, Yanhua Zhou, Jeffrey Yang & Subhendu Guha. *Effect of impurities on performance of hydrogenated nanocrystalline silicon solar cells.* Solar Energy Materials & Solar Cells, vol. 104, no. 0, pages 109–112, 2012.

[Zhang 04]   Jianming Zhang & Ellen R. Fisher. *Creation of SiOF films with SiF4/O2 plasmas: From gas-surface interactions to film formation.* Journal of Applied Physics, vol. 96, no. 2, pages 1094–1103, 2004.

[Zhang 08]   Q. Zhang, E. V. Johnson, Y. Djeridane, A. Abramov & P. Roca i Cabarrocas. *Decoupling crystalline volume fraction and V_{oc} in microcrystalline silicon pin solar cells by using a μc-Si:F:H intrinsic layer.* physica status solidi (RRL) – Rapid Research Letters, vol. 4, pages 154–156, 2008.

Publications as first author:

S. Hänni et al., "Highly crystalline Microcrystalline Silicon Solar Cells for Very High Infrared Absorption", (provisional title), in preparation.

S. Hänni et al., "Post-Deposition Treatment of Microcrystalline Silicon Solar Cells For Improved Performance on Rough Superstrates", in preparation.

S. Hänni et al., "Microcrystalline silicon solar cells with passivated interfaces for high open-circuit voltage", in preparation.

S. Hänni et al., "High-efficiency microcrystalline silicon single-junction solar cells", Progress in Photovolatics: Research and Applications, Vol. **21**, pp. 821-826, 2013.

S. Hänni et al., "On the Interplay Between Microstructure and Interfaces in High-Efficiency Microcrystalline Silicon Solar Cells", IEEE Journal of Photovoltaics, Vol. **3** (1), pp. 11-16, 2013.

S. Hänni et al., "TOWARDS BETTER UNDERSTANDING OF LONG-TERM STABILITY IN THIN FILM MICROCRYSTALLINE SILICON SOLAR CELLS", Proc. of the 27th EU-PVSEC, pp. 2699-2703, 2011.

Publications as co-author:

M. Boccard et al., "High-stable-efficiency multi-junction thin-film silicon solar cells incorporating conductive low-refractive index silicon-oxide interlayers", submitted, 2014.

R. Khazaka et al., "Silver versus white paste as a back reflector for microcrystalline silicon solar cells deposited on LPCVD-ZnO electrodes of various textures", submitted, 2014.

M. Boccard et al., "The role of front and back electrodes in parasitic absorption in thin-film solar cells", accepted in EPJ Photovoltaics, 2014.

J.-W. Schüttauf et al., "Thin film silicon triple junction solar cells on highly transparent front electrodes with stabilized efficiencies up to 12.8%", IEEE Journal of Photovoltaics, Vol. **4** (3), pp. 757-762, 2014.

G. Bugnon et al., "Silicon oxide buffer layer at the p–i interface in amorphous and microcrystalline silicon solar cells", Solar Energy Materials & Solar Cells, Vol. **120** (A), pp. 143-150, 2014.

R. Biron et al., "New progress in the fabrication of n–i–p micromorph solar cells for opaque substrates", Solar Energy Materials & Solar Cells, Vol. **114**, pp. 147-155, 2013.

R. Biron et al., "Optimization of the Asymmetric Intermediate Reflector Morphology for High Stabilized Efficiency Thin n-i-p Micromorph Solar Cells", IEEE Journal of Photovoltaics, Vol. **3** (1), pp. 41-45, 2013.

G. Bugnon et al., "A New View of Microcrystalline Silicon: The Role of Plasma Processing in Achieving a Dense and Stable Absorber Material for Photovoltaic Applications", Adv. Func. Mater. **22**, pp. 3665-3671, 2012.

F. Meillaud et al., "Latest developments of high-efficiency micromorph tandem silicon solar cells implementing innovative substrate materials and improved cell design", IEEE Journal of Photovoltaics, Vol. **2** (3), pp. 236-240, 2012.

M. Boccard et al., "Optimization of ZnO Front Electrodes for High-Efficiency Micromorph Thin-Film Si Solar Cells", IEEE Journal of Photovoltaics, Vol. **2** (3), pp. 229-235, 2012.

M. Despeisse et al., "Light harvesting schemes for high efficiency thin film silicon solar cells", in Conference Record of the 38th IEEE Photovoltaic Specialists Conference, Austin, USA, art. no. 6318218, pp. 3015-3019, 2012.

M. Boccard et al., "Nanometer- and Micrometer-Scale Texturing for High-Efficiency Micromorph Thin-Film Silicon Solar Cells", IEEE Journal of Photovoltaics, Vol. **2** (2), pp. 83-87, 2012.

M. Boccard et al., "Multiscale Transparent Electrode Architecture for Efficient Light Management and Carrier Collection in Solar Cells", Nano Lett. **12** (3), pp. 1344-1348, 2012.

C. Battaglia et al., "Advanced nanostructured materials for pushing light trapping towards the Yablonovitch limit", Optical Nanostructures and Advanced Materials for Photovoltaics, Austin, USA, November, 2011.

M. Despeisse et al., "Optimization of thin film silicon solar cells on highly textured substrates", Phys. Status Solidi A **208**, No. 8, 1863–1868, 2011.

G. Bugnon et al., "High rate deposition of microcrystalline silicon with silicon oxide doped layers: Highlighting the competing roles of both intrinsic and extrinsic defects on the cells performances", Proc. of the 37th IEEE PVSC, Seattle, USA, 2011.

M. Boccard et al., "Single to multi-scale texturing for high efficiency micromorph thin film silicon solar cell", Proc. of the 37th IEEE PVSC, Seattle, USA, 2011.

C. Ballif et al., "NOVEL MATERIALS AND SUPERSTRATES FOR HIGH-EFFICIENCY MICROMORPH SOLAR CELLS", Proc. of the 26th EU-PVSEC, 2010.

M. Despeisse et al., "LOW-CONDUCTIVITY DOPED LAYERS FOR IMPROVED PERFORMANCE OF THIN FILM SILICON SOLAR CELLS ON HIGHLY TEXTURED SUBSTRATES", Proc. of the 26th EU-PVSEC, 2010.

Publications prior to PhD thesis:

A. Chirila et al., "CIGS solar cells grown by a three-stage process with different evaporation rates", in Conference Record of the IEEE Photovoltaic Specialists Conference, art. no. 5411161, pp. 000812-000816, 2009.

162

Patents:

"Thin microcrystalline silicon solar cells", in preparation.

"METHOD FOR ANNEALING A THIN FILM PHOTOVOLTAIC CELL DEVICE", filled.

Presentations:

Oral presentation at the 25th International Conference on Amorphous and Nanocrystalline Semiconductors (ICANS25), in Toronto, Canada, August 2013 with the title: "Fundamental Limits of High-Efficiency Microcrystalline Silicon Thin-Film Solar Cells: The Role of Interfaces".

Oral presentation at the 38th IEEE PVSC, in Austin, USA, June 2012, with the title: "On the Interplay between Material Quality and Interfaces in High Efficiency Microcrystalline Silicon Solar Cells".

Poster presented at the 29th EUPVSEC in Paris, France, September 2013, with the title: "The Role of Interfaces in High-Efficiency Microcrystalline Silicon Thin-Film Solar Cells".

Poster presented at the 11. Nationale Photovoltaik-Tagung, Basel, Switzerland, March 2013, with the title "Recent Progress towards High-Efficiency Thin-Film Silicon Solar Cells".

Poster presented at the 27th EUPVSEC in Hamburg, Germany, September 2011, with the title: "TOWARDS BETTER UNDERSTANDING OF LONG-TERM STABILITY IN THIN FILM MICROCRYSTALLINE SILICON SOLAR CELLS".

Awards:

Best poster award (1st prize) at the 11. Nationale Photovoltaik-Tagung, Basel, Switzerland, March 2013, with the title "Recent Progress towards High-Efficiency Thin-Film Silicon Solar Cells".

Student award finalist at the 38th IEEE PVSC, in Austin, USA, with the title: "On the Interplay between Material Quality and Interfaces in High Efficiency Microcrystalline Silicon Solar Cells".

Simon HÄNNI
Master degree in Physics from ETH Zürich

16, Faubourg de l'Hôpital	sh.pvlab@gmail.com
2000 Neuchâtel	Nationality: Swiss
Switzerland	Age: 30

EXPERIENCE

01/2010 – 06/2014	**IMT – PV-lab, École Polytechnique Fédérale de Lausanne (EPFL)**	**PhD candidate in Material Science**: "Microcrystalline Silicon for High-Efficiency Thin-Film Photovoltaic Devices"
04/2009– 09/2010	**IMT – PV-lab, École Polytechnique Fédérale de Lausanne (EPFL)**	**Civilian service**
09/2008 – 01/2009	**Thin Film Physics Group Eidgenossische Technische Hochschule Zürich (ETHZ)**	**Master thesis in Physics**: "Cu(In,Ga)Se$_2$ Thin Film Solar Cells grown by Three-Stage-Process at Different Evaporation Rates"
06/2008	**Thin Film Physics Group Eidgenossische Technische Hochschule Zürich (ETHZ)**	**Semester work in Physics**: "Manufacture and Characterization of Alternative Buffer Layers for CIGS Thin Film Solar Cells by Ultrasonic Spray Pyrolysis"
2006–2007	**Ecole Primaire Sonceboz**	Intermittent teaching in elementary school

EDUCATION

08/2007 – 03/2009	**Eidgenössische Technische Hochschule Zürich (ETHZ):** Master of Science ETH in Physics
10/2003 – 08/2007	**Eidgenössische Technische Hochschule Zürich (ETHZ):** Bachelor of Science ETH in Physics
08/2000 – 06/2003	Maturité, Gymnase Français de Bienne, Switzerland

Language skills: French/Swiss German (mother tongue), German (fluent), English (fluent).
Computer skills: good knowledge of Office suite and LaTeX, basic knowledge of various simulation, mathematics and graphics tools such as PC1D, MATLAB, IGOR pro and Adobe Illustrator CS6.

SCIENTIFIC CONTRIBUTIONS

I coauthored 23 scientific contributions, including two peer-reviewed papers as a first author, and I am co-inventor on two patents. I took part to four international conferences, for which I gave two oral presentations. I was awarded the best poster award (1st prize) at the Swiss PV congress 2013 and was student award finalist at the 28th IEEE Photovoltaic Specialists Conference in 2012. A publication list is available on http://scholar.google.ch/citations?user=ase5VC8AAAAJ&hl=fr.

MISCELLANEOUS

During my PhD thesis at IMT–PV-lab, I was teaching assistant for the lecture "Opto- and macroelectronic materials" for two semesters, and supervised one master student internship and one civilian service. I like travelling, scuba diving, playing floorball and trekking. I'm an enthusiastic piano player and have been singing for 3 years in the choir of Neuchâtel University.